IDENTIFYING NOVEL REGULATORS OF EZRIN AND EPITHELIAL CELL MICROVILLI

A Dissertation

Presented to the Faculty of the Graduate School

Of Cornell University

In Partial Fulfillment of the Requirements for the Degree of

Doctor of Philosophy

by

Raghuvir (Ram) Viswanatha

January 2013

IDENTIFYING NOVEL REGULATORS OF EZRIN AND EPITHELIAL CELL MICROVILLI

Raghuvir (Ram) Viswanatha, Ph.D.

Cornell University 2013

Epithelial cells have a highly polarized cytoskeleton, in which microvilli, finger-like protrusions with filamentous actin (F-actin) cores, protrude only from the apical side. Ezrin, a plasma-membrane-F-actin crosslinker, is highly enriched in microvilli, and required for their presence in some cultured cell-lines. Numerous binding partners of ezrin are known, including ezrin-binding phosphoprotein 50 (EBP50) and CD44, but no systematic analysis of ezrin-binding partners in epithelial cells has been undertaken.

To better understand how ezrin works, we conducted a proteomic profiling of ezrin immunoprecipitates and identified 12 novel and 7 previously known interactors. The N- and C-termini of ezrin interact forming a dormant molecule, and this autoinhibition is released in a process dependent upon phosphorylation of a critical C-terminal residue, threonine-567, so we can control it through mutation of T567. By quantitatively comparing immunoprecipitates from open vs. closed ezrin mutants, I found that different ezrin binding partners respond differently to changes in ezrin autoinhibition.

In the course of my studies, I made the surprising observation that open ezrin variants lost their polarized distribution within microvilli, while they remained on the plasma membrane. This implied that a local cue, operating just in the apical domain, controls the normal opening of ezrin. A likely candidate was the hypothetical T567 kinase. Among the 12 novel ezrin-binding proteins, I noticed 2 potential T567 kinases, LOK and SLK, and confirmed that their presence was required for T567 phosphorylation and microvilli in two cell-lines. In additional

experiments, I determined that their apically-localized activity was required for ezrin's apical localization, which in turn, was required for the *de novo* presence of microvilli. Thus, a critical aspect of epithelial cytoskeletal polarity is the control of ezrin's partner interactions through the regulated release of autoinhibition mediated by apically polarized T567 phosphorylation.

BIOGRAPHICAL SKETCH

Raghuvir (Ram) Viswanatha was born in a Boston hospital to Hema and Alagawadi in the summer of 1982. He was fascinated with science—especially biology—from an early age, although he could never exactly pin down why. It was especially difficult when he was forced to write about himself in the third person. This interest eventually led him to enroll at Tufts University as a biochemistry major. It began to take a more concrete form in the summer following his freshman year when he was fortunate to be able to work in the lab of Dr. Laurence Rahme at Mass General Hospital on a project studying the innate immune response in *Drosophila*. The following summer, he worked on a biotechnology project at MIT Lincoln Laboratory with Dr. Todd Rider, and then, during his final three semesters at Tufts, on a senior research project with Dr. David Kaplan cloning the genes for emulsan biosynthesis. These small research projects succeeded in conveying the fun and excitement of science to our young hero, who, following his graduation from Tufts, attended Cornell as a BMCB graduate student.

Although his initial interest was in the mechanism of transcription, he was captivated instead by Dr. Tony Bretscher's description of the dynamic and beautiful cytokeleton. Even having never used a fluorescence microscope and having done fewer than three western blots in his life, he asked Dr. Bretscher for the opportunity to rotate in his lab and instantly fell in love with cell biology. Despite a long time with very little luck in his first three years after joining the lab (Appendices A,B,C), he persevered until, in his fourth, he had the start of quite an interesting story (Chapters 2,3). He hopes you will find it interesting, too.

ACKNOWLEDGEMENTS

This section is supposed to acknowledge the contribution (or merely the existence) of people without whom this PhD would not have materialized. However, that list is far too long, so here are some highlights, broken into six parts:

First, I'd like to thank my parents and extended family for supporting me and promoting science and critical thinking. I'd especially like to thank Dr. Gomathi Krishnan for the opportunity to work at Mass General Hospital, my first research position.

Second, I'd like to thank my friends here at Cornell that made it a fun place to live, including Yu-Fang, Laura, Pye Ton, Stephen, Srich, Damien, Song, Raga, Shamoni, Nasun, and Xin (in absolutely no order). The Asian gang will ride again.

Third, I'd like to thank all the members of our lab past and present for making it a fun and engaging place to work. Especially Janet Ingraffea for her invaluable contributions to the Nadrin project (Appendix B) and for general support over the years; Dr. Tal Ilani for introducing me to ERMs through her work on T-cells during my rotation; Dr. Julie Thoms for handing me a solid project before she left and help with cloning ezrin constructs; Dr. Abe Hanono for developing the cross-linking protocol for capturing the transient EBP50-ezrin interaction; Dr. Dave LaLonde for assistance with cell culture and immunoprecipitation; Dr. Damien Garbett for developing a protocol for efficient RNAi in Jeg-3 cells, invaluable microscopy support, and help with the IRSp53 project (Appendix C); Drs. David Hokanson and Felipe Santiago-Tirado for their help with liposome binding experiments; and Jessica Wayt for Jeg-3 cDNA. Their support made this work possible.

Fourth, I have to acknowledge the help of exceptional scientists from other labs. First, Dr. Marcus Smolka, Patrice Ohouo, and Dr. Francisco Bastos-de-Olivera. Their help with mass spectrometry and the SILAC procedure was pivotal. I'd also like to thank the other labs in Weill Institute for sharing reagents and knowledge, especially Dr. Yuxin Mao for structure-gazing with me and suggesting the I110-to-M point-mutation in LOK that resists inhibition by erlotinib. Early on, I relied on the advice of Drs. Raga Krishnakumar, Tong Zhang, and Nasun Hah from the Kraus lab and Dr. Volker Vogt to create stable cell-lines. Finally, I acknowledge the generous contribution of plasmids, antibodies, and cells over the years from the following scientists and their labs: Drs. Andrej Cybulsky (McGill), Pontus Apsenstrom (Karolinksa), James Bartles (Northwestern), Luc Sabourin (Ottowa), Stephen Shaw (NIH), Hajime Karasuyama (Tokyo), Monique Arpin (Curie), Steve Winder (Sheffield), Fenghua Hu (Cornell), Bill Brown (Cornell), Haiyuan Yu (Cornell), David Shalloway (Cornell), Wade Harper (Harvard), Rick Thorne (Newcastle), Yasu Fujita (UCL), Yuxin Mao (Cornell), Scott Emr (Cornell), Stefan Roberts (Buffalo), Matt Tyska (Vanderbilt), and Keith Mostov (UCSF).

Fifth, my funding source: the NIH and Cornell's NIH training grant. More generally, I'd like to acknowledge the NIH for investing in projects such as this one with no immediate therapeutic potential with the ultimate goal of gaining broad insights into the inner workings of humans to pinpoint what might go awry in disease.

Sixth, and most of all, I have to thank Tony, who has been invaluable at multiple levels: teaching a brilliant and engaging graduate course; being an unfettered thinker at times while showing more restraint than I could when more disciplined thinking was called for. In addition being the source of most of the insights that made this work possible, whenever I hit a roadblock,

Tony told me what I needed to hear to keep working. This was as essential to my Ph.D. as the technical and scientific help mentioned above.

TABLE OF CONTENTS

LIST OF FIGURES

LIST OF TABLES

CHAPTER 1

INTRODUCTION TO ERMS AND MICROVILLI

Life as we know it requires organizational and functional polarity at many levels. At its most fundamental level, that of the cell, life organizes spatially distinct regions specialized for particular functions. A few selected examples include polarization for bud-site selection which orients nuclear and cell division in the budding yeast *Saccharomyces cerevisea* (Pruyne et al., 2004; Figure 1.1A); the outgrowth of neuronal protrusions and then their subsequent assignment as either axons or dendrites (Dent et al., 2011; Figure 1.1B) and the formation of nutrient-absorptive microvilli just on lumen-facing side of intestine (Nambiar et al., 2010; Fehon et al., 2010; Figure 1.1C). Not only is the yeast bud, the neurite, and the microvillus compositionally distinct from the rest of the cell, but each also adopts a characteristic morphology. This is accomplished by differential restructuring of the common manifold underlying the plasma membrane: the cytoskeleton.

Microvilli: a model for cytoskeletal polarity

The cytoskeleton is largely made up of three filament-forming protein types—actin, comprising actin filaments (F-actin); tubulin, comprising microtubules; and keratins, vimentin, lamins, neurofilaments, and desmins, comprising intermediate filaments. The yeast bud, the neurite, and microvilli are primarily composed of actin filaments, directional polymers of a 43 kDa protein that grow and shrink from opposite ends (termed the plus and minus ends). Microvilli are composed of elongated F-actin bundles that protrude into the so-called terminal web region, where they connect with the underlying F-actin cortex (Figure 1.1C).

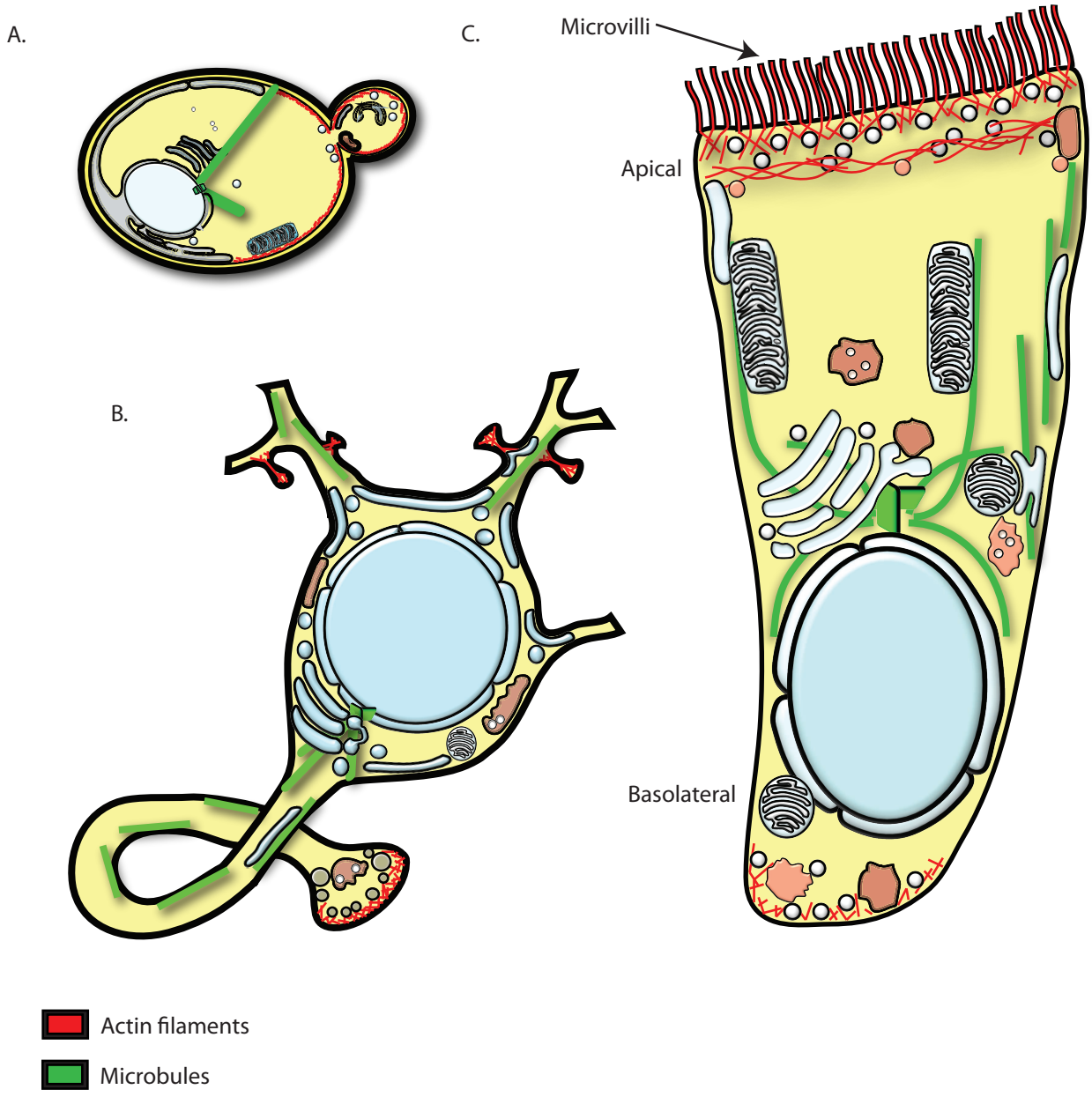

Figure 1.1 The eukaryotic cytoskeleton. Filamenous actin (red) and microtubule (green) cytoskeleton in a budding yeast (A), neuron (B), and epithelial cell (C). Note the apical microvilli rooted into the terminal web. Figures copyrighted 2011 by Felipe Santiago-Tirado. Used with permission.

The nucleation of actin from monomers into trimers is unfavorable *in vivo* and thus requires accessory proteins termed nucleation promoting factors (NPFs; Firat-Karalar and Welch, 2011). Particular NPFs appear to nucleate particular classes of actin filaments. For instance, the actin cables of the budding yeast are nucleated by formins whereas endocytic patch actin filaments are nucleated by the Arp2/3 complex (Evangelista et al., 2002). The microvillar F-actin core consists of parallel bundles with their growing end at the tip and their shrinking ends rooted in the terminal web. This suggests that the microvillar NPF is a component of the microvillar tip, which contains an electron-dense mass (Mooseker and Tilney, 1975), but due to pleiotropy and redundancy, the microvillar NPF has not yet been identified (Harris et al., 2010). A host of accessory proteins are additionally required to regulate filament elongation *in vitro* and in model systems (such as actin-based motility of invading bacteria and viruses). Several of these are present in microvilli, but only one has proved to be necessary for normal microvilli morphology *in situ* thus far, which is the processive capping-protein displacement factor Eps8 (Croce et al., 2004; Tocchetti et al., 2010). Consistent with the notion that it may be a critical component of the F-actin generation machinery, Eps8 is found preferentially towards the tip of microvilli (Croce et al., 2004).

Like most F-actin structures, microvillar cores consist of parallel actin bundles. The predominant F-actin bundling proteins in microvilli are fimbrin, espin, and villin, which were thought until recently to be necessary for microvillar core organization. In fact, fimbrin and villin, along with actin, ATP, and brush border myosin IA, are sufficient to form a microvillar core *in vitro* (Coluccio and Bretscher, 1989). Recent genetic analysis, however, has suggested that microvilli do not strictly require the major filament bundlers as slightly shortened but ultrastructurally intact microvilli are found in fimbrin-villin-espin triple knockouts (Revenu et

al., 2012). More detailed analysis suggested that actin bundlers are required to properly root the microvilli into the terminal web, but not for formation of the core, as their deletion led to fragile and leaky intestinal lumens (Revenu et al., 2012; Grimm-Gunter et al., 2009).

Finally, purified intestinal microvilli contain significant amounts of actin-binding protein ezrin and motor protein myosin IA (Bretscher, 1983). Both proteins bind directly to membranes, and therefore have the capacity to serve as cross-linkers between the microvillar core and the plasma membrane, but the lack of ultrastructural defects in the microvilli of myosin IA knockout mouse and presumed redundancy with other myosins (including myosin IC) has hindered a study of its cross-linking function (Tyska et al., 2005). Instead, recent research has focused on its role in generating vesicles containing digestive and protective enzymes from brush border microvilli tips, which is discussed further below. Ezrin and two related proteins, on the other hand, have been thought to be the primary actin-plasma membrane crosslinkers in microvilli, and these are the subjects of my studies.

Although microvilli are a common organelle, they have remained relatively understudied. The primary reason is that due to an exceptionally high degree of redundancy and pleiotropy among NPFs, actin cross-linking proteins, and membrane-actin cross-linking proteins, there is currently no gene knockout that selectively perturbs all of the microvilli in any organism. Furthermore, while a number of receptor signaling systems such as GluT receptor activation and internalization operate in microvilli (reviewed in Lange, 2011), to my knowledge, the need for these to be organized within microvilli has never been assessed. For instance, would signal transduction be attenuated in cells lacking microvilli or if the signaling apparatus was localized away from the apical plasma membrane? There are a few examples in which microvillus

organization *per se* has been shown or suggested to play a physiological role: photoreception, audition, nutrient absorption, and digestion.

Photoreception. The *Drosophila* photoreceptors are organized into clusters with a distinct apical membrane, covered in microvilli, facing into the center. Light-sensitive transient receptor potential channels TRP and TRPL are located in microvilli and may be anchored via dMoesin (Chorna-Ornan et al., 2005). The microvilli, and thus the organization of the photoreceptor cluster, were shown to be sensitive to the removal of dMoesin (Karagiosis and Ready, 2004), and, moreover, the overexpression of dominant dMoesin mutants, presumably perturbing microvilli formation, was shown to affect photoreception and cause photoreceptor degeneration in low-light conditions (Chorna-Ornan et al., 2005). Recently, an *in vitro* model of *Drosophila* photoreceptors was prepared, and this suggested to the authors that the clustered organization of photoreceptors into microvilli provides increased sensitivity in low-light (Song et al., 2012). Thus microvilli organization *per se*, and not simply the presence of their components, appears to be critical for photoreception.

Audition. The clearest model in which microvilli play a physiological role is in the specialized stereocillia of the inner ear, which function in vertebrate audition. Stereocilia, which are connected to one another by cadherin-based tip links, protrude into the vibration-sensing tectorial membrane. Shearing of the tectorial membrane by sound waves causes deflection of the stereocilia, resulting in a pulling force which opens stereocilia-resident voltage-gated calcium channels, resulting in a transient efflux of calcium ions, which activates neighboring neurons. This system relies on the ultrastructure of stereocilia to function in mechanotransduction. Many structural proteins such as myosins and actin-binding proteins are common between microvilli

and stereocilia. As mentioned below, radixin, one such actin-binding protein, was shown to be required for stereocilia (Kitajiri et al., 2004).

Nutrient absorption. Classically, it is believed that nutrient absorption in the intestine requires microvilli to increase available surface area, but this assertion has never been tested directly.

Pathogen barrier function. An intriguing aspect of microvillar organization has come from detailed analysis of the brush border myosin (MyoIA) knockout mouse. Wild-type brush border microvilli were shown to shed vesicles emanating from the distal tip into the intestinal lumen (McConnell et al., 2009). This activity was dependent on MyoIA, which can slide distally *in vitro* (Verner and Bretscher, 1983; Tyska et al., 2005; McConnell et al., 2009). The vesicles contained intestinal alkaline phosphatase (IAP), which was shown to inhibit bacterial colony formation in the intestinal lumen and *in vitro* (Shifrin et al., 2012). Thus the architecture of microvilli plays a role in epithelial barrier function.

Finally, microvilli are similar in morphology in invertebrates. Also, two gene deletions that cause complex microvillus abnormalities in mice, knockout of ezrin and Eps8, cause strikingly similar abnormalities in the invertebrate *Caenorhabditis elegans* (Tocchetti et al., 2010; Saotome et al., 2004; Casaletto et al., 2011; Van Furden et al., 2004; Segbert et al., 2004; Croce et al., 2004) and suggest that both their ultrastructual appearance and regulation is conserved among animals. Such a conserved process must be performing an important function even if it is hard to identify.

ERMs: regulated F-actin-plasma-membrane crosslinkers in cultured cell microvilli

ERMs are named for the founding members: ezrin, radixin, and moesin. These proteins are similar in size, primary sequence, and structure (Figure 1.2.A). Early biochemical studies

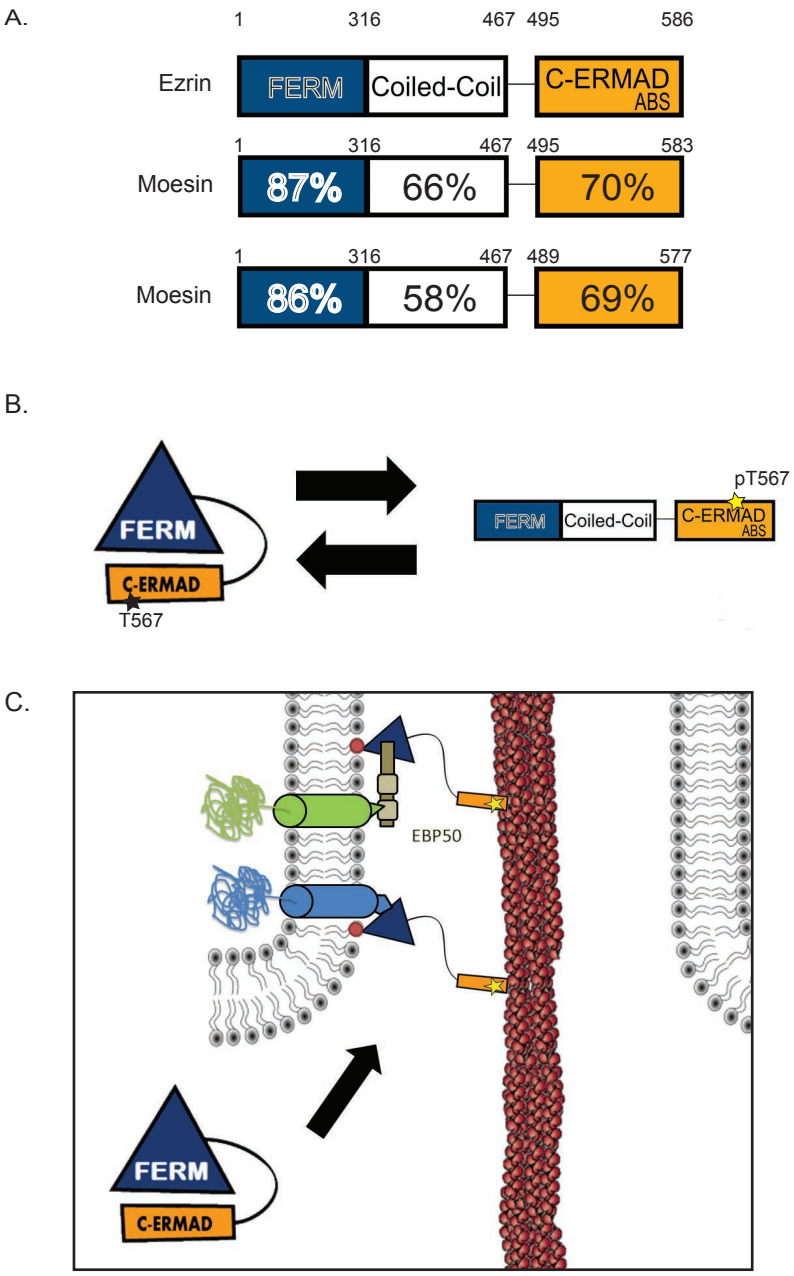

Figure 1.2 ERM homology, conformational change, and translocation to the plasma membrane. (A) Cartoon diagram of ezrin domain structure, and homology to radixin and moesin. *FERM*, Band 4.1-ERM homology domain; *C-ERMAD*, C-terminal ERM association domain; *ABS*, F-actin-binding site. Percent identities were calculated using CLUSTALW. (B) Conformational change in ezrin structure change the availability of the FERM domain and ABS. Star, T567 (in ezrin) which is phosphorylated to regulate the conformational change. (C) Translocation of dormant ezrin from the cytoplasm to microvilli is regulated by phosphorylation (yellow star) and PI(4,5)P_2 (red circle) binding. In microvilli it is thought to engage with various transmembrane proteins directly (like the blue transmembrane protein) or indirectly through ERM-binding phosphrotein 50 (brown; like the green transmembrane protein).

used cultured cell models to characterize their function, and these will be discussed in the first section. As mentioned, ERM orthologs are clearly present in all animals (possibly also fungi; Dagdas et al., 2012), and studies of ERM gene deletions has revealed that ERM gene function is essential for cell and tissue morphogenesis. I will review ERM genetics in the second section. Whereas early biochemical data established that ERM proteins were regulated intrinsically through conformational changes, contemporary studies have asked which molecules regulate these changes extrinsically. In the third section, I will consider potential ERM regulators: 1) the plasma membrane and membrane proteins and 2) kinases and phosphatases.

Initial observations pointed to the possibility that ezrin linked the plasma membrane and the underlying cytoskeleton in F-actin-rich protrusions. Ezrin was first isolated as a cytoplasmic protein enriched in brush border microvilli that localized to cell surface protrusions of numerous cell types (Bretscher, 1983). It was later revealed that ezrin is phosphorylated on serine, threonine, and tyrosine residues and hyperlocalizes in cell surface protrusions following EGF stimulation (Gould et al., 1986; Bretscher, 1989), an early indication that phosphorylation regulates its activity. By expressing and localizing tagged truncations, the N-terminal region of ezrin was found to localize at the plasma membrane whereas the C-terminal region localized indiscriminately to the F-actin cytoskeleton (Algrain et al., 1993). Finally, electron microscopy also supported this role. By immuno-ferritin electron microscopy of Jeg-3 cell microvilli (Pakkanen et al., 1987) or immuno-gold microscopy of chorionic and intestinal microvilli (Berryman et al., 1993), ezrin could be seen just beneath the limiting plasma membrane but some distance from the actin core. These initial observations led to studies of ezrin regulation *in vitro* and in the formation of cell surface protrusions.

ERMs undergo regulated intramolecular interaction. The critical inroads into understanding ERM regulation came from studies showing that the extreme N- and C-terminal regions of ERMs (termed the N- or C-terminal ERM association domain; N-/C-ERMAD) can directly bind to one another (Figure 1.2.B; Gary and Bretscher, 1995; Gary and Bretscher, 1993; Reczek et al., 1997). This model has been upheld by the crystal structure of the moesin N-ERMAD/C-ERMAD complex (Pearson et al., 2000) and that of a dormant, full-length ERM (Li et al., 2007). Subsequently, platelet moesin was found to be phosphorylated primarily on C-terminal T558, which is homologous to T567 in ezrin and T564 in radixin, and this phosphorylation was found to activate it (Nakamura et al., 1995). Radixin and ezrin were subsequently found to undergo similar phosphorylation (Barret et al., 2000; Gautreau et al., 2000; Hamada et al., 2000; Hirao et al., 1996; Matsui et al., 1998; Simons et al., 1998; Turunen et al., 1994). These studies showed that the F-actin binding site in the C-terminal region, and the protein interaction domain in the N-terminal region were self-masked in the dephosphorylated form and, together, established a coherent model: ERMs oscillate between a dormant, dephosphorylated state in which they are predominantly cytosolic, and then transition to an active, phosphorylated state, where they translocate to the plasma membrane and bind cortical or microvillar actin filaments (Figures 1.2.B,C). The remaining mystery was the mechanism of the translocation.

Phosphorylation influences ERM activity. The role of ezrin phosphorylation on serine and tyrosine is less well understood. While serine phosphorylation at position 66 has thus far only been shown to be relevant in gastric parietal cells (Zhou et al., 2003) and tyrosine phosphorylation appears to be relevant mainly in tubulogenesis in response to receptor tyrosine kinase activation (mostly hepatocyte growth factor receptor, HGF-R; Crepaldi et al., 1997; Prag et al., 2007; Naba et al., 2008; Zwaenepoel et al., 2012; Zaarour et al., 2012), neither the

interaction between these sites and the C-terminal threonine nor the effect on the open vs. closed state has been examined. Interestingly, tyrosine 477, which is phosphorylated directly by Src, is in the middle of the "acidic flap," a region that modulates the $PI(4,5)P_2$-dependent translocation of ezrin to the plasma membrane and will be discussed further below (Ben-Aissa et al., 2012). Phosphorylation at T235 by cyclin-dependent kinase 5 has also been shown to regulate ezrin activity in some contexts (Yang and Hinds, 2003; Yang and Hinds, 2006), but the generality of this regulation has not yet been demonstrated. The general sense in the field is that ERMs are primarily regulated by C-terminal threonine phosphorylation (T567 in ezrin; Figures 1.2.B,C).

ERM C-terminal threonine phosophorylation in cell surface structure regulation. In order to understand ERM regulation, it was first necessary to determine the phenotype of cells lacking ERMs. Several attempts have been made to determine this. Tsukita and colleagues found that inhibiting ERM translation by antisense RNA injection prevented the formation of microvilli, cell-cell junctions, and peripheral ruffles (Takeuchi et al., 1994), a global loss of actin-structures that has not since been reproduced. In retinal pigment epithelial cells both cultured and *in vivo*, ERM knockdown eliminated microvilli and basal infoldings but not junctions (Bonilha et al., 1999; Chuang et al., 2010; Bonilha et al., 2006). It is important to note that ezrin knockdown has not always resulted in the loss of microvilli, suggesting that the degree of ezrin suppression may need to be high in order to observe a defect, and that radixin and moesin may need to be suppressed along with ezrin (for example, D'Angelo et al., 2007). An alternative approach has been the use of dominant mutants. Overexpression of the FERM domain of ERMs inhibits the formation of microvilli and HGF signaling (Crepaldi et al., 1997) and has also been shown to inhibit the activity of a variety of interaction partners, the mechanism believed to involve the uncoupling of FERM domain binding partners away from endogenous ERMs, and thus F-actin.

Similarly, Arpin and colleagues have shown that the overexpression of dormant ezrin that cannot be activated by phosphorylation (T567A in ezrin) in epithelial cells impairs microvillus formation (Gautreau et al., 2000), while overexpression of phosphomimetic, constitutively activated ezrin (T567D) increases the density and length of microvilli (Gautreau et al., 2000; Fievet et al., 2006). The microvillus-formation ability of phosphomimetic ezrin appears to be more dramatic and reproducible in fibroblastic cell-lines which lack any apical protrusions under basal conditions that, when transfected with activated ezrin, produce microvilli-like actin-rich structures from their cell surface (Oshiro et al., 1998; Matsui et al., 1998; Yonemura et al., 1999). Together, these observations suggest that ERMs function by linking the plasma membrane and F-actin, and that in some cases, the regulation of ezrin activation by phosphorylation of the C-terminal threonine residue is rate-limiting for microvillus formation.

But phosphomimetic ezrin has not always been shown to enhance microvilli. First, it is worth noting that I and others could not reproduce the findings of Arpin and colleagues that epithelial cell microvilli elongate and grow denser when transfected with plasmids encoding activated ezrin (R. Viswanatha, J. Thoms and D. Chambers, unpublished), but this may have been due to the level of overexpression we were able to achieve. Second, in the developing mouse embryo, ezrin is polarized to microvilli and clears out of regions of cell-cell contact during the 4-cell stage (Dard et al., 2001; Louvet et al., 1996). This process was shown to be dependent upon both phosphorylation and dephosphorylation, as overexpression of either T567A or T567D ezrin-GFP but not wild-type ezrin-GFP interfered with the formation of microvilli (Dard et al., 2004). Finally, Karagiosis and Reddy found that *Drosophila* photoreceptor microvilli were sensitive to depletion of dMoesin, the ortholog of mammalian ERMs, and that phosphomimetic dMoesin failed to rescue the microvilli (Karagiosis and Ready, 2004). These

results suggest that in some cases, a complex interconversion between open and closed ezrin, and not simply the open form, is needed for ezrin function. Due to the complexity of these data, they have been summarized in Table 2.

ERM recruitment of EBP50. The existing evidence from cell culture as well as whole organism knockouts (reviewed below) suggests that ezrin functions as a cross-linker in numerous cases, but in addition to this role, work from Bretscher and colleagues have highlighted what is likely to be a second role: binding, thus recruiting, FERM-domain interaction partner ERM-binding phosphoprotein 50 (EBP50) to the apical membrane, which is also essential for microvilli (Hanono et al., 2006; LaLonde et al., 2010; Garbett et al., 2010; Garbett and Bretscher, 2012). Cells lacking EBP50 or expressing versions of EBP50 that cannot bind ezrin fail to form microvilli (Garbett et al., 2010; Hanono et al., 2006). Additionally, the defect in EBP50-depleted cells is limited to microvilli: surface-touching structures such as lamelipodia and filopodia are not as dramatically affected (D. Garbett and R. Viswanatha, unpublished observations). Importantly, the EBP50 knockout mouse supports a physiological role for ezrin-EBP50 linkage in microvillar morphology *in situ* (Morales et al., 2004). EBP50 is a scaffolding protein which interacts with a wide array of interaction partners through tandem PDZ protein-protein interaction domains (reviewed in Fehon et al., 2010), but the ligand or ligands critical for the formation of microvilli has not yet been identified. EBP50 is discussed in Appendices B and C.

In addition to EBP50, ERMs have been proposed to interact with numerous other transmembrane and cytoplasmic factors, but because it is unclear how these contribute to the regulation of its function in cell surface protrusions, they are listed in Table 1 but not discussed further.

ERM regulation of mitosis in Drosophila *S2 cells.* An intriguing role for dMoesin has emerged from studies of its function in *Drosophila* Schneider 2 and subline S2R+ cells (Carreno et al., 2008; Roubinet et al., 2011; Kunda et al., 2008; Kunda et al., 2012). These immortal cell lines derived from this *Drosophila* macrophage-like cell-line lack apico-basolateral polarity, so they cannot be used to assess polarized cell surface structures. Instead, knocking down dMoesin perturbs mitosis (Kunda et al., 2008; Carreno et al., 2008), which Baum and colleagues determined through atomic force microscopy studies was due to a defect in cortical rigidity (Kunda et al., 2008). Moreover, the dMoesin T579D mutant induced a 2-fold increase in stiffness, indicating that dMoesin acts to increase cortex stiffness (Kunda et al., 2008). The result of dMoesin depletion in S2R+ cells grown in suspension is that many cells arrest in metaphase with misoriented spindles and large plasma membrane blebs that fail to reconnect to the cortex (Kunda et al., 2008; Carreno et al., 2008). Furthermore, depleting *Slik*, the dMoesin kinase, or expressing T579A moesin phenocopied these defects (Kunda et al., 2008; Carreno et al., 2008). Thus, dMoesin contributes stiffness to the cortex which is essential for mitosis under some conditions.

More recent work in this system has revealed that the proper positioning of dMoesin activity is also important for mitosis (Roubinet et al., 2011; Kunda et al., 2012). Specifically, dMoesin activity is needed near to the presumptive cleavage furrow after metaphase, whereas it must clear out from the poles during the onset of anaphase (Roubinet et al., 2011; Kunda et al., 2012). This is achieved by two different extrinsic signals: first, phosphorylation by *Slik*, the dMoesin kinase, located at the cleavage furrow and dephosphorylation by PP1 phosphatase, located at the poles. The second is production of the activating plasma membrane phospholipid

$PI(4,5)P_2$ (see below), which is achieved by localization of specific enzymes (PTEN and Skittles) at the cleavage furrow.

This work reveals a role for ERMs in manipulating cortical stiffness. To my knowledge, there is no other system in which ERM depletion has been shown to decrease cortical stiffness or interfere with mitosis. However, the converse is true, as overexpression of phosphomimetic ezrin was recently shown to increase cortical stiffness in lymphocytes (Liu et al., 2012). Despite the lack of *in vivo* correlates, the work offers interesting insights into the biophysical roles ERMs might play, and the extrinsic cues that might regulate them. These regulatory mechanisms are discussed in a more physiological context in Chapter III.

Tagging ERMs. Epitope- or GFP-tagging ERMs has been shown to interfere with their function. The clearest example of this is in *Drosophila*, where two groups found that larval lethality due to *dMoesin* knockout could be partially rescued either by N-terminally myc-tagged dMoesin or dMoesin-T579D (Speck et al., 2003; Hipfner et al., 2004). By contrast, two groups showed that expression of dMoesin-T579D without a tag or with a C-terminal tag failed to rescue (Karagiosis and Ready, 2004; Roubinet et al., 2011). Especially given that the rescue was only partial even with wild-type dMoesin bearing an N-terminal myc tag (Hipfner et al., 2004) whereas it was complete with untagged or C-terminally GFP-tagged dMoesin (Roubinet et al., 2011), these results suggest that the presence of an N-terminal epitope tag reduces the activity and presumably the molecular openness of dMoesin.

This result from *Drosophila* is dramatically supported in Jeg-3 placental epithelial cells, where N-terminally Xpress-tagged ezrin accumulates diffusely similar to T567A ezrin, whereas C-terminally Xpress-tagged ezrin accumulates along with endogenous ezrin in microvilli (J.

Thoms, unpublished). Ezrin bearing a mutation in the N-ERMAD partially blocking association with the C-ERMAD (termed the N-mutant; Chambers and Bretscher, 2005) hyper-localizes to the cortex and fails to accumulate in microvilli, but strikingly, coupling this mutation with an N-terminal Xpress tag causes it to localize exclusively in microvilli (D. Chamers, J. Thoms, and R. Viswanatha, unpublished). This supports the notion that N-terminal tags reduce ERM openness.

C-terminal GFP tagging maintains dMoesin's functionality (Roubinet et al., 2011; Polesello et al., 2002) and ezrin's competence to form microvilli in Jeg-3 cells (Figure 3.6), causes aberrant localization to the plasma membrane in the background of the T567A mutation, which is cytoplasmic with an internal tag (R. Viswanatha, unpublished). This indicates that the presence of a C-terminal GFP tag partially increases openness, consistent with the extreme C-terminus of ezrin's being involved in critical contacts in the dormant ERM (Pearson et al., 2000; Li et al., 2007).

Thus ERMs have been proposed to have three related roles: 1) producing cell-surface structures; 2) serving as a scaffold for EBP50 and other binding partners (Table 1), increasing cortical rigidity, and these roles can be affected by the presence of epitope or GFP tags.

ERM knockouts support a role in microvillus formation

Due to redundancy and pleiotropy, mammalian ERMs have been difficult to functionally characterize. By contrast, in the fly *Drosophila melanogaster* as in the worm *Caenorhabditis elegans*, there is only one homolog of these three proteins, called dMoesin or ERM-1, respectively. The results in the vertebrate and invertebrate systems have been complementary, so both will be discussed.

Mouse ERM knockouts. All three ERM proteins have been knocked out of the mouse individually. Supporting the notion of functional redundancy among ERMs, moesin knockout mice are viable without any overt defects (Doi et al., 1999). The phenotypes of radixin knockout and ezrin knockout, however, are more informative.

The predominant tissue expression pattern of each ERM in the mouse (Ingraffea et al., 2002) correlates with the phenotypes of the knockouts. Radixin is predominantly expressed in the hair cell stereocilia and in the liver where it localizes to the apical bile canaliculi. Consequently, radixin knockout mice are deaf (Kitajiri et al., 2004). Deafness occurs despite upregulation of ezrin, which localizes aberrantly to the stereocilia during development but cannot fully compensate (Kitajiri et al., 2004). In addition to deafness, the mice display hyperbilirubinemia, due to mislocalization of multidrug-resistance protein 2 (MRP2), the conjugated bilirubin transporter, away from the bile canalicular membrane (Kikuchi et al., 2002). Moreover, it has been demonstrated that the apical localization of MRP2 is dependent on its binding to EBP50 (Harris et al., 2001; Li et al., 2010), and EBP50 knockout mice also display hyperbilirubinemia (Li et al., 2010). Thus, radixin knockout results in a defect in stereocilia (mechanism as yet unclear) and the loss of specific transporters from the liver cell apical membrane through defects in positioning of EBP50 and MRP2.

Although ezrin is distributed widely across all tissues examined (Ingraffea et al., 2002), it is the sole ERM expressed in intestinal epithelia. McClatchey and colleagues therefore generated ezrin null mice in order to examine the intestinal epithelium. Ezrin-null mice were born, but die of malnourishment shortly after weaning due to intestinal malformation (Saotome et al., 2004): specifically, a developmental transition, villi segregation at embryonic day 15.5, fails. The intestinal microvilli indeed lack all three ERMs; surprisingly, microvilli are present in the ERM-

null intestinal cells, but they are aberrant in morphology: the terminal web region is enlarged and the microvilli are short and disorganized (Saotome et al., 2004). McClatchey and colleagues have interpreted this as a defect in the terminal web, however, this type of defect might be envisioned if plasma membrane-cytoskeleton crosslinking were partially perturbed, the plasma membrane failing to wrap tautly around the microvillus core and splaying out like an opened umbrella. Importantly, the results argue for the existence of other plasma membrane-cytoskeleton cross-linkers exist in addition to ERMs in these cells. When a conditional ezrin allele was knocked out in the adult, multiple phenotypes were revealed. These included disorganization of microvilli and failure of villus fusion (as is seen in the embryonic null); blebs and breaks in the apical membrane where it appears to peel away from the F-actin cortex; mislocalization of apical junction components; a partial defect in mitotic spindle positioning leading to polarity defects; and the upregulation of activated RhoA (Casaletto et al., 2011). The basis for the additional defects is unclear. Thus, ezrin is required for multiple aspects of intestinal epithelial polarity, but importantly, one of those is structuring and shaping apical microvilli.

It will be interesting to cross the moesin or radixin knockout mice with the ezrin knockout mouse heterozygote to uncover further roles of ERMs during early development in the progeny, as has been predicted by dominant ezrin mutant expression during early embryogenesis (Dard et al., 2001).

Invertebrate ERM knockouts. In the *Drosophila* oocyte, three independent P-element insertions within the dMoesin gene have been shown to cause a defect in tethering the membrane to the F-actin cytoskeleton and a lack of retention of *Oskar* mRNA onto cortical F-actin, leading to larval lethality (Speck et al., 2003; Polesello et al., 2002; Jankovics et al., 2002). In the wing imaginal disc, the microvilli in the apical domain were replaced with large blebs, and the amount of F-

actin in the apical domain was increased (Speck et al., 2003). Whether the allele used in this study was a true null has been questioned (Karagiosis and Ready, 2004), but most of these defects were subsequently upheld by examining other alleles (Roubinet et al., 2011). In the photoreceptor cells, two *dMoesin* alleles or *dMoesin* RNAi disorganized the microvilli and caused loss of the photoreceptors, which normally reside in the microvilli (Karagiosis and Ready, 2004). Taken together, these results suggest that dMoesin functions in the maintenance of cross-linking between the F-actin cortex and the apical plasma membrane in multiple cell-types leading to the functional organization of microvilli.

A stunning finding from one dMoesin allele was that the mutant was partially rescued by suppressing the small GTPase *Rho1*, which is the homolog of mammalian RhoA/B/C (Speck et al., 2003). Furthermore, suppression of dMoesin rescued defects associated with a second mutant, *Dishevelled*, which causes a decrease in Rho1 activity on its own (Speck et al., 2003). These results have been doubted because the allele used in these experiments was conclusively shown not to be a null in some adult tissues (Karagiosis and Ready, 2004). However, the result has gained traction recently because knocking out ezrin in the adult mouse also elevates RhoA activity (Casaletto et al., 2011). Thus RhoA and ERM function appear to be antagonistic, but the molecular details remain elusive.

The worm *Caenorhabditis elegans* also possesses only one ERM family member called ERM-1, an essential gene. RNAi depletion of ERM-1 led to stage L1 lethality but also caused more informative phenotypes: cysts and obstructions along the intestine, as well as defects in properly positioning the apical domain as moves from a more lateral position during intestinal development (Van Furden et al., 2004; Gobel et al., 2004). Electron microscopy showed that microvilli were lost in the disorganized lumena and revealed regions where the plasma

membrane was peeling away from the cortex, consistent with the mouse and fly data (Gobel et al., 2004). Interestingly, ERM-1 depletion enhanced the loss of continuous apical junction staining incurred by loss of E-cadherin or α-catenin (Van Furden et al., 2004). This implied that ERM-1 collaborates to position apical junction components appropriately. The data suggest that ERM-1 has roles in apical membrane integrity and lumenogenesis, as well as a possible second role in apical junction positioning. To bring the latter role into the fold, Fehon and colleagues have suggested an alternative explanation: that ERM-1 may be facilitating formation of cell-cell boundaries under chaotic conditions, when cells are sliding past each other or dividing during lumen formation (Fehon et al., 2010).

Thus genetic ERM removal has suggested that ERMs have multiple roles *in situ*: microvillus morphology; scaffolding of protein interaction partners; villus fusion; cell-cell junction morphology; apical lumenogenesis; Rho GTPase regulation; and mitotic spindle polarization. The mechanism is unclear in most cases, and will depend on careful analysis of cell culture models as well as the identification of mutants in new genes that phenocopy some but not all of these defects.

Extrinsic regulation of ERM activation by PI(4,5)P_2, ERMBPs, kinases, and phosphatases

To date, two models for how ERMs bind membranes have been proposed. In the first, plasma membrane phospholipid PI(4,5)P_2 recruits ezrin to the plasma membrane. In the second, transmembrane ERM-binding partners (ERMBPs), interacting through the FERM domain, recruit and stabilize activated ezrin on the plasma membrane. Neither has been conclusively shown to be necessary and sufficient, so an interplay between them is the most likely scenario. As mentioned earlier, a second requirement for ERM activation is phosphorylation of a C-

terminal threonine (T567 in ezrin). The regulation of this phosphorylation has also received considerable attention and will be discussed in the third section. In the final section, I will try to integrate these regulatory modes with ERM function *in vivo*.

PI(4,5)P$_2$. The emerging model for ERM activation is that it involves synergy or coincidence detection between PI(4,5)P_2 on the plasma membrane and protein kinases that phosphorylate the C-terminal threonine. Functional evidence for an involvement with PI(4,5)P_2 was the discovery that PAO, which reduces the synthesis rate of its precursor, PI(4)P, also reduced moesin phosphorylation (Nakamura et al., 1995). In fibrobasts, PI(4)P-5 kinase Iα (PIPKIα, which generates PI(4,5)P_2, was strictly required for moesin phosphorylation, and microinjection of high doses of a PI(4,5)P_2 inhibitor, neomycin, reduced membrane-bound moesin (Matsui et al., 1999). The relevant protein kinase in fibroblasts has not yet been discovered, but this set up the possibility that binding PI(4,5)P_2 is required for subsequent C-terminal threonine phosphorylation by the kinase. Two groups showed that the FERM domain can specifically bind PI(4,5)P_2-containing liposomes, and that the accessibility of the FERM domain to bind the cytoplasmic region of CD44 is dependent on the presence of PI(4,5)P_2 (Hirao et al., 1996; Niggli et al., 1995). Finally, a recent study has confirmed that PI(4,5)P_2-liposome-bound ERMs undergo conformation opening *in vitro* (Maniti et al., 2012). These results suggest that PI(4,5)P_2 recruits ERMs to membranes via the FERM domain, allowing for subsequent phosphorylation (Figure 1.3.A).

Where on ezrin does PI(4,5)P_2 interact? Subsequently, Niggli and colleagues mutated four surface lysine residues to asparagine, severely impairing the interaction with PI(4,5)P_2 *in vitro* (Barret et al., 2000). These mutations (K253N, K254N, K262N, K263N in moesin; now referred to as K4N or PATCH mutations; Figure 1.3.B; Ben-Aissa et al., 2012) prevent the

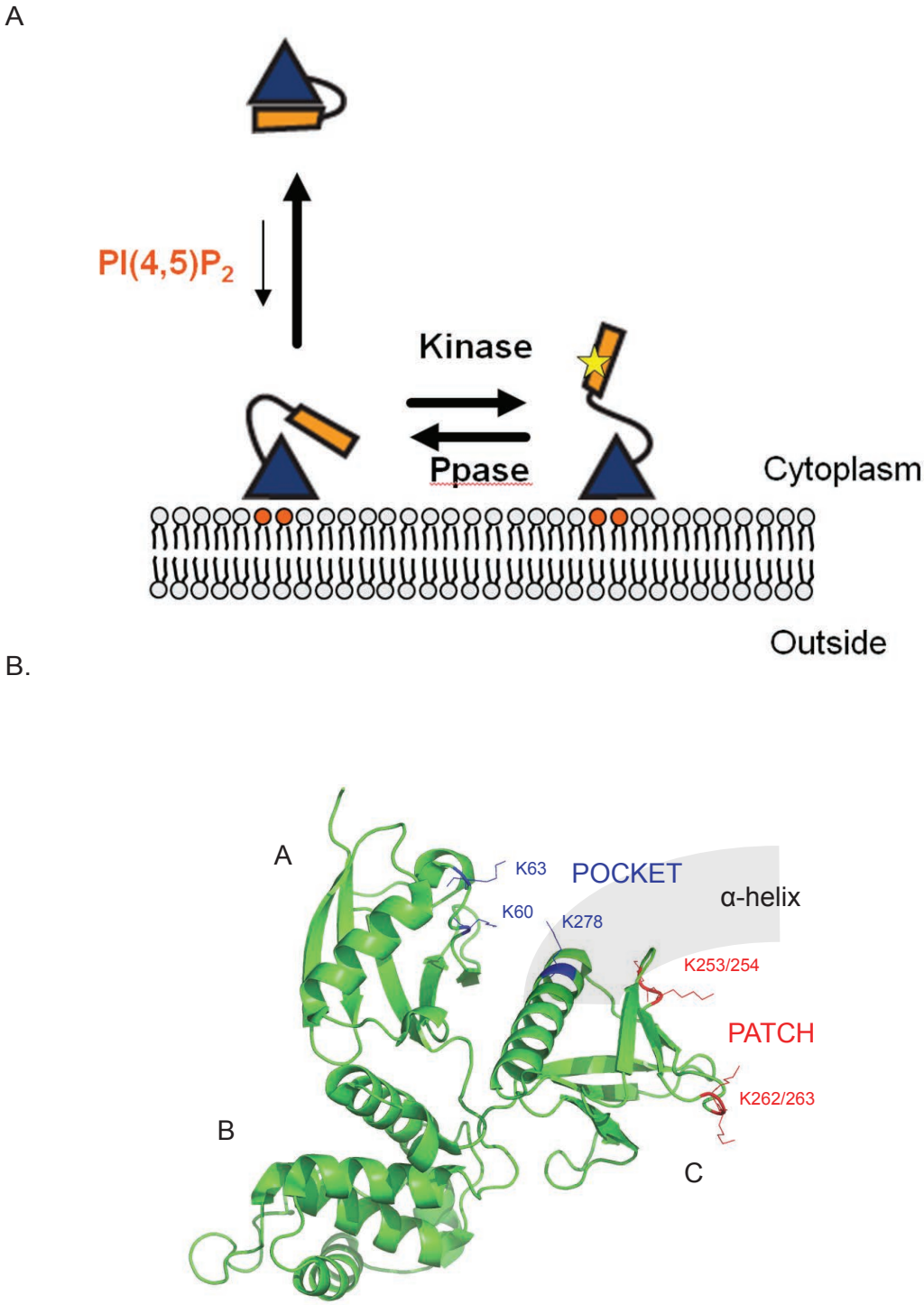

Figure 1.3 PI(4,5)P_2's role in ezrin activation. (A) The current model for ERM activation. PI(4,5)P_2 recruits dormant ERM to the plasma membrane, and this interaction stabilizes a conformation in which the kinases and phosphatases can reversibly phosphorylate the C-terminal threonine. (B) The FERM domain (1NI2) of ezrin with POCKET and PATCH residues illuminated. Based on Ben-Aissa et al., 2012.

translocation of full-length ERM to the membrane, but if PATCH-mutated ERM is additionally mutated to mimic C-terminal phosphorylation or truncated to just the FERM domain, membrane translocation is restored (Barret et al., 2000; Hao et al., 2009). A similar yin-yang effect between C-terminal phosphorylation and PI(4,5)P_2-engagement has been observed with *Drosophila* dMoesin (Roch et al., 2010). These results indicate that PI(4,5)P_2 engagement through PATCH residues regulates ERM autoinhibition. A detailed molecular mechanism has recently been proposed. The FERM PATCH can be seen overlapping with a portion of the C-ERMAD called the FLAP in the crystal structure of full-length, closed ERM (Li et al., 2007). It was recently demonstrated that competition between the FLAP and PI(4,5)P_2 binding at the PATCH can regulate the accessibility and membrane occupancy of moesin (Ben-Aissa et al., 2012), but the applicability of these observations *in vivo* and to radixin and ezrin remain to be determinined.

PI(4,5)P_2 binding has been shown to additionally require positive charges on K63 and K64 (now called the POCKET; Figure 1.3.B; Barret et al., 2000; Ben-Aissa et al., 2012). This site was shown to interact with PI(4,5)P_2's head group, IP_3 in crystals (Hamada et al., 2000). Furthermore, recent work suggests that the same molecule of PI(4,5)P_2 cannot simultaneously bind both the PATCH and the POCKET (Ben-Aissa et al., 2012). The authors favor a model in which one molecule of PI(4,5)P_2 translocates along the surface of the FERM domain from the PATCH to the POCKET as the FERM domain becomes progressively more accessible. However, the authors overlooked an important test: mutation of both the PATCH and the POCKET simultaneously. As early work shows that there is synergy between these mutations (Barret et al., 2000), ERMs may bind two molecules of PI(4,5)P_2 simultaneously. *In vivo* studies have not yet examined the effects of mutating these sites on the plasma-membrane localization of the isolated FERM domain, leaving room for debate as to whether PI(4,5)P_2-engagement is

sufficient for the plasma-membrane localization of the FERM domain, and leave open the possibility of partner interactions regulating ERM occupancy at the membrane.

Functional studies have confirmed that $PI(4,5)P_2$ is required for ERM activation, but have been similarly ambivalent as to whether an exposed FERM domain can still be enriched on the plasma membrane independently of $PI(4,5)P_2$. Using rapamycin-induced plasma membrane-translocation of a cytoplasmic $PI(4,5)P_2$ phosphatase, Shaw and colleagues showed that both ezrin and moesin are efficiently removed from the lymphocyte plasma membrane concomitant with the loss of a $PI(4,5)P_2$ reporter (Hao et al., 2009). This agrees with long-term $PI(4,5)P_2$ depletion studies in other systems (Matsui et al., 1999; Gervais et al., 2008). However, the loss of phosphomimetic moesin from the membrane following $PI(4,5)P_2$ depletion was incomplete (Hao et al., 2009). Thus, although $PI(4,5)P_2$ has a clear role in ERM activation and tethering, it has not yet been conclusively demonstrated whether there is still room for other determinants. Also, the localization of these determinants to the plasma membrane may also require the presence of $PI(4,5)P_2$.

Regulation by ERM Binding Proteins (ERMBPs). A hypothesis that has received relatively less attention is that many transmembrane proteins might coordinately regulate ezrin's attachment to the plasma membrane by recruiting ezrin via the basic patches in their cytoplasmic tails. According to this hypothesis, ezrin may have evolved to bind a large number of transmembrane proteins, which may explain the large number of diverse ligands proposed for ERMs (Table 1). Moreover, removal of no single ERMBP would cause microvilli collapse, consistent with the existing data (for instance, CD44 knockdown does not alter microvilli appearance; Legg et al., 2002). Tsukita and colleagues reasoned that the overexpression of ERMBPs, however, might increase the clustering of activated ezrin, leading to the formation of microvilli-like structures in

fibroblasts (Yonemura et al., 1999). They found this to be the case with the intracellular portions of ICAM-2, CD44, and CD43 artificially fused to E-cadherin's extracellular and transmembrane domains for normalization and detection purposes. Furthermore, microvilli-like structures failed to coalesce when mutations to block ezrin binding were introduced into the cytoplasmic tails. This effect was not observed in epithelial cells, where, perhaps, ERMBP availability is not rate-limiting for microvilli formation (Yonemura et al., 1999). Thus, ERMBPs may anchor ezrin to the plasma membrane in addition to $PI(4,5)P_2$.

In reality, a combination of both strategies may be operational. This is supported by the fact that *in vitro*, phosphomimetic ezrin is not fully open, but only partially open (Chambers and Bretscher, 2005), suggesting that the binding of accessory factors *in vivo* may be needed to sustain active, membrane-linked molecules.

ERM regulation by kinases and phophatases. A primary role for kinases and phosphatases in regulating ERM accessibility was recognized early on. Early *in vitro* experiments suggested that Protein kinase C Θ was capable of phosphorylating moesin at T558, but no functional data connected these two *in vivo* (Simons et al., 1998; Pietromonaco et al., 1998). Initial *in vivo* work from Tsukita and colleagues suggested that Rho-activated kinase (ROCK) was the relevant kinase in tissue culture fibroblasts (Oshiro et al., 1998; Matsui et al., 1998), but this has been questioned (Matsui et al., 1999; Yokoyama et al., 2005). Subsequently, myotonic dystrophy related Cdc42-interacting kinase (MRCK), a known effector of Cdc42 and regulator of microvilli (Leung et al., 1998), was suggested to phosphorylate ERMs only in filopodia stimulated by activated Cdc42, but not in microvilli-like structures stimulated by activated RhoA (Nakamura et al., 2000). However, this result has not been consistent with subsequently identified phenotypes associated with MRCK depletion. Protein kinase C α was shown to regulate ERM

phosphorylation during fibroblast migration, but the relevance to microvilli has not been investigated (Ng et al., 2001). Finally, Salas and colleagues showed that PKCι, one of the isoforms of atypical protein kinase C known to be involved in determining the polarity of the apical domain of epithelial cells, could phosphorylate ezrin at T567 in Caco-2 cells and be required for microvilli (Wald et al., 2008), but an unbiased *in vitro* screen for ERM-phosphorylating kinases by a different group failed to detect any activity for the activated PKCι kinase domain towards ezrin at T567 *in vitro* in direct contradiction to the Salas group (ten Klooster et al., 2009). Thus, the identity of the ERM kinase operational in mammalian tissue culture cells has remained elusive.

A key contribution of the identification of the ERM ortholog in *Drosophila* was the ability to identify genetically interacting kinases based on whole-organism phenotypes. A gain-of-function screen for genes whose overexpression leads to an increase in tissue size identified Sterile-20 kinase-like (*Slik*; Hipfner and Cohen, 2003). The authors then generated mutations in the Slik gene. *Slik* mutants gave two distinct defects: 1) reduced proliferation, consistent with the *Slik* overexpression phenotype, which could be suppressed by the overexpression of Raf (Hipfner and Cohen, 2003), and 2) a loss of apical integrity in the wing imaginal disc epithelial and photoreceptor cells (Hipfner et al., 2004). Based on the appearance of the photoreceptors in dMoesin knockouts (Karagiosis and Ready, 2004), the authors reasoned that one defect could be in the phosphorylation of dMoesin, and they subsequently showed that dMoesin phosphorylation was compromised in *Slik* knockout larvae and in S2 tissue cultured cells knocked down for *Slik* (Hipfner et al., 2004). Finally, they showed that activated dMoesin (overexpressed dMoesin bearing an N-terminal myc tag and T579D mutation) can partially rescue *Slik* mutants, consistent with some of the Slik mutant phenotype's being due to reduced dMoesin phosphorylation

(Hipfner et al., 2004). That Slik is genetically upstream of dMoesin has been upheld by a number of subsequent studies (Kunda et al., 2008; Hughes et al., 2010; Yang et al., 2012). Furthermore, while one group has claimed that dRok, ortholog of mammalian ROCK, can also control dMoesin phosphorylation during larval development using immunostaining techniques (Verdier et al., 2006), their result was directly contradicted by another group using quantitative Western blotting (Neubueser and Hipfner, 2010). This leaves the general sense in the field that *Slik* is the predominant upstream kinase for dMoesin in all cell-types in *Drosophila*.

A side-point is that the proliferative defect in *Slik* mutants may be due to a defect in phosphorylation of dMerlin, the ortholog of mammalian merlin, as marked *Slik* mutant imaginal disc clones have a defect in dMerlin phosphorylation, and Slik can directly phosphorylate dMerlin *in vitro* (Hughes and Fehon, 2006). This is not terribly surprising as merlin and ezrin are similar in primary sequence, and since the phosphorylation site is roughly conserved between them (reviewed in McClatchey and Fehon, 2009). Only one publication has examined the role of mammalian merlin phosphorylation at this site (T576 in mouse and human merlin), and, unbelievably, they concluded that phosphorylation at T576 does not contribute to regulation, whereas phosphorylation at an adjacent site, S518, mediated by p21-activated kinase, does (Surace et al., 2004). The interplay between phosphorylation at the two sites has not yet been examined, so whether this regulatory mode contributes anything in mammalian cells remains to be addressed. Thus Slik appears to be upstream of both ERMs and merlin in *Drosophila*.

Recent studies of ERM regulation in mammalian cells have offered fresh insights. There are two orthologs of Slik in mammalian cells: lymphocyte-oriented kinase (LOK) and Ste20-like kinase (SLK). Knockout of LOK in mice yields no overt phenotype, but a careful examination of several tissues shows a slight decrease in phosphorylation of all three ERMs systemically

(Belkina et al., 2009). The mice also show a deficiency in lymphocyte activation in response to SDF-1, similar to moesin knockdown (Belkina et al., 2009). SLK has not yet been connected with ERM regulation. These results suggest that LOK is necessary for a portion of ERM phosphorylation, in agreement with *Drosophila* studies, but suggests that other kinase(s) are also involved.

Surprisingly, an entirely different model has been put forth by Clevers and colleagues (ten Klooster et al., 2009; Baas et al., 2004; Gloerich et al., 2012). Using the W4 enterocyte-derived cell line in which the membrane localization and activation of polarity-inducing Lkb1, the mammalian homolog of *C elegans* PAR-4, can be synchronously triggered by doxycycline treatment, they showed that polarization of an apical domain containing microvilli can occur in suspension-growing, isolated cells (Baas et al., 2004). Furthermore, an examination of cells made to lack Lbk1 by RNAi (Baas et al., 2004) or cells with greatly reduced Lkb1 (Xu et al., 2010) suggests that Lkb1 expression is part of the normal apical polarity pathway. Clevers and colleagues later identified proteins interacting with the membrane-bound Lkb1 complex and identified the serine/threonine kinase MST4 (ten Klooster et al., 2009). According to this group, MST4 expression was necessary for ezrin phosphorylation and brush border formation following Lkb1 translocation in Ls174T-W4 cell-lines, and that it was capable of phosphorylating ezrin *in vitro* with a catalytic rate similar to those of several kinases previously identified as ERM kinases in various other systems (ten Klooster et al., 2009). Its reduction in Caco-2 cells also caused a decrease in the formation of microvilli, suggesting a general role (ten Klooster et al., 2009). MST4 has a clearly discernible ortholog in *Drosophila*, called germinal center kinase III (GCKIII). The homology is evident not only on the basis of protein identity within the catalytic domain, but in the regulatory domain outside the catalytic domain, clearly establishing their

evolutionary origin (R. Viswanatha, data not shown). Thus, the existing data support the intriguing notion that while the predominant kinase for ERMs in *Drosophila* is Slik (LOK/SLK), in mammalian cells it is MST4 (GCKIII), suggesting a major evolutionary switch in pathway wiring with only minor changes in the key players. Two alternative solutions are 1) both kinases are capable of phosphorylating ezrin *in vitro*, whereas only one of them directly phosphorylates ezrin in both *in vivo* systems; and 2) both kinases lie in the same pathway; i.e., the activation of one leads ultimately to the activation of the other. This remains to be tested. Thus, MST4 is claimed to be important for ezrin phosphorylation *in vivo*.

Nonetheless, the currently held notion is that a strikingly wide array of kinases phosphorylates ezrin at T567 *in vitro* and *in vivo* (Figure 1.4). These kinases fall into two broad evolutionary categories, the PKC A/γ/C (AGC) branch and the germinal center kinase (GCK) branch (Figure 1.4). The diversity is also apparent by their enormously different regulatory domains, which directly interact with various signaling inputs such as calcium (in the case of PKC isoforms) and activated Cdc42 (in the case of PKCι, ROCK, or MRCK; Figure 1.4). Thus numerous already-established molecular pathways may have evolved connectivity to ezrin through these kinases as a means by which to couple various signals to cytoskeleton regulation.

In contrast to kinases, phosphatases have received less attention. Protein phosphatase 1's (PP1s), very large multisubunit complexes, have been most often invoked as the ERM phosphatase. Calyculin A and okadaic acid treatment has long been known to inhibit ERM dephosphorylation, but these drugs target PP1, PP2, and PP6 catalytic subunits, so it is unclear from these experiments which phosphatase is actually required. In support of a general role for PP1s, Sds22, a common structural subunit of PP1 complexes including those based on catalytic subunits PP1-87B (α/β) and Flapwing (δ/γ), was shown to be necessary for dMoesin

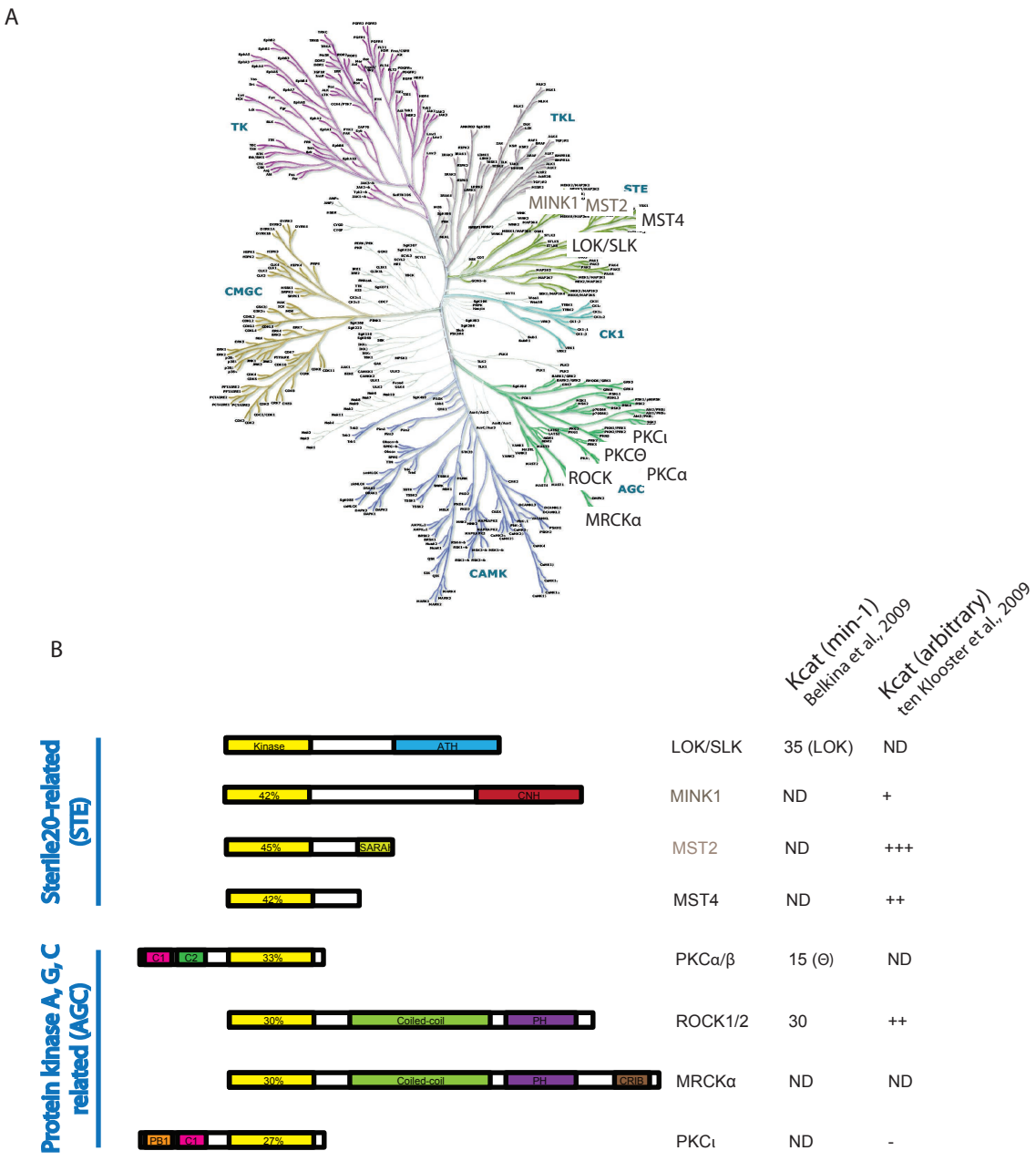

Figure 1.4 The ERM-kinome. (A) The human kinome with illuminated proteins known to phosphorylate ezrin *in vivo* or *in vitro*. (B) Cartoon diagram of kinases in A, homology to LOK and SLK kinase domain, and catalytic rate of indicated isolated kinase domain for ezrin C-terminal domain *in vitro*. *CNH*, Citron homology, a small GTPase effector binding domain; *SARAH*, Salvador/Rassf/Hippo homology, a protein-protein interaction domain and dimerization domain; *C1*, *C2*, cysteine-rich domains mediating divalent ion-dependent protein-lipid interactions; *PH*, Phox homology, lipid-binding domains; *CRIB*, Cdc42/Rac1-interaction domain; *PB1*, Phox and Bem1p homology, a heterodimerization domain.

dephosphorylation in *Drosophila* imaginal discs (Kunda et al., 2012; Grusche et al., 2009), and its human homolog, PPP1R7, was shown to be necessary for ERM dephosphorylation in human A431 cells (Grusche et al., 2009). DFlapwing was uncoupled from dMoesin in *Drosophila* S2 cells but necessary for dMoesin dephosphorylation *in vivo* (Roubinet et al., 2011; Yang et al., 2012), whereas PP1-87B has been shown to be necessary for dMoesin dephosphorylation in S2 cells (Roubinet et al., 2011). PP1s are targeted via another set of accessory subunits. While the situation may be complicated *in vivo* (Lee and Treisman, 2004), in cultured mammalian cells, MYPT1/MBS (myosin-binding subunit) is thought to target PP1's catalytic subunit to moesin (Fukata et al., 1998). This was difficult to test because the regulation of MYPT1's localization was unclear in early reports. However, the finding that PP1Cδ, a mammalian homolog of DFlapwing, could translocate to the cytoplasm from the nucleus upon co-overexpression with MYPT1 (Eto et al., 2005) may prove a useful tool. Thus PP1 appears to mediate ERM dephosphorylation in most cases, and the details remain to be elucidated.

Regulating the regulators. The ERM regulators mentioned here ($PI(4,5)P_2$, transmembrane ERMBPs, and kinases and phosphatases) must be integrated to regulate ERM-dependent processes. In selected cases, this regulation has been fleshed out.

$PI(4,5)P_2$ is one of the critical determinants of the apical domain, as reversing its mild gradient towards the apical domain leads to a general loss of apical polarity (Martin-Belmonte et al., 2007). Overexpressing type I phosphatidylinositol-4-phosphate 5 kinase α (PIP5KIα) causes a dramatic increase in $PI(4,5)P_2$ at the expense of PI(4)P (Yamamoto et al., 2001). This has multiple effects on actin-binding proteins, including increasing actin-bound ezrin (Matsui et al., 1999; Yamamoto et al., 2001). In turn, this was shown to increase phosphorylated ezrin and microvillus formation in NIH 3T3 fibroblasts (Matsui et al., 1999). Furthermore, when PIP5KIα

was very highly overexpressed in A431 cells, it accumulated in vesicles also containing phosphorylated ezrin (Yonemura et al., 2002). As an aside, Yonemura et al. go further and conclude that ERM activation can be accomplished by high enough $PI(4,5)P_2$ levels, bypassing the need for phosphorylation (Yonemura et al., 2002). They suggest this because A431 cells can be made to ruffle in response to EGF even following pre-treatment with staurosporine to completely dephosphorylate their ERMs (Yonemura et al., 2002). This argument is incorrect because it presupposes that the ezrin is necessary for ruffling in response to EGF, which was proposed because it unquestionably localizes to the ruffles (Bretscher, 1989) but never verified by ezrin gene disruption. By contrast, my findings are that ezrin depletion by RNAi has no statistically significant effect on EGF-induced ruffling in A431 or Jeg-3 cells (R. Viswanatha, unpublished). Thus $PI(4,5)P_2$ levels could be limiting for ERM engagement relative to potential tethering factors and kinase activity under some circumstances, so regulating its levels could regulate ERM phosphorylation.

How might PIP5KIα be regulated? Two pathways have been proposed: a Rho-ROCK pathway and Rho-dependent, ROCK-independent pathway (Yamamoto et al., 2001). Since ROCK inhibition is uncoupled from ERM phosphorylation in some systems (Matsui et al., 1999), the most likely scenario is that PIP5KIα is activated directly by Rho GTPases. Thus, Rho GTPase activation should act synergistically with ERM phosphorylation, which it does in some cases (Matsui et al., 1999; Yonemura et al., 2002; Hayashi et al., 1999; Antoine-Bertrand et al., 2011; Batchelor et al., 2007; Pujuguet et al., 2003). However, in ERM-deficient mouse intestinal cells (Casaletto et al., 2011a) and *Drosphila* wing epithelial cells (Speck et al., 2003), RhoA and ezrin act antagonistically. The reason for this difference is unclear.

Relatively less is known about the regulation of ERM kinases. Although much is known about ROCK regulation, its identity as an ERM kinase is suspect (Matsui et al., 1999), and nothing is known about its regulation of ERM phosphorylation. In *Drosophila*, Slik is the ERM kinase, which also controls proliferation presumably through dMerlin (Hipfner and Cohen, 2003; Hughes and Fehon, 2006). Slik's proliferative role may be regulated by Raf (Hipfner and Cohen, 2003), but nothing is known about how its role in ERM phosphorylation is regulated. ten Klooster et al. (2009) have shown that the ERM kinase in polarized single-cells is MST4 (ten Klooster et al., 2009). MST4 activation requires an apically-localized Lkb1 complex, but additionally requires a complex signaling pathway originating from activated small GTPase Rap2A (Gloerich et al., 2012). Curiously, MST4 is concentrated not in the microvilli, the site of activated ezrin, but in the terminal web region below the brush border, suggesting an action-at-a-distance or molecular hand-off mechanism (ten Klooster et al., 2009). Also, its distribution at the plasma membrane is presumably regulated by polarized membrane trafficking due to its partial co-localization in vesicles with Rab11 (ten Klooster et al., 2009). Thus there is an as yet murky view of ERM kinase regulation.

Finally, several lines of evidence have pointed out an interesting requirement of any ERM regulatory mechanism: it has to be fast! First, microvilli have been shown to come and go with a half-life of approximately 5 minutes (Garbett and Bretscher, 2012; Gorelik et al., 2003). Ezrin's steady-state enrichment in microvilli suggests that it is constantly trained on a moving target. Consistently, measurement of ezrin turnover rates from the plasma membrane using fluorescence bleaching techniques of ezrin-GFP have suggested that it turns over with a half-life of 40 seconds – 2 minutes (Garbett and Bretscher, 2012; Coscoy et al., 2002), slightly faster than that of microvilli, themselves, allowing dynamic ezrin redirection to growing microvilli as

needed. Two groups have examined the redirection of ERMs during more dramatic morphological transitions. Sanchez-Mateos and colleagues examined moesin recruitment to the dorsal region of adhering melanoma cells as they were plated from suspension and found that it cleared from the ventral side within 5 minutes of re-plating, suggesting dynamic cellular control of the ERM regulatory network (Estecha et al., 2009). Similarly, Simons and colleagues showed that podocalyxin, a transmembrane protein that interacts with EBP50, cleared from the ventral surface of freshly plated MDCK cells within 1 hour of plating and accumulated in dorsal domain (Meder et al., 2005). This clearing was faster than non-EBP50-binding apical transmembrane proteins which take greater than 4 hours and is thought to depend upon polarized membrane trafficking, and it also required that podocalyxin contain a motif that allows interaction with EBP50 (Meder et al., 2005). Because EBP50 requires ezrin to localize at the plasma membrane (R. Viswanatha, unpublished; Garbett et al., 2010), this suggests that ezrin can identify and target the dorsal surface specifically before it is defined by polarized membrane trafficking, a hypothesis that has been upheld by a very recent study (Galvagni et al., 2012). These observations suggest that ERM regulation by $PI(4,5)P_2$, transmembrane ERMBPs, and/or kinases/phosphatases is a system tuned to functioning in chaotic and rapidly changing situations.

This thesis will address two of the issues brought forth in this discussion. If there are ERM membrane tethers, they would be expected to interact directly with ERMs. In the first chapter, I conduct an unbiased proteomic screen of ezrin-bound material in a microvillus-decorated cell-line to determine the identity, location, and function of ERMBPs. In the second chapter, I address the ERM regulatory network, asking how the influence of kinases affects ERM polarity.

Most of this work was performed in Jeg-3 choriocarcinoma cells. In the first appendix, I attempt to recapitulate the findings in a kidney epithelial cell-line, LLC-PK1.CL4.

As mentioned above, interaction between ezrin and scaffolding protein EBP50 is required for microvilli in Jeg-3 cells. EBP50 can simultaneously bind to a number of ligands through two PDZ protein-protein interaction domains. In the second and third appendices, I conducted an unbiased proteomic profiling of EBP50-bound proteins to ask which of these ligand(s) of EBP50 is required for this function.

Table 1 Ezrin interactions and selected publication list

Interaction partner	Selected References	Proposed binding mode	Proposed function	Expressed in Jeg-3/Identified here?
Aquaporin-0	1	Unknown	Unknown	ND/No
CD146	2	Unknown	ERM regulation of melanoma cell migration through control of ERM-RhoGDI interaction	ND/No
CD43	3-7	Positive cluster in cytoplasmic tail interacts with acidic groove in FERM domain lobe F3	ERM regulation of lymphocyte migration via PKCϴ-mediated phosphorylation of CD43 tail; tethering of ERMs to plasma membrane for micovillus formation	No/No
CD44	3, 5, 8-14	Positive cluster in cytoplasmic tail interacts with acidic groove in FERM domain lobe F3	ERM regulation of migration speed and directionality; lymphocyte polarization; tethering of ERMs to plasma membrane for micovillus formation	No/No
Clic-3/-4/-5	15, 16	Unknown	Microvillus formation in RPE cells	Yes/Yes (Clic-3 and Clic-4)
Dbl	17-22	Ezrin FERM interacts with a basic cluster within the PH domain of Dbl	ERM modulation of Cdc42 signaling, general function unknown	ND/No
DCC	23, 24	Positive cluster in cytoplasmic tail interacts with acidic groove in FERM domain lobe F3	Ezrin regulation of Netrin-induced axon guidance	ND/No
Dlg	25, 26	FERM domain of ezrin interacts with Dlg1	Ezrin regulation of immune synapse formation	Yes/No
EBP50/E3KARP	27-32	Occupies a region of the FERM domain which overlaps with C-ERMAD interaction site	ERM regulation of microvilli formation and receptor clustering	Yes/Yes
E-cadherin	33	T567D only binds E-cadherin	Activated ezrin-dependent interference with E-cadherin trafficking	Yes/No
Eps8 /-L1a	34	Coiled-coil domain of ezrin harboring an NPxY motif interacts with the SH3 domain of Eps8 when ezrin is phosphorylated on Y477	ERM regulation of microvillus length and spacing	Yes/No
Fes	35	Coiled-coil domain of ezrin harboring an NPxY motif interacts with the SH2 domain of Fes when ezrin is phosphorylated on Y477	ERM control of cell spreading and migration in response to HGF	ND/No
ICAM-1/-2/-3	36-41	Positive cluster in cytoplasmic tail interacts with acidic groove in FERM domain lobe F3	Polarization of ICAMs to the urpod in migrating lymphocytes; tethering of ERMs to plasma membrane for micovillus formation	ND/No

L1CAM	42, 43	FERM domain binds L1CAM	ERM regulation of neurite outgrowth	ND/No
Myo18aα	44	Unknown	Unknown, detected in activated B cells	ND/No
NHE-1	45, 46	Positive cluster in cytoplasmic tail interacts with acidic groove in FERM domain lobe F3	ERM regulation of migration speed and directionality	ND/No
NHE-3	47	Positive cluster in cytoplasmic tail interacts with acidic groove in FERM domain lobe F3	ERM regulation of NHE-3 surface distribution in OK cells	Yes/No
PACE-1	48	C-terminal region of ezrin	Unknown	Yes/Yes
Palladin	49, 50	Residues 278-585 of ezrin interact with Ig2 or Ig3 of palladin.	Unknown	Single enriched peptide detected
PDZD8	51	Unknown	Moesin control of glutamylated microtubule abundance and HSV-1 viral entry	ND/No
PLEKHG6	52	FERM domain of ezrin interacts with a C-terminal region of unknown function in PLEKHG6	ERM regulation of macropinocytotic ruffling	Yes/No
Podocalyxin	53	Unknown	Unknown	ND/No
PSGL-1	39, 54-57	Positive cluster in cytoplasmic tail interacts with acidic groove in FERM domain lobe F3	ERM regulation of lymphocyte rolling on P-selectin	ND/No
Ras	58	FERM domain of ezrin interacts with activated Ras	Promotes Ras activity	ND/No
RhoGDI	17, 59, 60	FERM, details unknown	ERM modulation of the RhoA signaling, general function unknown	ND/No
S100P	61, 62	FERM domain lobe F2 of ezrin, in a region that partially overlaps with PI(4,5)P2 binding site interacts with S100P	Ezrin regulation of cell migration	ND/No
SAP97	63	Unknown	Unknown	ND/No
SOS	58	FERM domain of ezrin interacts with the DH/PH domain of SOS	Promotes SOS activity, and thus active Ras	ND/No
Syndecan-2	64, 65	Positive cluster in cytoplasmic tail interacts with acidic groove in FERM domain lobe F3	Unknown	Yes/Yes
Vps11/HOPS	66	Coiled-coil domain of ezrin interacts with Vps11	ERM regulation of endocytosis	ND/No
WWOX	67	Coiled-coil domain of ezrin harboring an NPxY motif interacts with WWOX when ezrin is phosphorylated on Y477	Control of ERM-mediated secretion in gastric parietal cells	ND/No
WWP-1	68	Coiled-coil domain of ezrin harboring an NPxY motif	ERM control of HGF-induced migration, requiring	ND/No

		interacts with WWP-1 when ezrin is phosphorylated on Y477	ubiquitylation by WWP-1	
ZAP-70	69	Unknown	Ezrin regulation of immune synapse formation	ND/No
β4 integrin	70	FERM domain of ezrin interacts with β4 integrin	Regulation of β4 integrin level	ND/No
β-Dystroglycan	20, 71	Positive cluster in cytoplasmic tail interacts with acidic groove in FERM domain lobe F3	ERM regulation of filopodia formation in C2C12 cells co-transfected with active Cdc42	Yes/Yes

1. Wang, Z. & Schey, K. L. Aquaporin-0 interacts with the FERM domain of ezrin/radixin/moesin proteins in the ocular lens *Invest. Ophthalmol. Vis. Sci.* 52, 5079-5087 (2011).

2. Luo, Y. *et al*. Recognition of CD146 as an ERM-binding protein offers novel mechanisms for melanoma cell migration *Oncogene* 31, 306-321 (2012).

3. Yonemura, S. *et al*. Ezrin/radixin/moesin (ERM) proteins bind to a positively charged amino acid cluster in the juxta-membrane cytoplasmic domain of CD44, CD43, and ICAM-2 *J. Cell Biol.* 140, 885-895 (1998).

4. Serrador, J. M. *et al*. CD43 interacts with moesin and ezrin and regulates its redistribution to the uropods of T lymphocytes at the cell-cell contacts *Blood* 91, 4632-4644 (1998).

5. Yonemura, S., Tsukita, S. & Tsukita, S. Direct involvement of ezrin/radixin/moesin (ERM)-binding membrane proteins in the organization of microvilli in collaboration with activated ERM proteins *J. Cell Biol.* 145, 1497-1509 (1999).

6. Cannon, J. L. *et al*. CD43 interaction with ezrin-radixin-moesin (ERM) proteins regulates T-cell trafficking and CD43 phosphorylation *Mol. Biol. Cell* 22, 954-963 (2011).

7. Ilani, T., Khanna, C., Zhou, M., Veenstra, T. D. & Bretscher, A. Immune synapse formation requires ZAP-70 recruitment by ezrin and CD43 removal by moesin *J. Cell Biol.* 179, 733-746 (2007).

8. Tsukita, S. *et al*. ERM family members as molecular linkers between the cell surface glycoprotein CD44 and actin-based cytoskeletons *J. Cell Biol.* 126, 391-401 (1994).

9. Hirao, M. *et al*. Regulation mechanism of ERM (ezrin/radixin/moesin) protein/plasma membrane association: possible involvement of phosphatidylinositol turnover and Rho-dependent signaling pathway *J. Cell Biol.* 135, 37-51 (1996).

10. Legg, J. W. & Isacke, C. M. Identification and functional analysis of the ezrin-binding site in the hyaluronan receptor, CD44 *Curr. Biol.* 8, 705-708 (1998).

11. Legg, J. W., Lewis, C. A., Parsons, M., Ng, T. & Isacke, C. M. A novel PKC-regulated mechanism controls CD44 ezrin association and directional cell motility *Nat. Cell Biol.* 4, 399-407 (2002).

12. Li, Y. *et al*. Phosphorylated ERM is responsible for increased T cell polarization, adhesion, and migration in patients with systemic lupus erythematosus *J. Immunol.* 178, 1938-1947 (2007).

13. Mori, T. *et al*. Structural basis for CD44 recognition by ERM proteins *J. Biol. Chem.* 283, 29602-29612 (2008).

14. Hao, J. J. *et al*. Phospholipase C-mediated hydrolysis of PIP2 releases ERM proteins from lymphocyte membrane *J. Cell Biol.* 184, 451-462 (2009).

15. Berryman, M. & Bretscher, A. Identification of a novel member of the chloride intracellular channel gene family (CLIC5) that associates with the actin cytoskeleton of placental microvilli *Mol. Biol. Cell* 11, 1509-1521 (2000).

16. Chuang, J. Z., Chou, S. Y. & Sung, C. H. Chloride intracellular channel 4 is critical for the epithelial morphogenesis of RPE cells and retinal attachment *Mol. Biol. Cell* 21, 3017-3028 (2010).

17. Takahashi, K. *et al*. Interaction of radixin with Rho small G protein GDP/GTP exchange protein Dbl *Oncogene* 16, 3279-3284 (1998).

18. Tran Quang, C., Gautreau, A., Arpin, M. & Treisman, R. Ezrin function is required for ROCK-mediated fibroblast transformation by the Net and Dbl oncogenes *EMBO J.* 19, 4565-4576 (2000).

19. Prag, S. *et al*. Activated ezrin promotes cell migration through recruitment of the GEF Dbl to lipid rafts and preferential downstream activation of Cdc42 *Mol. Biol. Cell* 18, 2935-2948 (2007).

20. Batchelor, C. L. *et al*. Recruitment of Dbl by ezrin and dystroglycan drives membrane proximal Cdc42 activation and filopodia formation *Cell. Cycle* 6, 353-363 (2007).

21. Yang, H. S. & Hinds, P. W. Phosphorylation of ezrin by cyclin-dependent kinase 5 induces the release of Rho GDP dissociation inhibitor to inhibit Rac1 activity in senescent cells *Cancer Res.* 66, 2708-2715 (2006).

22. Ognibene, M. *et al*. The tumor suppressor hamartin enhances Dbl protein transforming activity through interaction with ezrin *J. Biol. Chem.* 286, 29973-29983 (2011).

23. Martin, M. *et al*. DCC regulates cell adhesion in human colon cancer derived HT-29 cells and associates with ezrin *Eur. J. Cell Biol.* 85, 769-783 (2006).

24. Antoine-Bertrand, J., Ghogha, A., Luangrath, V., Bedford, F. K. & Lamarche-Vane, N. The activation of ezrin-radixin-moesin proteins is regulated by netrin-1 through Src kinase and RhoA/Rho kinase activities and mediates netrin-1-induced axon outgrowth *Mol. Biol. Cell* 22, 3734-3746 (2011).

25. Lue, R. A., Brandin, E., Chan, E. P. & Branton, D. Two independent domains of hDlg are sufficient for subcellular targeting: the PDZ1-2 conformational unit and an alternatively spliced domain *J. Cell Biol.* 135, 1125-1137 (1996).

26. Lasserre, R. *et al*. Ezrin tunes T-cell activation by controlling Dlg1 and microtubule positioning at the immunological synapse *EMBO J.* 29, 2301-2314 (2010).

27. Reczek, D., Berryman, M. & Bretscher, A. Identification of EBP50: A PDZ-containing phosphoprotein that associates with members of the ezrin-radixin-moesin family *J. Cell Biol.* 139, 169-179 (1997).

28. Reczek, D. & Bretscher, A. The carboxyl-terminal region of EBP50 binds to a site in the amino-terminal domain of ezrin that is masked in the dormant molecule *J. Biol. Chem.* 273, 18452-18458 (1998).

29. Finnerty, C. M. *et al*. The EBP50-moesin interaction involves a binding site regulated by direct masking on the FERM domain *J. Cell. Sci.* 117, 1547-1552 (2004).

30. Hanono, A., Garbett, D., Reczek, D., Chambers, D. N. & Bretscher, A. EPI64 regulates microvillar subdomains and structure *J. Cell Biol.* 175, 803-813 (2006).

31. LaLonde, D. P., Garbett, D. & Bretscher, A. A regulated complex of the scaffolding proteins PDZK1 and EBP50 with ezrin contribute to microvillar organization *Mol. Biol. Cell* 21, 1519-1529 (2010).

32. Garbett, D., LaLonde, D. P. & Bretscher, A. The scaffolding protein EBP50 regulates microvillar assembly in a phosphorylation-dependent manner *J. Cell Biol.* 191, 397-413 (2010).

33. Pujuguet, P., Del Maestro, L., Gautreau, A., Louvard, D. & Arpin, M. Ezrin regulates E-cadherin-dependent adherens junction assembly through Rac1 activation *Mol. Biol. Cell* 14, 2181-2191 (2003).

34. Zwaenepoel, I. *et al*. Ezrin regulates microvillus morphogenesis by promoting distinct activities of Eps8 proteins *Mol. Biol. Cell* 23, 1080-1094 (2012).

35. Naba, A., Reverdy, C., Louvard, D. & Arpin, M. Spatial recruitment and activation of the Fes kinase by ezrin promotes HGF-induced cell scattering *EMBO J.* 27, 38-50 (2008).

36. Helander, T. S. *et al*. ICAM-2 redistributed by ezrin as a target for killer cells *Nature* 382, 265-268 (1996).

37. Heiska, L. *et al*. Association of ezrin with intercellular adhesion molecule-1 and -2 (ICAM-1 and ICAM-2). Regulation by phosphatidylinositol 4, 5-bisphosphate *J. Biol. Chem.* 273, 21893-21900 (1998).

38. Serrador, J. M. *et al*. Moesin interacts with the cytoplasmic region of intercellular adhesion molecule-3 and is redistributed to the uropod of T lymphocytes during cell polarization *J. Cell Biol.* 138, 1409-1423 (1997).

39. Alonso-Lebrero, J. L. *et al*. Polarization and interaction of adhesion molecules P-selectin glycoprotein ligand 1 and intercellular adhesion molecule 3 with moesin and ezrin in myeloid cells *Blood* 95, 2413-2419 (2000).

40. Hamada, K. *et al*. Structural basis of adhesion-molecule recognition by ERM proteins revealed by the crystal structure of the radixin-ICAM-2 complex *EMBO J.* 22, 502-514 (2003).

41. Oh, H. M. *et al*. RKIKK motif in the intracellular domain is critical for spatial and dynamic organization of ICAM-1: functional implication for the leukocyte adhesion and transmigration *Mol. Biol. Cell* 18, 2322-2335 (2007).

42. Dickson, T. C., Mintz, C. D., Benson, D. L. & Salton, S. R. Functional binding interaction identified between the axonal CAM L1 and members of the ERM family *J. Cell Biol.* 157, 1105-1112 (2002).

43. Sakurai, T. *et al*. Interactions between the L1 cell adhesion molecule and ezrin support traction-force generation and can be regulated by tyrosine phosphorylation *J. Neurosci. Res.* 86, 2602-2614 (2008).

44. Matsui, K., Parameswaran, N., Bagheri, N., Willard, B. & Gupta, N. Proteomics analysis of the ezrin interactome in B cells reveals a novel association with Myo18aalpha *J. Proteome Res.* 10, 3983-3992 (2011).

45. Denker, S. P., Huang, D. C., Orlowski, J., Furthmayr, H. & Barber, D. L. Direct binding of the Na--H exchanger NHE1 to ERM proteins regulates the cortical cytoskeleton and cell shape independently of H(+) translocation *Mol. Cell* 6, 1425-1436 (2000).

46. Denker, S. P. & Barber, D. L. Cell migration requires both ion translocation and cytoskeletal anchoring by the Na-H exchanger NHE1 *J. Cell Biol.* 159, 1087-1096 (2002).

47. Cha, B. *et al*. The NHE3 juxtamembrane cytoplasmic domain directly binds ezrin: dual role in NHE3 trafficking and mobility in the brush border *Mol. Biol. Cell* 17, 2661-2673 (2006).

48. Sullivan, A., Uff, C. R., Isacke, C. M. & Thorne, R. F. PACE-1, a novel protein that interacts with the C-terminal domain of ezrin *Exp. Cell Res.* 284, 224-238 (2003).

49. Mykkanen, O. M. *et al*. Characterization of human palladin, a microfilament-associated protein *Mol. Biol. Cell* 12, 3060-3073 (2001).

50. Rachlin, A. S. & Otey, C. A. Identification of palladin isoforms and characterization of an isoform-specific interaction between Lasp-1 and palladin *J. Cell. Sci.* 119, 995-1004 (2006).

51. Henning, M. S. *et al*. PDZD8 is a novel moesin-interacting cytoskeletal regulatory protein that suppresses infection by herpes simplex virus type 1 *Virology* 415, 114-121 (2011).

52. D'Angelo, R. *et al*. Interaction of ezrin with the novel guanine nucleotide exchange factor PLEKHG6 promotes RhoG-dependent apical cytoskeleton rearrangements in epithelial cells *Mol. Biol. Cell* 18, 4780-4793 (2007).

53. Orlando, R. A. *et al*. The glomerular epithelial cell anti-adhesin podocalyxin associates with the actin cytoskeleton through interactions with ezrin *J. Am. Soc. Nephrol.* 12, 1589-1598 (2001).

54. Snapp, K. R., Heitzig, C. E. & Kansas, G. S. Attachment of the PSGL-1 cytoplasmic domain to the actin cytoskeleton is essential for leukocyte rolling on P-selectin *Blood* 99, 4494-4502 (2002).

55. Takai, Y., Kitano, K., Terawaki, S., Maesaki, R. & Hakoshima, T. Structural basis of PSGL-1 binding to ERM proteins *Genes Cells* 12, 1329-1338 (2007).

56. Serrador, J. M. *et al*. A juxta-membrane amino acid sequence of P-selectin glycoprotein ligand-1 is involved in moesin binding and ezrin/radixin/moesin-directed targeting at the trailing edge of migrating lymphocytes *Eur. J. Immunol.* 32, 1560-1566 (2002).

57. Spertini, C., Baisse, B. & Spertini, O. Ezrin-radixin-moesin-binding sequence of PSGL-1 glycoprotein regulates leukocyte rolling on selectins and activation of extracellular signal-regulated kinases *J. Biol. Chem.* 287, 10693-10702 (2012).

58. Sperka, T. *et al*. Activation of Ras requires the ERM-dependent link of actin to the plasma membrane *PLoS One* 6, e27511 (2011).

59. Hirao, M. *et al*. Regulation mechanism of ERM (ezrin/radixin/moesin) protein/plasma membrane association: possible involvement of phosphatidylinositol turnover and Rho-dependent signaling pathway *J. Cell Biol.* 135, 37-51 (1996).

60. Takahashi, K. *et al*. Direct interaction of the Rho GDP dissociation inhibitor with ezrin/radixin/moesin initiates the activation of the Rho small G protein *J. Biol. Chem.* 272, 23371-23375 (1997).

61. Koltzscher, M., Neumann, C., Konig, S. & Gerke, V. Ca2+-dependent binding and activation of dormant ezrin by dimeric S100P *Mol. Biol. Cell* 14, 2372-2384 (2003).

62. Austermann, J., Nazmi, A. R., Muller-Tidow, C. & Gerke, V. Characterization of the Ca2+ -regulated ezrin-S100P interaction and its role in tumor cell migration *J. Biol. Chem.* 283, 29331-29340 (2008).

63. Bonilha, V. L. & Rodriguez-Boulan, E. Polarity and developmental regulation of two PDZ proteins in the retinal pigment epithelium *Invest. Ophthalmol. Vis. Sci.* 42, 3274-3282 (2001).

64. Granes, F., Urena, J. M., Rocamora, N. & Vilaro, S. Ezrin links syndecan-2 to the cytoskeleton *J. Cell. Sci.* 113 (Pt 7), 1267-1276 (2000).

65. Granes, F. *et al*. Identification of a novel Ezrin-binding site in syndecan-2 cytoplasmic domain *FEBS Lett.* 547, 212-216 (2003).

66. Chirivino, D. *et al*. The ERM proteins interact with the HOPS complex to regulate the maturation of endosomes *Mol. Biol. Cell* 22, 375-385 (2011).

67. Jin, C. *et al*. PKA-mediated protein phosphorylation regulates ezrin-WWOX interaction *Biochem. Biophys. Res. Commun.* 341, 784-791 (2006).

68. Zaarour, R. F. *et al*. Ezrin ubiquitylation by the E3 ubiquitin ligase, WWP1, and consequent regulation of hepatocyte growth factor receptor activity *PLoS One* 7, e37490 (2012).

69. Ilani, T., Khanna, C., Zhou, M., Veenstra, T. D. & Bretscher, A. Immune synapse formation requires ZAP-70 recruitment by ezrin and CD43 removal by moesin *J. Cell Biol.* 179, 733-746 (2007).

70. Li, M. *et al*. NHERF-1 binds to Mrp2 and regulates hepatic Mrp2 expression and function *J. Biol. Chem.* 285, 19299-19307 (2010).

71. Spence, H. J. *et al*. Ezrin-dependent regulation of the actin cytoskeleton by beta-dystroglycan *Hum. Mol. Genet.* 13, 1657-1668 (2004).

Table 2 Function of phosphomimetic and phosphoinhibitory ERMs in selected publications

	Phosphomimetic (T>D/E)		Phosphoinhibitory (T>A)	
	Rescues/Promotes	Fails/Inhibits	Rescues/Promotes	Fails/Inhibits
Microvilli	Increase in microvillus length and density [1, 2] Presence of microvilli when endogenous ezrin cannot be phosphorylated, overexpression, T567D-VSV-G [3] Increase in microvillus-like structures in fibroblasts [4-6]	Microvilli in *Drosophila* photoreceptor cells, T559D overexpresion [7] 4-cell mouse embry microvilli, T567D [8]		Microvilli formation, Ezrin-T567D-VSV-G overexpression [1, 2] Microvillus-like structure formation, Moesin T558A/Ezrin T567A [4-6] Presence of microvilli when endogenous ezrin cannot be phosphorylated, overexpression, T567A-VSV-G [3] 4-cell mouse embry microvilli, T567A [8]
Spreading	Spreading of S2R+ cells on ConA [9] Spreading of A549 cells with elevated cAMP [10]	Spreading of BLM melanoma cells [11]		Spreading of BLM melanoma cells [11] Spreading of S2R+ cells on ConA [9]
Viability	*Drosophila* Viability, myc-dMoesin T559D (N-terminal tag) overexpression, partial [12, 13]	*Drosophila* viability, dMoesin T559D or T559D-GFP overexpression [14, 15]	*Drosophila* viability, dMoesin T559A or T559A-GFP overexpression, partial [14]	*Drosophila* viability, dMoesin T559A or T559A-GFP overexpression [12,13,15]
Other	Oriented mitotic spindle in S2 cells [16] T-cell migration (moesin T558D or ezrin T567D) [17, 18]	Secretion in gastric parietal cells, overexpression of T567D-CFP [19] T-cell migration (T567D)[20, 21]		Oriented mitotic spindle in S2 cells [16]

1. Barret, C., Roy, C., Montcourrier, P., Mangeat, P. & Niggli, V. Mutagenesis of the phosphatidylinositol 4,5-bisphosphate (PIP(2)) binding site in the NH(2)-terminal domain of ezrin correlates with its altered cellular distribution *J. Cell Biol.* 151, 1067-1080 (2000).

2. Fievet, B. T. *et al*. Phosphoinositide binding and phosphorylation act sequentially in the activation mechanism of ezrin *J. Cell Biol.* 164, 653-659 (2004).

3. ten Klooster, J. P. *et al*. Mst4 and Ezrin induce brush borders downstream of the Lkb1/Strad/Mo25 polarization complex *Dev. Cell.* 16, 551-562 (2009).

4. Oshiro, N., Fukata, Y. & Kaibuchi, K. Phosphorylation of moesin by rho-associated kinase (Rho-kinase) plays a crucial role in the formation of microvilli-like structures *J. Biol. Chem.* 273, 34663-34666 (1998).

5. Matsui, T. *et al*. Rho-kinase phosphorylates COOH-terminal threonines of ezrin/radixin/moesin (ERM) proteins and regulates their head-to-tail association *J. Cell Biol.* 140, 647-657 (1998).

6. Yonemura, S., Tsukita, S. & Tsukita, S. Direct involvement of ezrin/radixin/moesin (ERM)-binding membrane proteins in the organization of microvilli in collaboration with activated ERM proteins *J. Cell Biol.* 145, 1497-1509 (1999).

7. Karagiosis, S. A. & Ready, D. F. Moesin contributes an essential structural role in Drosophila photoreceptor morphogenesis. *Development* 131, 725-732 (2004).

8. Dard, N. *et al*. In vivo functional analysis of ezrin during mouse blastocyst formation *Dev. Biol.* 233, 161-173 (2001).

9. Kunda, P., Pelling, A. E., Liu, T. & Baum, B. Moesin controls cortical rigidity, cell rounding, and spindle morphogenesis during mitosis *Curr. Biol.* 18, 91-101 (2008).

10. Ross, S. H. *et al*. Ezrin is required for efficient Rap1-induced cell spreading *J. Cell. Sci.* 124, 1808-1818 (2011).

11. Estecha, A. *et al*. Moesin orchestrates cortical polarity of melanoma tumour cells to initiate 3D invasion *J. Cell. Sci.* 122, 3492-3501 (2009).

12. Speck, O., Hughes, S. C., Noren, N. K., Kulikauskas, R. M. & Fehon, R. G. Moesin functions antagonistically to the Rho pathway to maintain epithelial integrity. *Nature* 421, 83-87 (2003).

13. Hipfner, D. R., Keller, N. & Cohen, S. M. Slik Sterile-20 kinase regulates Moesin activity to promote epithelial integrity during tissue growth *Genes Dev.* 18, 2243-2248 (2004).

14. Roubinet, C. *et al*. Molecular networks linked by Moesin drive remodeling of the cell cortex during mitosis *J. Cell Biol.* 195, 99-112 (2011).

15. Polesello, C., Delon, I., Valenti, P., Ferrer, P. & Payre, F. Dmoesin controls actin-based cell shape and polarity during Drosophila melanogaster oogenesis. *Nat. Cell Biol.* 4, 782-789 (2002).

16. Carreno, S. *et al*. Moesin and its activating kinase Slik are required for cortical stability and microtubule organization in mitotic cells *J. Cell Biol.* 180, 739-746 (2008).

17. Cernuda-Morollon, E., Millan, J., Shipman, M., Marelli-Berg, F. M. & Ridley, A. J. Rac activation by the T-cell receptor inhibits T cell migration *PLoS One* 5, e12393 (2010).

18. Lee, J. H. *et al*. Roles of p-ERM and Rho-ROCK signaling in lymphocyte polarity and uropod formation *J. Cell Biol.* 167, 327-337 (2004).

19. Zhou, R. *et al*. Phosphorylation of ezrin on threonine 567 produces a change in secretory phenotype and repolarizes the gastric parietal cell *J. Cell. Sci.* 118, 4381-4391 (2005).

20. Liu, Y. *et al*. Constitutively active ezrin increases membrane tension, slows migration, and impedes endothelial transmigration of lymphocytes in vivo in mice *Blood* 119, 445-453 (2012).

21. Belkina, N. V., Liu, Y., Hao, J. J., Karasuyama, H. & Shaw, S. LOK is a major ERM kinase in resting lymphocytes and regulates cytoskeletal rearrangement through ERM phosphorylation *Proc. Natl. Acad. Sci. U. S. A.* 106, 4707-4712 (2009).

CHAPTER 2

DEFINING THE ACTIVATION-DEPENDENT EZRIN INTERACTOME

Numerous ERM binding partners have been identified (Table 1), but binding partners have never been identified systematically from epithelial cells. Experiments in which affinity matrices were pre-adsorbed with ezrin ("GST-pulldown-type" experiments) have concluded that CD44 (Hirao et al., 1996; Yonemura et al., 1998; Legg and Isacke, 1998; Mori et al., 2008) or EBP50 (Reczek et al., 1997; Reczek and Bretscher, 1998) are the tightest-binding interaction partners of the isolated ezrin FERM domain. However, these experiments overlook several key issues: 1) interactions of weaker affinity could proceed in cells if the local concentration of the binding partner is higher at sites of ezrin enrichment; 2) ERMs could interact with partners through motifs other than the FERM domain, and could interact with proteins in the dormant state rather than the open state; 3) the interactions could be transient.

To address these issues, I used the method of cross-linking co-immunoprecipitation to capture tagged ezrin along with proteins in its proximity without the bias of interaction strength or longevity. Using mass spectrometry, I identified 19 ezrin interactors, some of which represent novel microvillar components. I also took advantage of the ezrin activation cycle to show that ERM-interaction partners respond differently to changes in ERM activation.

MATERIALS AND METHODS

Plasmid construction, cell-lines, and antibodies. Transient ezrin expression constructs were generated in pIRES2EGFP (Clontech) for bicistronic expression with EGFP. T567A and T567E mutations were generated by Julie Thoms in pENTR3C (Invitrogen) between EcoRI and XhoI. pIRES2EGFP was cut BamHI and appended by direct ligation with annealed primers

RV20F1/R1 (5’-TCGACCGGATCCGAATTCTCGCGGCCGCACTCGAG-3’ and 5’-GATCCTCGAGTGCGGCCGCGAGAATTCGGATCCGG-3’) to generate pIRES2EGFP_ReMCS, introducing an EcoRI and XhoI site in MCS. pIRES2EGFP_ReMCS was then cut with EcoRI and XhoI, and ezrin mutants introduced from pENTR3C. All mutants were initially mutagenized to generate resistance to siEzrin2 using QuickChange mutagenesis (Agilent) and RV39F1/R1 (5'-GCTCAGGACCTGGAAATGTATGGAATCAATTACTTTGAAATAAAAAACAAGAAAGGAACAGACCTTTG-3' and 5'-CAAAGGTCTGTTCCTTTCTTGTTTTTTATTTCAAAGTAATTGATTCCATACATTTCCAGGTCCTGAGC-3'). Additional ezrin mutations were created in this backbone.

An internal flag tag was introduced into pIRES2EGFP_ReMCS/Ezrin T567E by inverse tailored PCR using RV29F1/R1 (5’-GACTACAAAGACGATGACGACAAGgagagcttgcaggatgagggc, 5’-gtacacgggtggtggtggaggc-3’). The resulting vector was further reverted or mutated to 567T or 567A using RV30F1/R1 (5’-Gccgggacaagtacaagacgctgcggcagatc-3’ and 5’-Gatctgccgcagcgtcttgtacttgtcccggc-3’) or RV30F2/R2 (5’-Gggacaagtacaaggccctgcggcagatccgg-3’ and 5’-Ccggatctgccgcagggccttgtacttgtccc-3’), respectively.

The K4N mutations (K253N, K254N, K262N, K263N; Barret et al., 2000) were generated using the QuickChange kit and primers RV71F1/R1 (5’- CCCATCGAC AAC AAC GCACCTGACTTTGTGTTTTATGCCCCAC-3’ and 5’-TTTAATGACAAAGTTATTGTCATTGAAAGAGATGTTCCTGATTTCACTCC-3’).

To generate stable cell-lines, ezrin mutants were amplified using primers RV33F1/R1 (5'- TTCACT GCGGCCGC ATGCCGAAACCAATCAATGTCCGAGTTAC-3' and 5'-ACGAAGAATTCTTACAGGGCCTCGAACTCGTCGATG-3') and ligated into the NotI-EcoRI of pQCXIP. These were then transiently transfected into Pheonix-Ampho packaging cells, and the resulting viral supernatant was used to infect log-phase Jeg-3 cell cultures, which were then selected in 2 μg/mL puromycin.

Ezrin 1-478-Flag was generated using RV20F2/36R3 (5'- AGTGGTTCGA GAATTC ATGCCGAAACCAATCAATGTCCGAGTTAC-3' and 5'-GATCAACTCTCGAGTTACTTGTCATCGTCGTCCTTGTAGTCGTACACGGGTGGTGGT GGAGGC-3') and then cloning the resulting fragment into pIRES2EGFP or using RV33F1/38R1 (5'- TTCACT GCGGCCGC ATGCCGAAACCAATCAATGTCCGAGTTAC-3' and 5'- ACGAAGAATTCTTACTTGTCGTCATCGTCTTTGTAGTCgtacac-3') and cloning the resulting fragment into pQCXIP. Ezrin 1-583-iFlag was generated using RV20F2/36R5 (5'-AGTGGTTCGA GAATTC ATGCCGAAACCAATCAATGTCCGAGTTAC-3' and 5'-GATCAACTCTCGAGTTACTCGAACTCGTCGATGCGCTGC-3') and then cloning the resulting fragment into pIRES2EGFP or using RV33F1/38R2 (5'- TTCACT GCGGCCGC ATGCCGAAACCAATCAATGTCCGAGTTAC-3' and 5'-ACGAAGAATTCTTACTCGAACTCGTCGATGCGCTGC-3') and cloning the resulting fragment into pQCXIP.

Ezrin-GFP was made by amplifying ezrin mutants using RV72F1/R1 (5'-TTCACTCTCGAGATGCCGAAACCAAT-3' and 5'-ACGAAGAATTCcagggcctcgaactcgtcgatgc-3') and ligating the resulting product into pEGFP-N2 (Clontech) cut with XhoI/EcoRI. Ezrin-GFP and variants were then amplified using

RV33F1/53R1 (5'-5'- TTCACT GCGGCCGC ATGCCGAAACCAATCAATGTCCGAGTTAC-3' and 5'-ACGAAGAATTCTTACTTGTACAGCTCGTCCATGCCGAG-3'), cut with NotI, and the products were inserted into pQCXIP cut with EcoRI, flushed with mung bean nuclease (New England Biolabs) to generate a blunt end, and cut with NotI.

Full-length TROP-2 was amplified from Jeg-3 cDNA using RV56F2k/R2 (5'- GTTCGA GGATCC ATGGCTCGGGGCCCCGGC-3' and 5'-TCGAACGAATTCCAAGCTCGGTTCCTTTCTCAACTCCC-3') and inserted into pcDNA3.1/MycHis (Invitrogen) or pcDNA3.1/V5His (Invitrogen) cut with BamHI/EcoRI. To engineer TROP-2 lacking an extracellular domain, TROP-2 was amplified using RV56F2k/R3 (5'- GTTCGA GGATCC ATGGCTCGGGGCCCCGGC-3' and 5'-TCGAACGAATTCGATCACCAGGACGGCCATGCCG -3') and inserted into pcDNA3.1/V5His.

The following primers were used to engineer basic patch mutations within pcDNA3.1/TROP-2-V5His:

"ΔA", R300A, R301A, K302A	RV84F1/R1	5'- GGC CGT CCT GGT GAT CAC CAA CGC GGC AGC GTC GGG GAA GTA CAA GAA GGT G-3'	5'- CAC CTT CTT GTA CTT CCC CGA CGC TGC CGC GTT GGT GAT CAC CAG GAC GGC C-3'
"ΔA6", K305A, K307A	RV84F2/R2	5'- CGT CCT GGT GAT CAC CAA CGC GGC AAA GTC GGG GAA GTA CAA G -3'	5'- CTT GTA CTT CCC CGA CTT TGC CGC GTT GGT GAT CAC CAG GAC G-3'
"ΔA1", K300A	RV84F3/R3	5'- CCT GGT GAT CAC CAA CGC GAG AAA GTC GGG GAA G-3'	5'- CTT CCC CGA CTT TCT CGC GTT GGT GAT CAC CAG G-3'

“ΔBC”, K305A, K307A, K308A	RV78F2/R2	5'-ACC AAC CGG AGA AAG TCG GGG GCG TAC GCG GCG GTG GAG ATC AAG GAA CTG GG-3'	5'-CCC AGT TCC TTG ATC TCC ACC GCC GCG TAC GCC CCC GAC TTT CTC CGG TTG GT-3'

For stable cell-lines expressing TROP-2-V5His, TROP-2 was amplified with RV56F2k/83R1 (5’- GTTCGA GGATCC ATGGCTCGGGGCCCCGGC-3’ and 5’-ACGAACAATTGTCAATGGTGATGGTGATGATGACCGGTAC -3’), cut with BamHI/MfeI and inserted into pQCXIP cut with BamHI/EcoRI. This was then transiently transfected into Pheonix-Ampho packaging cells, and the resulting viral supernatant was used to infect log-phase Jeg-3 cell cultures, which were then selected in 2 μg/mL puromycin.

To create GST-TROP-2-tail, residues 298-323 were amplified using RV50F1/R1 (5’-GTTCGA GGATCC ACCAACCGGAGAAAGTCGGGGAAG-3’ and 5’-CCACTGCGGCCGCCTACAAGCTCGGTTCCTTTCTCAACTCC-3’) and pasted into pGEX6P1 cut with BamHI/NotI. The following mutations were engineered in the tail using the following primers and the QuickChange kit:

“ΔA”, R300A, R301A, K302A	RV78F1/R1	5’- GGC CCC TGG GAT CCA CCA ACG CGG CAG CGT CGG GGA AGT ACA AGA AGG-3’	5'-CCT TCT TGT ACT TCC CCG ACG CTG CCG CGT TGG TGG ATC CCA GGG GCC-3'
“ΔBC”, K305A, K307A, K308A	RV78F2/R2	5'-ACC AAC CGG AGA AAG TCG GGG GCG TAC GCG GCG GTG GAG ATC AAG GAA CTG GG-3'	5'-CCC AGT TCC TTG ATC TCC ACC GCC GCG TAC GCC CCC GAC TTT CTC CGG TTG GT-3'
“ΔD”, K312A	RV78F3/R3	5'-TAC AAG AAG GTG GAG ATC GCG GAA CTG GGG GAGT TGA G-	5'-CTC AAC TCC CCC AGT TCC GCG ATC TCC ACC TTC TTG TA-3'

		3'	
S303D	RV78F4/R4	5'-GAT CCA CCA ACC GGA GAA AGG ATG GGA AGT ACA AGA AGG TGG A-3'	5'-TCC ACC TTC TTG TAC TTC CCA TCC TTT CTC CGG TTG GTG GAT C-3'
R300A,R301A, from ΔA	RV81F6/R6	5'-GGG ATC CAC CAA CGC GGC AAA GTC GGG GAA GTA C-3'	5'- GTA CTT CCC CGA CTT TGC CGC GTT GGT GGA TCC-3'
R301A,K302A, from ΔA	RV81F7/R7	5'-ATC CAC CAA CCG GGC AGC GTC GGG GAA GTA CAA G-3'	5'- CTT GTA CTT CCC CGA CGC TGC CCG GTT GGT GGA T-3'
R300A,K302A, from ΔA	RV81F8/R8	5'-GAT CCA CCA ACG CGA GAG CGT CGG GGA AGT ACA AGA-3'	5'- TCT TGT ACT TCC CCG ACG CTC TCG CGT TGG TGG ATC-3'
R300A	RV81F1/R1	5'- CTG GGA TCC ACC AAC GCG AGA AAG TCG GGG AA-3'	5'-TTC CCC GAC TTT CTC GCG TTG GTG GAT CCC AG-3'
R301A	RV81F2/R2	5'-GGG ATC CAC CAA CCG GGC AAA GTC GGG GAA GTA C-3'	5'-GTA CTT CCC CGA CTT TGC CCG GTT GGT GGA TCC C-3'
K302A	RV81F3/R3	5'- GAT CCA CCA ACC GGA GAG CGT CGG GGA AGT ACA AGA-3'	5'- TCT TGT ACT TCC CCG ACG CTC TCC GGT TGG TGG ATC-3'
K300R,K301R,R302K	RV81F4/R4	5'- GCC CCT GGG ATC CAC CAA CAA GAA AAG GTC GGG GAA GTA CAA GAA G-3'	5'- CTT CTT GTA CTT CCC CGA CCT TTT CTT GTT GGT GGA TCC CAG GGG C-3'
N299R,K300N	RV81F5/R5	5'- CAG GGG CCC CTG GGA TCC ACC AGG AAT AGA AAG TCG GGG AAG TAC-3'	5'- GTA CTT CCC CGA CTT TCT ATT CCT GGT GGA TCC CAG GGG CCC CTG-3'

ATP11C was obtained from the ATCC, Clone ID 40146750, and amplified using primers RV48F1/R1 (5'- GTTCGA GGTACC A ATGCAGATGGTCCCATCTCTCCCTCC-3' and 5'-

TCGAACCTCGAGTTACAATACATTAGATTCGTCTGAGAATGTTCGTAAAAGAAG-3') and inserted into pFLAG-CMV7.1 (Sigma) cut with KpnI/XhoI which placed it in-frame of an N-terminal 3XFlag tag. Additional experiments verified that the tag had to be on the N-terminus to express any protein (data not shown).

PACE-1-myc expression plasmid was a generous gift from Dr. Rick Thorne (University of Newcastle).

ATB(0) was cloned from Jeg-3 cDNA using primers RV58F2k/R1 (5'-GTTCGAGAATTCACCATGGTGGCCGATCCTCCTCGAGAC-3' and 5'-TCGAACGCGGCCGCTTCATGACTGATTCCTTCTCAGAGGCGACC-3').

BASP-1 was cloned from Jeg-3 cDNA using primers RV66F1/R1 (5'- GTTCGA GGATCC ACC ATGGGAGGCAAGCTCAGCAAGAAGAAG-3' and 5'-TCGAACGAATTCCTCTTTCACGGTTACGGTTTGGTCGG-3') and inserted into pcDNA3.1/MycHis to generate BASP-1-MycHis or pEGFP-N2 to generate BASP-1-EGFP. BASP-1-EGFP was further mutated using the following primers in tailored inverse PCR:

"ΔEDA", K7-10→AAAA	RV68F2/R1	5'-GCG GCG GCT GCC GGC TAC AAT GTG AAC GAC GAG AAA GCC-3'	5'- GGC TAC AAT GTG AAC GAC GAG AAA GCC-3'
"ΔED"	RV68F3/R1	5'-GGC TAC AAT GTG AAC GAC GAG AAA GCC -3'	5'- GGC TAC AAT GTG AAC GAC GAG AAA GCC-3'
G2A	RV68F1/R2	5' GGC TAC AAT GTG AAC GAC GAG AAA GCC-3'	5'- GCT GAG CTT GCC TGC CAT GGT AGA TCT GAG TCC GG-3'
ΔED, G2A	RV68F3/R2	5'-GGC TAC AAT	5'- GCT GAG CTT

		GTG AAC GAC GAG AAA GCC -3’	GCC TGC CAT GGT AGA TCT GAG TCC GG-3’

SiRNA sequences for Ezrin (5’-GGAAUCAACUAUUUCGAGAtt-3’), BASP-1 (5’-CAACAGUAAUAAAGUUAAAtt-3’ and 5’- GAUUUCUCAUGACGAGUUAtt-3’), and ATP11C (5’-CCCAAUAACUCUGUCGAUAtt-3’) were from Ambion. Dicer substrate dsRNAs for TROP-2 knockdown were 5’-GCUUAAAUGAGUUUAGAUGGGAAAT-3’ and 5’-AGUUGAGAAAGGAACCGAGCUUGTA-3’ from Integrated DNA Technologies.

For SILAC, cells expressing ezrin-iFlag or empty vector were grown for at least 2 weeks in MEM (Pierce) containing dialyzed FBS (Invitrogen) and either C-13 arginine and lysine or C-12 arginine and lysine (Sigma), respectively.

TROP-2 antibody was mouse monoclonal GA733.1 (Abcam) or a rabbit polyclonal antibody (Santa Cruz). Flag M2 antibody and affinity gel were from Sigma. Myc antibody was mouse monoclonal 9E10 (Roche). GFP antibody was from Santa Cruz. V5 antibody was mouse monoclonal V5.11 (Invitrogen).

Immunoprecipitations and mass spectrometry. Prior to lysis, cells were treated with warm PBS containing 1.25 mM DSP (Pierce), a cell permeable, thiol-reversible crosslinking agent, for 2 minutes at 37^{O}C. Excess crosslinker was quenched by extensive washing in TBS for 15 minutes at room temperature. Cells were then solubilized in cold IP buffer (25 mM Tris pH 7.4, 5% glycerol, 150 mM NaCl, 50 mM NaF, 0.1 mM Na_3VO_4, 10 mM βGP, 8.7 mg/mL pNPP, 0.5% Triton X-100, 0.1 μM calyculin A, Roche protease inhibitor tablet) and immunoprecipitated for 2 hours using Flag M2 Affinity Gel (Sigma). For western blots, immunoprecipitates were

extensively washed in IP wash buffer (25 mM Tris pH 7.4, 5% glycerol, 150 mM NaCl, 50 mM NaF, 0.2% Triton X-100) and then eluted in 200 μg/mL 3XFlag peptide, and then denatured in Laemmli buffer, resolved by SDS-PAGE, transferred to PVDF and then interrogated with specific antibodies.

For mass spectrometry, immunoprecipitates were eluted in 50 mM Tris pH 8.0 containing 1% SDS, trypsin-digested, desalted, dried, and reconstituted in 80% acetonitrile and 1% formic acid, and fractionated by hydrophilic interaction chromatography. Fractions were dried, reconstituted in 0.1% trifluoroacetic acid, and analyzed by LC-MS/MS using an Orbitrap XL mass spectrometer (Thermo). Database search and quantitation of heavy/light peptide isotope ratios were performed as previously described (Smolka et al., 2007) with the following modification: interacting proteins were limited to those for which at least 2 peptides were discovered with a Sorcerer probability score of greater than 90% and a heavy-vs.-light enrichment greater than 3.0.

Immunofluorescence and image analysis. Cells grown on glass coverslips were fixed in 3.7% formalin/PBS for 15 minutes at room temperature for most experiments Cells were then washed with PBS and blocked with IF buffer (PBS + 0.5% BSA + 0.5% goat serum + 0.1% Triton-X 100) for 10 minutes. Primary and secondary antibodies were then applied in IF buffer containing 1% FBS. Alexa-fluor conjugated phalloidin (Invitrogen), to stain F-actin, was added to the secondary as required. The cells were mounted in Vectashield reagent, imaged using a CSU-X spinning disk microscope (Intelligent Imaging Innovations) with spherical aberration correction device, 63x 1.4 NA objective on an inverted microscope (Leica), acquired with either a QuantEM EMCCD camera or an HQ2 CCD camera (Photometrics) using Slidebook software (Intelligent Imaging Innovations). Maximum or summed intensity projections were assembled in

Slidebook and exported to Adobe Illustrator software. For clarity, side projections were vertically expanded 5-fold using Illustrator.

Plasmid and siRNA transfection. All transient plasmid DNA transfections were performed for ~18 hours using Polyethylenimine reagent (PolyPlus) using a previously established protocol (Hanono et al., 2006). Phoenix-Ampho retrovirus producer cells (ATCC) were cultured in DMEM (Invitrogen) with 10% FBS. Retroviruses were prepared following a standard transfection protocol using the Phoenix-Ampho cell-line and the retroviral vector pQCXIP. The recombinant retroviruses were used to transduce Jeg-3 cells, which were then selected with 2.0 μg/ml puromycin (Sigma). All siRNAs were transfected at 30 nM into ~25% confluent cultures of Jeg-3 cells using Lipofectamine RNAiMAX (Invitrogen) using the manufacturer's protocol. Cells were processed for immunofluorescence or lysis 3 days after transfection.

The presence or absence of microvilli was scored as described previously (Hanono et al., 2006; LaLonde et al., 2010; Garbett et al., 2010).

Ezrin FERM domain was produced and purified in vitro according to Reczek et al., 1997. $PI(4,5)P_2$ (Avanti) micelles were prepared and added to interaction assays at either 25 or 50 μg/mL according to Hirao et al., 1996.

RESULTS

Tagged ezrin binds to EBP50 in a cross-linker and activation-dependent manner

In order to examine the localization and interaction partners of ezrin mutants, it was necessary to tag them. Functional studies that have tagged both the N-terminus and C-terminus of ERMs have generally concluded that N-terminal tags are function-disrupting due to favoring a

more closed conformation whereas C-terminal tags are function-preserving, although there have been some exceptions (Figure 2). The recent crystal structure of full-length ERM (Li et al., 2007) as well as biochemical experiments (Chambers and Bretscher, 2005) have hinted that the extreme C-terminus participates in important contacts in the closed ERM. To avoid disrupting either terminus by tag addition, I introduced a flag tag (DYKDDDK) into a disordered loop in the ERM crystal structure (Li et al., 2007) which is poorly conserved amongst ERM family members (Figure 2.1.A). Activation mutants were then introduced into this construct, which was cloned into an internal-ribosome-entry-site-puromyicin-resistance vector which allows stable batch selection of Jeg-3 choriocarcinoma cells. Following selection in 2 μg/mL puromycin beyond two weeks, the level of transfected ezrin-iFlag per population was less than or equal to the level of endogenous ezrin (Figure 2.1.B), and 85-90% of cells in the population expressed ezrin-iFlag regardless of mutation (data not shown). Interestingly, the expression level of activated mutants was always less than that of deactivated mutants (data not shown). Furthermore, microvilli (quantified in Figure 3.3.B) and the localization of EBP50 (data not shown) were unaltered in the stable cell-lines.

To determine whether *in vivo* EBP50 interaction was dependent on conformation switching as it is *in vitro* (Reczek and Bretscher, 1998), I immunoprecipitated EBP50 in the stable cell-lines and revealed bound ezrin-iFlag. Chemical cross-linker DSP was used to preserve the otherwise transient interaction between ezrin and EBP50 (Figure 2.1.C). DSP-assisted immunoprecipitation experiments demonstrated a minor but reproducible increase in the amount of EBP50 that bound to wild-type ezrin relative to T567A ezrin (Figure 2.1.D), consistent with a role for activation in regulating this interaction in cells. Unexpectedly, there was no increase in EBP50-binding to T567E ezrin, but an alternative constitutively open form, 1-583, bound vastly

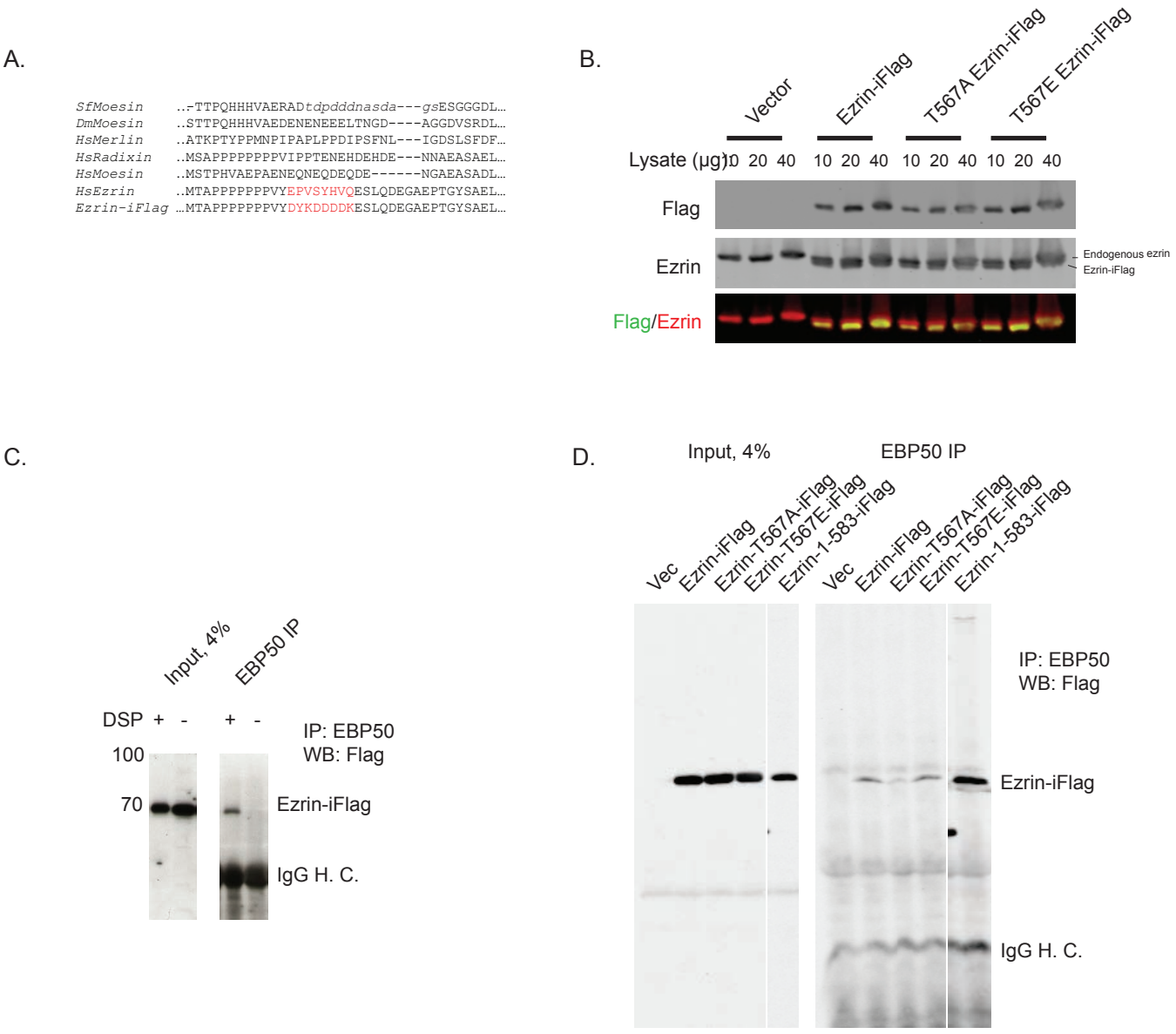

Figure 2.1 Creation of stable cell-lines expressing internally-flag tagged ezrin and interaction with EBP50.

(A) Multiple sequence alignment of the region between the ERM coiled-coiled domain and the C-ERMAD (residues 467-503 in ezrin) from various ERMs highlighting the disordered region in the *Sf*Moesin structure (italics) and the substitution made to introduce an internal flag tag into *Hs*Ezrin (red). (B) Anti-flag and anti-ezrin two-color fluorescent Western blot showing the stable incorporation of internally flag-tagged ezrin (which runs faster than untagged ezrin) and phosphomutants in Jeg-3 cells. (C) EBP50 immunoprecipitates from cells treated or untreated with DSP as indicated, Western blotted with anti-Flag. (D) EBP50 immunoprecipitates from stable cell-lines expressing indicated ezrin-iFlag protein and treated with DSP, Western blotted with anti-Flag.

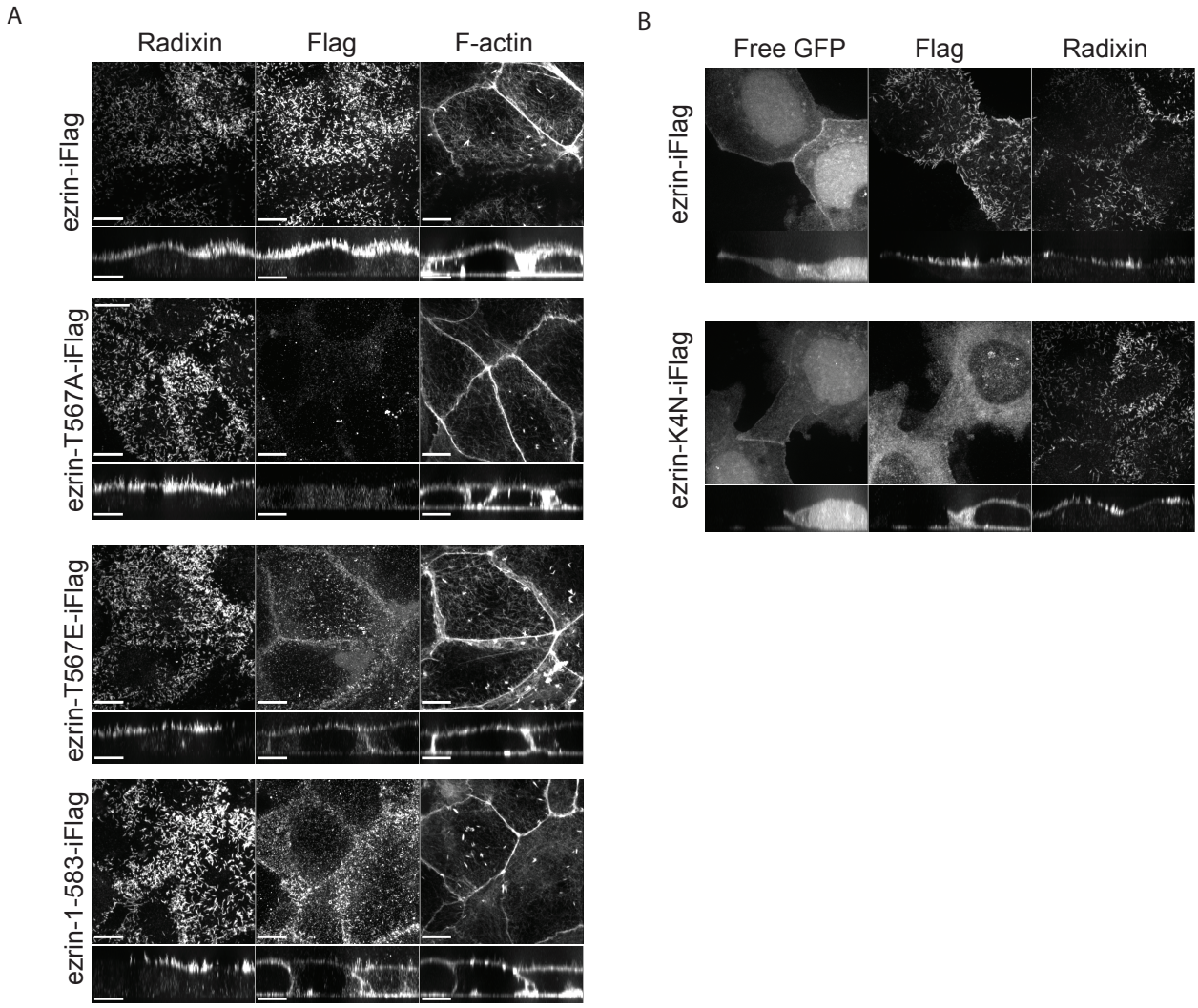

Figure 2.2 Ezrin-iFlag localization in microvilli is dependent on phosphocycling, conformation switching, and lipid interaction .

(A) Three-color, confocal immunofluorescent detection of radixin, flag, and F-actin (phalloidin) in stable cell-lines expressing indicated ezrin-iFlag protein shown *en face* (upper panels) and as a projection of Z-stacks through a vertical cross-section, stretched 5-fold (lower panels). (B) Transient transfection of wild-type ezrin-iFlag or K4N mutant (K253N,K254N,K262N,K263N) expressed in internal-ribosome-entry vectors, allowing bicistronic expression of free GFP as a reporter of the transfection level.

more. The difference between T567E and 1-583 can be accounted for by considering the difference in openness between these two mutants, as Chambers and Bretscher measured in similar mutants (Chambers and Bretscher, 2005).

I next examined the localization of the ezrin-iFlag constructs in the stable cell-lines (Figure 2.2). Ezrin and radixin have identical localizations in Jeg-3 cell microvilli (D. Chambers, unpublished). Wild-type ezrin-iFlag localized just like endogenous radixin in microvilli, whereas the T567A mutant was predominantly cytoplasmic (Figure 2.2.A). Interestingly, the amount of staining was also reduced, suggesting that the protein was partially extracted during the immunofluorescence procedure. Both the T567E mutant and the 1-583 mutant were distributed evenly along the membrane rather than being concentrated in microvilli (Figure 2.2.A), suggesting that conformation switching is important for accumulation of ezrin in apical microvilli, which is explored further in chapter 3. Importantly, taken together with the EBP50 IP results (Figure 2.1.D) and the fact that 1-583 is more open that T567E (Chambers and Bretscher, 2005), these data suggest that DSP-assisted immunoprecipitations integrate binding affinity and localization: whereas wild-type ezrin co-localizes with EBP50 very well, only a portion (the activated form) binds tightly; whereas T567E ezrin binds tightly to EBP50, only a portion of it co-localizes with EBP50; 1-583 localizes as poorly with EBP50, but binds it extremely tightly whenever it comes in contact with it.

Activation of ezrin by phosphorylation has been suggested to be preceded by PIP_2 binding both *in vitro* (Pietromonaco et al., 1998; Hirao et al., 1996) and *in vivo* (Fievet et al., 2004). Therefore, I also examined the effect of mutations that block PIP_2-binding. The so-called K4N (K253N, K254N, K262N, K263N) mutant, which has reduced binding to $PI(4,5)P_2$ *in vitro* (Barret et al., 2000) also failed to localize to microvilli in Jeg-3 cells (Figure 2.2.B).

A.

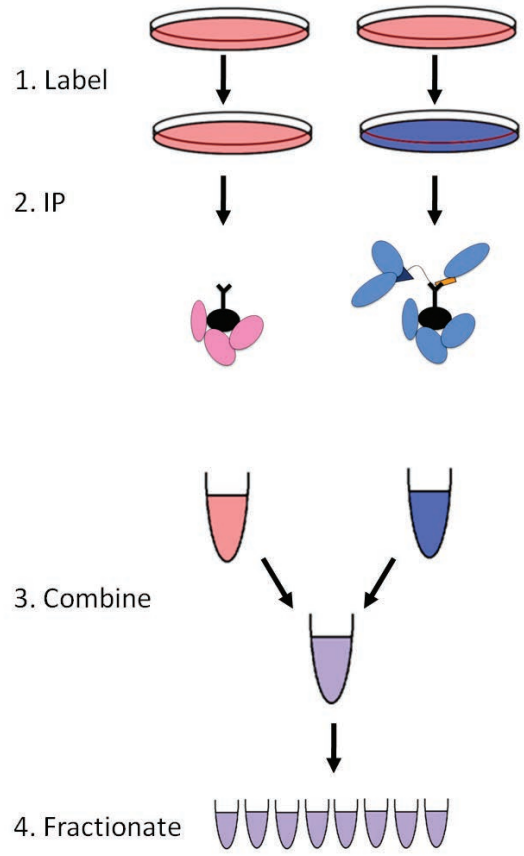

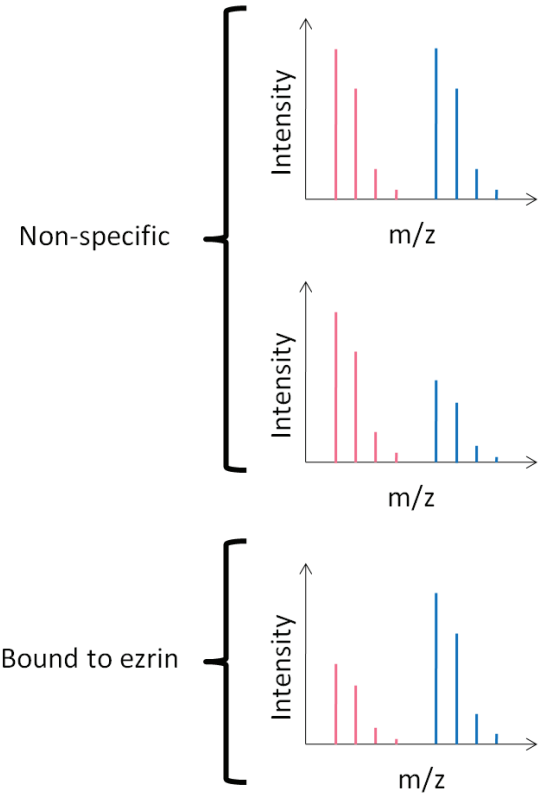

B.

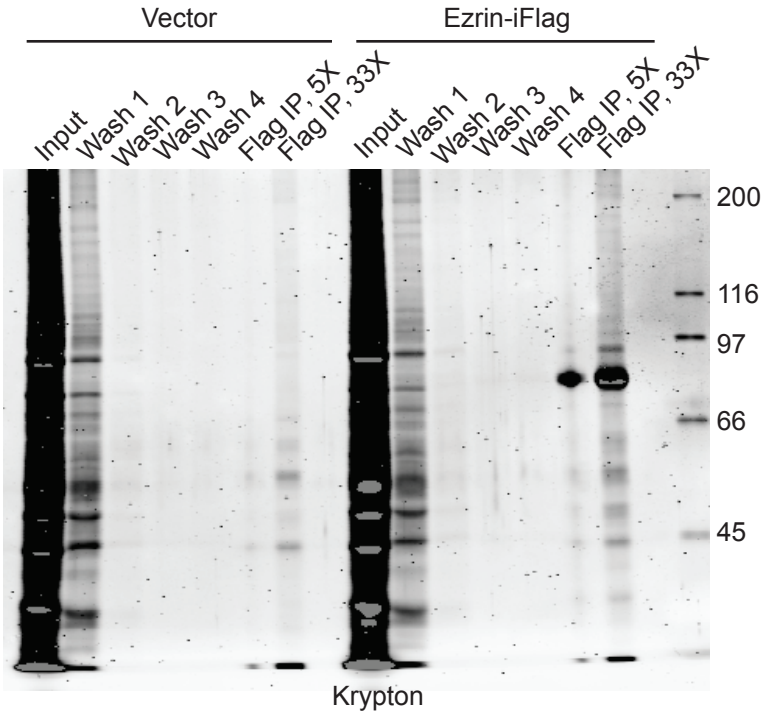

C.

	Ezrin-iFlag/Control	# Peptides	
Candidates			
FHOD-1	18.9	13	
TROP-2	18.0	9	
CLIC-4	17.7	2	*
JAM-A	17.5	6	
Radixin (Unique)	16.1	26	*
RasGAP-1	12.6	6	
Syndecan-2	12.1	3	*
EBP50	10.6	17	*
PACE-1	9.8	10	*
β-Dystroglycan	9.8	10	*
BASP-1	8.7	5	
ATP11C	6.6	6	
EGF-R	6.2	5	
LOK	5.3	13	
CLIC-3	5.1	16	*
β1-Integrin	4.7	11	
SLK	3.8	9	
Claudin-6	3.2	2	
ATB(0)	3.0	5	

	Ezrin-iFlag/Control	# Peptides
Selected Background		
α-Enolase	2.7	51
IQGAP	1.9	85
Fatty acid synthase	1.8	120
Dynein-1 H. C.	1.6	61
p97 VCP	1.2	45
GRP78	0.5	81
52 kDa Ro Protein	0.5	76

Figure 2.3 The ezrin interactome as identified by SILAC-mass spectometry

(A) Graphical outline of the stable-isotope labeling of amino acids in cell culture (SILAC) procedure as applied to identifying the ezrin interactome. Peptides are labeled by feeding C-13- (heavy) or C-12- (light) -containing amino acids (1), the DSP-assisted immunoprecipitation is performed from cells stably expressing ezrin-iFlag or control cells (2), the immunoprecipitates are combined (3), and fractionated using hydrophobic interaction liquid chromatography (4). Proteins are then proteolyzed and subjected to mass spectrometry, where the sequence and heavy/light ratio is determined. Proteins bound to ezrin will have high ratios, whereas bead-binding background proteins will have ratios close to 1. (B) Fractions from the immunoprecipitations resolved by SDS-PAGE. (C) A list of candidate interactors (those for which two peptides were found with an average enrichment greater than 3.0) and selected bead-binding background (those for which at least 40 peptides were found with an average enrichment less than 3.0) highlighting known ERM interactors (red asterisks).

Identification of 19 proteins bound to ezrin-iFlag

In order to determine whether the interaction of other proteins with ezrin also depended upon conformational and phosphorylation status, I compared ezrin-iFlag mutant immunoprecipitates. To begin these studies, it was necessary to first determine the interactome of wild-type ezrin-iFlag in Jeg-3 cells. To do this, I used the SILAC procedure (Ong et al., 2002). Briefly, two populations of cells were shifted into medium containing heavy (C-13) or light (C-12) arginine and lysine. One population was stably transfected with an empty vector, whereas the other expressed ezrin-iFlag. Both populations were subjected to parallel DSP-assisted immunoprecipitations, which recovers bead-binding background proteins in both populations, but also ezrin-iFlag-binding proteins in one population. The immunoprecipitates are combined and trypsin-digested. The tryptic fragments are subjected to hydrophobic interaction liquid chromatography, an orthogonal separation technique, and fractionated to reduce complexity. Each fraction is then analyzed by an Orbitrap mass spectrometer (Figure 2.3.A), which determines the ratio of heavy to light peptides and then determines the sequence of the peptide. Prior to trypsin-digestion, a small aliquot of the sample was resolved by SDS-PAGE (Figure 2.3.B). This revealed a host of proteins bound to ezrin-iFlag, whereas no single binding partner approached ezrin-iFlag abundance (Figure 2.3.B) This suggests that the vast majority of ezrin is unbound to any specific ligand in cells (Figure 2.3.B).

A list of proteins for which greater than two peptides with a mean enrichment greater than 3.0 is presented in Figure 2.3.C. Besides EBP50, other candidates have been previously identified as ERM-binding proteins (Figure 2.3.C, red asterisks), validating the results. These included proteins interacting with the ezrin FERM domain such as radixin, syndecan-2 (Granes et al., 2000; Granes et al., 2003), β-dystroglycan (Spence et al., 2004; Batchelor et al., 2007), as

A.

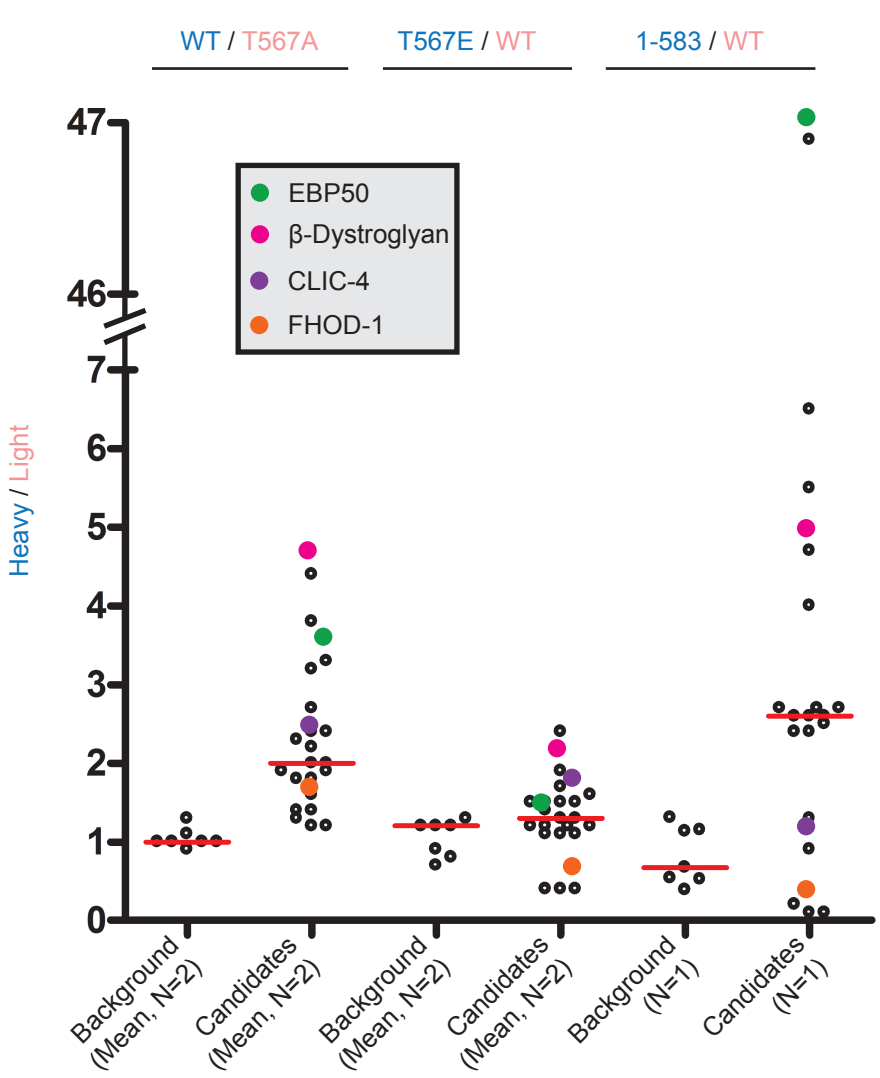

B.

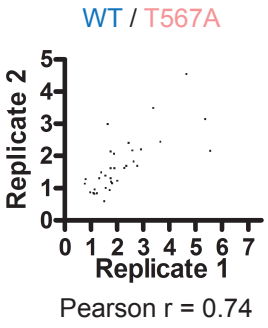

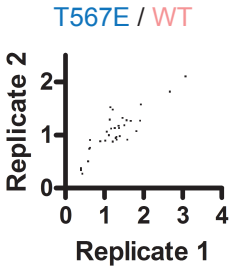

C.

	WT/T567A	T567E/WT	1-583/WT	# of peptides	
Class I - EBP50					
EBP50	3.2	1.2	46.9	152	*

	WT/T567A	T567E/WT	1-583/WT	# of peptides	
Class II - β-Dystroglycan-like					
Radixin (Unique)	2.0	1.2	2.7	460	*
LOK	2.2	1.3	2.4	85	
β-Dystroglycan	4.4	1.9	4.7	76	*
β1-Integrin	1.4	1.6	2.6	68	
SLK	2.0	1.5	5.5	60	
ATB(0)	2.4	1.2	2.7	58	
ATP11C	3.8	2.4	6.8	57	
JAM-A	1.8	1.7	4.0	54	
TROP-2	3.3	1.2	2.6	39	
EGF-R	1.4	1.1	2.6	39	
Syndecan-2	2.4	1.5	1.7	21	*
Claudin-6	1.6	1.4	2.5	13	

	WT/T567A	T567E/WT	1-583/WT	# of peptides	
Class III - CLIC-4-like					
CLIC-3	2.3	1.5	0.9	108	*
CLIC-4	1.9	1.2	1.3	29	*

	WT/T567A	T567E/WT	1-583/WT	# of peptides
Class IV - FHOD-1-like				
FHOD-1	1.3	0.4	0.1	231
RasGAP-1	1.2	0.4	0.1	44
PACE-1	1.2	0.4	0.2	39

	WT/T567A	T567E/WT	1-583/WT	# of peptides
Inadequate data				
BASP-1	2.7	1.5	ND	21

	WT/T567A	T567E/WT	1-583/WT	# of peptides
Selected Background				
Fatty acid synthase	1.0	0.7	0.6	856
IQGAP	1.0	1.2	1.0	745
GRP78	1.0	1.2	1.3	515
Dynein-1 H. C.	1.0	0.8	0.5	486
α-Enolase	1.0	0.9	0.5	408
52 kDa Ro Protein	1.3	1.2	1.1	347
p97 VCP	0.9	1.3	0.7	284

D.

	Pearson r	p-value	Significant?
Class II	0.58	0.03	Yes
Background	0.31	0.68	No

Figure 2.4 The candidate ezrin interactors respond in four different ways to manipulations of ezrin conformation.

(A) Result of SILAC experiment comparing wild-type ezrin-iFlag (Figure 2.3) to each indicated conformation mutant showing which population was labeled heavy (blue) or light (pink). Plots enrichment of each candidate ezrin interactor or selected bead-binding background protein in Figure 2.3.C on the heavy vs. light ezrin-iFlag protein highlighting a representative of each interactor class. Red line indicates mean enrichment of all proteins plotted. Class I (green): prefers wild-type to T567A, no preference for T567E, and an enormous preference for 1-583 (note: Y-axis cut); Class II (magenta): prefers wild-type to T567A, mild preference for T567E, and a slightly greater preference for 1-583; Class III (purple): prefers wild-type to T567A, no preference for T567E, no preference for 1-583; Class IV (orange): no preference for wild-type vs. T567A, prefers wild-type over T567E, prefers wild-type over 1-583. (B) Plot of each biological replicate for given SILAC experiment against the other, showing that the enrichment statistics are reproducible. (C) List of proteins contained in each class highlighting known interactors (red asterisks). (D) Pearson correlation between WT vs. T567A and T567E vs. WT for Class II and bead-binding background proteins.

well as proteins interacting with C-terminus of ezrin, including chloride ion chanel-3 and -4 (CLIC-3 and -4; Berryman and Bretscher, 2000) and Protein Associated with the C-terminus of Ezrin (PACE-1; Sullivan et al., 2003). Representative bead-binding background proteins were also selected as controls in future analyses (Figure 2.3.C, lower section). I did not obtain the very first ERM-binding protein ever identified, CD44, as it is not expressed in these cells (data not shown). I also failed to identify many of the known mammalian ERM interaction partners (Figure 2.3.C; Table 1.1), but I have not explored the reason in any other case.

Interactors respond differently to changes in ezrin activation

To determine how ezrin conformation affects its interactome, I performed SILAC comparisons of DSP-assisted immunoprecipitates from wild-type ezrin-iFlag ('WT') relative to either ezrin-T567A-iFlag ('T567A'), ezrin-T567E-iFlag ('T567E'), or ezrin-1-583-iFlag ('1-583'). The results are presented in Figure 2.4. Two biological replicates of WT vs. T567A and T567E vs. WT were performed, and a moderately high Pearson's correlation suggests that the enrichment statistics of the binding partners are reasonably reproducible (Figure 2.4.B), but more importantly, the same proteins were found in both sets with almost no deviations. I found that the ezrin interaction partners fell into four classes (I-IV). Class I was EBP50, which reacted to the ezrin changes uniquely. EBP50-binding was decreased by ezrin T567A mutation, unmoved by T567E mutation, and dramatically increased by 1-583 mutation. I propose that these changes are an integration of binding and co-localization between ezrin-iFlag and EBP50, the latter only present on the plasma membrane in microvilli, regardless of ezrin location (data not shown). Binding to Class II partners (the predominant and expected class) was also decreased by T567A mutation, but moderately increased by either T567E mutation or 1-583 truncation. Interestingly, there was a statistically significant correlation between the decrease in affinity for T567A and the

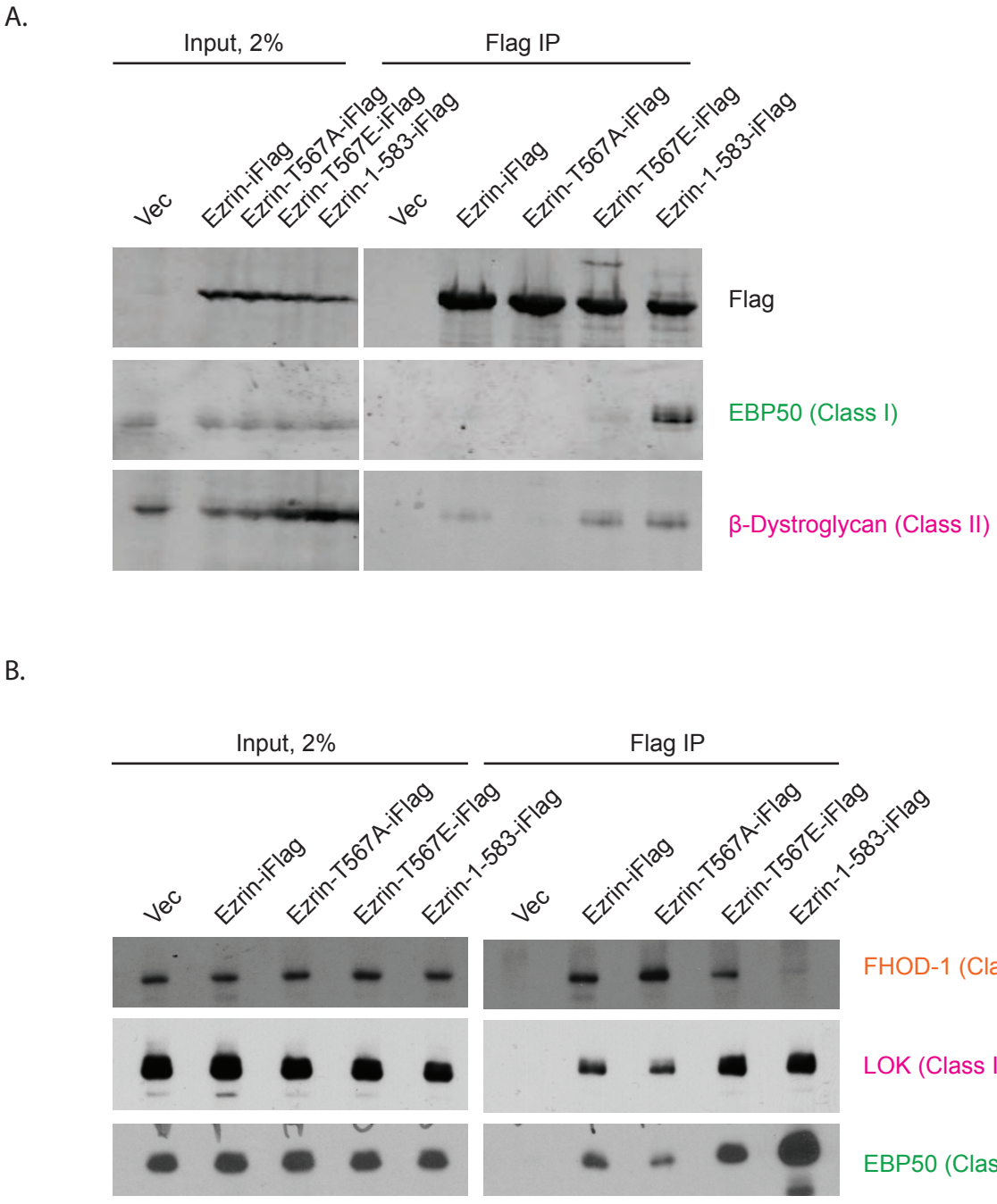

Figure 2.5 Confirmation of selected interactions by DSP-crosslinking immunoprecipitation and Western blot.

(A,B) Crosslinking flag immunoprecipitates from stable cells expressing the indicated ezrin-iFlag protein were Western blotted for indicated protein with indicated class designation (Figure 2.4).

increase in affinity for T567E (Figure 2.4.C). Thus binding to these ligands may be largely based on ezrin conformation, but their weak affinity for open ezrin may preclude spectacular binding as is seen with EBP50. Binding to Class III partners (the CLICs) was also decreased by T567A mutation, but it was unchanged in both hyperactivated mutants. Ezrin interaction with these proteins may be limited by another mechanism besides conformation switching, such as binding to a second ligand or membrane translocation. Finally, binding to Class IV partners (the formin FHOD-1, PACE-1, and RasGAP-1) was largely unchanged by T567A mutation and *decreased* in hyperactivated mutants. Thus conformation is perceived differently for different ligands.

Along with Jessica Wayt, I confirmed the results of the mass spectrometry experiments by manual immunoprecipitation and western blotting using available antibodies. As predicted EBP50, β-dystroglycan, and LOK preferred more open forms of ezrin, whereas FHOD-1 preferred more closed forms of ezrin (Figure 2.5).

Some novel Class II interactors localize in microvilli

I next examined the localization of several candidates. Given that they consistently bind more activated ezrin, Class I and Class II interactors should be components of microvilli. Consistently, EBP50 (Reczek et al., 1997) and β-dystroglycan (Spence et al., 2004) are highly enriched in microvilli. Although we did not verify the localization of Syndecan-2 and β-1 integrin, each (Granes et al., 2000; Garbi et al., 1996) has been shown to be a component of filopodia in fibroblastic cell-lines. Next, I focused on the novel candidates. These were expressed as affinity tag-fusions and localized in Jeg-3 cells. TROP-2 strongly localizes in microvilli, and ATP11C, ATB(0), and BASP-1 were distributed throughout the plasma membrane, although they demonstrated an apical bias (Figure 2.6). CLIC-4 and a related family member CLIC-5 were

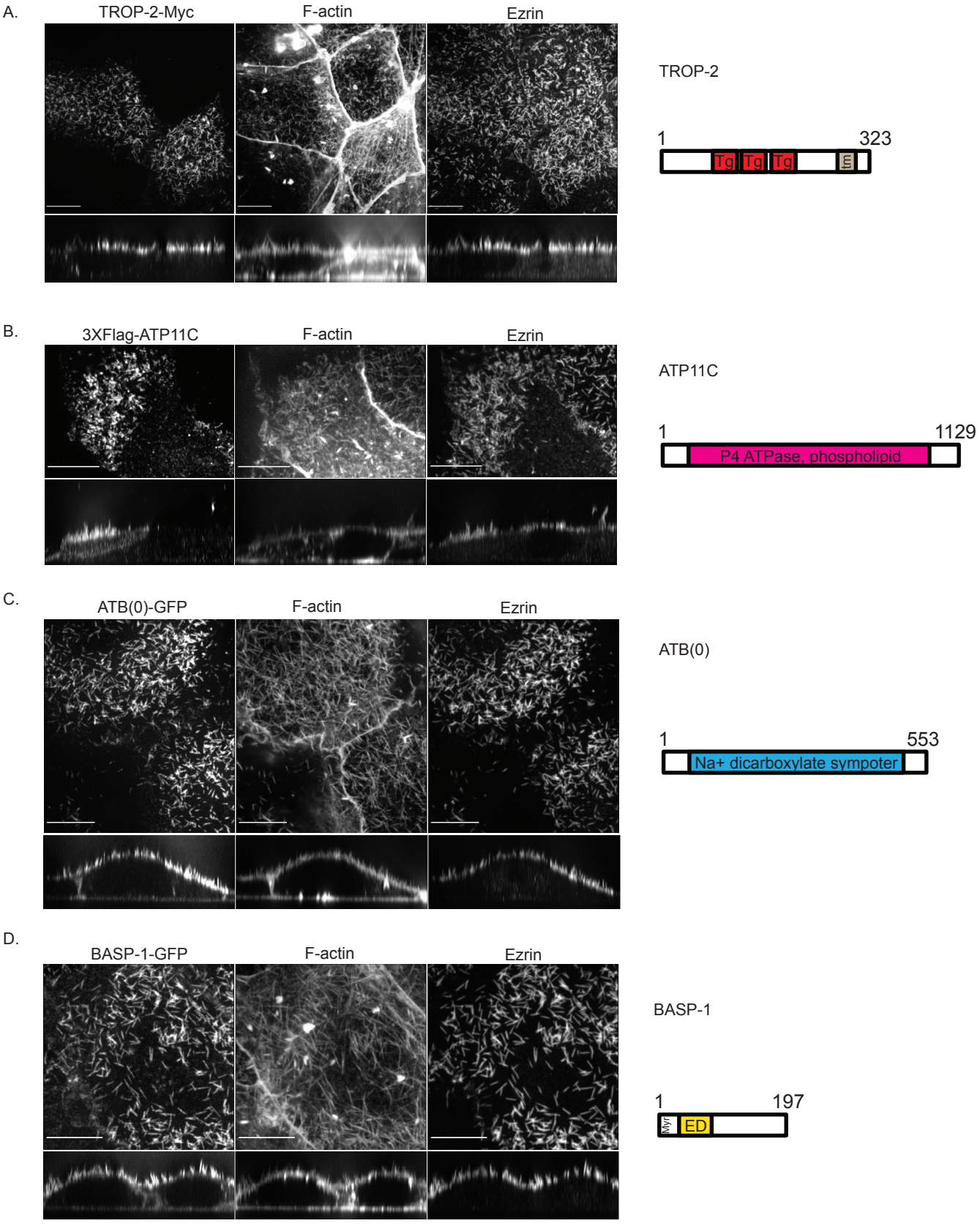
A.
TROP-2-Myc
F-actin
Ezrin
TROP-2
1
323
Tg
Tg
Tg
tm
B.
3XFlag-ATP11C
F-actin
Ezrin
ATP11C
1
1129
P4 ATPase, phospholipid
C.
ATB(0)-GFP
F-actin
Ezrin
ATB(0)
1
553
Na+ dicarboxylate sympoter
D.
BASP-1-GFP
F-actin
Ezrin
BASP-1
1
197
Myr
ED

Figure 2.6 Microvillus localization of selected novel candidates.

(A,B) Three-color, confocal immunofluorescent detection of TROP2-myc (A) or 3XFlag-ATP11C (B) along with F-actin (phalloidin) and ezrin following transient transfection of Jeg-3 cultures *en face* (upper panels) or as a projection of Z-stacks through a vertical cross-section, stretched 5-fold (lower panels). (C,D) Three-color, confocal immunofluorescent detection of ATB(0)-GFP (C) or BASP1-GFP (D) along with F-actin (phalloidin) and ezrin following stable transfection and selection of Jeg-3 cultures. Schematics of the proteins are provided at right. *Tg*, Thyroglobulin repeat; *ED*, Basic Effector Domain.

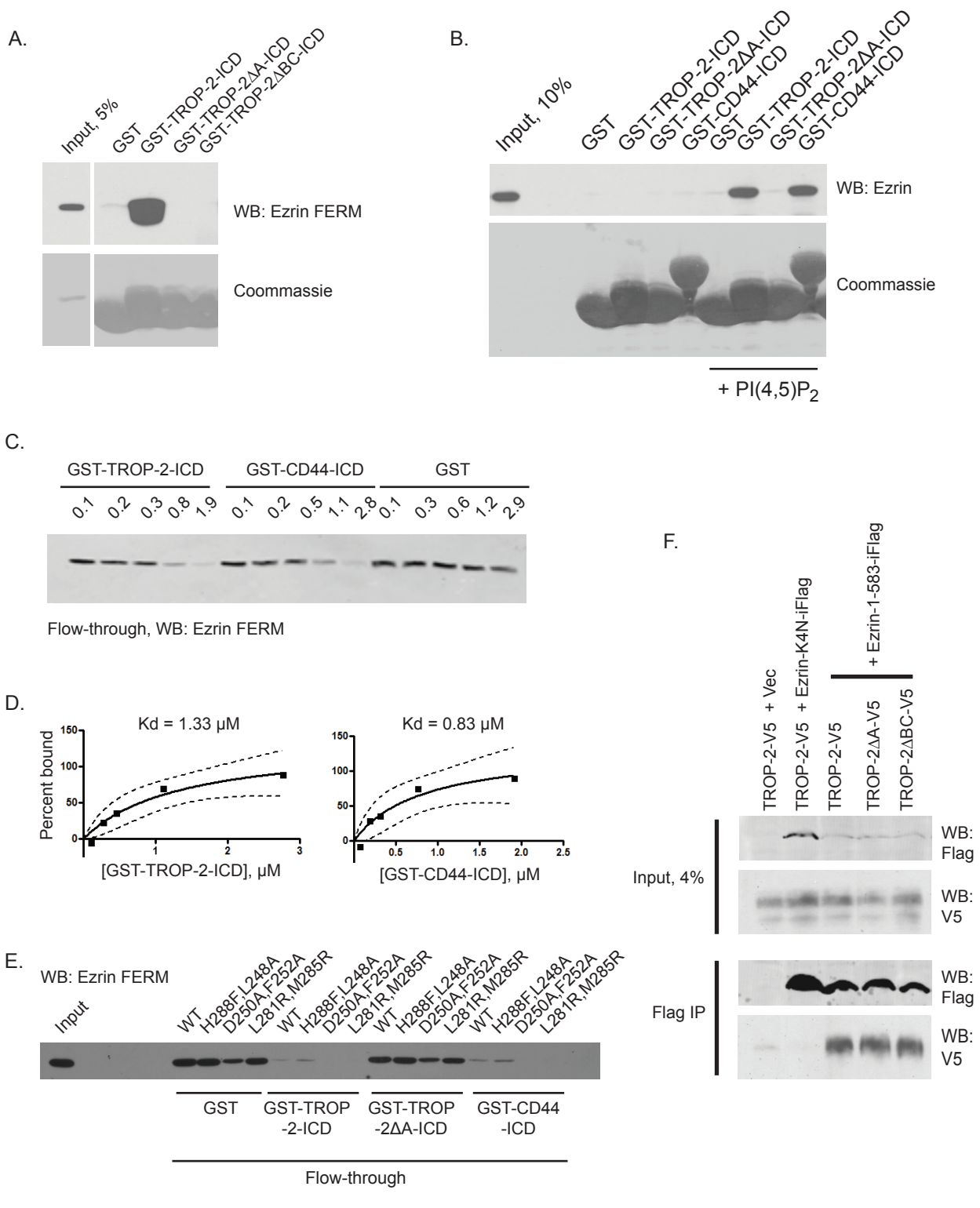
A.
Input, 5%
GST
GST-TROP-2-ICD
GST-TROP-2ΔA-ICD
GST-TROP-2ΔBC-ICD
WB: Ezrin FERM
Coommassie
B.
Input, 10%
GST
GST-TROP-2-ICD
GST-TROP-2ΔA-ICD
GST-CD44-ICD
GST
GST-TROP-2-ICD
GST-TROP-2ΔA-ICD
GST-CD44-ICD
WB: Ezrin
Coommassie
+ PI(4,5)P2
C.
GST-TROP-2-ICD
GST-CD44-ICD
GST
0.1 0.2 0.3 0.8 1.9
0.1 0.2 0.5 1.1 2.8
0.1 0.3 0.6 1.2 2.9
Flow-through, WB: Ezrin FERM
D.
Kd = 1.33 μM
Kd = 0.83 μM
Percent bound
[GST-TROP-2-ICD], μM
[GST-CD44-ICD], μM
E.
WB: Ezrin FERM
Input
WT
H288F,L248A
D250A,F252A
L281R,M285R
GST
GST-TROP -2-ICD
GST-TROP -2ΔA-ICD
GST-CD44 -ICD
Flow-through
F.
TROP-2-V5 + Vec
TROP-2-V5 + Ezrin-K4N-iFlag
+ Ezrin-1-583-iFlag
TROP-2-V5
TROP-2ΔA-V5
TROP-2ΔBC-V5
Input, 4%
WB: Flag
WB: V5
Flag IP
WB: Flag
WB: V5

Figure 2.7 BASP-1 is marginally required for microvilli and localizes to the microvilli through its basic effector domain which may interact with negatively-charged plasma membrane phospholipids.

(A) Ezrin-iFlag or an empty vector were co-transfected with BASP-1-GFP expression plasmid into Jeg-3 cells, and ezrin-iFlag immunoprecipitated with or without DSP cross-linking. The results show very marginal, DSP-independent co-precipitation of BASP1-GFP. (B) Cells were transfected with the indicated siRNAs for 3 days, then fixed and stained for ezrin, and the percentage of cells with microvilli scored. Ezrin depletion causes the loss of ~40% of microvilli-baring cells, while two siRNAs targeting BASP1 but not control cause a very mild loss of ~20% of microvilli-baring cells. Non-targetting GL2 luciferase siRNA ('siGL2') or an siRNA against ATP11C had no effect. (C) Immobilized, CNBr-coupled ezrin FERM domain was incubated with Jeg-3 cell extract transfected with BASP1-GFP expression plasmid where indicated in the presence or absence of $PI(4,5)P_2$ micelles. The results suggest that PIP_2 can bridge an interaction between ezrin and BASP1-GFP *in vitro*. (D) BASP1-GFP or mutants were transfected and localized relative to ezrin staining in Jeg-3 cells. Deletion or mutation of the basic effector domain of BASP1 prevents localization to microvilli and the plasma membrane. (E) A small region of the apical domain of a BASP1-GFP-expressing, ezrin-stained cell was blown up to reveal that BASP1-GFP can be seen in a number of apical membrane structures devoid of ezrin staining.

both shown to be components of microvilli, correlating with their activation-dependent interaction with ezrin (Berryman and Bretscher, 2000; Chuang et al., 2010). By contrast, the two examined Class IV members, PACE-1 and FHOD-1, were not found in microvilli: PACE-1 accumulates on Golgi membranes and in the cytoplasm (Sullivan et al., 2003), while FHOD-1 is predominantly cytoplasmic (Jessica Wayt, personal communication). Thus the dependence of an interactor on ezrin conformational openness appears to be a clear predictor of its localization in microvilli.

Investigations of BASP-1 in Jeg-3 cells

In order to investigate the role of the novel interactions, I more closely examined BASP-1 (brain acid-soluble protein-1) and TROP-2 (trophoblast antigen-2). BASP-1 interacted very weakly with ezrin-iFlag, but the interaction did not depend upon DSP cross-linking (Figure 2.7.A). Two siRNAs against BASP-1 were found to cause mild loss of microvilli compared to ezrin depletion (Figure 2.7.B), suggesting that BASP-1 is necessary for ezrin accumulation in microvilli. *In vitro* (Zakharov and Mosevitsky, 2010; Takaichi et al., 2012) and *in vivo* (Takaichi et al., 2012; Toska et al., 2012) analysis of BASP-1 and its homology to MARCKS and GAP43 (Mosevitsky et al., 1997) suggest that it binds to and regulates $PI(4,5)P_2$ levels or clustering in cells through a group of basic residues in the extreme N-terminus called a "basic effector domain" or "ED" (see diagram in Figure 2.6). To test whether $PI(4,5)P_2$ was necessary for the interaction between BASP-1 and ezrin, bacterially-expressed FERM domain was purified, coupled to resin by CNBr crosslinking, and added to cell extract containing BASP-1-GFP. I found that the FERM domain could pull down BASP-1-GFP only if it was mixed with micellar $PI(4,5)P_2$ in the method of Tsukita and colleagues (Hirao et al., 1996; Figure 2.7.C), suggesting that the interaction is dependent upon high levels of $PI(4,5)P_2$. Others have determined that the

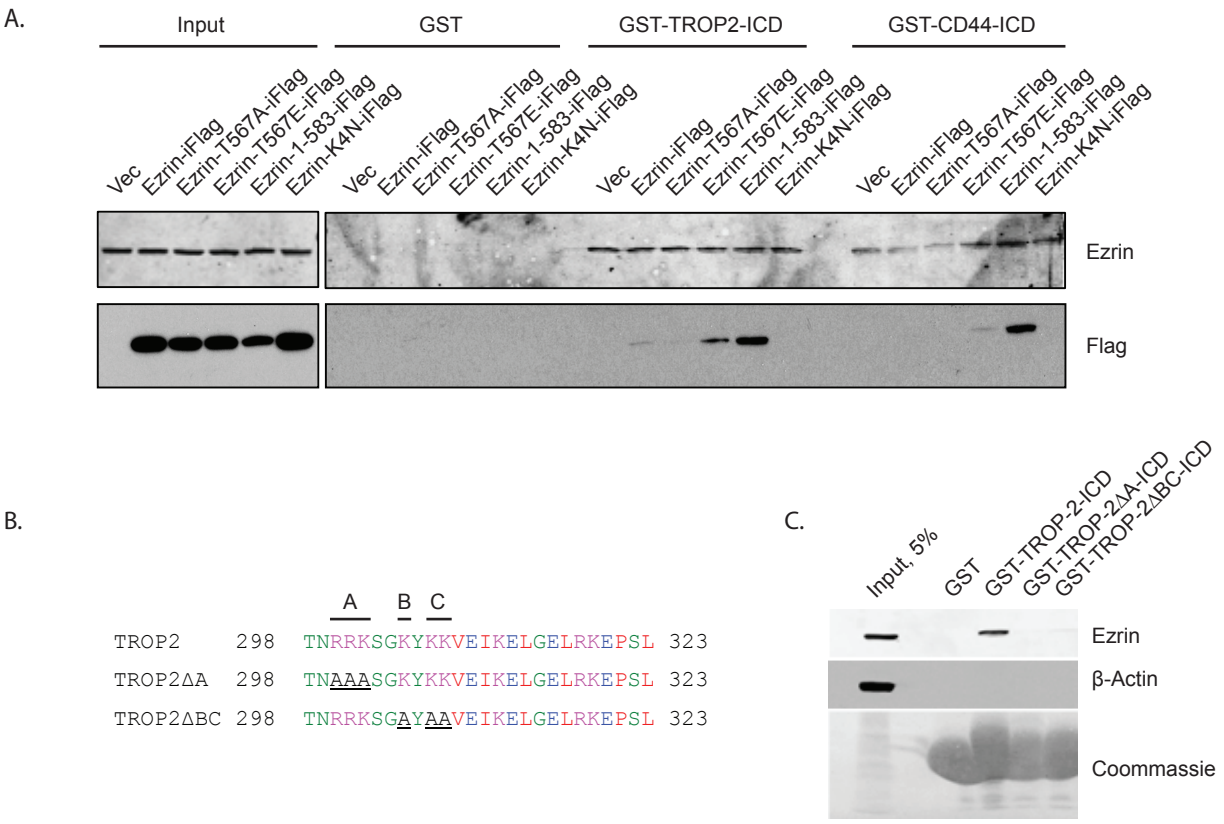

Figure 2.8 Immobilized TROP-2 binds to ezrin in cell lysate prepared in low-ionic strength buffers

(A) Alignment of the TROP-2 and TROP-1 cytoplasmic tails. (B) Glutathione resin containing GST-fused TROP-2 but not TROP-1 cytoplasmic tail retrieves ezrin from a complex lysate prepared in 40 mM salt buffer, similarly to the positive control CD44 cytoplasmic tail. (C) The GST-fused TROP-2 and CD44 tails but not GST alone selectively retrieve more conformationally open forms of ezrin from a cell lysate prepared in 40 mM salt buffer. (D) Sequence alignment of TROP-2 tail highlighting three basic segments (A, B, C) and two mutants which remove selected patches by alanine mutagenesis as indicated. (E) Glutathione resin containing GST-fused TROP-2 but not TROP-2 basic patch mutants retrieves ezrin from a complex lysate prepared in 40 mM salt, whereas other such as actin are left behind.

ED is needed for the interaction with $PI(4,5)P_2$ (Takaichi et al., 2012; Toska et al., 2012). Consistently, the ED was necessary for BASP-1's localization to the plasma membrane and microvilli, as deleting or neutralizing it greatly diminished its plasma-membrane and microvilli enrichment (Figure 2.7.D). BASP-1-GFP also marked regions of the plasma membrane that were not (yet) positive for ezrin following fixation and immunostaining, suggesting that BASP-1 can translocate to the plasma membrane independently of ezrin.

Investigations of the TROP-2-ezrin interaction *in vitro*

I also examined the Class II interactor TROP-2, a transmembrane protein highly expressed in normal trophoblasts as well as in gastrointestinal and pancreatic cancers, where its upregulation may be necessary for cancer progression (Basak et al., 1998; Fornaro et al., 1995; Wang et al., 2008; Schon and Orfanos, 1995; Guerra et al., 2012; Trerotola et al., 2012; Wang et al., 2011). I began by attempting GST-pulldowns according to Legg and Isacke to see whether GST-fusions of the short TROP-2 intracellular tail can precipitate ezrin from a lysate prepared in low (40 mM) salt as has been shown for that of CD44 (Legg and Isacke, 1998). Both GST-TROP-2 tail and control tail GST-CD44 could precipitate endogenous ezrin whereas GST alone could not (Figure 2.8.A). Furthermore, when ezrin-iFlag mutants were transfected into Jeg-3 cells, both GST-TROP-2 and GST-CD44 displayed a preference for binding to only the activated forms of ezrin-iFlag from low-salt extracts (Figure 2.8.A). Ezrin binding in these assays has been proposed to proceed through ezrin recognition of juxtamembrane basic patches within the intracellular tails (Yonemura et al., 1998; Legg and Isacke, 1998; Serrador et al., 2002; Hamada et al., 2000). The sequence of the predicted cytoplasmic tail of TROP-2 contains three such patches of basic residues (A, B, C; Figure 2.8.B). Mutating patch A, or B and C in combination to alanine, effectively neutralizing the charge, prevents the interaction with ezrin (Figure 2.8.C).

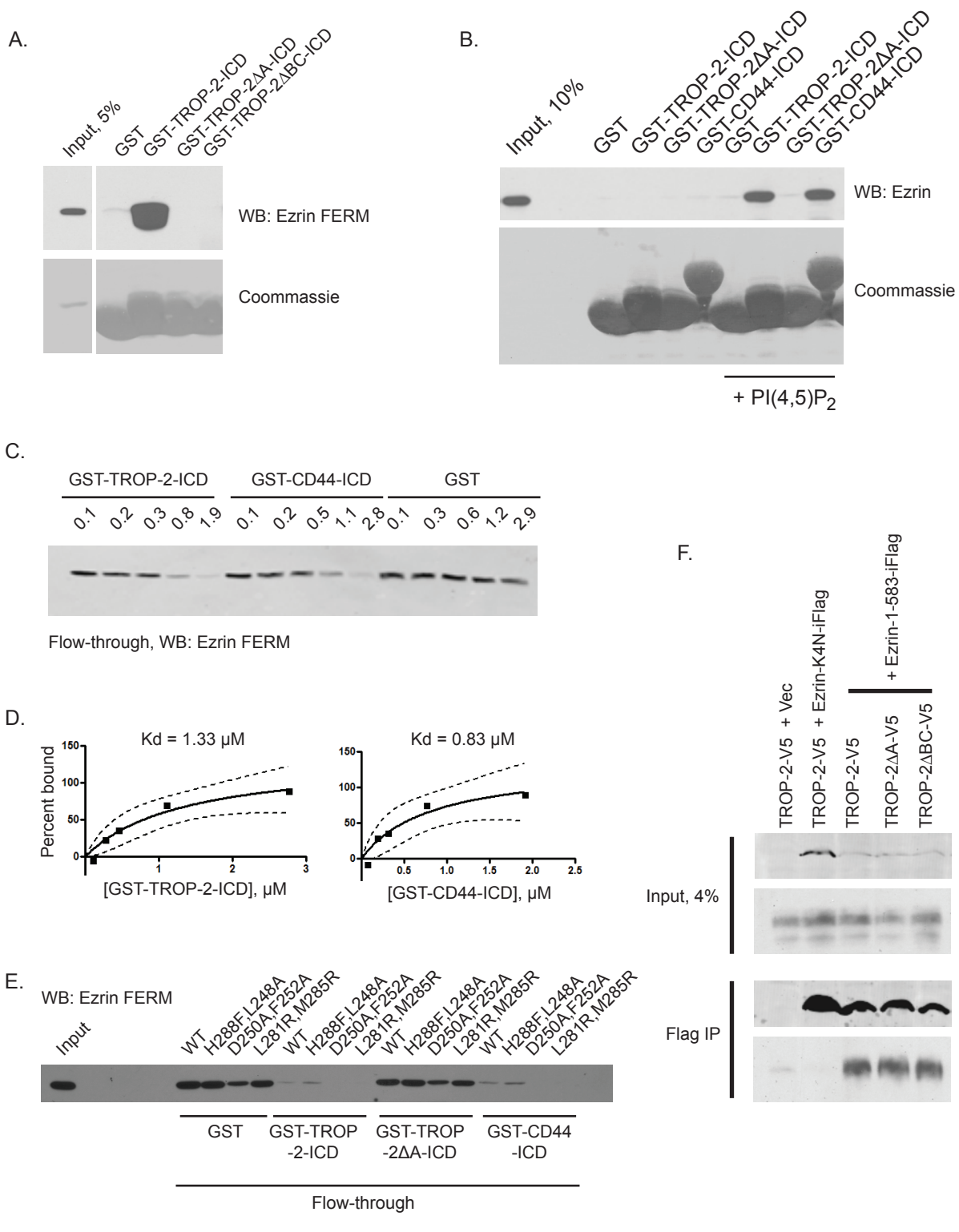
A.
Input, 5%
GST
GST-TROP-2-ICD
GST-TROP-2ΔA-ICD
GST-TROP-2ΔBC-ICD
WB: Ezrin FERM
Coommassie
B.
Input, 10%
GST
GST-TROP-2-ICD
GST-TROP-2ΔA-ICD
GST-CD44-ICD
GST
GST-TROP-2-ICD
GST-TROP-2ΔA-ICD
GST-CD44-ICD
WB: Ezrin
Coommassie
+ PI(4,5)P2
C.
GST-TROP-2-ICD
GST-CD44-ICD
GST
0.1 0.2 0.3 0.8 1.9
0.1 0.2 0.5 1.1 2.8
0.1 0.3 0.6 1.2 2.9
Flow-through, WB: Ezrin FERM
D.
Kd = 1.33 μM
Kd = 0.83 μM
Percent bound
[GST-TROP-2-ICD], μM
[GST-CD44-ICD], μM
E.
WB: Ezrin FERM
Input
WT
H288F,L248A
D250A,F252A
L281R,M285R
GST
GST-TROP -2-ICD
GST-TROP -2ΔA-ICD
GST-CD44 -ICD
Flow-through
F.
TROP-2-V5 + Vec
TROP-2-V5 + Ezrin-K4N-iFlag
+ Ezrin-1-583-iFlag
TROP-2-V5
TROP-2ΔA-V5
TROP-2ΔBC-V5
Input, 4%
WB: Flag
WB: V5
Flag IP
WB: Flag
WB: V5

Figure 2.9 Immobilized TROP-2 strongly interacts with the FERM domain of ezrin *in vitro* in physiological buffer, but there are additional determinants for the interaction *in vivo*.

(A) Glutathione resin containing GST-fused TROP-2 but not TROP-2 basic patch mutants retrieves ezrin FERM in physiological salt buffer. (B) GST-fused TROP-2 but not TROP-2 basic patch mutants retrieves full-length ezrin in physiological buffer only when soluble $PI(4,5)P_2$ is added to the solution, similarly to the positive control CD44 cytoplasmic tail. (C) Ezrin FERM was depleted from solution by addition of varying concentrations of immobilized GST-TROP-2 or GST-CD44 cytoplasmic tails, and the flow-through analyzed by Western blot. (D) The percent of starting FERM domain bound to the resin was calculated and plotted, and the resulting curve used to determine the Kd. (E) Indicated, immobilized, GST-fused cytoplasmic tail was mixed with FERM domain mutants baring indicated mutations and the flow-through analyzed by Western blot. (E) Indicated TROP-2 mutants in the context of full-length TROP-2-V5 were transiently transfected in cells along with indicated ezrin-iFlag mutant. Mutations in TROP-2 that block the interaction with the FERM domain *in vitro* (panels A, B, E) and ezrin in lysate binding experiments (Figure 2.7.D,E) fail to disrupt the interaction *in vivo*.

Interestingly, while GST-pulldown-type interactions with either TROP-2 or CD44 were exquisitely salt-sensitive (disappearing entirely in 75 mM salt), *in vitro* binary interactions in the absence of lysate was more tolerant of buffers containing salt concentrations (up to 175 mM; data not shown). This may have been because the presence of some factor in cell lysate affects charge-screening. Nonetheless, it allowed me to more stringently analyze the interaction entirely *in vitro*. I used the physiological salt buffer system of Denker and Barber to test binding of GST-tagged tails to the untagged FERM domain of ezrin *in vitro* (Denker et al., 2000; Denker and Barber, 2002). Similar to the GST-pulldown experiment, GST-TROP-2 tail bound to the FERM domain only when the basic patches were present (Figure 2.9.A). Full-length ezrin is autoinhibited *in vitro*, but this inhibition can be released by addition of $PI(4,5)P_2$ micelles, which then allows binding of the FERM domain to transmembrane tails (Hirao et al., 1996). I used this system to test whether basic patch interaction with the FERM domain was entirely sufficient to explain ezrin interaction with TROP-2. Even full-length ezrin activated by $PI(4,5)P_2$ micelles failed to interact with TROP-2 lacking the basic patches, thus confirming that the interaction between TROP-2 and ezrin proceeds through the juxtamembrane basic patches (Figure 2.9.B).

To explore this interaction further, I measured the K_d by varying the concentration of GST-fusion protein and measuring the amount of ezrin depleted from the flow-through. These experiments determined that the K_d was around 1 μM for both TROP-2 and CD44 tails (Figure 2.9). By crystalizing radixin bound to CD44 tail, the interaction was thought to proceed by the cytoplasmic tail lying in a groove created by an α-helix and a β-strand in the third subdomain of the clover-shaped FERM domain (Mori et al., 2008), but surprisingly, mutation of several of these residues to remove hydrogen bond coordination (H288A), hydrophobic interaction (L248A, D250A, F252A), or to create charged protrusions into the groove (L281R, M285R), all

A.

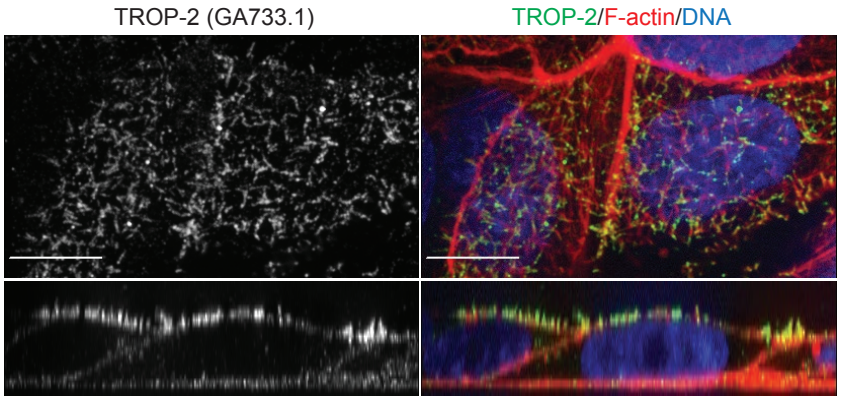
TROP-2 (GA733.1)
TROP-2/F-actin/DNA

B.

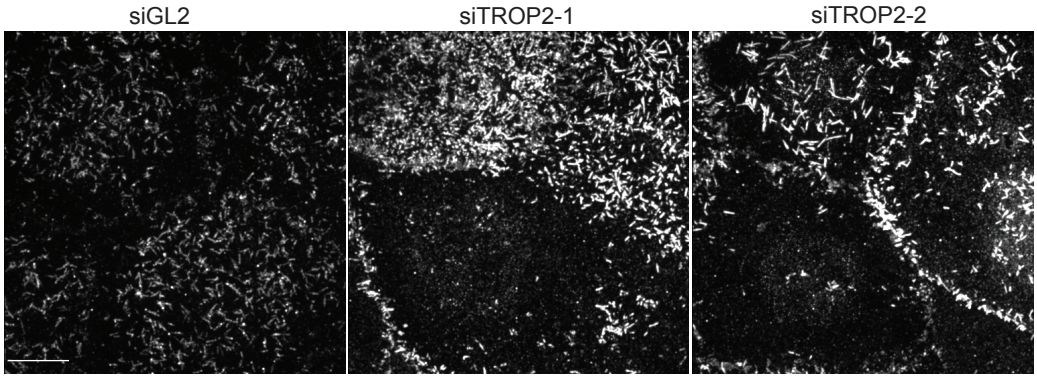
siGL2
siTROP2-1
siTROP2-2

C.

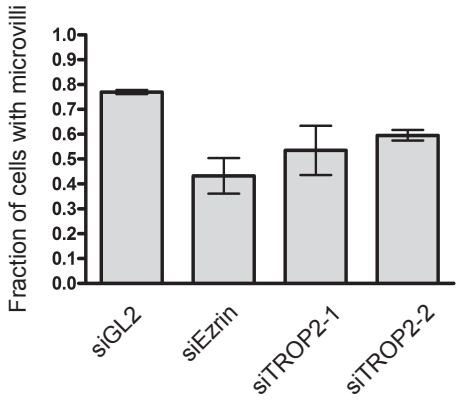
Fraction of cells with microvilli
1.0
0.9
0.8
0.7
0.6
0.5
0.4
0.3
0.2
0.1
0.0
siGL2
siEzrin
siTROP2-1
siTROP2-2

D.

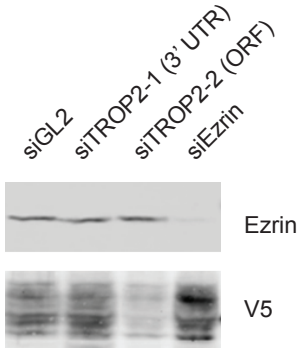
siGL2
siTROP2-1 (3' UTR)
siTROP2-2 (ORF)
siEzrin
Ezrin
V5

E.

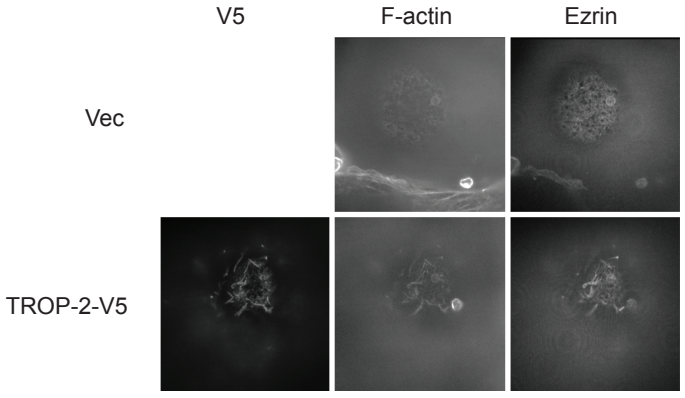
V5
F-actin
Ezrin
Vec
TROP-2-V5

F.

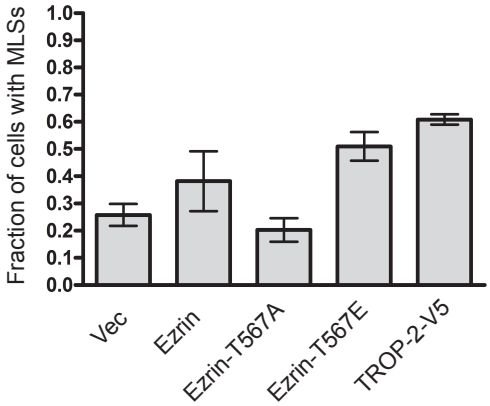
Fraction of cells with MLSs
1.0
0.9
0.8
0.7
0.6
0.5
0.4
0.3
0.2
0.1
0.0
Vec
Ezrin
Ezrin-T567A
Ezrin-T567E
TROP-2-V5

Figure 2.10 Endogenous TROP-2 is an important component of Jeg-3 microvilli and promotes dorsal F-actin-containing protrusion formation when overexpressed in COS7 cells.

(A) Three-color, confocal immunofluorescent detection of endogenous TROP-2 (GA733.1 monoclonal antibody), F-actin (phalloidin), and DNA in Jeg-3 cells *en face* (upper panels) or as a projection of Z-stacks through a vertical cross-section stretched 5-fold (lower panels). (B) RNAi knockdown of TROP-2 with either of two siRNA sequences in Jeg-3 cells causes an occasional loss of microvilli. (C) Quantification of B. (D) Cells stably overexpressing TROP-2-V5 were transiently transfected with siRNAs as in B and C, then analyzed by Western blot. As expected, siTROP2-1, which targets the 3'-UTR (not present in the overexpression plasmid), fails to reduce TROP-2-V5 levels. However, TROP2-2, which targets the ORF, is capable of diminishing the overexpression by >4-fold. (E) Immunofluorescent detection of V5 tag, F-actin (phalloidin) and ezrin in COS7 cells transfected with empty vector or TROP-2-V5. (F) Quantification of the results in panel E with additional controls.

failed to disrupt either the TROP-2 or CD44 interaction (Figure 2.9.E). These results strongly suggest that the solution interaction between CD44 tail and the FERM domain occurs differently than it does in the crystal structure (Mori et al., 2008), also throwing into question other such crystal structures (Takai et al., 2007; Hamada et al., 2003).

Investigations of a possible functional interaction between TROP-2 and ezrin *in vivo*

I next examined TROP-2 function in Jeg-3 cells. I first examined the distribution of endogenous TROP-2 in Jeg-3 cells using the GA733.1 monoclonal antibody. This antibody preferentially illuminated microvilli (Figure 2.10.A), agreeing with the distribution of tagged TROP-2 (Figure 2.6.A). Knockdown of TROP-2 with two independent siRNAs showed that TROP-2 is partially required for microvilli (Figure 2.10.B,C). Because our TROP-2 antibodies could not easily detect endogenous TROP-2 by western blot, to confirm that TROP-2 levels were reduced upon siRNA transfection, a stable cell-line expressing TROP-2-V5 was generated, and the siRNA treatment repeated in these cells. siTROP-2-2, which targets the TROP-2 ORF, was capable of knocking down the stably overexpressed TROP-2-V5 as expected. Unexpectedly, the stable TROP-2-V5-expressing cell-line had inconsistent microvilli, and was not suitable for knockdown-rescue experiments. Nonetheless, microvilli formation appears to partially require TROP-2.

The excessive activation of ezrin (Oshiro et al., 1998) or the overexpression of ezrin-binding transmembrane proteins (Yonemura et al., 1999) has been shown to increase the number of microvilli-like structures in fibrobastic cell-lines such as COS and L cells. To explore whether the overexpression of TROP-2 has a similar effect, COS7 cells were transfected with high levels of ezrin, ezrin phospho-mutants, or TROP-2-V5 and assessed for the number of cells with finger-

like, F-actin-containing structures on their dorsal surface. Overexpression of TROP-2-V5 (Figure 2.10.E,F) or ezrin or phosphomimetic ezrin (Figure 2.10.F) all led to an increase in microvilli-like structures, whereas overexpression of ezrin-T567A partially suppressed microvilli-like structures (Figure 2.10.F). Consistent with Figure 2.9.F, the basic patch mutations did not inhibit binding to ezrin-iFlag in COS7 cells, and all led to a similar increase in microvilli-like structures as wild-type TROP-2-V5 overexpression (data not shown). These data suggest that the presence of TROP-2 can stimulate microvillus formation.

DISCUSSION

The results presented in this chapter represent a pioneering attempt to discover the interaction partners of ERM proteins systematically. These interaction partners have been elusive due to the transient nature of the interactions coupled with the fact that modulating the openness of ezrin changes its distribution in cells. I took the approach of chemical cross-linking coupled with an analysis of how the ezrin interactome responds to ezrin mutations rendering it more closed or more open. Consistent with the proposed function of ezrin activation to increase its partner binding, I find that most interaction partners favor more open ezrin, although there are some exceptions, i.e., proteins that interact preferentially with the closed form. It will be interesting to repeat these studies in other cell-lines of epithelial and other origin to determine their generality.

Among the unknown proteins identified, I discovered a new interaction with Ig-CAM-like molecule TROP-2. Ezrin can interact with the very short intracellular tail of TROP-2 *in vitro*, although whether the *in vitro* binding proceeds in the same manner as the interaction by co-immunoprecipitation is questionable. In support of a functional role between the two, TROP-

2 depletion causes a partial loss of microvilli in Jeg-3 cells, a phenotype also caused by depletion of ezrin, while TROP-2 overexpression creates microvilli-like dorsal structures in COS7 cells, a phenotype also caused by activation of ezrin. Another connection between ezrin and TROP-2 is that both molecules are upregulated in cancer, elevate metastatic potential, and are being considered as drug targets in human chemotherapy. It will be interesting to investigate whether ERMs are functionally connected with TROP-2 in other ways. 1) Adding antibodies against the extracellular domain of TROP-2 was shown to induce calcium transients in cells (Ripani et al., 1998), so it would be interesting to repeat this experiment in cells depleted of ezrin and radixin (see Figure 3.1.A) to determine the contribution of ERM engagement in this system. 2) Trypsinized cell aggregation was shown to be dependent on TROP-2 homotetramerization (Trebak et al., 2001; Basak et al., 1998), so it would be interesting to determine the contribution of ERM engagement in this assay. 3) TROP-2 expression assists in anchorage-independent growth and invasion into Matrigel (Schon and Orfanos, 1995; Trerotola et al., 2012; Basak et al., 1998), so it would be interesting to determine whether and to what extent ERM-knockdown cells are defective in these functions.

My results have also raised question about the nature of solution interactions between the FERM domain and transmembrane tails in solution, as mutations predicted to abolish these interactions based on co-crystal structures (Mori et al., 2008; Takai et al., 2007; Hamada et al., 2003) failed to affect them in solution binding experiments (Figure 2.9.E). It will be interesting to undertake 5-residue-by-5-residue alanine scanning mutagenesis of the FERM domain to determine the regions critical for the solution interactions. A problem plaguing the analysis ERM-binding transmembrane tails is potential redundancy among them. Having such mutants may be helpful here, as well. For instance, one could identify the general role of transmembrane

tail binding in the context of ezrin function in microvilli by testing the mutants in microvillar complementation assays as described below (Figure 3.5 and 3.6).

CHAPTER 3[1]

PHOSPHORYLATION CYCLING BY LOK AND SLK KINASES RESTRICTS EZRIN APICALLY

Ezrin and radixin are exquisitely localized in epithelial microvilli, but how this strikingly polarized distribution is achieved is unknown. The hypothesis driving the experiments in the previous chapter was that unknown transmembrane ligands direct ezrin toward the apical domain. Indeed, such a mechanism seems likely because transmembrane ERM binding partners can cluster ERMs on the cell surface (Yonemura et al., 1999), and apical polarity proteins are thought to interact directly with ERMs (Pilot et al., 2006; Medina et al., 2002). Additionally, $PI(4,5)P_2$ which binds directly to the ezrin FERM doamin (Nakamura et al., 1996; Hirao et al., 1996; Matsui et al., 1998; Simons et al., 1998; Pietromonaco et al., 1998; Fievet et al., 2004; Gautreau et al., 2000; Pearson et al., 2000) is preferentially localized in apical membranes in polarized cells (Martin-Belmonte et al., 2007). In the course of the experiments, however, I realized that this is incorrect: in fact, ezrin apical-vs.-basolateral polarity can be explained simply by extrinsic regulation by apically localized kinases and delocalized phosphatase activity.

First, I examine the dynamics of ezrin phosphorylation in human epithelial cells and show that cycling of T567 phosphorylation is required to restrict ezrin function to the apical membrane. I find that two related serine-threonine kinases, LOK and SLK, associate specifically with ezrin-iFlag, and are together required for ezrin phosphorylation in a number of cell-lines. Moreover, I show that the kinases themselves are components of apical microvilli and their local activation is required for the polarized distribution of ezrin.

[1] Some of the experiments presented in this chapter were published in Viswanatha et al., 2012.

MATERIALS AND METHODS

Reagents, cDNAs, and siRNAs. Phos-Tag reagent (Wako Chemicals, USA) was added at 50 μM to standard Tris-Glycine-SDS polyacrylamide gels according to the manufacturer's recommendations. Krypton (Pierce) staining was performed according to the manufacturer's protocol. Calyculin A and staurosporine were from Enzo Lifesciences. Erlotinib was from Cayman Chemical.

Ezrin antibody was CPCT-Ezrin-1 from the Developmental Studies Hybridoma Bank or a previously characterized rabbit polyclonal antibody (Bretscher, 1989). Pan-ERM antibody was from Cell Signaling. Anti-Radixin (Shcherbina, 1999) and anti-phospho ERM (Hanono et al., 2006) have also been described. Anti-LOK was from Bethyl Laboratories. Anti-Flag and anti-Tubulin were from Sigma. Anti-E-cadherin was from BD Biosciences. Anti-TagRFP was from Evrogen. Anti-GFP was from Santa Cruz.

The pDEST47 Gateway vector (Invitrogen) so that it encoded a C-terminal EGFP (pDESTCEGFP), C-terminal TagRFP-T (pDEST47red), or C-terminal TagRFP-T-integrin binding site (pDEST47IBR) instead of C-terminal Cycle3GFP. pDESTCEGFP was made by replacing the NheI-XhoI fragment in pDEST47 with EGFP, amplified pEGFP-N2 using RV94F4/R4 (5'- TCTAGAATGGCTAGCATGGTGAGCAAGGGCGAGGAGCTG-3' and 5'-GTTGTACTCGAGTTACTTGTACAGCTCGTCCATGCCGAG-3'). pDEST47red was made by replacing the NheI-XhoI fragment with TagRFP amplified from pcDNA3/TagRFP-T using RV94F1/R1 (5'- TCTAGAATGGCTAGCAAGGGCGAAGAGCTGATTAAGGAGAAC-3' and 5'-GTTGTACTCGAGTTAATTAACTTGTACAGCTCGTCCATGCCATTAAGTTTG-3'), which also adds a 3' PacI site. This vector was then cut with PacI/XhoI and talin 1958-2541,

which was amplified from Jeg-3 cDNA using RV94F2/R2 (5'- TACAACCGATCGAA GCTGTGTCTGGTATCATTGCTGACCTC-3' and 5'-GTTGTACTCGAGTTAGTGCTCATCTCGAAGCTCTGAAGGC-3'), was ligated into it. All cloning to this point was done in the DB3.1 *E coli* strain in the presence of chloramphenicol to maintain the ccdB-resistance cassette in the Gateway constructs.

LOK and truncations thereof were generated by tailored PCR using whole cDNA, which was made using mRNA isolated from Jeg-3 cells and the SuperScript III kit (Invitrogen), and subcloned into pDONR221 by BP recombination (Invitrogen) using primers RV59F1/R1 (5'-GGGG ACA AGT TTG TAC AAA AAA GCA GGC TTT ATGGCTTTTGCCAATTTCCGCCGCATC-3' and 5'- GGGG AC CAC TTT GTA CAA GAA AGC TGG GTA AGAAGCATCCGCAGAACTGTAGGGGAAG-3'). They were then transferred into the modified destination vectors as indicated above. The linking region between the ORF and the tags encoded the following peptide sequence: Y-P-A-F-L-Y-K-V-V-R-S-R. The K65R mutation was generated using the QuickChange kit and primers RV90F1/R1 (5'-Gtgctttggctgcggccagagtcattgaaaccaag-3' and 5'-cttggtttcaatgactctggccgcagccaaagcac-3'). Additional truncations of LOK were generated using the following primers.

LOK 757 reverse	RV93R1	GGGG AC CAC TTT GTA CAA GAA AGC TGG GTA CAGCTGGTGCCTCTCCTGCAGCT
LOK 589 reverse	RV93R2	GGGG AC CAC TTT GTA CAA GAA AGC TGG GTA GCAGCTCATGCTTGTTACTCAGCTR
LOK 310 forward	RV93F4	GGGG ACA AGT TTG TAC AAA AAA GCA GGC TCC ATG GCCAAGGCCGAGGTGATGGAAG
LOK 586 forward	RV93F3	GGGG ACA AGT TTG TAC AAA AAA GCA GGC TCC ATG AAGCATGAGCTGCAGCTGGAGCAAAT

LOK 348 reverse	RV93R4	GGGG AC CAC TTT GTA CAA GAA AGC TGG GTA ACTCACCTCAGAGGAGTTCTGAGTATGG
LOK 715 forward	RV93F5	GGGG ACA AGT TTG TAC AAA AAA GCA GGC TCC ATG GACAACAGGCGGGAGATCTGTG
LOK 615 forward	RV93F6	GGGG ACA AGT TTG TAC AAA AAA GCA GGC TCC ATG AACCTGGAGCGTCAGCAAAAGCAGC
LOK 801 reverse	RV93R7	GGGG AC CAC TTT GTA CAA GAA AGC TGG GTA CTGTTGCTGCCGCACCTTCAGC
LOK 884 reverse	RV93R8	GGGG AC CAC TTT GTA CAA GAA AGC TGG GTA CTGCTGCAGCTCGCTCATGTTGC

The murine long isoform of SLK and truncations thereof were amplified by PCR from EST # BC131675 from Open Biosystems and then cloned into pDONR223 by BP recombination using RV91F1/R1 (5'- GGGG ACA AGT TTG TAC AAA AAA GCA GGC TTT ACC ATGTCCTTCTTCAATTTCCGTAAGAT-3' and 5'- GGGG AC CAC TTT GTA CAA GAA AGC TGG GTA TGATCCGGTGGAATGCAAGCTGGGAATAGG-3'). They were then transferred into the same set of modified Gateway vectors by LR recombination, with one exception: SLK-310-1233 was transferred into pcDNA-DEST53 (Invitrogen), which adds an N-terminal (rather than C-terminal) GFP because this resulted in higher expression of this construct. K63R mutant of SLK was a kind gift of Dr. Luc Saborin (Inst. de Recherche de l'Hopital d'Ottowa). Various truncations of SLK were prepared using the following primers:

SLK 353 reverse	RV91R2	GGGG AC CAC TTT GTA CAA GAA AGC TGG GTA AAGTTTATCTTCTTCAGAGCTGGCAATG
SLK 310 forward	RV91F3	GGGG ACA AGT TTG TAC AAA AAA GCA GGC TTT ACC GAAGTAACAGAAGAAGTTGAAGATGG

For kinase assays, a C-terminal Flag tag was added to the 3' end by tailored PCR of LOK-GFP or SLK-GFP and derivatives using primers RV97F1 for LOK (5'- TTCACT GCGGCCGC ATGGCTTTTGCCAATTTCCGCCGCATC-3') or F2 for SLK (5'- TTCACT GCGGCCGC ACCatgtccttcttcaatttccgtaagatcttcaag-3') and RV97R1 (5'- CATGGACGAGCTGTACAAG ATG gac tac aag gac gac gat gac aag TAA CAATTG AGTTG-3'), digested with NotI and MfeI, and the products ligated into pQCXIP cut with NotI and EcoRI.

The actin binding sequence of espin was a generous gift of James Bartles (Northwestern University). It was cloned first into pEGFP by Damien Garbett, and then the Espin-EGFP cassette was then cloned by tailored PCR into pQCXIP, and ezrin deriviates were ligated 5' of the cassette as needed.

siRNAs were from Ambion or Dharmacon with the following sequences: 5'-AAAGUCAGGUGCCUUCUUGuu-3' (Ezrin, sequence 1); 5'-GGAAUCAACUAUUUCGAGAtt-3' (Ezrin, sequence 2); 5'-UGAAGAUGUUUCUGAGGAAuu-3' (Radixin); 5'-GAAGAGCAUCGGAACCAGAtt-3' (LOK, sequence 1); 5'-GGACUACACCAGGUUCCAAtt-3' (LOK, sequence 2); 5'-GAUCGAUAUCUUUACAAGAtt-3' (SLK, sequence 1); 5'-GCAGAAACAGACUAUCGAAtt-3' (SLK, sequence 2); 5'-GCUUUACCACCGUACGAAAtt-3' (MST4); 5'-GAAUCCCGCUGACAAACCAtt-3' (MINK1). siGL2, targeting GL2 luciferase, was previously described (Hanono et al., 2006).

Caco-2 cells (American Type Culture Collection, ATCC) were maintained in a 5% CO_2 humidified atmosphere at 37°C in MEM (Invitrogen) with 20% FBS (Invitrogen). LLC-

PK1.CL4 cells were kindly provided by Matthew J.Tyska (Vanderbilt University). They were grown in MEMα + 10% FBS. MDCK cells were kindly provided by Keith Mostov, and HEK293T cells originally by Gary Nolan (Stanford University), and primary mouse embryo fibroblasts by Jan Lammerding (Cornell University). All were grown in DMEM + 10% FBS.

All transient plasmid DNA transfections were performed for ~18 hours using Polyethylenimine reagent (PolyPlus) using a previously established protocol (Hanono et al., 2006). Phoenix-Ampho retrovirus producer cells (ATCC) were cultured in DMEM (Invitrogen) with 10% FBS. Retroviruses were prepared following a standard transfection protocol using the Phoenix-Ampho cell-line and the retroviral vector pQCXIP. The recombinant retroviruses were used to transduce Jeg-3 cells, which were then selected with 2.0 μg/ml puromycin (Sigma).

SILAC, mass spectrometry, and immunoprecipitations were as described in Chapter 2.

All siRNAs were transfected at 30 nM into ~25% confluent cultures of Jeg-3 cells or Caco-2 cells using Lipofectamine RNAiMAX (Invitrogen) using the manufacturer's protocol. In all but one case, cells were processed for immunofluorescence or lysis 3 days after transfection. For combined siRNA transfection of LOK and SLK, cells were treated with the indicated first siRNA for 2 days, reseeded, and then, on the third day, transfected with the indicated second siRNA for an additional 3 days, and processed on the sixth day.

For analysis of tagged ezrin phosphorylation, cells transfected with ezrin-iFlag plasmid plus LOK or SLK expression vector were rapidly boiled in 50 mM Tris pH 8.0 containing 1% SDS. Lysates were then diluted 10-fold with IP buffer, clarified, the protein abundance quantified and adjusted using the Pierce 660 nm assay (Thermo), and immunoprecipitated as described above.

Western blotting and densitometry. Western blots were performed as previously described (Hanono et al., 2006). For all densitometry, western blotting was carried out with a mixture of mouse CPCT-Ezrin-1 or mouse Flag and rabbit pERM antibodies, detected with infrared fluorescent secondary antibodies (Invitrogen or LI-COR). Membranes were imaged using an Odyssey scanner (LI-COR). On every membrane in this study, dilutions of lysate were run alongside the samples so that standard curves for both total ezrin and pERM could be generated in the Odyssey software (LI-COR). These were then used to determine the relative intensity of in-range pERM and ezrin or Flag signals from experimental lanes. These data were exported to Graphpad Prism software where all further quantitative and statistical analyses were performed.

Immunofluorescence microscopy and image analysis. Cells grown on glass coverslips were fixed in 3.7% formalin/PBS for 15 minutes at room temperature for most experiments except where indicated. In the remaining cases, cells were fixed in cold 10% trichloroacetic acid for 15 minutes as described (Hayashi et al., 1999). Cells were then washed with PBS and blocked with IF buffer (PBS + 0.5% BSA + 0.5% goat serum + 0.1% Triton-X 100) for 10 minutes. Primary and secondary antibodies were then applied in IF buffer containing 1% FBS. Alexa-fluor conjugated phalloidin (Invitrogen), to stain F-actin, was added to the secondary as required. The cells were mounted in Vectashield reagent, imaged using a CSU-X spinning disk microscope (Intelligent Imaging Innovations) with spherical aberration correction device, 63x 1.4 NA objective on an inverted microscope (Leica), acquired with either a QuantEM EMCCD camera or an HQ2 CCD camera (Photometrics) using Slidebook software (Intelligent Imaging Innovations). Maximum or summed intensity projections were assembled in Slidebook and exported to Adobe Illustrator software. For clarity, side projections were vertically expanded 5-fold using Illustrator.

The presence or absence of microvilli was scored as described previously (Hanono et al., 2006; LaLonde et al., 2010; Garbett et al., 2010).

For scoring of ezrin localization to the basolateral domain induced by delocalized LOK expression, the cell middle or cell base was identified by confocal microscopy using F-actin staining for 50 transfected cells per sample per trial, and the presence or absence of ezrin stain in transfected cells relative to surrounding non-transfected cells was reported.

For line-intensity analysis, a line was drawn along a single microvillus from base to tip (the orientation was verified by scanning through multiple Z sections), the intensity of ezrin immunofluorescent staining, GFP, and F-actin were each calculated in Slidebook, and exported into Microsoft Excel software. Ezrin and GFP were each divided by F-actin to minimize aberrations in microvilli geometry, and the resulting data were plotted in Prism.

Kinase assays. Kinase assays were essentially as described (Jackson and Dickson, 1999). GST-ezrin-474-585 was purified from Rosetta2DE3pLysS bacteria (Novagen) onto glutathione agarose (Sigma) and then washed extensively in TBS. pQCXIP plasmids encoding kinase constructs were transiently transfected into Phoenix-Ampho cells for ~18 hours, and cells were Flag immunoprecipitated in IP Buffer for 2 hours, and the resin extensively washed in TBS. Immunoprecipitates were eluted in TBS containing 200 μg/mL 3XFlag peptide and quickly resolved by SDS-PAGE to verify purity and determine concentration. ~0.2 μM GST-ezrin-474-585 beads were added to ~0.2 μM soluble kinase in kinase assay buffer (150 mM NaCl, 20 mM Tris pH 7.4, 50 mM $MnCl_2$, 100 mM $MgCl_2$, 0.1 μM Na_3VO_4, 0.1 μM calyculin A, 20 μM ATP) and the reactions incubated at 30^{o}C for 1 hour with agitation and then terminated by boiling in Laemmli buffer.

RESULTS

ERMs are required for microvilli in Jeg-3 cells

In order to investigate the role of ERMs, it was first necessary to find a way to reduce their expression and observe the phenotype. ERMs have been suppressed in tissue culture by antisense oligonucleotide expression or RNAi with a wide range of effects including ablation of all F-actin-containing structures (Tsukita et al., 1994), destruction of microvilli and basal infoldings (Bonilha et al., 1999), and reduction in circular dorsal ruffles with no effect on microvilli (D'Angelo et al., 2007). *In situ*, ezrin-lacking epithelial cells that do not express radixin or moesin have terminal web defects leading to stunting and deformation of the microvilli, while the structures themselves are intact (Saotome et al., 2004). These variations perhaps reflect differences in experimental procedure and cell type. By contrast, the Bretscher lab has found that Jeg-3 placental cells transfected with siRNAs targeting EBP50, a key ERM binding partner, lose microvilli without apparent defects in any other F-actin-containing structure (Hanono et al., 2006). Thus, I used the same methods in this cell-line to generate ezrin-suppressed cells.

Cells were transfected with either of two ezrin siRNAs for 3 days. Western blots using a pan-ERM antibody showed that both were specific for ezrin, because ezrin expression decreased while radixin expression was mildly elevated, perhaps due to compensatory gene upregulation (Figure 3.1.A). Approximately 80% of Jeg-3 cells have microvilli (Hanono et al., 2006; LaLonde et al., 2010; Garbett et al., 2010), and transfecting either siEzrin1 or siEzrin2 led to a reduction in microvilli-baring cells to 26% or 47%, respectively (Figure 3.1.B), while microvilli always seem to remain along the regions of cell-cell contact. Since siEzrin1 had a greater effect but knocked

A.

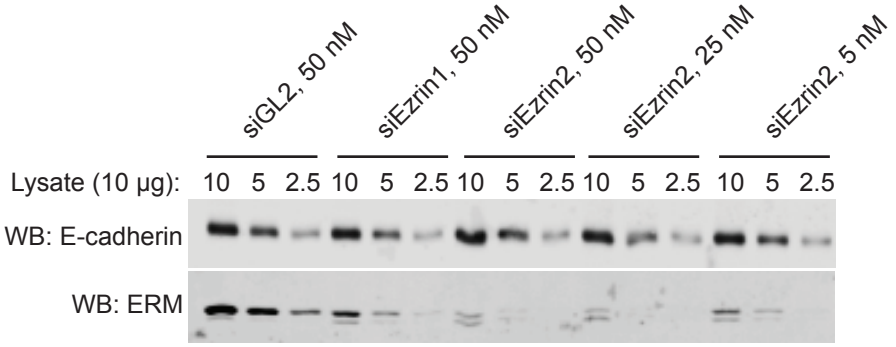

B.

	ERM content, % of control	Ezrin content, % of control	% with microvilli (N=2)	% Abnormal (N=2)
siGL2, 50 nM	100	100	81 ± 4	5 ± 3
siEz1, 50 nM	38	32	26 ± 4	19 ± 6
siEz2, 50 nM	26	8	47 ± 5	3 ± 1
siEz2, 25 nM	25	8	50 ± 7	5 ± 1
siEz2, 5 nM	31	14	47 ± 6	5 ± 3

C.

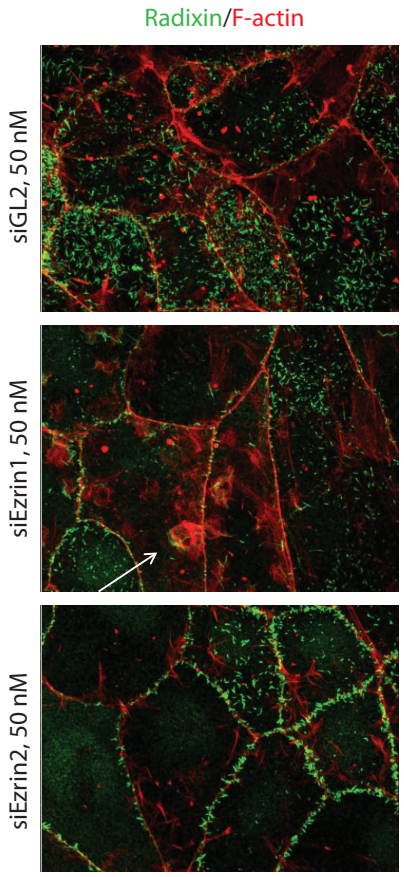

D.

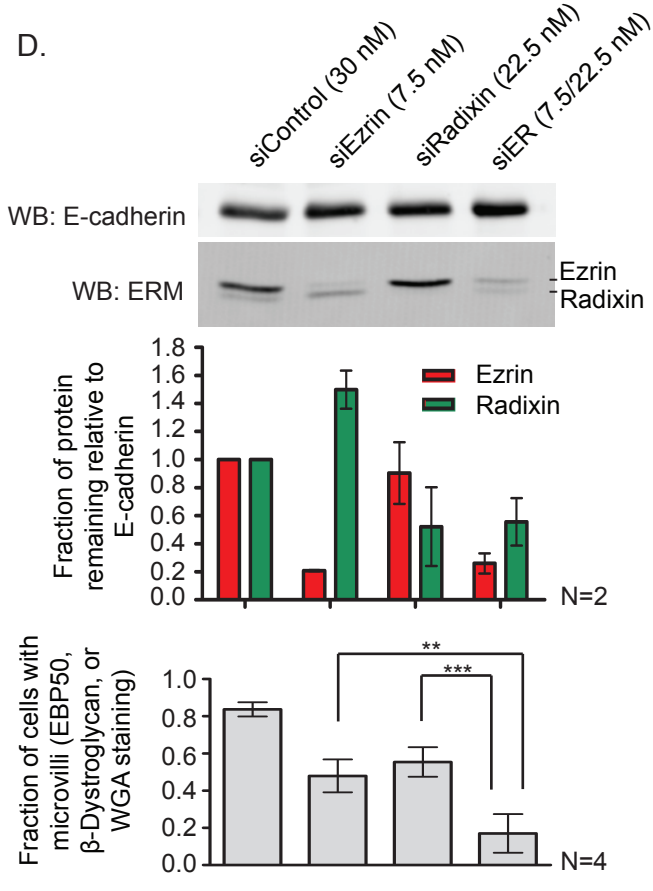

Figure 3.1 Ezrin and radixin RNAi-mediated depletion causes a loss of microvilli in Jeg-3 cells

(A) Western blot showing depletion of ezrin relative to E-cadherin by two siRNA sequences. (B) Quantification of the Western blot in panel A and determination of microvilli abundance by WGA-staining or radixin and F-actin staining. siEzrin1 causes greater microvillus loss, but less ezrin depletion, and therefore must have off-targets, whereas siEzrin2 results in ezrin depletion. Additionally, siEzrin1 causes many more cells with abnormal cytoskeletons. (C) Representative images from one of the analyses quantified in panel B, showing abnormality caused by siEzrin1 (arrow). (D) Cells were treated with ezrin and/or radixin siRNA as indicated, analyzed by western blot to determine amount of ezrin and radixin remaining following the knockdown and fixed and stained for various microvillar markers (EBP50, β-dystroglycan, or WGA) and scored to determine the degree of microvillus loss. Ezrin depletion leads to the mild compensatory upregulation of radixin. Ezrin and radixin are each independently required for microvilli, and microvilli are almost entirely dependent on ezrin and radixin.

down ezrin more poorly, I more closely examined the effects. siEzrin1 transfection caused the formation of circular dorsal ruffles (Figure 3.1.C, arrow; scored as 'abnormal' cells in A), skewing the scoring results perhaps as a consequence of an off-target suppression of another protein, while siEzrin2 caused the loss of microvilli without grossly affecting the F-actin cytoskeleton in any other way (Figure 3.1.C,B). Thus siEzrin2 (hereafter simply called 'siEzrin') was used for the subsequent studies.

To determine whether ezrin and radixin act in parallel to form microvilli, they were silenced individually or together. Western blots and densitometry confirmed the specificity of each knockdown (Figure 3.1.D). The cells were fixed and stained for the presence of microvillar markers EBP50 or β-dystroglycan and additionally stained with fluorescent wheat germ agglutinin (WGA) prior to permeablization to localize the dominant cell-surface proteoglycans which illuminate the plasma membrane. Cells were scored for the presence or absence of microvilli, and the scores pooled. The results show that regardless of the marker observed, ezrin and radixin are each required for microvilli individually, and there was statistically significant enhancement of the phenotype when the two siRNAs were co-transfected, even though their protein levels were not further diminished in the combined knockdown. Thus, ezrin and radixin act in parallel to generate microvilli in Jeg-3 cells, and Jeg-3 cells are almost entirely dependent upon ERMs for microvilli.

Ezrin undergoes rapid threonine-567 phosphorylation cycling

Threonine 567 (T567) is the major site of phosphorylation regulating ezrin activation, yet the fraction of the protein phosphorylated in epithelial cells has not been explored. Using Phos-Tag gels (Kinoshita et al., 2006), in which the mobility of phosphorylated proteins is specifically

retarded, ezrin from Jeg-3 cells resolves into two species of approximately equal abundance (Figure 3.2.A). The slower migrating band is selectively recognized by an antibody specific for ERM C-terminal threonine phosphorylation (pERM), and is absent from expressed T567A ezrin (Figure 3.1.A,B). The cell-permeable phosphatase inhibitor calyculin A is known to reduce ezrin dephosphorylation (Chen et al., 1995), so I explored if treatment enhances the relative abundance of ezrin T567 phosphorylation. Five minutes' treatment with 1 μM calyculin A resulted in essentially complete ezrin phosphorylation (Figure 3.1.A,B). These results show that about half of the ezrin is phosphorylated in these cells, and the other half can be rapidly phosphorylated *in vivo* in the absence of opposing phosphatase activity.

To explore the dynamics of phosphorylation of ezrin on T567 in more detail, I followed the extent of phosphorylation as a function of time after adding either the general kinase inhibitor staurosporine (1 μM) or calyculin A (1 μM). Of the ERM proteins, Jeg-3 cells express ezrin and radixin, which have an identical sequence in the region of ezrin T567, so the antibody detects the phosphorylated state of both proteins. In all experiments, the percentage of ezrin and radixin that is phosphorylated is similar so I considered them together. Quantitative western blotting with the pERM antibody was used to determine the degree of C-terminal threonine phosphorylation. The lifetime of the dephosphorylated species in the presence of phosphatase inhibitor and that of the phosphorylated species in the presence of kinase inhibitor were each approximately 2 minutes (3.1.C,D). The results show that ezrin and radixin undergo constant C-terminal phosphocycling *in vivo*.

Ezrin phosphocycling is necessary for ezrin localization to microvilli

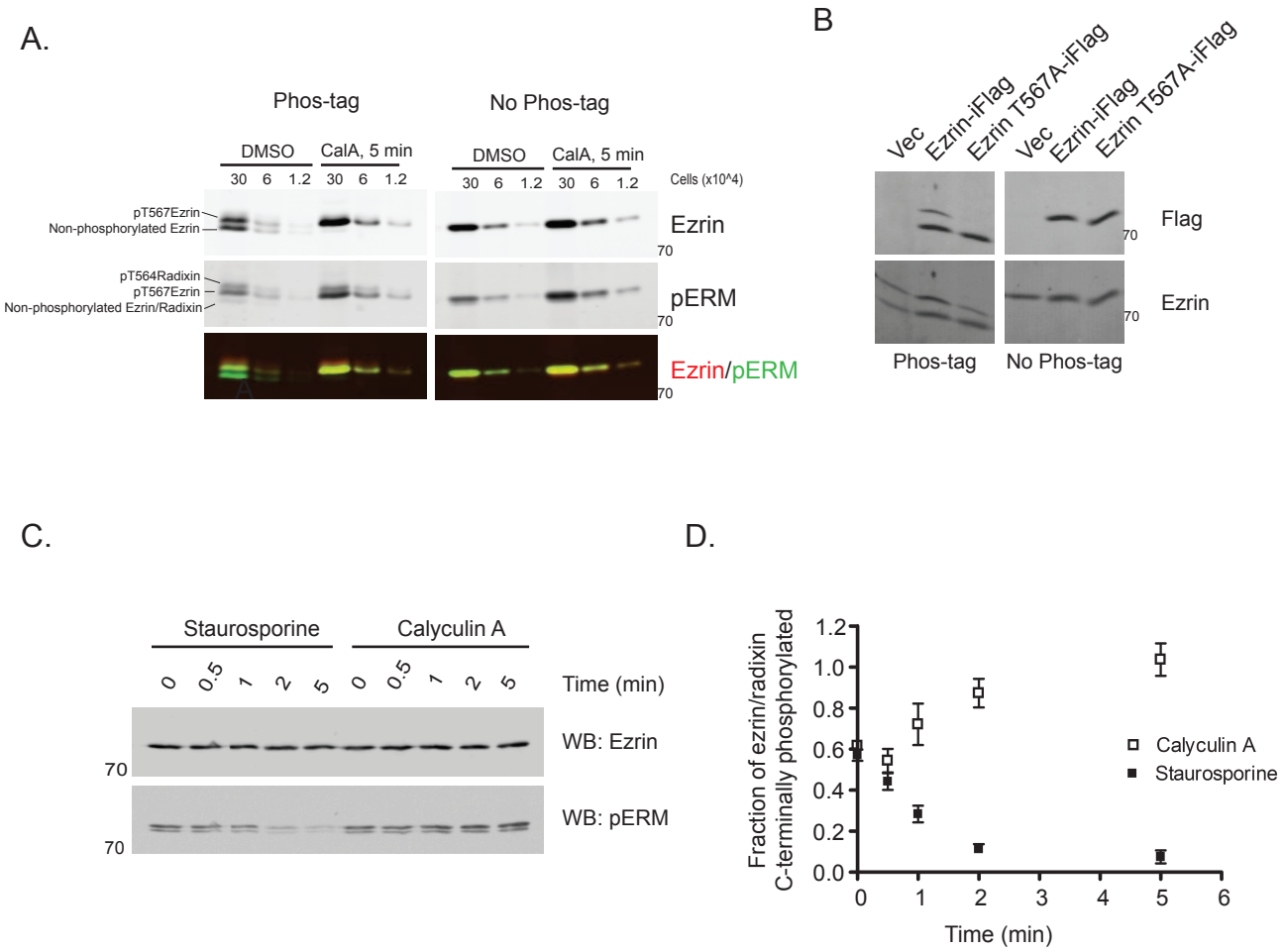

Figure 3.2 Half of ezrin is phosphorylated, and phospho-ezrin has a turnover time of approximately 2 minutes.

(A) A 5-fold dilution series of lysates of Jeg-3 cells treated as indicated was resolved by SDS-PAGE with or without Phos-Tag and western blotted for ezrin. The abundance of phosphorylated and non-phosphorylated ezrin is nearly equal; ezrin is nearly quantitatively phosphorylated after treatment with calyculin A for five minutes. (B) Cells transiently transfected to express ezrin-T567A-iFlag (see Figure S2A) does not shift on Phos-Tag gels, so the majority of ezrin phosphorylation is on T567. Note that transiently transfected ezrin-iFlag is phosphorylated to a lesser extent than endogenous ezrin. (C) Time-course of treatment of cells with 1µM Staurosporine or 1µm CalyculinA on the level of phospho-ERM (pERM) and total ezrin as seen by western blotting. (D) Quantification of data in B from three independent experiments. Means ± s.d. are shown.

I next explored whether the T567E phosphomimetic mutant of ezrin, or the T567A phosphodeficient mutant, localizes appropriately. Numerous previous studies have used a C-terminal tag to follow expressed ezrin. However, as the C-terminus makes important contacts with the FERM domain to maintain an inhibited conformation (Pearson et al., 2000), I was concerned that a C-terminal tag might affect the regulation of the protein. I therefore explored the possibility of introducing an internal tag, and chose a region between the α-helical ERM coiled-coil and the tail that is not ordered in the X-ray structure and also poorly conserved within the ERM family (Li et al., 2007; Figure 3.3.A). Cell-lines were stably transfected and selected such that they expressed nearly identical levels of ezrin-iFlag compared with endogenous ezrin (Figure 2.1.B). The ezrin-iFlag reagent proved useful for immunoprecipitation analyses and recapitulates many aspects of ezrin regulation, so I asked whether it can complement ezrin depletion. I engineered ezrin-iFlag stable cell-lines resistant to siEzrin, and confirmed the expression by western blot (Figure 3.3.C). I then scored microvilli in the cells treated with control siRNA or depleted of endogenous ezrin (Figure 3.3.D). The results show Ezrin-iFlag partially complements the depletion of endogenous ezrin, although to a lesser extent than untagged ezrin. As expected, the tagged protein localized precisely in microvilli and therefore served as a good control for testing the effect of targeted mutations on ezrin distribution

Wild-type ezrin-iFlag localized precisely in microvilli with endogenous radixin, whereas ezrin-T567A-iFlag could not be detected in microvilli and showed dim fluorescence in the cytoplasm (Fig 3.4.A). Unexpectedly, ezrin-T567E-iFlag was poorly concentrated in microvilli, with the vast majority mislocalized all over the plasma membrane, including to the basolateral membrane, a site where wild-type ezrin is never enriched, and importantly without disturbing the apical localization of radixin (Fig 3.4.A). To see if this is a general property of open ezrin

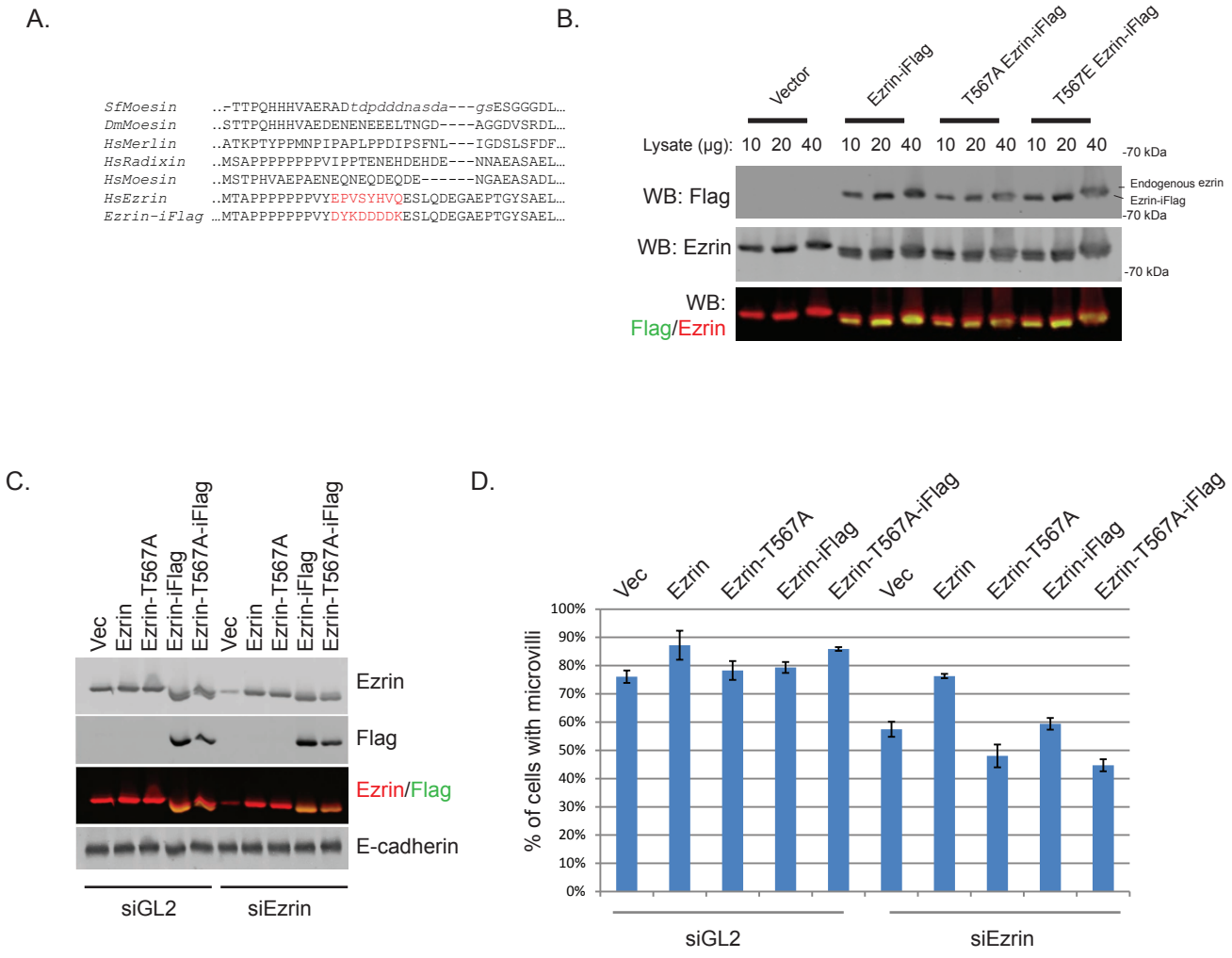

Figure 3.3 Characterization of the ezrin-iFlag stable cell-lines

(A) Sequence alignment of ezrin-iFlag along with indicated ERMs, based upon Li et al., 2007. (B) Western blots of ezrin-iFlag and phosphomutant stable cell-lines. Note the shift due to the internal flag tag. (C) Western blots of ezrin-iFlag and phosphomutants treated with indicated siRNA. (D) Analysis of microvilli-baring cells from panel A. Ezrin-iFlag reproduces some aspects of ezrin, but is incapable of restoring normal microvilli in the absence of endogenous ezrin.

mutants, I also explored the localization of ezrin-1-583-iFlag and ezrin 1-479-Flag, in which the C-terminal tail of ezrin is truncated or deleted rendering the protein completely open, and ezrin Nm-iFlag, which is open due to a mutation in the FERM domain that blocks binding to its otherwise functional C-terminal tail (Chambers and Bretscher, 2005; Finnerty et al., 2004). All constructs localized more generally to the plasma membrane than wild-type ezrin-iFlag, and none affected the localization of radixin (Fig 3.4.B).

To explore the effect of stable C-terminal threonine phosphorylation of endogenous ezrin, I examined the localization of ezrin after brief calyculin A treatment. This resulted in the localization of ezrin not only in microvilli, but also generally to the plasma membrane, including the basolateral membrane (Figure 3.4.C). Taken together, these results imply that phosphocycling of ezrin regulates its distribution by controlling its open state.

Phosphoregulatory control of ezrin localization is necessary for microvilli formation

As my data show that ezrin hyper-phosphorylation resulting from phosphatase inhibition results in partial mislocalization, I wished to determine if T567 phosphocycling is necessary for microvilli formation. Depletion of ezrin alone by siRNA reduces the number of cells expressing microvilli on their surface from about 80% to about 47%, with some microvilli remaining over regions of cell-cell contact (Figure 3.1, 3.5), as is also seen when the microvillar component ERM-binding phosphoprotein 50 kDa (EBP50) is depleted (Hanono et al., 2006; Garbett et al., 2010). Therefore, this provides a system to ask if phosphomimetic variants of ezrin can contribute to the formation of microvilli. Jeg-3 cells stably expressing siRNA-resistant untagged wild-type ezrin, ezrin-T567A or ezrin-T567E at near-endogeneous ezrin levels were generated and all found to have microvilli as seen by radixin staining. Endogeneous ezrin was then

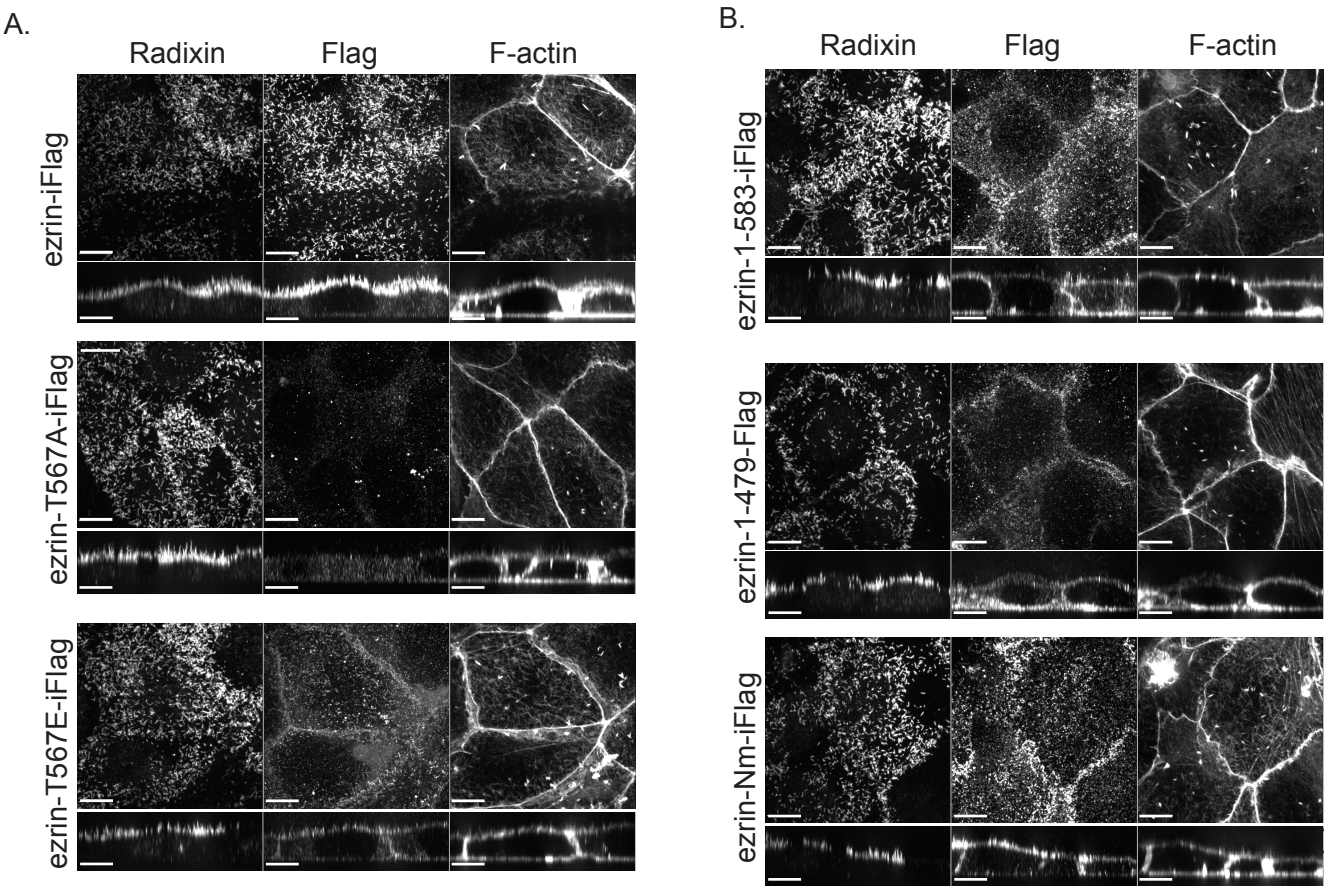

Figure 3.4 Constitutively open ezrin loses apical-versus-basal polarity.

(A) Jeg-3 cells expressing ezrin-iFlag or its T567 phospho-mutants (see Fig. S1C,D) were stained using a Flag antibody and the localization compared to endogenous radixin and F-actin. For every sample, a maximum-intensity projection of the apical surface *en face* as well as a vertical cross-section is shown. (B) Cells stably expressing ezrin C-terminal truncation mutants or the N-mutant (Nm), all of which are known to be constitutively open, were processed and imaged as in A. Compromising the FERM/C-terminus interaction in ezrin reduces ezrin-iFlag accumulation in microvilli, without affecting the polarized distribution of radixin. (C) Cells were treated with DMSO or 0.1 μM calyculin A for 5 minutes, and ezrin and F-actin localized. Calyculin A treatment causes ezrin to mislocalize. Scale bars, 10 μm. Vertical sections were expanded 5-fold for clarity.

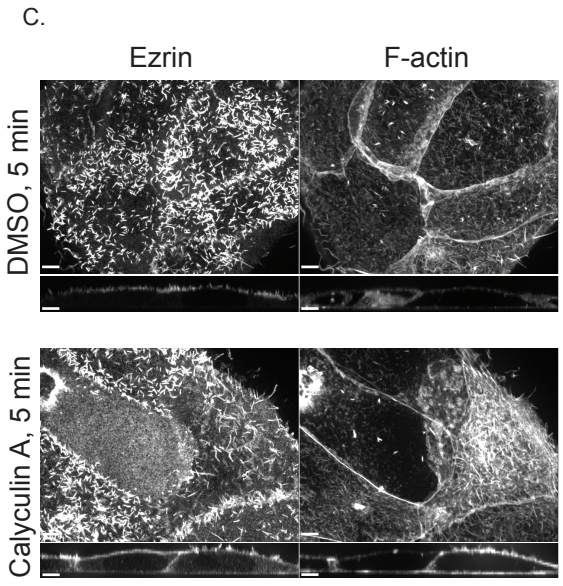

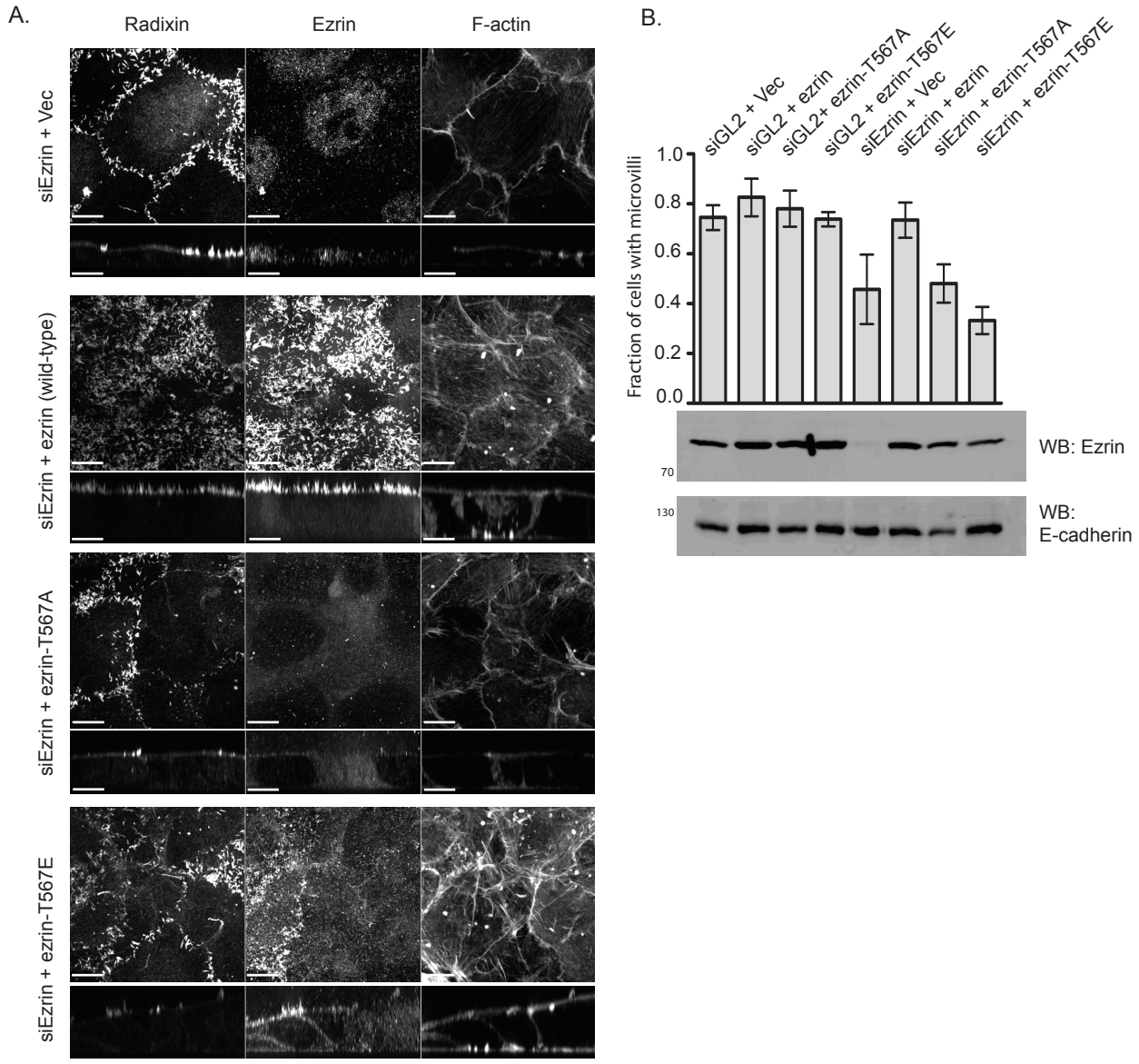

Figure 3.5 Phosphomimetic, activated ezrin cannot rescue microvilli when endogenous ezrin is depleted by RNAi.

(A) Cells stably expressing the indicated ezrin protein or vector control were treated for 3 days with siRNA to deplete endogenous ezrin, and microvilli were revealed by radixin and F-actin staining. (B) Quantification of the presence of microvilli as reported by radixin or F-actin staining. Wild-type ezrin but neither phosphodeficient nor phosphomimetic ezrin restores microvilli after knockdown of endogenous ezrin. Data are means ± s.d. of four independent experiments, and >150 cells were scored per treatment in each experiment. Scale bars, 10 μm. Cross-sections were expanded 5-fold vertically for clarity.

depleted in these cells by siRNA treatment and the presence of microvilli scored (Figure 3.5). Whereas expression of wild-type ezrin completely restored the presence of microvilli, neither ezrin-T567A nor ezrin-T567E was able to bring back microvilli.

I also examined the functionality of the widely used C-terminally-tagged GFP constructs. In contrast to untagged or internally tagged ezrin-T567A, I found that ezrin-T567A-GFP is membrane-targeted, consistent with my concern that it might be slightly activated. Nonetheless, neither siRNA-resistant T567A nor T567E in the context of ezrin-GFP rescued microvilli, whereas siRNA-resistant wild-type ezrin-GFP rescued microvilli in the absence of endogenous ezrin (Figures 3.6). I conclude that while ezrin-GFP may be partially activated relative to untagged ezrin, it still requires phosphocycling to perform its function in microvillus biogenesis. Taken together, these results indicate that the precise spatial control of ezrin phosphocycling is necessary for microvilli.

The ability to tag ezrin on the C-terminus without grossly interfering with its function allowed me to ask what would happen to an ezrin molecule that was constitutively open due to a second actin-binding site which could not be masked by the FERM domain. For these experiments, I expressed the actin-binding site (ABS) of espin, which nonspecifically localizes with the bulk of F-actin (Figure 3.7.A) and does not affect the presence of Jeg-3 microvilli on its own (Figure 3.7.B). I fused the ABS to the C-terminus of ezrin to create a constitutively F-actin-targetted molecule (Figure 3.7.C). Intriguingly, while siRNA-resistant ezrin-GFP accumulated in and rescued microvilli following siEzrin transfection, ezrin-GFP-ABS mislocalized to all cortical F-actin and failed to rescue completely (Figure 3.7.D,E). Furthermore, when T567E ezrin was replaced within the construct, it became partially deleterious towards endogenous ezrin function

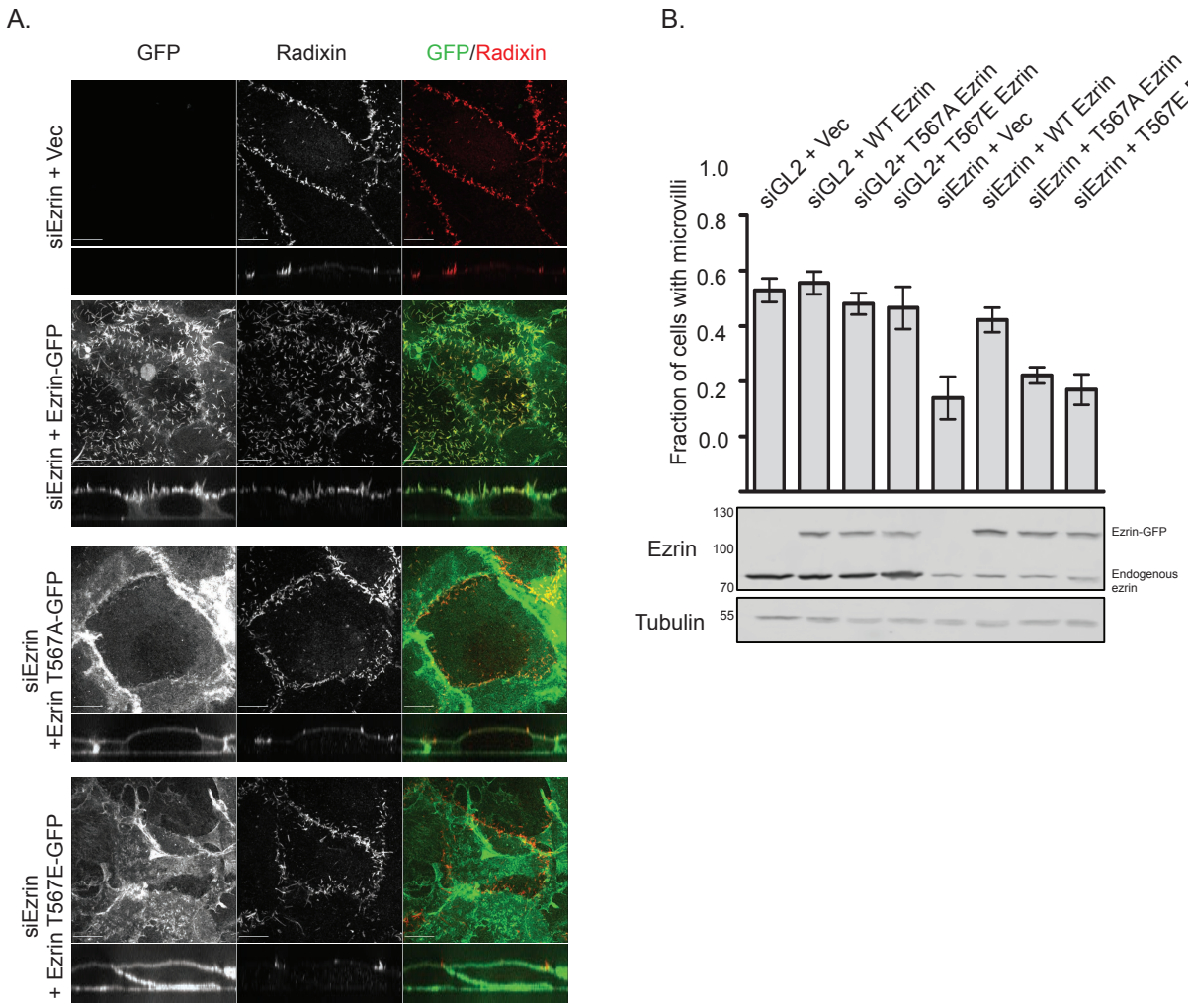

Figure 3.6 C-terminally GFP-tagged ezrin also rescues microvilli in a phosphocycling-dependent manner

(A) Cells stably expressing indicated RNAi-resistant ezrin-GFP or vector control were treated for 3 days with siRNA to deplete endogenous ezrin, and microvilli were revealed by radixin and F-actin staining. Similar to Figure 3.5, where untagged ezrin is employed, RNAi knockdown of ezrin causes ~40% of cells to lose central microvilli as revealed by radixin or F-actin staining, and the re-expression of GFP-tagged, wild-type ezrin reverses the deficiency. However, microvilli are not restored by expression of T567A- nor T567E-ezrin-GFP. (B) Quantification of cells with microvilli as seen by radixin or F-actin staining. Expression of the ezrin-GFP constructs was verified by western blot. Data are means ± s.d. of three independent experiments. All scale bars, 10 μm. Cross-sections were expanded 5-fold vertically for clarity.

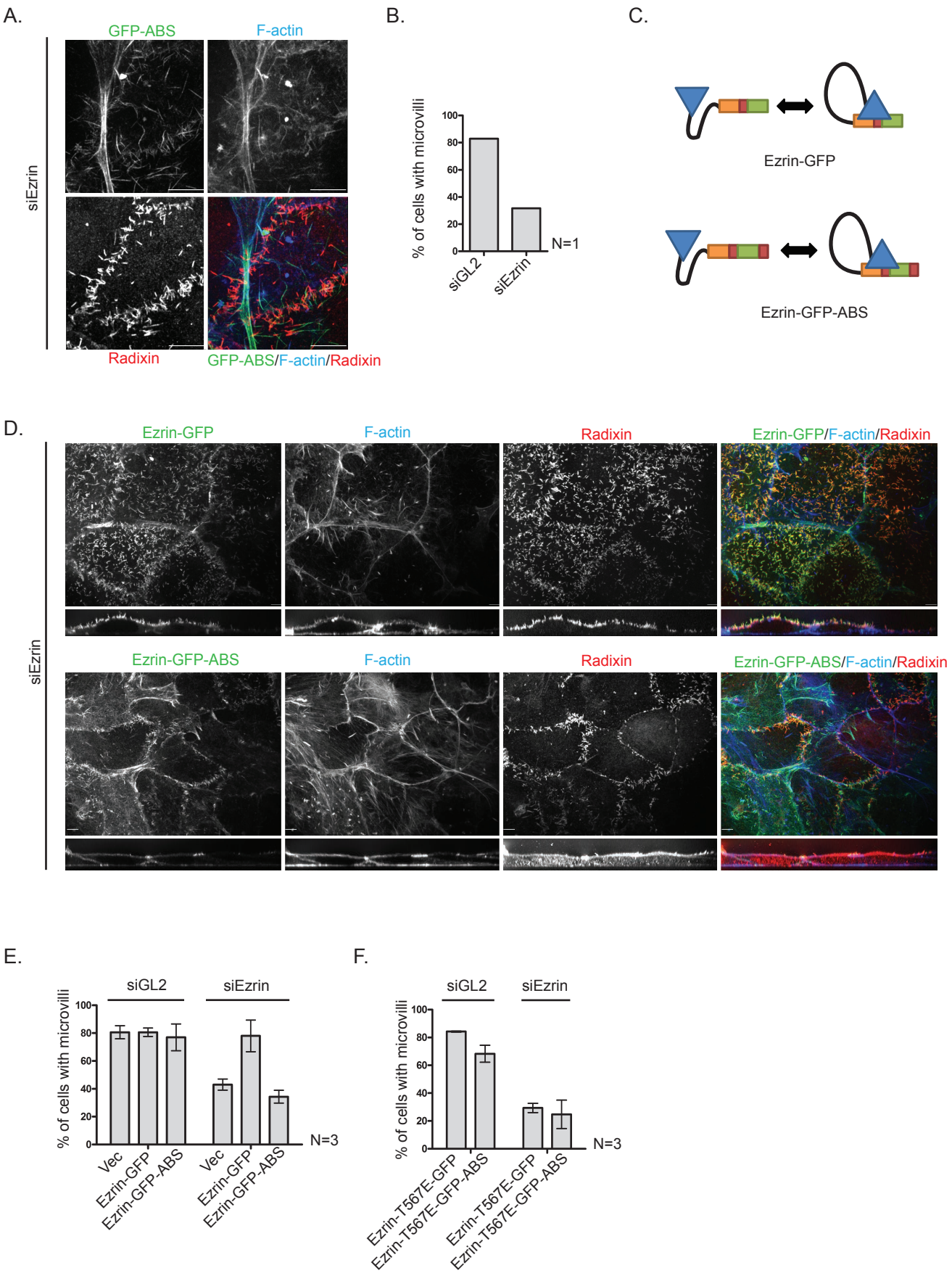
A.
GFP-ABS
F-actin
siEzrin
Radixin
GFP-ABS/F-actin/Radixin
B.
% of cells with microvilli
100
80
60
40
20
0
siGL2
siEzrin
N=1
C.
Ezrin-GFP
Ezrin-GFP-ABS
D.
Ezrin-GFP
F-actin
Radixin
Ezrin-GFP/F-actin/Radixin
siEzrin
Ezrin-GFP-ABS
F-actin
Radixin
Ezrin-GFP-ABS/F-actin/Radixin
E.
siGL2
siEzrin
% of cells with microvilli
100
80
60
40
20
0
Vec
Ezrin-GFP
Ezrin-GFP-ABS
N=3
F.
siGL2
siEzrin
% of cells with microvilli
100
80
60
40
20
0
Ezrin-T567E-GFP
Ezrin-T567E-GFP-ABS
N=3

Figure 3.7 Appending the actin binding/bundling sequence from espin to ezrin-GFP causes it to mislocalize and inhibits its activity

(A) Cells stably expressing GFP-tagged F-actin binding site (ABS) from espin were fixed and stained as indicated. GFP-ABS is found within most F-actin containing structures. (B) Cells stained as in A were scored for radixin-containing microvilli. GFP-ABS does not promote microvilli in the absence of ezrin. (C) Schematic of constructs. Espin ABS is expected to be available even when the endogenous ABS within ezrin is self-masked. (D) Cells stably expressing RNAi-resistant ezrin-GFP or ezrin-GFP-ABS were depleted of endogenous ezrin, stained with indicated markers. (E). Cells stained as in B or control siRNA-transfected cells were scored for the presence or absence of radixin-containing microvilli. Fusion with the ABS causes ezrin to fail to rescue microvilli. (F) Cells expressing indicated constructs and transfected with indicated siRNAs and scored for the presence or absence of microvilli. Activating ezrin in the context of the ezrin-GFP-ABS chimera causes a mild synthetic enhancement of microvilli defects. All scale bars, 10 μm. Cross-sections were expanded 5-fold vertically for clarity.

on its own (Figure 3.7.F). These results suggest that appending an unmasked actin-binding site to ezrin exerts a dominant inhibition of its apical localization and its ability to form microvilli.

LOK and SLK are the major kinases involved in ezrin phosphorylation

The results presented so far hint that phosphoregulatory control of ezrin controls its localization, and that tightly compartmentalized ezrin localization is necessary for microvilli. To test this hypothesis, we hunted for the relevant kinase(s). I reexamined my mass spectrometry of ezrin-iFlag immunoprecipitates (Figure 2.3) to identify the kinases in Jeg-3 cells responsible for phosphorylating ezrin. Although more than 18 kinases were identified, the four enriched more than two-fold in ezrin-iFlag immunoprecipitates are shown in Figure 3.8.A. The most highly enriched serine/threonine kinases were the evolutionary homologs LOK and SLK (Delpire, 2009). Immunoprecipitation of ezrin-iFlag co-precipitates some LOK-GFP (Figure 3.8.B) thereby supporting the mass spectrometry results.

If LOK and SLK are the relevant kinases for ezrin phosphorylation, I would expect the level of T567 phosphorylation to decrease when the level of LOK and/or SLK is reduced. Depletion of LOK by siRNA treatment resulted in about a 50% decrease in T567 phosphorylation (Figure 3.8.C). SLK depletion had a minimal effect on T567 phosphorylation, but, importantly, knocking down both LOK and SLK reduced ezrin T567 phosphorylation even further to about 20% of control levels (Figure 3.8.C), implying that ezrin is a substrate of both LOK and SLK in these cells. Consistent with a major role for LOK, fewer cells knocked down for LOK exhibited microvilli on their apical surface (Figures 3.8.D,E), an effect similar to that seen when ezrin is depleted by siRNA (Figure 3.1,3.5,3.6).

A.

Serine/threonine kinase	# of peptides recovered	Enrichment on ezrin-iFlag
STK10/LOK	13	4.0
SLK	9	3.6

B.

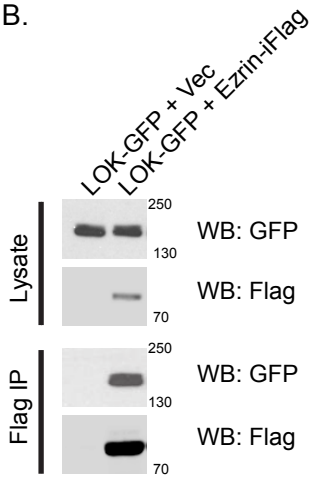

C.

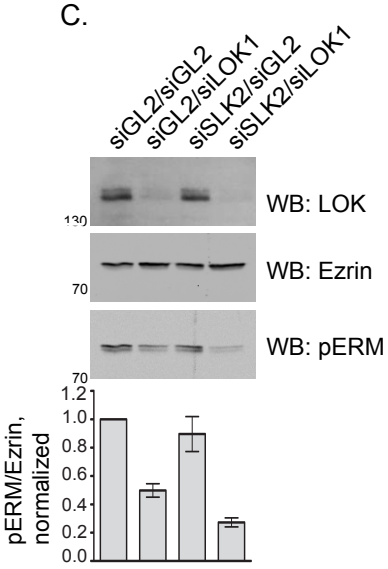

D.

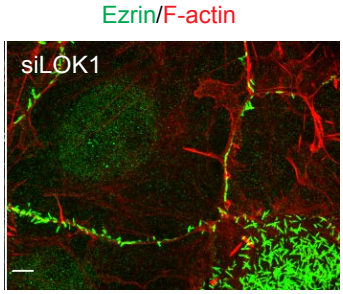

E.

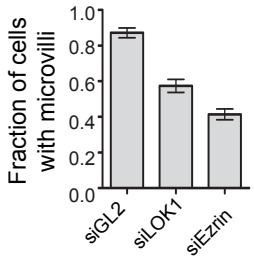

F.

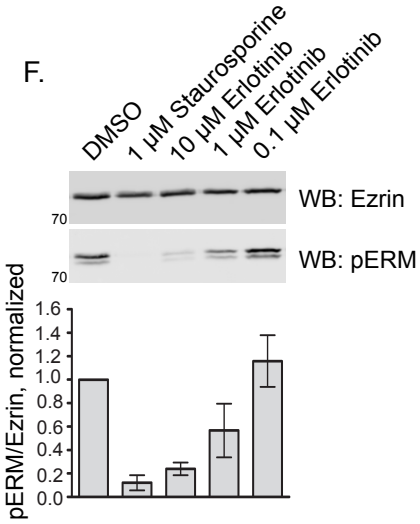

G.

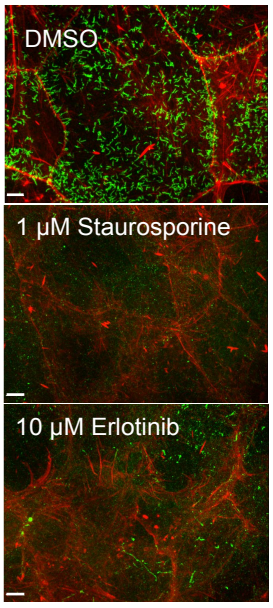

H.

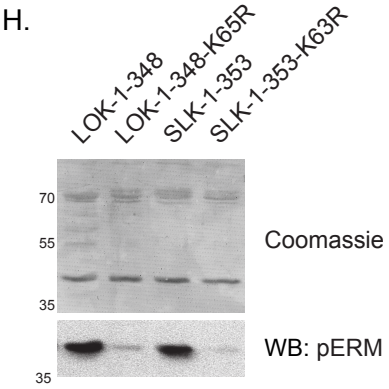

I.

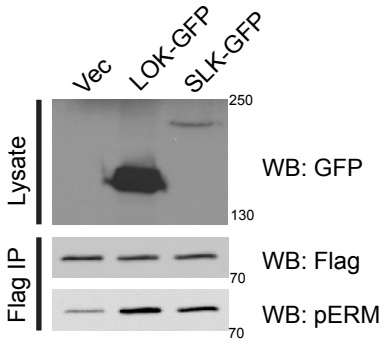

Figure 3.8 LOK and SLK are responsible for ezrin/radixin C-terminal phosphorylation in Jeg-3 cells.

(A) Enrichment statistics for LOK and SLK from mass spectrometry analysis of ezrin-iFlag cross-linking immunoprecipitates. LOK and SLK were the most highly enriched serine/threonine kinases binding to ezrin-iFlag. (B) LOK-GFP was co-expressed with empty vector or Ezrin-iFlag and cells were subjected to cross-linking immunoprecipitation using anti-Flag (Flag IP). LOK-GFP co-immunoprecipitates with ezrin-iFlag. (C) Cells were treated with indicated combinations of validated siRNAs against LOK (siLOK1) or SLK (siSLK2) or control (siGL2) and western blotted for LOK to measure knockdown efficiency. The level of phosphorylated ezrin and radixin was determined by western blot and quantified by densitometry. (D) Cells were treated with siLOK1 for 3 days and then fixed and stained for ezrin and F-actin. Knockdown of LOK causes loss of microvilli similar to the knockdown of ezrin (Fig. 3). (E) The presence of microvilli on cells treated with indicated siRNA was assessed following ezrin and F-actin staining. (F) Cells were treated with DMSO, staurosporine, or erlotinib at indicated concentrations for 5 minutes at 37^{O}C and phospho-ERM levels measured by western blot. (G) Cells treated as in F were fixed and stained for ezrin and F-actin. Erlotinib treatment causes a severe reduction in ezrin-containing microvilli. (H) GFP-Flag-tagged kinase constructs were immunoprecipitated using the Flag tag after expression in HEK293T cells, and then combined with purified GST-tagged ezrin C-terminus in the presence of ATP, which was then subjected to pERM western blot. Both LOK and SLK kinase domains are able to phosphorylate the ezrin C-terminal tail *in vitro*. (I) Cells were co-transfected with an empty vector or GFP fusions of either LOK or SLK along with ezrin-iFlag. The cells were lysed, and ezrin-iFlag was immunoprecipitated with anti-Flag (Flag IP) and the phosphorylation of ezrin-iFlag was detected by western blot. Both LOK-GFP and SLK-GFP overexpression cause an increase in the overall level of ezrin-iFlag phosphorylation. Data in C, E, and F are means ± s.d. of three independent experiments.

Erlotinib, a small molecule inhibitor of the epidermal growth factor receptor (EGFR) tyrosine kinase, was recently shown to inhibit LOK and SLK when used at higher concentrations (Yamamoto et al., 2011). A five minute treatment with 10 μM erlotinib resulted in the loss of ezrin phosphorylation and loss of microvilli from Jeg-3 cells, similar to 1 μM of the general kinase inhibitor staurosporine (Figures 3.8.F,G). Functional but not kinase-dead LOK or SLK kinase domains could each phosphorylate T567 in the context of the C-terminal domain of ezrin *in vitro* (Figure 4H), confirming that LOK and SLK each possess similar kinase activity towards ezrin. Moreover, overexpression of LOK-GFP or SLK-GFP increased the phosphorylation of co-transfected ezrin-iFlag *in vivo* (Figure 3.8.I).

I performed some additional experiments to support my conclusion that LOK and SLK are the ERM kinases. I found that ezrin-iFlag stable cell-lines could precipitate endogenous LOK (3.9.A). The effect of the LOK siRNA in Figure 3.8.C was corroborated with a second LOK-specific siRNA (Figure 3.9.B). Jeg-3 cells also express MST4 and MINK1, two kinases that phosphorylate ezrin *in vitro* (ten Klooster et al., 2009), but validated siRNAs against these kinases had no effect on the level of ezrin phosphorylation (Figure 3.9.B). Furthermore, ROCK inhibitor Y-27632 and CDK inhibitor roscovitine had no effect on T567 phosphorylation in Jeg-3 cells (data not shown). Collectively, my results show that LOK and SLK are functionally the major relevant kinases involved in the steady-state phosphorylation of ezrin in Jeg-3 cells.

LOK activity is localized and restricted apically via the C-terminal domain

LOK has an N-terminal kinase domain and a C-terminal domain predicted to be similar to the AT1-46 homology (ATH) domain of SLK (Sabourin et al., 2000) (Figure 3.10.A).To dissect the molecular organization of LOK, I constructed a series of truncation mutants as well as

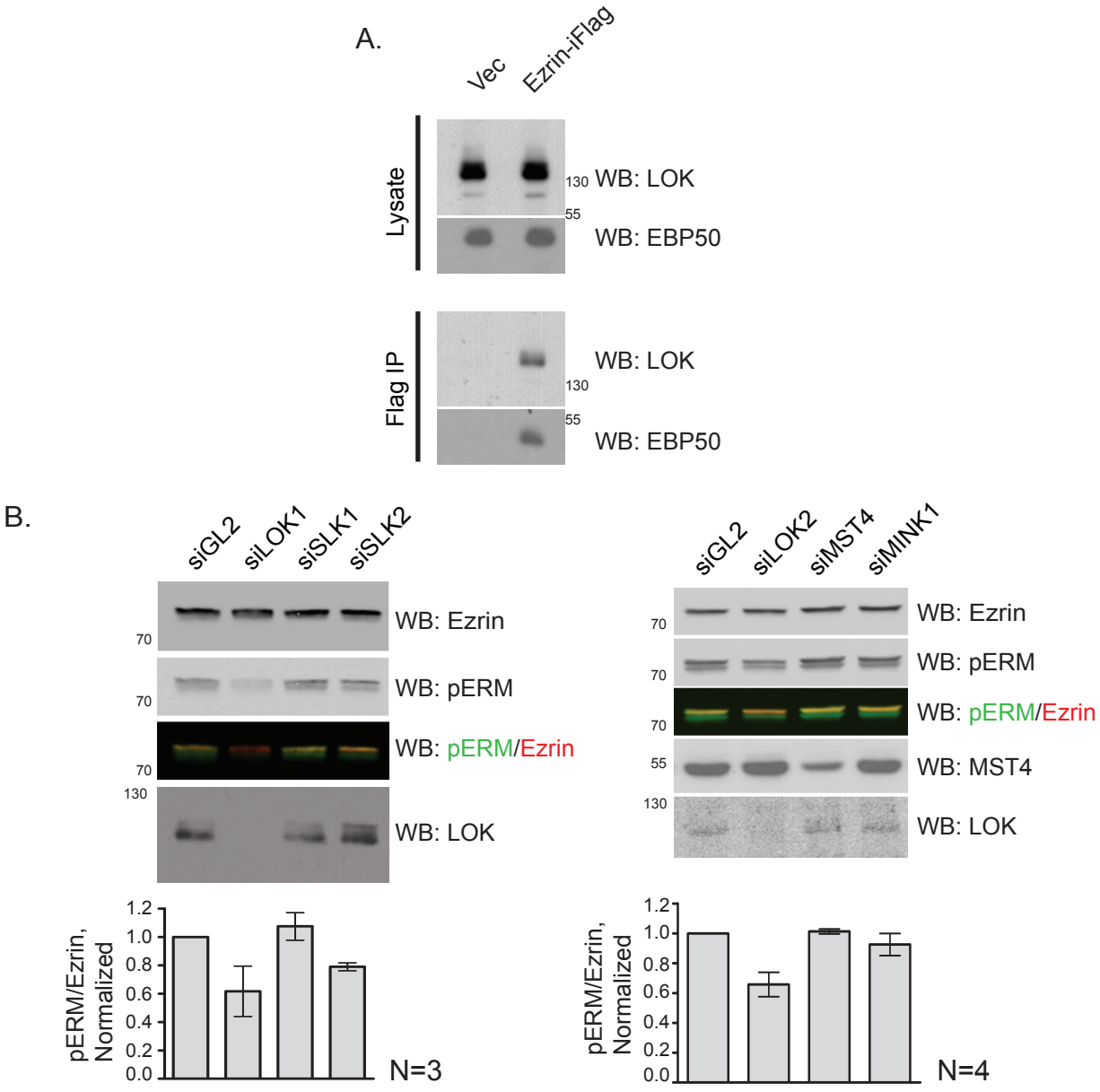

Figure 3.9 Additional experiments verifying that LOK and SLK are upstream of phospho-ezrin and radixin in Jeg-3 cells.

(A) Cells stably expressing empty vector or ezrin-iFlag were cross-linked and immunoprecipitated using anti-Flag (Flag IP), and the immunoprecipitate was western blotted to detect ezrin-binding phosphoprotein 50 (EBP50), a known interaction partner of ezrin, and LOK. Endogenous LOK interacts with stably transfected ezrin-iFlag. (B) Cells were treated with indicated siRNA and phospho-ERM was measured by western blot. siRNAs against other known ERM kinases (siMST4 and siMINK1) fail to cause any reduction in phospho-ERM levels, whereas two siRNAs against LOK (siLOK1 and siLOK2) cause a 40-50% reduction, and one siRNA against SLK (siSLK2) causes a 20% reduction. Data are means ± s.d. of three independent experiments.

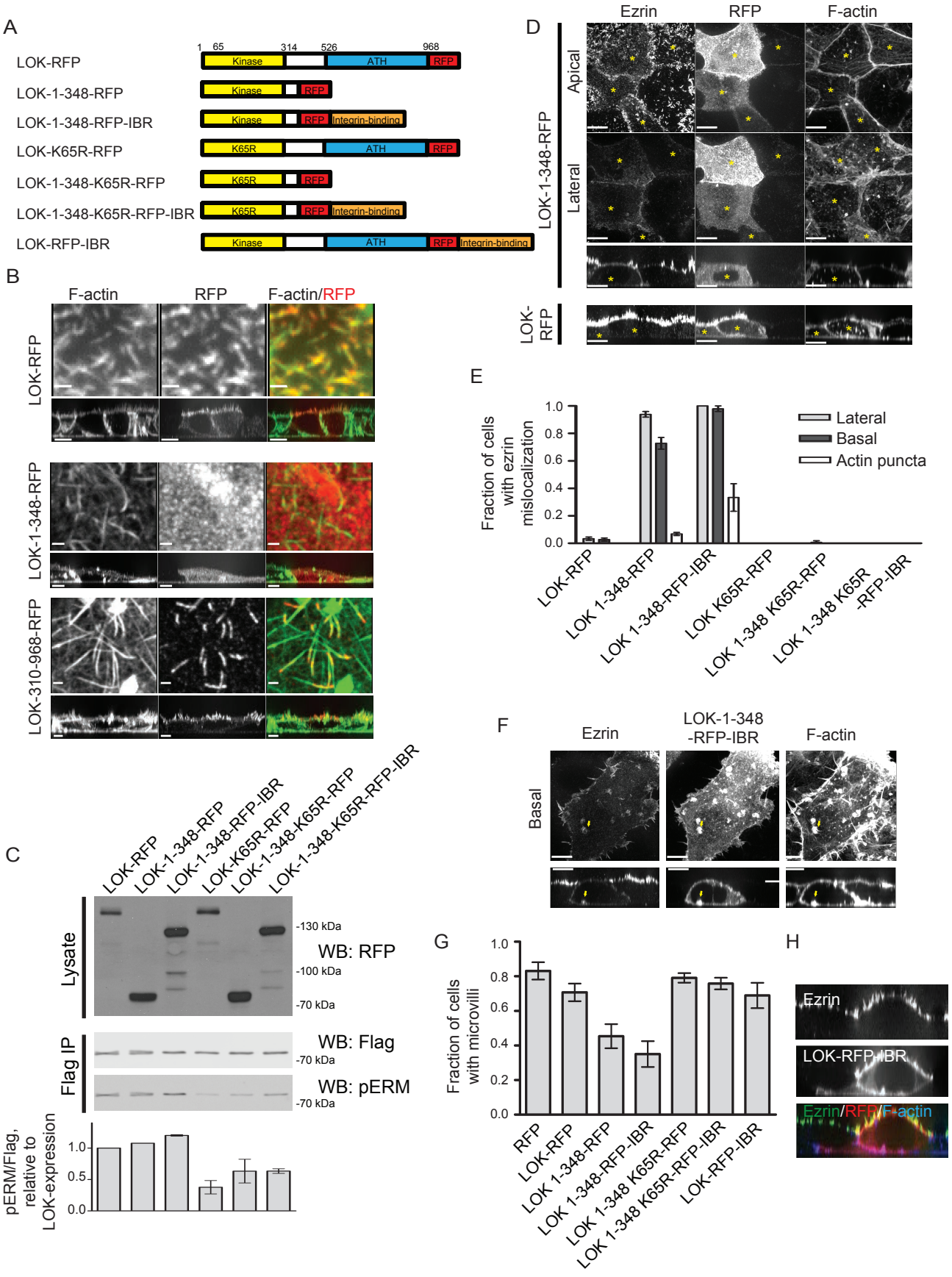
A
LOK-RFP
LOK-1-348-RFP
LOK-1-348-RFP-IBR
LOK-K65R-RFP
LOK-1-348-K65R-RFP
LOK-1-348-K65R-RFP-IBR
LOK-RFP-IBR
Kinase
ATH
RFP
Integrin-binding
K65R
1
65
314
526
968
B
F-actin
RFP
F-actin/RFP
LOK-RFP
LOK-1-348-RFP
LOK-310-968-RFP
C
LOK-RFP
LOK-1-348-RFP
LOK-1-348-RFP-IBR
LOK-K65R-RFP
LOK-1-348-K65R-RFP
LOK-1-348-K65R-RFP-IBR
Lysate
Flag IP
WB: RFP
WB: Flag
WB: pERM
-130 kDa
-100 kDa
-70 kDa
pERM/Flag, relative to LOK-expression
1.0
0.5
0.0
D
Ezrin
RFP
F-actin
Apical
Lateral
LOK-1-348-RFP
LOK-RFP
E
Fraction of cells with ezrin mislocalization
1.0
0.8
0.6
0.4
0.2
0.0
Lateral
Basal
Actin puncta
LOK-RFP
LOK 1-348-RFP
LOK 1-348-RFP-IBR
LOK K65R-RFP
LOK 1-348 K65R-RFP
LOK 1-348 K65R -RFP-IBR
F
Ezrin
LOK-1-348 -RFP-IBR
F-actin
Basal
G
Fraction of cells with microvilli
1.0
0.8
0.6
0.4
0.2
0.0
RFP
LOK-RFP
LOK 1-348-RFP
LOK 1-348-RFP-IBR
LOK 1-348 K65R-RFP
LOK 1-348 K65R-RFP-IBR
LOK-RFP-IBR
H
Ezrin
LOK-RFP-IBR
Ezrin/RFP/F-actin

Figure 3.10 Unregulated LOK causes ezrin depolarization

(A) Schematic of truncation constructs and chimeras used. (B) LOK-RFP and truncations were localized relative to F-actin. LOK and the LOK C-terminal domain localized to microvilli, whereas the N-terminal kinase domain did not. For clarity, only a small region of the apical domain is shown, and the full cell is shown in vertical cross-section. (C) Cells were co-transfected with indicated RFP-tagged LOK constructs along with ezrin-iFlag. The cells were lysed and ezrin-iFlag was immunoprecipitated (Flag IP), and phosphorylation of ezrin-iFlag was measured by quantitative western blot. The fold-increase in ezrin phosphorylation due to each LOK truncation was normalized to the overexpression of full-length LOK. (D) Cells expressing the RFP-tagged LOK N-terminal kinase domain alone (LOK-1-348-RFP) were stained for ezrin and F-actin and presented as either an apical, basolateral, or side view, and cells transfected with full-length LOK-RFP (lower panels) are presented in side view. Cells expressing the LOK kinase domain alone exhibit delocalized ezrin staining, whereas cells expressing full-length LOK do not. (E) Cells expressing indicated LOK-RFP fusion proteins were stained as in D, and the ezrin depolarization phenotypes were quantified by confocal microscopy. Only when the LOK kinase domain is functional but unregulated does it cause ezrin to mislocalize. (F) Cells overexpressing a fusion of the LOK kinase domain to the integrin-binding region (IBR) of talin were processed as in D. Arrows point to one F-actin containing basal-membrane associated structure. When the kinase domain alone is intentionally mislocalized, ezrin is preferentially located around these structures. (G) Cells expressing LOK-RFP and derivatives were stained with ezrin and F-actin and the presence of microvilli was scored as in Figs. 3B, 4D. (H) Cell expressing full-length LOK fused to the IBR and stained for ezrin and F-actin. Even when intentionally mislocalized basally, full-length LOK does not cause ezrin to mislocalize, indicating that it is only active in the apical domain. Active, mislocalized LOK constructs cause cells to lose microvilli. Data in B, E, and H are means ± s.d. of three or four independent experiments. *En face* images in C: scale bars, 1 μm. All other scale bars, 10 μm. Cross-sections were expanded 5-fold vertically for clarity, and yellow asterisks (*) mark transfected cells.

generating the K65R kinase-dead mutant previously shown to inhibit LOK activity (Belkina et al., 2009) (Figure 3.10.A).

LOK has been shown to localize to the membrane of peripheral blood lymphocytes (Belkina et al., 2009), but a more precise location has not been reported. Although I was unable to determine the localization of endogenous LOK, LOK-RFP is mostly apical but also partially basolateral (Figure 3.10.B). The N-terminal kinase domain failed to localize to any specific region, whereas low-level expression of the C-terminal domain localized specifically to apical microvilli (Figure 3.10.B). Thus LOK is localized to microvilli via the C-terminal domain.

To determine whether LOK distribution is important for its activity toward ezrin *in vivo*, I expressed truncations of LOK and their kinase-dead derivatives along with ezrin-iFlag and measured the effect on ezrin-iFlag phosphorylation (Figure 3.10.C). Unexpectedly, I found that all constructs containing the active N-terminal kinase domain—even those that did not contain the C-terminal domain necessary for localization to microvilli—yielded a similar increase in ezrin-iFlag phosphorylation relative to constructs lacking kinase activity (Figure 3.10.C).

Since the overexpression of either microvillus-localized LOK or the delocalized N-terminal kinase domain could both raise the level of phosphorylated ezrin to a similar extent (Figure 3.10.C), this allowed me to explore the contribution of localizing the kinase activity to ezrin distribution. Cells overexpressing full-length LOK were unaffected: ezrin was still highly enriched in microvilli (Figure 3.10.D). By contrast, cells overexpressing a delocalized kinase ('LOK-1-348-RFP') consistently exhibited mislocalized ezrin including on the basolateral plasma membrane below cell-cell junctions, a location at which ezrin is never normally enriched (Figure 3.10.D, E). This effect is due to the mislocalized kinase activity, because overexpression

of either the kinase domain harboring the K65R mutation ('LOK-1-348-K65R-RFP') or full-length LOK never caused ezrin to localize basolaterally (Figure 3.10.D, E). Kinase-dead LOK-RFP ('LOK-K65R-RFP') has a mild dominant-negative effect reducing the number of cells with microvilli as discussed below (Figure 3.15.C), but the remaining ezrin did not mislocalize to basolateral membranes, consistent with a requirement for kinase activity in order for LOK constructs to have this effect. Taken together, these data suggest that LOK kinase activity must be apically restricted via the C-terminal domain to maintain microvilli.

I next asked whether intentionally mistargetting just the N-terminal kinase domain to a specific region of the basolateral membrane would cause ezrin to accumulate in that region. The C-terminus of talin has been shown to bind integrins (Xing et al., 2001), so I generated a construct containing the LOK kinase domain fused to talin's integrin binding region (IBR). Cells expressing the kinase-domain- IBR chimera ('LOK-1-348-RFP-IBR') mislocalized ezrin on the basal plasma membrane as well as to basal actin puncta to a significantly greater extent than those expressing the kinase domain alone ('LOK-1-348-RFP') (Figure 3.10.F, arrows; quantified in Figure 3.10.E). Therefore ezrin enrichment coincides with the location of unregulated LOK activity.

Consistent with this and my earlier data showing that phosphomimetic ezrin cannot support microvillus formation, overexpression of a delocalized, active LOK kinase domain ('LOK-1-348-RFP' or 'LOK-1-348-RFP-IBR') greatly reduced the number of microvilli, whereas overexpression of full-length LOK ('LOK-RFP') did not (Figure 3.10.G). Kinase activity was also required, because kinase-dead versions of the delocalized kinases ('LOK-1-348-K65R-RFP' or 'LOK-1-348-K65R-RFP-IBR') also failed to reduce microvilli (Figure 6G).

Thus the correct targeting and activation of LOK to microvilli by a mechanism involving its C-terminal domain is critical for the normal function and distribution of ezrin.

Overexpressed LOK was found to be partially mislocalized along basolateral membranes, but ezrin was never found associated with it (Figure 3.10.D). Furthermore, when the full-length kinase was fused to the IBR ('LOK-RFP-IBR'), the chimera localized basolaterally to a greater extent, but ezrin remained strictly polarized in microvilli (Figure 3.10.H) and microvilli remained intact (Figure 3.10.G). Thus in the context of the full-length protein, factors must exist that restrict LOK activity apically.

I performed additional experiments to verify that the effects of the kinase domain constructs acted by re-localizing phosphorylated ezrin, and that these effects could also be seen with SLK. By immunolocalizing phospho-T567 ezrin and phospho-T564 radixin, I could show that delocalized ezrin caused by overexpression of the LOK N-terminal kinase domain was due to delocalized ERM phosphorylation (Figure 3.11.A, upper two panels). SLK has a domain architecture similar to LOK, and the N-terminal kinase domain and the C-terminal ATH domain are conserved between them, whereas the linker region is variable in length and sequence, consistent with its not being required for the effects shown below (Figure 3.15). Consistently, overexpression of SLK or just the N-terminal kinase domain (1-353) gave equivalent results to those obtained with LOK and its derivatives (Figures 3.11.C-E). Thus, I conclude that the LOK and SLK activity must be restricted by factors in the apical domain acting through the C-terminal ATH region, giving rise to apically polarized ezrin and microvilli.

Localized LOK/SLK activity is sufficient for microvillus formation

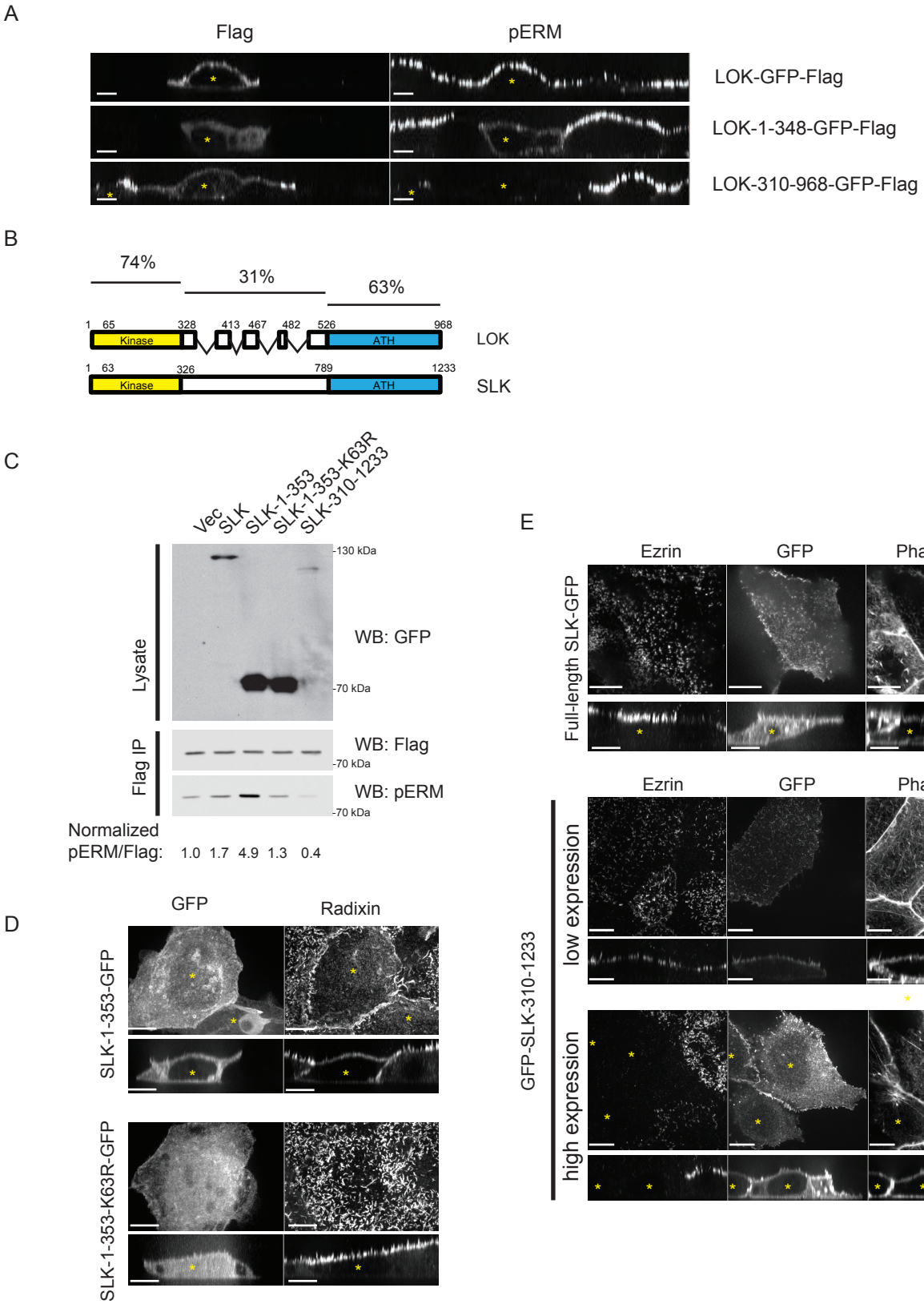
A
Flag
pERM
LOK-GFP-Flag
LOK-1-348-GFP-Flag
LOK-310-968-GFP-Flag
B
74%
31%
63%
1 65 328 413 467 482 526 968
Kinase
ATH
LOK
1 63 326 789 1233
Kinase
ATH
SLK
C
Vec
SLK
SLK-1-353
SLK-1-353-K63R
SLK-310-1233
130 kDa
70 kDa
Lysate
WB: GFP
Flag IP
WB: Flag
70 kDa
WB: pERM
70 kDa
Normalized
pERM/Flag: 1.0 1.7 4.9 1.3 0.4
D
GFP
Radixin
SLK-1-353-GFP
SLK-1-353-K63R-GFP
E
Ezrin
GFP
Phalloidin
Full-length SLK-GFP
Ezrin
GFP
Phalloidin
GFP-SLK-310-1233
low expression
high expression

3.11 Additional experiments verifying that phospho-ezrin polarity requires polarized LOK and SLK activity

(A) Cells expressing indicated LOK-GFP-Flag fusion proteins were acid-fixed and stained with pERM and Flag antibodies. LOK effects on ezrin and radixin localization are due to the redistribution of the phosphorylated species. (B) LOK and SLK alignments. Percent identities in various domains were scored using CLUSTALW. The kinase domain and the C-terminal domain are highly conserved, whereas the linking region (which is dispensable for the dominant effects described in Figure 7 and S5) is more divergent. (C) Cells were co-transfected with ezrin-iFlag along with various GFP fusions or vector control as indicated, lysed, and the Flag tag immunoprecipitated and phosphorylation measured by western blot. Co-transfection of SLK leads to an increase in the phosphorylation of ezrin-iFlag so long as the kinase domain is present and functional. As with LOK, expression of the C-terminal domain inhibits ezrin-iFlag phosphorylation (see Figure 7B). Note that phosphorylation on T567 of ezrin-iFlag exceeds 2-fold. This happens because transiently transfected ezrin-iFlag is less phosphorylated than endogenous ezrin (Figure S1B). (D) Cells overexpressing functional or kinase-dead SLK N-terminal kinase domain were stained for radixin and F-actin. Overexpression of the functional but not the inactive (K63R) kinase domain causes ERM depolarization. (E) SLK and its derivatives were expressed in Jeg-3 cells as GFP fusions and the cells stained for ezrin and F-actin. Full-length SLK is present but not highly enriched in microvilli, whereas, at low expression level, the C-terminal domain is localized specifically in apical microvilli. At high expression level, the C-terminal region causes the dominant inhibition of membrane-localized ezrin, similar to LOK's C-terminal region (see Figure 7). All scale bars, 10 μm. For clarity, yellow asterisks (*) mark transfected cells.

To assess the importance of LOK and SLK in microvillus formation, I set out to generate erlotinib-resistant forms of the kinases. Erlotinib was first identified as an inhibitor of EGFR (Pao et al., 2005; Pao and Chmielecki, 2010). Threonine-766 of EGFR becomes mutated to methionine in some erlotinib-resistant cancers and has been shown to cause the occlusion of erlotinib from the ATP-binding site (Pao et al., 2005). I asked whether the homologous mutation could be used to develop erlotinib-resistant LOK and SLK, which could then be used to test microvilli formation in the absence of endogenous LOK/SLK activity. Structural analysis revealed that the residues in the homologous positions as T766 in EGFR are I110 in LOK (Figure 3.12.A) and I108 in SLK. When modeled into the LOK ATP binding site, erlotinib is also close to L85, so we mutated this residue to M as well (Figure 3.12.A). Expression of LOK-I110M-GFP or LOK-L85M,I110M-GFP both similarly abrogated the loss of microvilli induced by erlotinib treatment after a five minute's treatment in most cells, while overexpression of wild-type LOK was less effective (Figure 3.12.B). To optimize the assay, cells transiently transfected with a control plasmid (GFP targeted to the nucleus with a nuclear localization sequence) and a separate population of cells expressing LOK-I110M-GFP, which enters the nucleus, were mixed and treated with erlotinib at different concentrations (not shown) and for different amounts of time (Figure 3.12.C,D). These experiments showed that ~15 minutes in 20 μM erlotinib gave the maximal difference between treated and untreated cells.

Next, the assay was used to determine whether positional LOK phosphorylation affects the formation of microvilli. Strikingly, expression of just the erlotinib-resistant LOK kinase domain failed to rescue microvillus loss in the presence of erlotinib to a similar extent to the kinase-dead variant or the control plasmid (Figures 3.13A), and this result was highly

A.

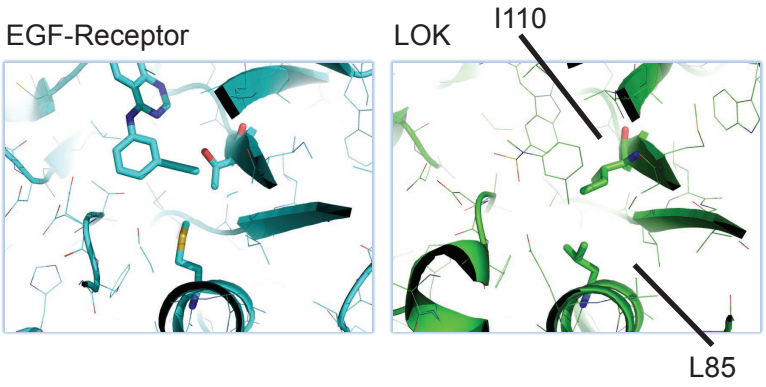
EGF-Receptor
LOK
I110
L85

B.

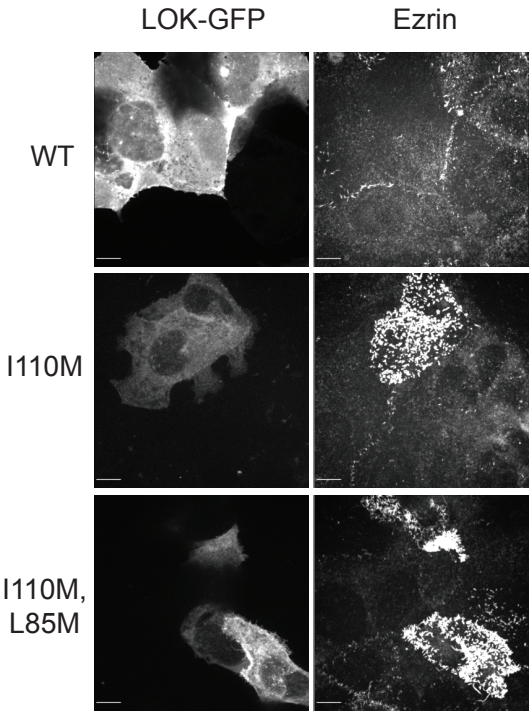
LOK-GFP
Ezrin
WT
I110M
I110M,
L85M

C.

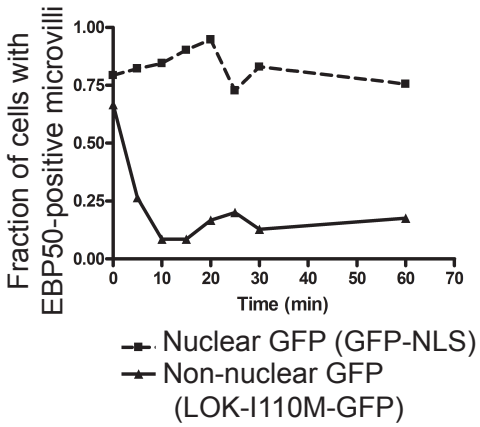
Fraction of cells with
EBP50-positive microvilli
1.00
0.75
0.50
0.25
0.00
0
10
20
30
40
50
60
70
Time (min)
Nuclear GFP (GFP-NLS)
Non-nuclear GFP
(LOK-I110M-GFP)

D.

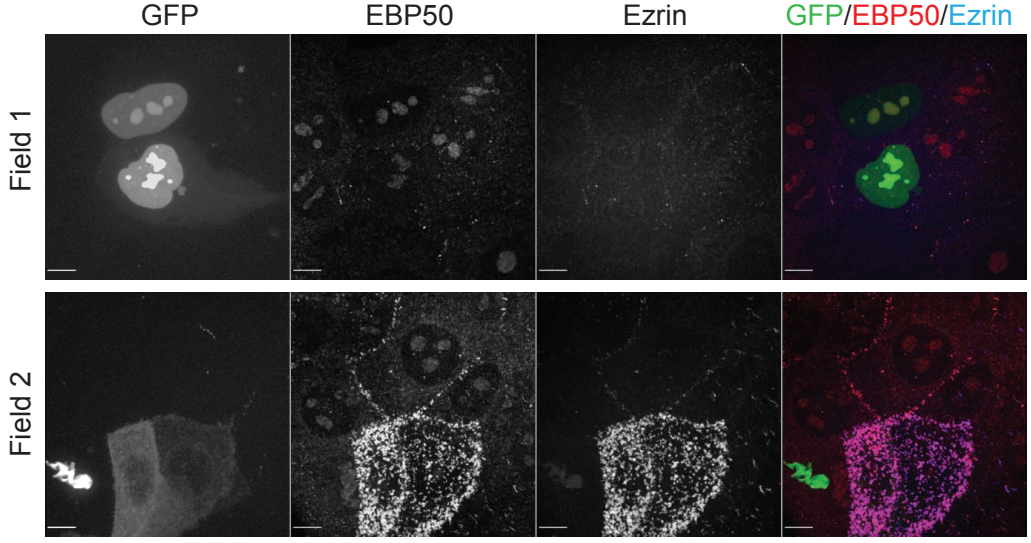
GFP
EBP50
Ezrin
GFP/EBP50/Ezrin
Field 1
Field 2

Figure 3.12 Creating drug-resistant LOK.

(A) *Green*: structure of EGFR (cartoon) bound to erlotinib (sticks; Stamos et al., 2002). *Blue*: structure of LOK kinase domain with residue I110 highlighted (Pike et al., 2008). The homolog of T766 (EGFR) is I110, which, along with L85, is also poised to infiltrate the ATP binding pocket (LOK). (B) Cells transfected as indicated (along with non-transfected surrounding cells) were first treated with 10 μM erlotinib for 5 minutes to induce ezrin dephosphorylation then fixed and stained for ezrin. Cells transfected with LOK mutation always had more ezrin staining than surrounding non-transfected cells. (C) Cells were first transfected with LOK_110M-GFP or GFP-tagged nuclear localization sequence (NLS) as a control, then the cells were trypsinized and mixed and placed onto coverslips. Each coverslip was treated with 20 μM erlotinib for indicated time, then fixed and stained for ezrin and EBP50. Cells were first analyzed for the expression of nuclear GFP (which must have been GFP-NLS) or non-nuclear GFP (which must have been LOK-I110M-GFP) and then scored for EBP50-positive microvilli. (D) Representative fields from C. Bar is 10 μm.

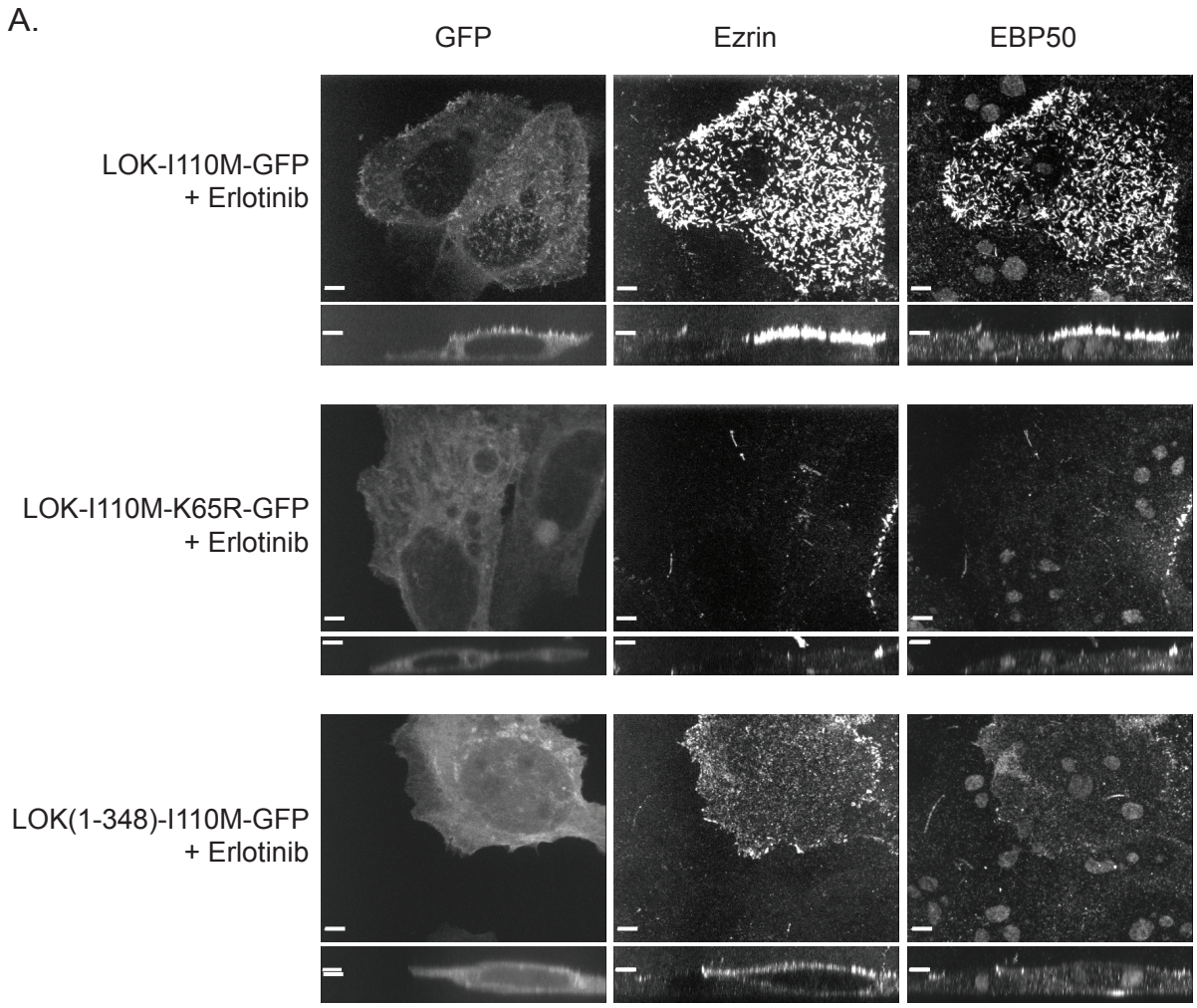

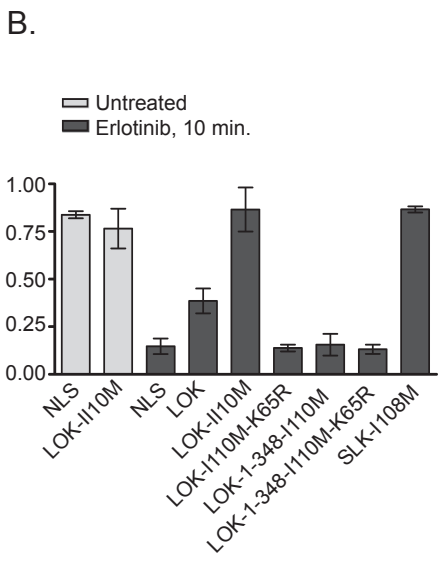

Figure 3.13 Regulated LOK activity is necessary and sufficient for microvilli in the presence of erlotinib.

(A) Cells expressing erlotinib-resistant mutants of LOK as indicated were treated with 20 μM erlotinib for 10 minutes. LOK-I110M-GFP-transfected cells (or SLK-I108M-GFP-transfected cells, Figs. 3.14.A,B) but not neighboring untransfected cells, are protected from microvillus loss due to erlotinib. Cells transfected with LOK-1-348-I110M-GFP have membrane-enriched depolarized ezrin, but do not form microvilli. (C) Quantification of results in Figs. B and 3.13.A. Data are means ± s.d. of three independent experiments.

reproducible (Figure 3.13.B). Thus, the regulation of LOK activity via the C-terminal domain is necessary for the presence of microvilli.

I asked whether erlotinib-resistant SLK could also protect microvilli from erlotinib-induced collapse. SLK-I108M-GFP-transfected cells continued to have microvilli despite treatment with erlotinib (Figure 3.14.A). Thus LOK and SLK are each sufficient for microvilli in the presence of erlotinib.

Finally, I verified that phosphorylated ezrin and radixin could be seen in microvilli following erlotinib treatment in LOK-I110M-GFP-transfected cells. Strikingly, it was present in microvilli when full-length LOK was transfected, but in a delocalized fashion all over the plasma membrane when the erlotinib-resistant N-terminal kinase domain alone was transfected (Figure 3.14.B), thus confirming that erlotinib causes microvillus collapse by specifically inhibiting LOK/SLK activity, which is necessary and sufficient for polarized phospho-ERM.

The LOK C-terminal domain both localizes and regulates the N-terminal kinase domain

To further investigate the localization of LOK activity, I examined the effect of expressing either full-length constructs or the C-terminal domain alone (Figure 3.15.A). Low-level expression of the C-terminal domain of LOK (Figure 3.15.B) or the equivalent region in SLK (Figure 3.11.B, middle panels) showed that it localizes preferentially to microvilli. Strikingly, however, high level expression of the entire LOK C-terminal domain (residues 310-968) or a smaller segment (residues 586-968) caused a significant reduction in overall ezrin phosphorylation (Figure 3.15.B) and a nearly complete elimination of microvilli (Figure 3.15.C). In addition to accumulating at cell junctions and in the cytoplasm, expression of the LOK C-terminal domain caused and accumulated in long protrusive F-actin-containing structures devoid

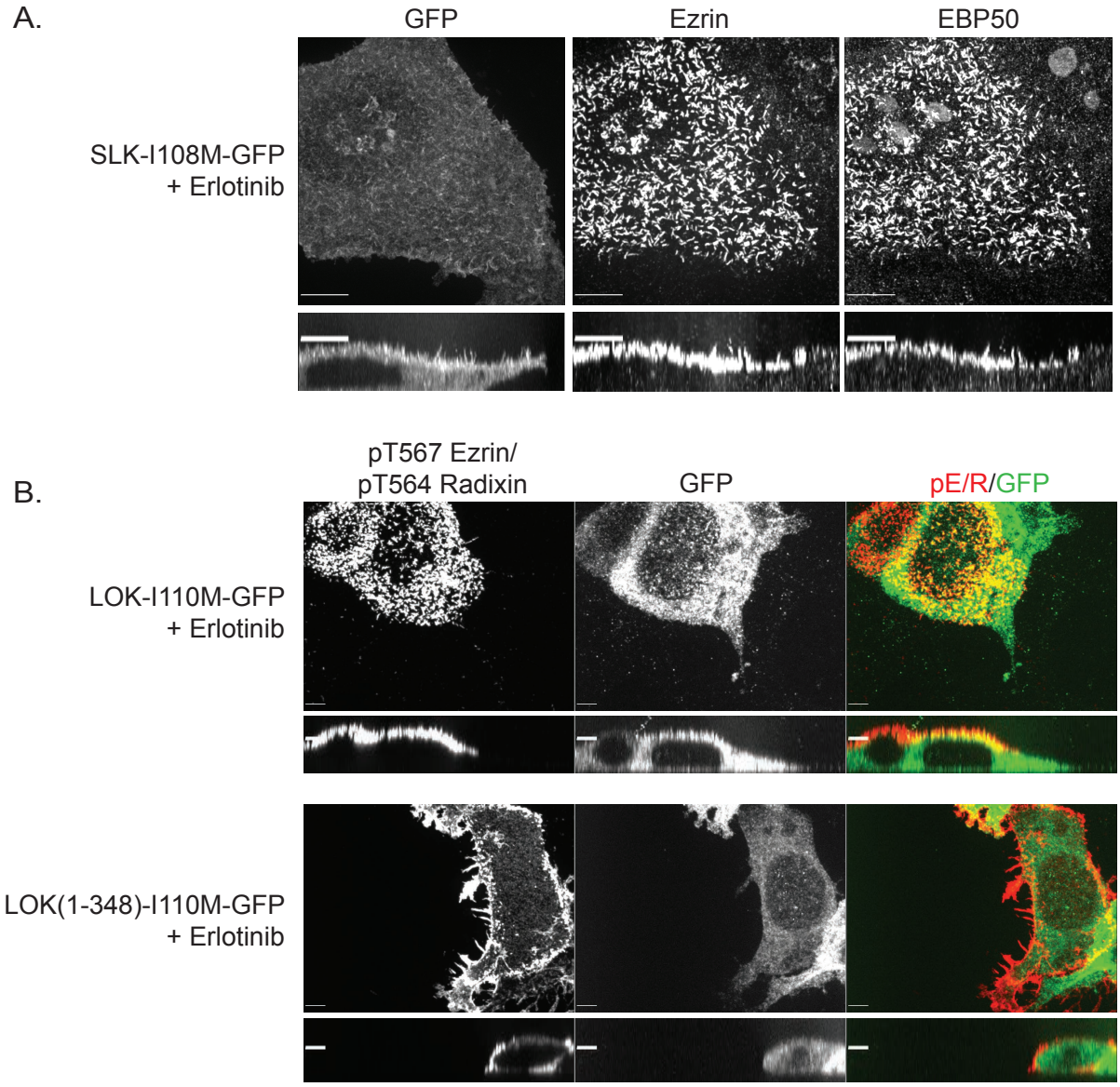

Figure 3.14 Design and utilization of drug-resistant LOK and SLK mutants.

(A) Cells transfected to transiently express SLK-I108M-GFP were stained for ezrin and EBP50. Just like LOK-I110M-GFP, SLK-I108M-GFP also restores apical ezrin and EBP50 distribution following erlotinib treatment. Quantified in 3.12.C. (B) Cells transfected to transiently express indicated GFP fusion proteins were acid-fixed and stained with pERM and GFP antibodies. LOK(1-348)-I110M cannot support apically-positioned phospho-T567 ezrin/phospho-T564 radixin following inhibition of endogenous LOK/SLK function due to erlotinib treatment. All scale bars, 10 μm.

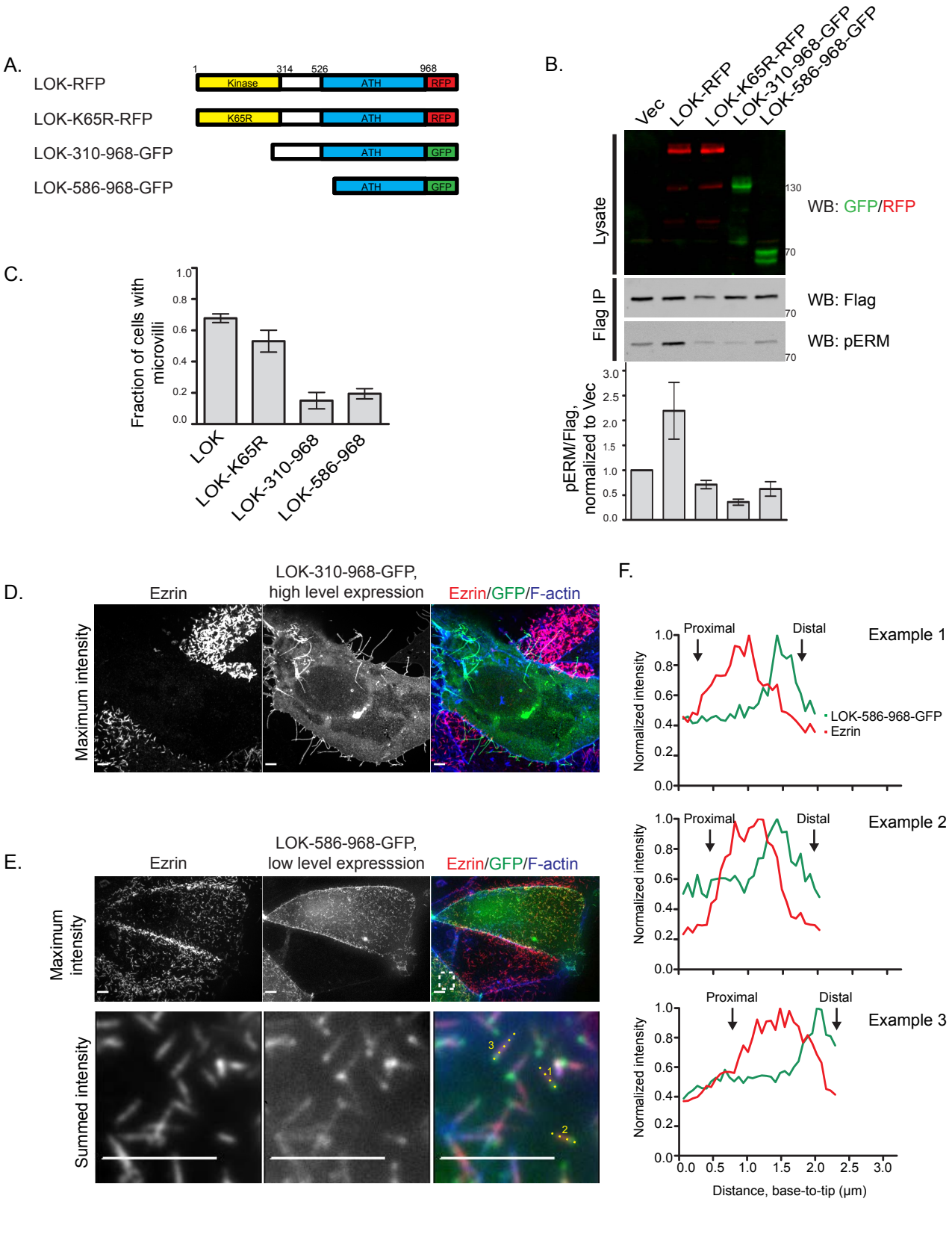
A.
LOK-RFP
LOK-K65R-RFP
LOK-310-968-GFP
LOK-586-968-GFP
Kinase
K65R
ATH
RFP
GFP
1
314
526
968
B.
Vec
LOK-RFP
LOK-K65R-RFP
LOK-310-968-GFP
LOK-586-968-GFP
Lysate
Flag IP
WB: GFP/RFP
WB: Flag
WB: pERM
130
70
pERM/Flag, normalized to Vec
C.
Fraction of cells with microvilli
LOK
LOK-K65R
LOK-310-968
LOK-586-968
D.
Ezrin
LOK-310-968-GFP, high level expression
Ezrin/GFP/F-actin
Maximum intensity
E.
Ezrin
LOK-586-968-GFP, low level expresssion
Ezrin/GFP/F-actin
Maximum intensity
Summed intensity
F.
Proximal
Distal
Example 1
Example 2
Example 3
LOK-586-968-GFP
Ezrin
Normalized intensity
Distance, base-to-tip (μm)

Figure 3.15 Overexpression of the LOK C-terminal domain inhibits membrane association of ezrin, and this effect can be limited to extremely small regions within microvilli.

(A) Schematic of tagged truncation constructs used. (B) Cells were co-transfected with empty vector or GFP or RFP fusions of LOK along with ezrin-iFlag. The cells were lysed and ezrin-iFlag was immunoprecipitated with anti-Flag (Flag IP) and phosphorylation of ezrin-iFlag was detected by western blot and quantified. When the LOK C-terminal domain is overexpressed without an active kinase domain, ezrin-iFlag phosphorylation is inhibited. (C) Cells expressing indicated LOK-GFP or -RFP fusions were stained for ezrin and F-actin and assessed for the presence of microvilli. LOK fusions that cause decreased phospho-ERM also cause microvillus loss. (D) Cells expressing high levels of the LOK C-terminal domain (LOK-310-968-GFP) were stained for ezrin and F-actin. The overexpression of the LOK C-terminal domain causes the loss of microvilli and formation of F-actin positive protrusions lacking ezrin. (E) Cells expressing a low level of the shorter region of the LOK C-terminal domain (LOK-586-968-GFP) were stained for ezrin and F-actin. Bottom panels show an enlargement of the region boxed in the upper right panel. (F) Fluorescence intensity along the lines indicated in E of three microvilli from their proximal to distal ends as marked. The minimal overexpression of the LOK C-terminal region often causes a loss of ezrin staining from the distal ends of microvilli. Data in B and C are means ± s.d. of three independent experiments. All scale bars, 10 μm.

of ezrin mostly emanating from the basolateral membrane, suggesting the possibility that it imparts additional defects (Figure 3.15.D). Expression of the equivalent region of SLK promoted a similar reduction in phospho-ERM as well as the loss of microvilli (Figures 3.11.C, E, lower panel).

Surprisingly, expression of full-length kinase-dead LOK was much less efficient at reducing the number of cells with microvilli (Figure 3.15.C), suggesting that the strong inhibitory effect of the C-terminal domain is partially masked in the context of the full-length protein.

At low levels of expression in the rare cells that have normal microvilli, the smaller fragment of the LOK C-terminal domain, LOK-586-968-GFP, localized preferentially to the distal ends of microvilli (Figure 3.15.E). In individual microvilli, the intensities of ezrin and LOK-586-968-GFP display a partially mutually exclusive relationship along microvilli (Figure 3.15.E,F), and therefore appear to represent targeted inhibition of ezrin accumulation in discrete regions.

To investigate the localization of LOK-586-968-GFP in more detail, additional cells were carefully imaged. Ezrin exclusion was observed in all cells expressing this domain and still retaining microvilli, but often it was observed at both the tip and base of the microvilli. An example is shown in Figure 3.16.A. Even in these examples, however, the bulk of LOK-586-968-GFP is located toward the microvillus tip. Neither ezrin exclusion nor concentration at the microvillus tip was observed with full-length LOK (Figure 3.16.B), possibly hinting at regulatory masking in full-length LOK of a localization determinant within its C-terminal region. Thus, because LOK-586-968-GFP is typically more concentrated on the tip than at the base of

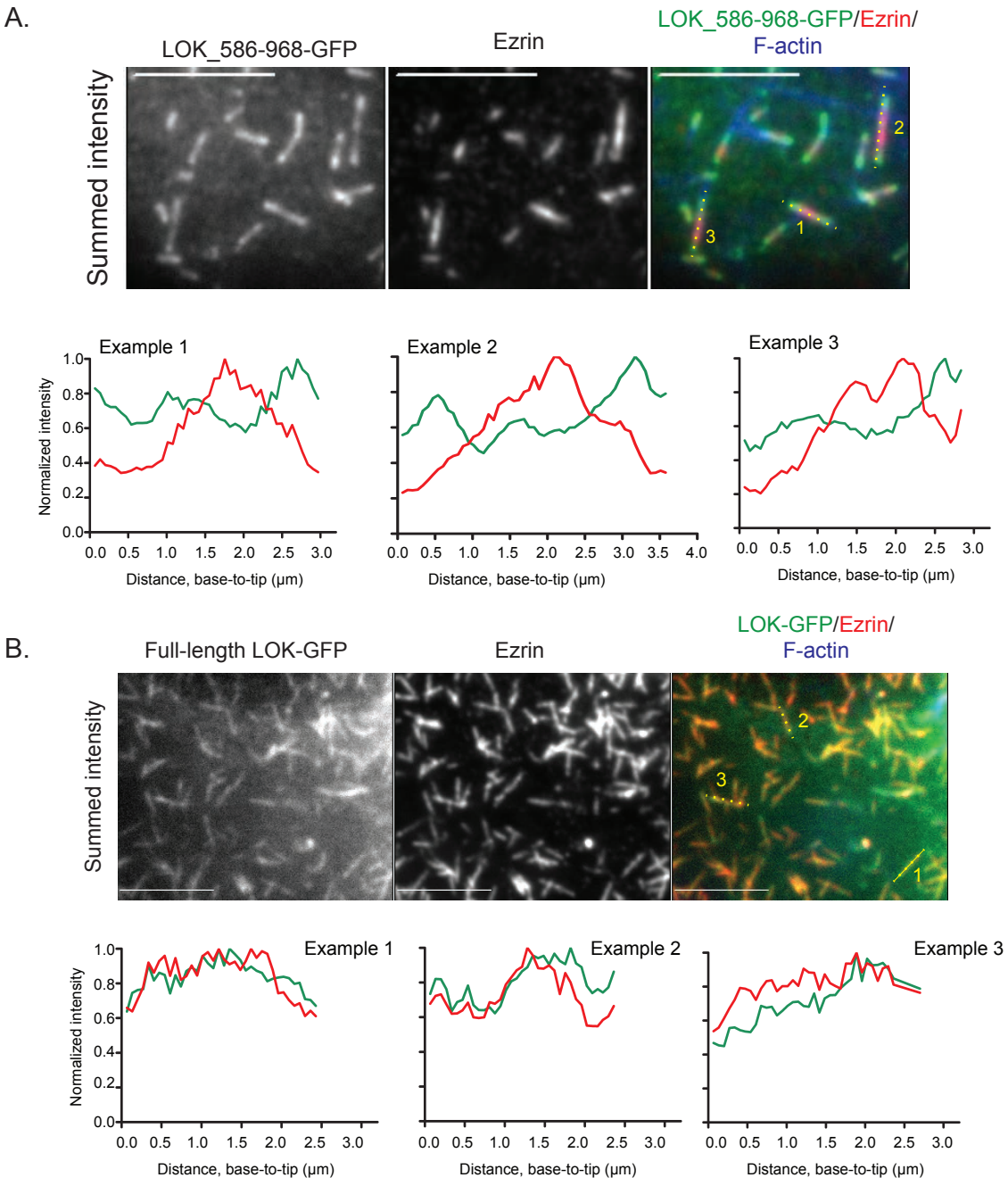

Figure 3.16 Additional controls verifying that the LOK C-terminus localizes to the ends of microvilli

(A and B) Summed-intensity projection of cells expressing a dominant-negative region of the LOK C-terminal domain (A) or full-length LOK (B) stained for ezrin and F-actin. A portion of the apical membrane is shown, and line intensities for three microvilli in each image are shown. (A) In these microvilli, membrane-bound ezrin is reduced in both the base and the tip, as seen in three base-to-tip line intensity plots. (B) This is not the case for full-length LOK-GFP, which stains the whole microvillus, its intensity rising and falling with that of ezrin in the three examples. All scale bars, 10 μm.

microvilli (Figures 3.14.E, F), these results hint that endogenous kinase activity may be directed towards the growing, distal tip of microvilli, and that the C-terminus can locally displace factors involved in activating or derepressing LOK and SLK.

Preliminary attempts to uncover the regulatory mechanism of LOK and SLK

To add weight to the hypothesis that the C-terminus of LOK regulates kinase activity, a series of C-terminal truncation mutants of LOK were constructed as RFP fusions and expressed in cells. As shown in Figure 3.10.E, expression of the N-terminal kinase domain alone, but not the full-length causes ezrin mislocalization to basal and lateral membranes. Intermediate effects are seen with 1-884, but full mislocalization is achieved with 1-801 (Figure 3.17.A). Thus, residues lying between 801 and 968 are strictly required for ezrin's apical restriction, while residues from 884-968 are partially required.

As shown in Figure 3.15.C, the C-terminal region of LOK causes inhibition of microvilli *in trans*, most likely by inhibiting LOK and SLK activity. Thus I asked what effect the C-terminal truncation series would have when introduced in the context of the C-terminal domain. Maximal inhibition is achieved with the full C-terminal domain from 310-968, and severing off the linker region (586-968) does not greatly diminish the effect (Figure 3.15.C, Figure 3.17.B). In fact, the construct can be shortened further from the N-terminus to 615-968 without loss of inhibitory activity (data not shown). However, truncating from the C-terminal end to 801 (either 310-801 or 586-801) renders the domains completely incompetent to inhibit microvilli, while intermediate effects are seen with 310-884 or 586-884 (Figure 3.17.B). These observations correlate strikingly well with ezrin mislocalization in the context of full-length LOK (Figure

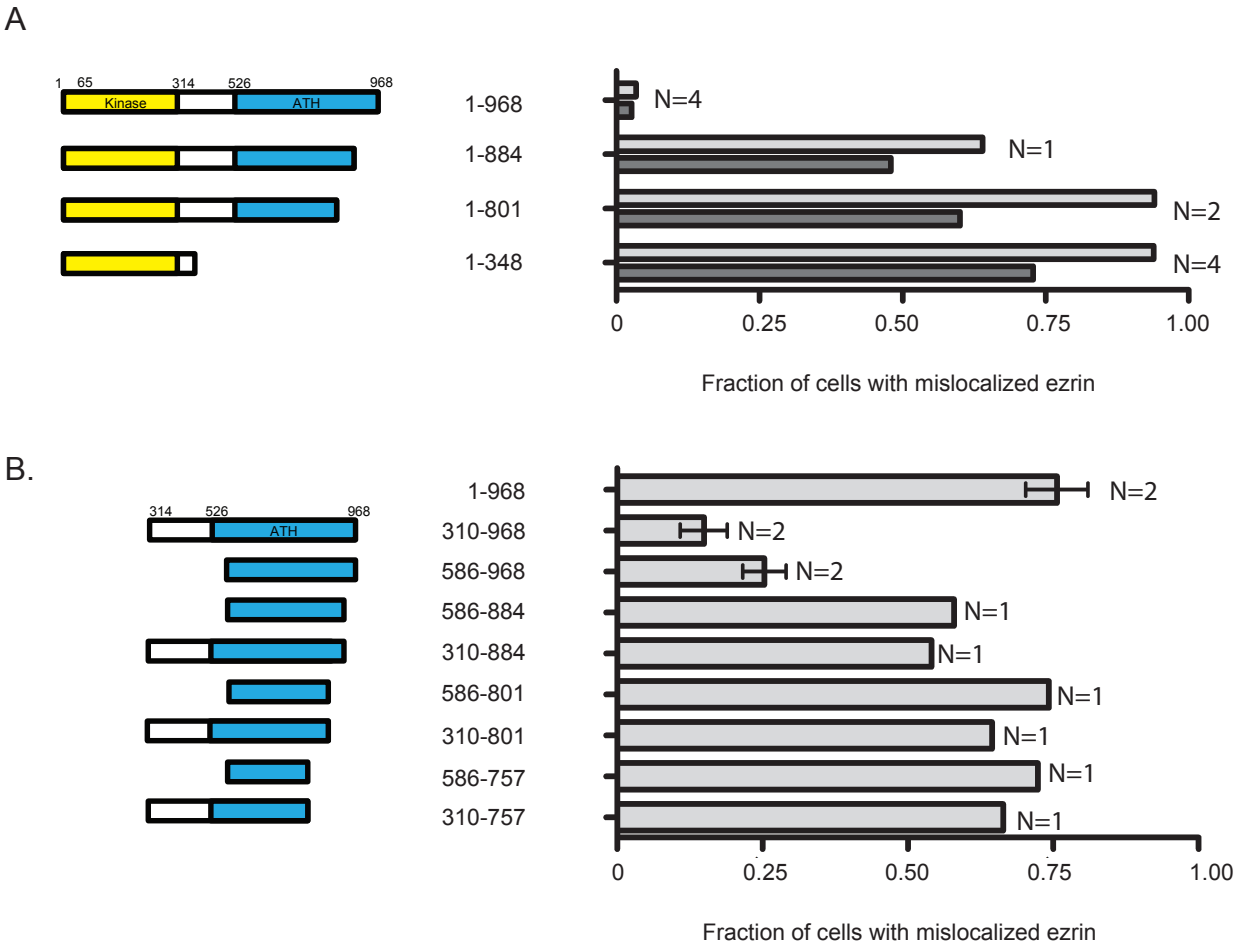

Figure 3.17 Residues at the extreme C-terminus of LOK are necessary for ezrin polarity and inhibition of ezrin phosphorylation in *trans.*

(A) Cells expressing the indicated truncation of LOK were stained for ezrin and F-actin (phalloidin) and ezrin localization to lateral (light gray) or lateral (dark gray) membranes was scored as in 3.10.E. (B) Cells expressing the indicated truncation of LOK were stained for ezrin and F-actin (phalloidin) and the presence of microvilli was scored.

3.17.A). Thus, residues at the extreme C-terminal end of LOK appear to be necessary both for restriction of LOK activity *in cis* and inhibition of LOK activity *in trans*.

I also used the newly developed erlotinib protection assay to discover LOK and SLK mutants incapable of rescuing polarized ezrin distribution. Many mutants were used in the assay as indicated in Figure 3.18.A, including S951 and T952 which are abundantly phosphorylated in LOK but have never been connected with any function (Hornbeck et al., 2012). Mutating these either to alanine or phosphomimetic residues had no effect in my assay (Figure 3.18). SLK regulation is better studied. Phosphorylation at S347 and S348 by casein kinase II was shown to inactivate SLK, and this was shown to regulate SLK function in focal adhesion dynamics and its phosphorylation of RhoA (Cordes et al., 2008; Guilluy et al., 2008). Phosphomimetics did not reproduce this inactivation in the microvillus assay, a discrepancy I can't explain (Figure 3.18). A number of additional post-translational modifications still remain (curated on Phosphosite), and these may prove valuable in uncovering the mechanism of LOK/SLK regulation.

Interestingly, an isoform of SLK generously provided to us by Luc Sabourin was found to lack a small region within the C-terminal ATH domain ('SLK_short'). This is an isoform that could be produced by alternatively splicing the SLK gene, and thus could be expressed *in vivo*, though it does not appear to be the predominant isoform (Sabourin and Rudnicki, 1999). Intriguingly, both this isoform and the cognate deletion in LOK ('LOK_short') fail to protect against erlotinib-induced microvillus collapse in roughly half of the cells (Figure 3.18). In these cells, ezrin is partially mislocalized to basolateral membranes (data not shown), implicating this region of the ATH domain (residues 663-693 in LOK or 925-955 of SLK) in restricting kinase activity, as well.

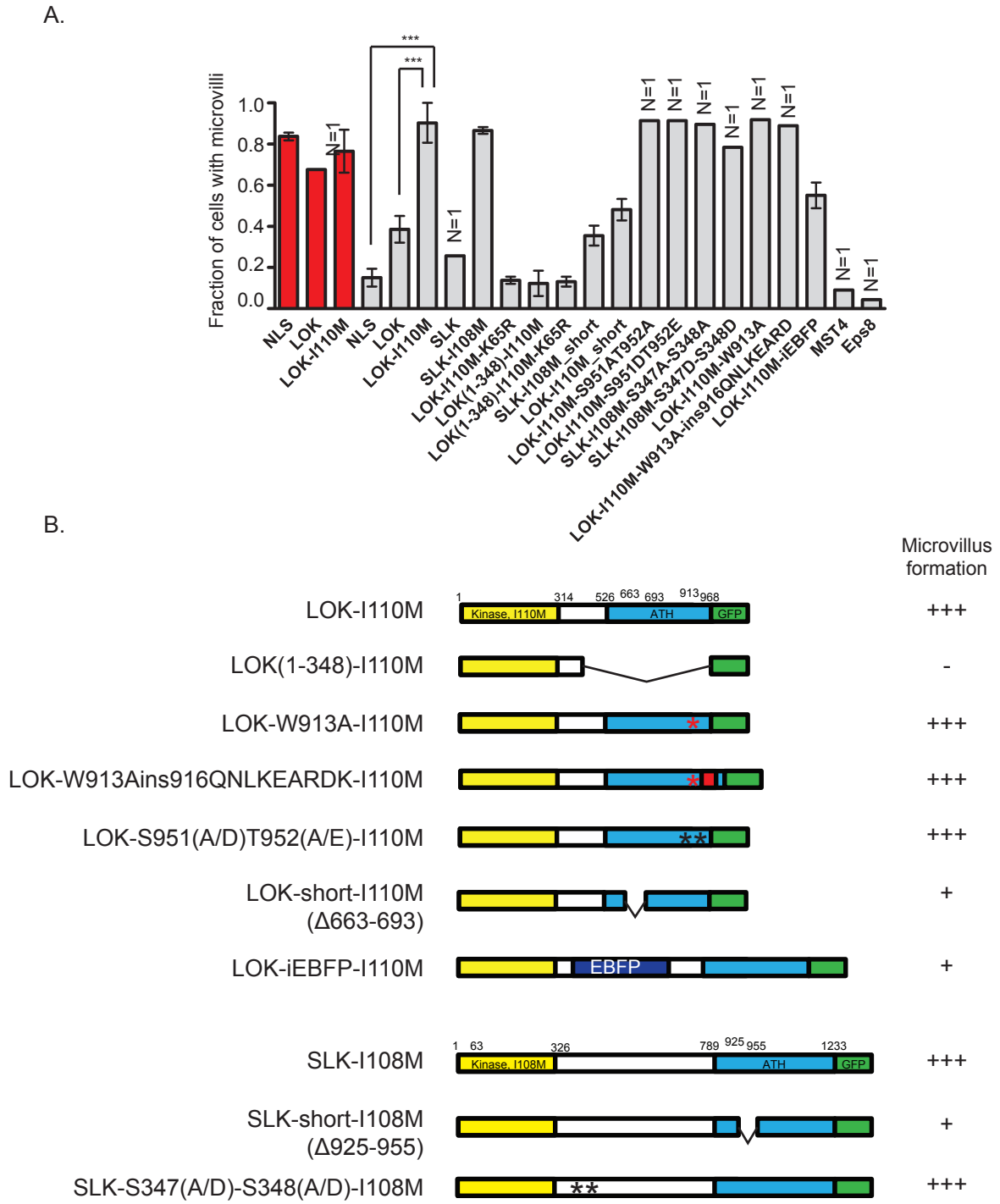

Figure 3.18 Attempts to uncover the regulatory mechanism of LOK using erlotinib-rescue assays.

(A) Cells expressing GFP-nuclear localization signal ('NLS') or indicated LOK or SLK protein with a C-terminal GFP tag were treated (gray) or not treated (red) with 20 μM erlotinib for 15 min and then fixed and stained for EBP50, and the presence or absence of microvilli was scored as in figure 3.13. (B) Graphical summary of key observations from A.

Tryptophan (W) is often involved in coordinating protein interactions. The only W residue between 801 and 968 is W913, however mutating this residue has no effect on its protection abilities (Figure 3.18). Amazingly, a PCR-induced insertion of 9 residues following the mutated W also functioned fully in erlotinib protection.

In an attempt to determine whether an intramolecular interaction between the N- and C-terminal regions is necessary, the enhanced blue fluorescent protein (EBFP) open reading frame was inserted into the linker region, prying the two domains apart a bit more than normal. Although this partially impaired its erlotinib-protection ability (Figure 3.18), it fully restores microvilli in around half of the transfected cells. This makes it seem less likely that a critical intramolecular interaction regulates LOK and SLK activity in microvilli.

Two speculative molecular models of LOK and SLK restriction

Several lines of evidence in the last section (sufficiency as assessed by erlotinib-protection assays, dominant-positive redistribution of ezrin as assessed by ezrin localization, and dominant-negative inhibition of microvilli) have highlighted the importance of two regions (Region 1: 615-693, and Region 2: 801-912) within the C-terminal domain in regulating LOK and SLK activity. How might this be accomplished at the molecular level? One possibility is that of intra- or intermolecular regulation (Figure 3.19.A). In this model the C-terminal domain directly interacts with the N-terminal domain on basolateral membranes. The inhibitory interaction is released upon binding of activating factor(s) to Regions 1 and 2 of the tail. Thus deleting these regions would keep the molecule constitutively active, and high levels of an intact tail or a LOK/SLK kinase-dead protein would titrate away these activating factors from endogenous LOK and SLK, thereby maintaining their repressed state. Preliminary attempts to

Figure 3.19 Two possible models for the restriction of LOK activity to the apical domain of epithelial cells.

(A) Model 1: In this model, the C-terminal domain inhibits the N-terminal kinase domain in *cis*. Region 1 and 2 of the C-terminal make critical contacts with an unknown, apically-localized factor(s) which derepresses LOK apically but not basolaterally, leading to phosphatase-opposed T567 ezrin phosphorylation. (B) Model 2: In this model, LOK is bound to an inhibitory ligand ('Repressor') which is displaced by an unknown, apically localized factor(s) which derepresses LOK apically but not basolaterally, leading to phosphatase-opposed T567 ezrin phosphorylation.

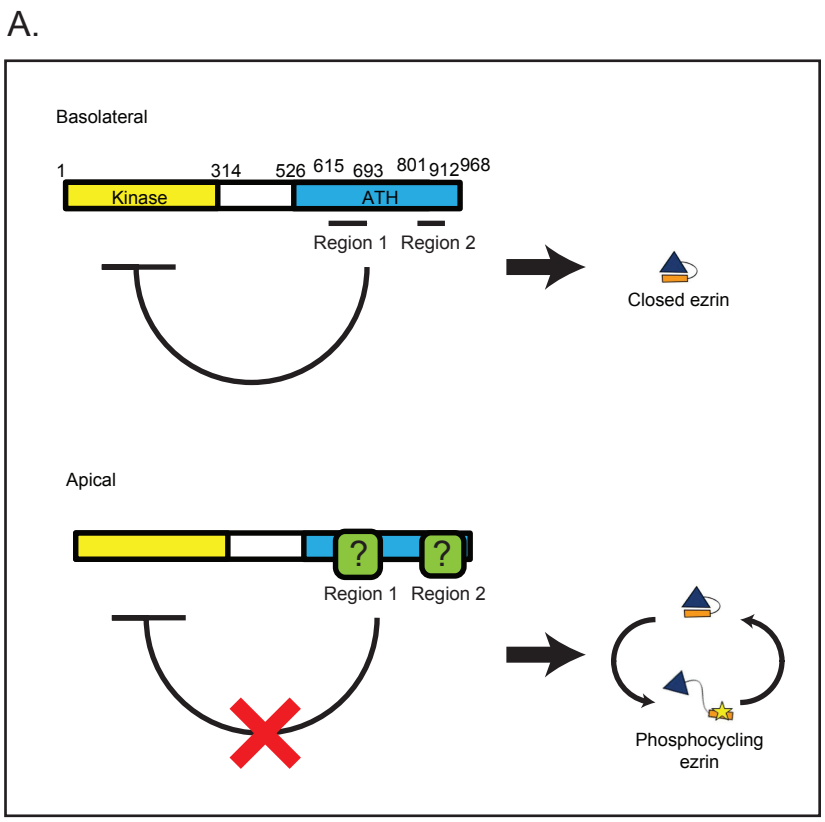

validate this model as is have been difficult. First, the N- and C-terminal domains of LOK interact poorly in co-immunoprecipitation experiments (data not shown), and, as shown in Figure 3.18, disrupting the distance between the domains by insertion of an EBFP only occasionally disrupts its regulatory ability.

A second, and more likely model, builds on the first but invokes another unknown factor interacting with both the N-terminal and C-terminal domains of LOK and SLK and repressing their activity when bound (Figure 3.19.B). In this model, the repressor is displaced by engagement with apically-localized, derepressing factor(s).

It should be noted that the activating factor(s) could represent proteins such as kinases, phosphatases, or ubiquitin ligases that post-translationally modify LOK and SLK, changing their activation status. Indeed, large-scale phosphoproteome analysis has identified two unexamined phosphorylation sites (S679 and S844) and two predicted ubiquitination sites (K621 and K690) within regions 1 and 2 as well as another unexamined phosphorylation site just outside Region 2 (S954) (Hornbeck et al., 2012). It is possible that mutation of these residues will affect LOK and SLK function, further elucidating the mechanism.

LOK and SLK are the general ERM kinases in epithelial and fibroblastic cells

Finally, I asked whether LOK and SLK C-terminally phosphorylate ERMs in other cell-lines in addition to their role in placentally-derived Jeg-3 cells. I first examined ERM phosphorylation in colon-derived Caco-2 cells. Just as with Jeg-3, Caco-2 cells express ezrin and radixin but no moesin. Interestingly, Caco-2 cells express slightly more SLK and much less LOK than Jeg-3 cells, but steady-state ezrin and radixin C-terminal phosphorylation is nearly identical (Figure 3.20.A). This suggests that SLK is more active than LOK in these cells.

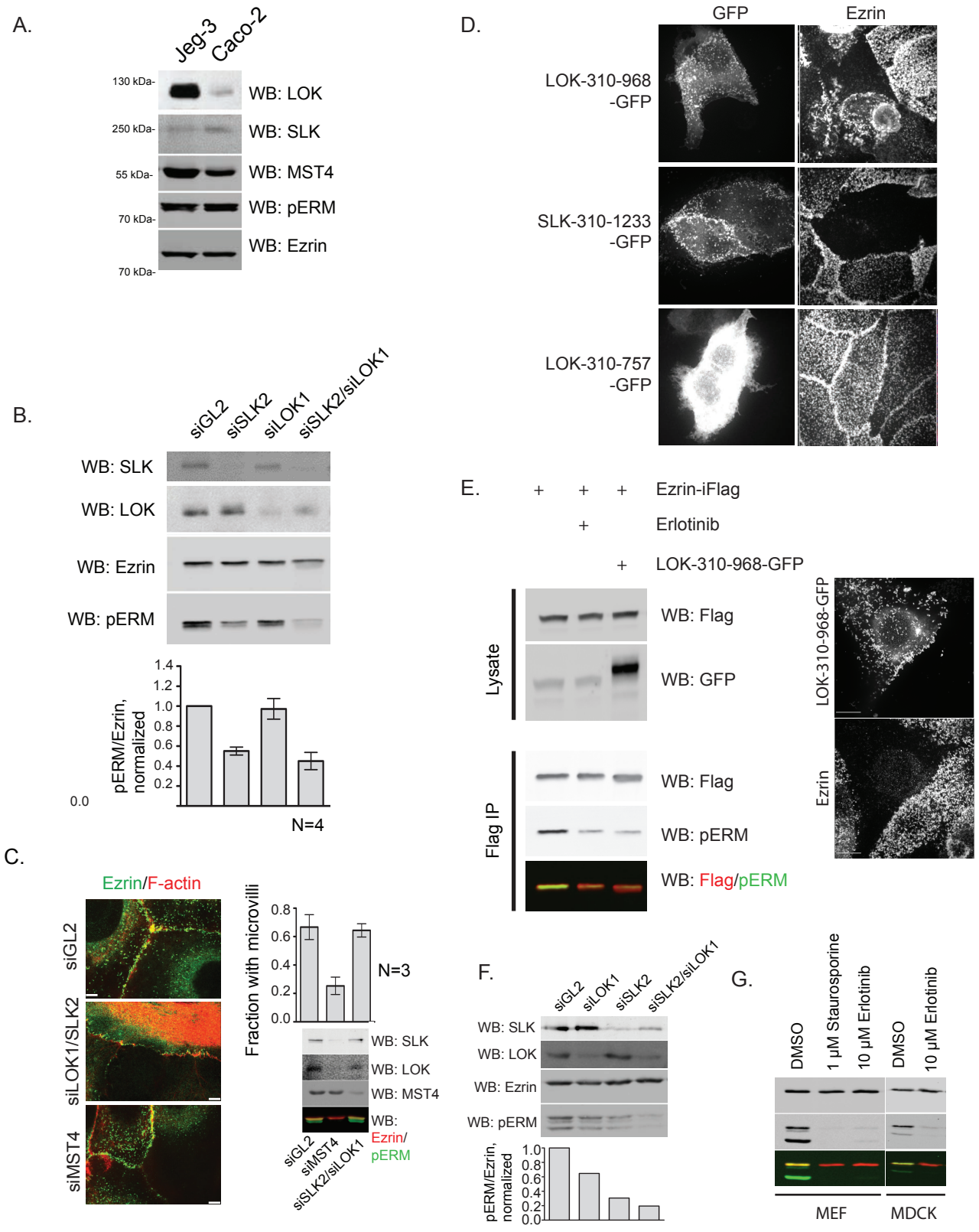
A.
Jeg-3
Caco-2
130 kDa-
WB: LOK
250 kDa-
WB: SLK
55 kDa-
WB: MST4
70 kDa-
WB: pERM
70 kDa-
WB: Ezrin
B.
siGL2
siSLK2
siLOK1
siSLK2/siLOK1
WB: SLK
WB: LOK
WB: Ezrin
WB: pERM
pERM/Ezrin, normalized
1.4
1.2
1.0
0.8
0.6
0.4
0.2
0.0
N=4
C.
Ezrin/F-actin
siGL2
siLOK1/SLK2
siMST4
Fraction with microvilli
0.8
0.6
0.4
0.2
0.0
N=3
WB: SLK
WB: LOK
WB: MST4
WB: Ezrin/ pERM
siGL2
siMST4
siSLK2/siLOK1
D.
GFP
Ezrin
LOK-310-968 -GFP
SLK-310-1233 -GFP
LOK-310-757 -GFP
E.
+ + + Ezrin-iFlag
+ Erlotinib
+ LOK-310-968-GFP
Lysate
WB: Flag
WB: GFP
Flag IP
WB: Flag
WB: pERM
WB: Flag/pERM
LOK-310-968-GFP
Ezrin
F.
siGL2
siLOK1
siSLK2
siSLK2/siLOK1
WB: SLK
WB: LOK
WB: Ezrin
WB: pERM
pERM/Ezrin, normalized
1.0
0.8
0.6
0.4
0.2
0.0
G.
DMSO
1 μM Staurosporine
10 μM Erlotinib
DMSO
10 μM Erlotinib
MEF
MDCK

Figure 3.20 LOK and SLK function upstream of ERMs in several other epithelial cell models.

(A) Nearly equivalent amounts of Jeg-3 and Caco-2 cell lysate were subjected to western blots with indicated antibodies, and the results reveal that Caco-2 cells express ~4-fold less LOK than Jeg-3 cells and ~2-fold more SLK. (B) Caco-2 cells treated with siRNAs as indicated for 4 days were subjected to pERM and ezrin Western blot to measure the percentage of T567-phosphorylated ezrin and T564-phosphorylated radixin, plotted below. SLK and not MST4 is the primary ERM kinase in Caco-2 cells, and LOK and SLK siRNA exhibit partial synthetic pERM inhibition. (C) Cells as in B were stained for ezrin and F-actin (phalloidin) to reveal that microvilli are depleted in coverlip-grown Caco-2 cells depleted of LOK and SLK, but not MST4. In one replicate, the very same cells were lysed and analyzed by western blot to confirm the transfections. (D) Ezrin stainined of Caco-2 cells expressing GFP-tagged LOK or SLK tail, but not a truncated variant (see 3.17), causes loss of ezrin-staining microvilli. Phalloidin-staining microvilli-baring cell fraction was scored. (E) Left: LLC-PK1.CL4 cells were transiently transfected to express ezrin-iFlag along with GFP-tagged LOK C-terminus or treated with 10 μM erlotinib for 10 minutes as indicated, and then a denaturing Flag IP was performed, and the immunoprecipitate subjected to Western blot as in panel B. The fraction of pERM is plotted below. Right: As in Caco-2, expression of the LOK tail causes a loss of ezrin-staining microvilli. (F) HEK293T cells were treated with indicated siRNAs and processed as in B. SLK is the primary ERM kinase in HEK293T cells. (G) Primary mouse embryo fibroblasts (MEF) or MDCK cells were treated with indicated drugs for 10 minutes and then processed as in B. ERM phosphorylation is sensitive to erlotinib in MEFs and MDCK cells.

Consistently, siRNA-mediated depletion of SLK alone causes a 50% decrease in phospho-ERM level, whereas depletion of LOK has no measurable effect on its own (Figure 3.20.B); however, combining LOK and SLK siRNAs revealed a marginal synergy between them ($p < 0.05$, Fig 3.19.C). Depletion of MST4, the ERM kinase in the single polarized Ls174T-W4 cells (ten Klooster et al., 2009), had no effect on ezrin phosphorylation in Caco-2 (Figure 3.20.B) or Jeg-3 cells (Figure 3.9.B). An examination of Caco-2 cultures knocked down for LOK and SLK revealed a reproducible 2-fold loss of microvilli-bearing cells; whereas no such loss was observed when MST4 was depleted (Figure 3.20.C). I also found that similar to their expression in Jeg-3 cells, the expression of the intact C-terminus of either LOK or SLK inhibited ezrin accumulation in the apical domain of Caco-2 cells, whereas a truncated C-terminal region which could not inhibit microvilli in Jeg-3 cells did not (Figure 3.20.D). These results suggest that LOK and SLK are the ERM kinases in Caco-2 cells, and that the regulatory mechanism is conserved between the cell-lines.

Because my siRNAs target human mRNA, I could not knock down LOK and SLK in porcine kidney-derived LLC-PK1.CL4 cells, which have been widely used for studies of microvilli. However, expression of the LOK C-terminus inhibited co-transfected ezrin-iFlag phosphorylation and the accumulation of endogenous ezrin in microvilli, and erlotinib inhibited ezrin phosphorylation to a similar extent to its effect in Jeg-3 cells (Figure 3.20.E). Interestingly, many LLC-PK1.CL4 cells expressing the LOK C-terminal domain erupted in mostly apical bulbous projections resembling cortical blebs, but importantly, these lacked ezrin. This may support a role for ezrin in resolving blebs into the cortex, as Mitchison and colleagues have suggested (Charras et al., 2006). Other cells produced protrusions from both the apical and

basolateral membrane, but all were negative for ezrin (data not shown). The results suggest that LOK and SLK are the ERM kinases in LLC-PK1.CL4 cells.

Lastly, I also examined human kidney-derived HEK293T cells by siRNA (3.20.F), and primary mouse embryonic fibroblasts (MEFs) and dog kidney-derived MDCK cells by erlotinib treatment (3.20.G), and my data were always consistent with a critical role for LOK and SLK in phosphorylating ERMs. This is especially surprising because HEK293T cells and MEFs lack a truly polarized apical domain and do not possess organized microvilli, but both incorporate ezrin specifically into surface structures, thus retaining a crude sort of ezrin polarity (HEK293T: Jessica Wayt personal communication; MEF: Heiska and Carpen, 2005). Thus LOK and SLK appear to have a very general role in ERM phosphorylation in mammalian cell-lines regardless of the tissue-of-origin, morphology, or differentiation status.

DISCUSSION

Functional polarity requires the targeting of appropriate membrane proteins to specific domains but also defining the morphology of the domain by cytoplasmic factors, about which little is known. Here I uncover how ezrin function is restricted to the apical membrane. I first demonstrate that phosphocycling on T567 is critical. Second, I identify the relevant kinases in epithelial cells as LOK and SLK. Third, I show that the kinases are enriched in microvilli through their C-terminal domain. Fourth, I show that the kinases are locally activated in microvilli.

Extensive characterization of the ERM phosphomimetic corresponding to ezrin T567D/E has shown that it reflects the activated form (Chambers and Bretscher, 2005; Charras et al., 2006; Kunda et al., 2008; Matsui et al., 1999; Polesello et al., 2002; Carreno et al., 2008; Speck et al.,

2003). Earlier studies of epithelial cells suggested that overexpressing the ezrin phosphomimetic can provide more numerous microvilli, but these studies were performed in the presence of endogenous ezrin (Fievet et al., 2004; Crepaldi et al., 1997). By contrast, I show that expression of the phosphomimetic in the absence of endogenous ezrin, or unopposed phosphorylation of ezrin, or ezrin phosphorylated by a non-localized kinase, all lead to its mislocalization to the basolateral membrane and the loss of its function. My results are consistent with the finding in fly photoreceptor cells that re-expression of wild-type Moesin but not the phosphomimetic T559D Moesin can restore apical microvilli following *Moesin* gene disruption (Karagiosis and Ready, 2004).

I find that the normal ezrin phosphorylation cycle is about two minutes, which is similar to the turnover rate as measured by FRAP of ezrin-GFP in the same cells (Garbett and Bretscher, 2012). Thus, my data imply that the apical membrane is a dynamic system of local ezrin phosphorylation. Since microvilli have been shown to undergo constant remodeling (Gorelik et al., 2003; Garbett and Bretscher, 2012), phosphocycling ensures that activated ezrin can be recruited into growing microvilli as needed.

To identify the relevant kinases for ezrin T567 phosphorylation, I used an unbiased proteomic approach, leading me to LOK and SLK, two evolutionary homologs, which I found are necessary and sufficient for microvilli formation by localized ezrin. LOK has previously been shown to regulate moesin in lymphocytes. However, mice with the LOK gene knocked out have reduced ERM phosphorylation and alterations in chemokine-stimulated lymphocyte migration and polarization, but the mice are viable (Belkina et al., 2009). I suspect that in such knockout mice, SLK is providing a compensating function, and predict that a double LOK and SLK knockout mouse would be inviable. Since the ERM kinase in *Drosophila* is Slik, the

homolog of LOK and SLK, this implies that regulation of ERM proteins by this family of kinases has an ancient evolutionary origin.

Earlier work has shown that in single epithelial Ls174T-W4 cells a signal transduction pathway from LKB1/Strad results in the activation of the kinase MST4 to phosphorylate ezrin necessary for morphological assembly of the apical domain (ten Klooster et al., 2009; Gloerich et al., 2012). Moreover, these studies reported that phosphomimetic ezrin targets and restores microvilli in these MST4 knockdown cells, in apparent contradiction to my work. Although the expression level of phosphomimetic ezrin relative to endogenous ezrin was not reported, these results suggest that other mechanisms may exist under some circumstances to polarize ezrin apically. Furthermore, ten Klooster et al. (2009) also reported that knockdown of MST4 in Caco-2 cells induced defects in apical morphology (ten Klooster et al., 2009). By contrast, I have found that knockdown of LOK and SLK, but not MST4, in either Jeg-3 or Caco-2 results in reduced ezrin phosphorylation and loss of apical microvilli. I can offer no simple explanation for the difference in results between my and these studies.

Although both LOK in mammalian lymphocytes and *Drosophila* Slik have been implicated in ERM phosphorylation, it was not known how their function was restricted to a specific domain. I now show that the C-terminal region of both LOK and SLK target the kinase to apical microvilli and restrict their activity apically. Accordingly, overexpression of the LOK C-terminal domain uncoupled from the kinase domain acts as a dominant-negative to inhibit ERM phosphorylation, leading to the destruction of microvilli. I find a similar effect in colon epithelial Caco-2 cells and kidney epithelial LLC-PK1.CL4 cells (Fig 3.19.), suggesting that LOK and SLK may be the general ERM kinases in epithelial cells.

We have previously shown that phospho-ezrin and -radixin are enriched towards the tip of the microvillus, and suggested that ezrin is phosphorylated at the microvillus tip and then moves down with treadmilling actin (Hanono et al., 2006). I now find a region within the LOK protein which, when expressed at low levels, is often confined to the tip of microvilli, as would be expected if it is the relevant kinase. I therefore propose that some factor enriched at the microvillus tip, recruits LOK and activates it there locally. Ezrin becomes phosphorylated, and, as it moves down the microvillus, it begins to become dephosphorylated by a cytoplasmic phosphatase and ultimately releases from the membrane and F-actin at the base.

Interestingly, ERM-anchorage has been invoked as a means for maintaining the protein composition of the apical domain in the absence of polarized membrane trafficking (Meder et al., 2005). The phosphocycling mechanism I describe, and thus polarized LOK/SLK, may therefore be a critical component of this "pre-apical" polarity pathway.

The work presented here has uncovered local regulation of ERM proteins by LOK and SLK through an unidentified microvillar component. So far, no interactors of LOK are known, but several binding partners of SLK have been reported, including microtubules (Cordes et al., 2008; Wagner et al., 2002; Burakov et al., 2005), F-actin (Sabourin et al., 2000), PDZ-domain containing protein PDZK1 (Gisler et al., 2003), and the transcription factors Lbd1/2 (Storbeck et al., 2009). My current efforts are aimed at determining whether these or other interactors are responsible for the polarized activity of LOK and SLK.

In establishing the phenotype associated with ERM depletion, I made two striking observations which point to the limitations of this work in providing mechanisms for microvillus biogenesis. In contrast to two previous reports using potentially nonspecific antisense

oligonucleotide synthesis to reduce ERM expression (Tsukita et al., 1994; Bonilha et al., 1999), siRNAs-mediated depletion of ERMs in Jeg-3 cells cause a loss of a very specific class of F-actin structure—microvilli—but not others, including cell-cell junctions, lamellipodia, or even filopodia, which are nearly structurally identical to microvilli. The same very specific defect occurs when EBP50 is depleted in Jeg-3 cells (Damien Garbett, personal communication). Secondly, I found that Caco-2 cell microvilli are only lost from cells treated with LOK and SLK siRNA prior to reaching confluence. When the cells were replated in smaller dishes following the siRNA transfection and thus allowed to reach confluence prior to the analysis, the microvillus defect was fully reversed (data not shown). Furthermore, in confluent Caco-2 cells, ERM dephosphorylation by staurosporine or erlotinib treatment caused ezrin to translocate away from microvilli, but did not alter the apical microvilli as observed by F-actin staining (Cécile Sauvanet, personal communication). Similar results were seen in EGF-stimulated A431 cells pretreated with staurosporine (Yonemura et al., 2002). Finally, LLC-PK1.CL4 cells made to almost completely lack ERMs have mostly intact microvilli, although their organization is significantly affected, and the results do not seem to depend upon plating density (Appendix A). Taken together with the observation that intestinal cells *in situ* retain microvilli despite severe morphological defects (Saotome et al., 2004), these findings hint that other pathways than the ERM-dependent pathway described in this thesis can provide cross-linking function between the plasma membrane and the cytoskeleton. It also suggests at extensive diversity in the use of these pathways in regulating apical morphology among different cell-types. In short, a microvillus is not a microvillus is not a microvillus. How might plasma membrane-cytoskeletal cross-linking be performed in the absence of ERMs? Obvious candidates are myosins (classes I, VI, VII, X, XI, and XV) which possess membrane anchoring domains in addition to their F-actin-binding

and motor properties. It will be interesting to test whether these or other pathways are additionally required for microvilli in the exceptional cases mentioned.

APPENDIX A

ERM SUPPRESSION IN LLC-PK1.CL4 CELLS CAUSES VILLIN UPREGULATION

LLC-PK1.CL4 cells have been used extensively for studies of microvilli, particularly in studies of brush border myosin IA. Thus, I sought to characterize the role of ezrin, radixin, and moesin in the microvilli of these cells.

MATERIALS AND METHODS

LLC-PK1.CL4 cells were kindly provided by Matthew J.Tyska (Vanderbilt University). They were grown in MEMα + 10% FBS at 37^{O}C in a humid incubator containing 5% CO_2.

Anti-villin antibody was rabbit polyclonal H148 (Anthony Bretscher) or 1D2C3 mouse monoclonal (Santa Cruz). Anti-Fimbrin and Anti-Myosin II heavy chain antibody was from Anthony Bretscher.

shRNA sequences (5'-GATATGGGCTGAATACAAA-3' for GL2 Luciferase control; 5'-GGAAGAGGATGATGTGTTC-3' for villin) were cloned into pSUPER.retro.puro (Oligoengine) following the manufacturer's instructions. They were packaged in the Pheonix Ampho cell-line, and the supernatant was used to infect LLC-PK1.CL4 cells, which were then selected in 2 μg/mL puromycin.

siRNAs were as follows: AAAGUCAGGUGCCUUCUUGuu-3' (Ezrin); UGAAGAUGUUUCUGAGGAAuu-3' (Radixin); 5'-GGCUGAAACUCAAUAAGAAuu-3' (Moesin). These were premixed at a ratio of siEzrin:siRadixin:siMoesin::1.7:1:1.6 (siERM), which reflects the expression level difference between ezrin, radixin, and moesin in LLC-

PK1.CL4 cells. 50 nM of siERM were transfected by Lipofectamine 2000 (Invitrogen) following the manufacturer's protocol into LLC-PK1.CL4 cells three times over 9 days prior to processing.

All immunofluorescence, western blotting, and additional antibodies were as described in chapters 2 and 3.

RESULTS AND DISCUSSION

Transfection of siERM into LLC-PK1.CL4 cause knockdown to undetectable levels for each ERM (Fig. A.1.A). Blotting for other microvillar components showed that fimbrin and EBP50 remained constant, myosin II went slightly down, whereas the levels of villin dramatically increased (Fig. A.1.A). An examination of the proteoglycans on the cell surface using pre-permealization WGA revealed few cells lacking microvilli following the depletion of ERMs (Fig. A.1.B), however the composition of the microvilli changed, as more microvilli now contained villin, whereas it was predominantly cytoplasmic in control cells (Fig. A.1.C).

To test whether the upregulation of villin was obscuring a defect in microvilli, I suppressed villin in addition to knocking down ERMs. This works, because cells treated with both villin shRNA and ERM siRNA indeed had undetectable levels of phosphorylated ERMs while still having less villin than cells treated without any targeted RNAi (Fig. A.1.D)

The downregulation of villin on its own or in combination with ERM suppression had no effect on the number of cells with microvilli (data not shown). ERM knockdown in LLC-PK1.CL4 cells caused a general disorganization of the apical surface of cells. Blindly scoring the subjective attribute showed that villin suppression rendered no enhancement of this defect regardless of plating density (Fig. A.1.E). Thus, villin upregulation is a genuine consequence of

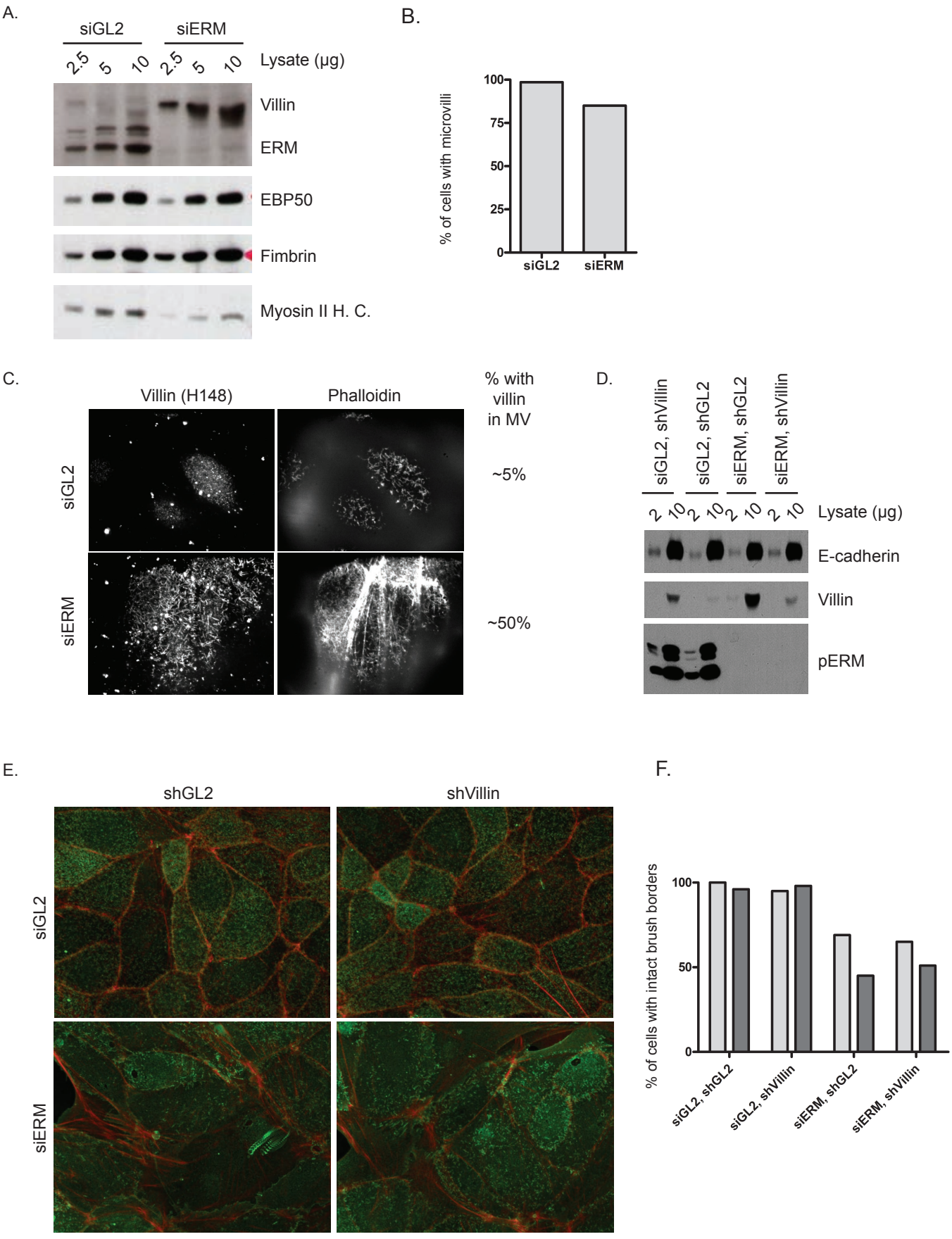
A.
siGL2
siERM
2.5
5
10
2.5
5
10
Lysate (µg)
Villin
ERM
EBP50
Fimbrin
Myosin II H. C.
B.
% of cells with microvilli
100
75
50
25
0
siGL2
siERM
C.
Villin (H148)
Phalloidin
% with villin in MV
siGL2
siERM
~5%
~50%
D.
siGL2, shVillin
siGL2, shGL2
siERM, shGL2
siERM, shVillin
2
10
2
10
2
10
2
10
Lysate (µg)
E-cadherin
Villin
pERM
E.
shGL2
shVillin
siGL2
siERM
F.
% of cells with intact brush borders
100
50
0
siGL2, shGL2
siGL2, shVillin
siERM, shGL2
siERM, shVillin

Figure A.1 Ezrin, radixin, and moesin depletion in LLC-PK1.CL4 causes villin upregulation and disorganization of the apical membrane without loss of microvilli-baring cells

(A) LLC-PK1.CL4 cells transiently transfected with control siRNA or siRNAs against all three ERMs for 9 days were western-blotted with indicated antibodies. ERM removal causes a specific increase in the expression of villin, but no increase in the levels of ERM-associated EBP50 or another actin cross-linked protein, fimbrin. (B) Cells as in B were grown on glass coverslips, fixed and stained with fluorescent WGA to illuminate the plasma membrane (as in E) and scored for the presence of microvilli. ERM removal has a marginal impact on the number of microvilli-baring cells. (C) Control or ERM-depleted cells were stained for villin and F-actin. ERM-depletion resulted in a 10-fold increase in the number of cells expressing villin in microvilli. (D) Cells stably transfected to express indicated shRNA were transiently transfected to deplete ERMs and western blotted as indicated. Note that the level of villin in villin shRNA-expressing, ERM-depleted cells is *less* than the amount of villin in control/control cells. (E,F) Cells as in D were stained with WGA (green) and phalloidin (red), and the number of disorganized brush-borders scored. Note: all cultures had similar numbers of cells with microvilli, and ERM-depletion-induced loss of brush border organization was *not* synthetically enhanced by villin depletion.

ERM suppression, perhaps reflecting accelerated differentiation of a subset of cells. However, this specific change does not affect microvillar morphology.

ERM suppression *in situ* causes many specific developmental defects (Saotome et al., 2004; Casaletto et al., 2011) which cannot easily be explained by its biophysical role in imparting membrane tension or its cell biological role in microvillar morphology. For instance, villus fusion is blocked in ERM-deficient developing intestinal epithelial cells (Saotome et al., 2004). The work here suggests that expression-level changes are caused—however indirectly—by ERM suppression in tissue culture cells, as well. Examining these systematically (by microarray or whole-proteome SILAC methods) may prove useful to explain the changes *in situ*.

APPDENDIX B

INVESTIGATIONS INTO THE FUNCTION OF NADRIN, AN EBP50 PDZ LIGAND

Nadrin (also known as RICH-1 or ARHGAP17) was identified as a ligand of the first PDZ domain of EBP50 (Reczek and Bretscher, 2001). Thus we asked whether Nadrin and EBP50 biology intersect in some way. EBP50 has an established role in microvillar morphology (Hanono et al., 2006b). During these investigations, a second role for Nadrin in establishing tight junctions (Wells et al., 2006) and Nadrin ligand Par3 in primary ciliogenesis (Sfakianos et al., 2007) were claimed. Therefore we asked what role Nadrin plays in these three processes.

MATERIALS AND METHODS

T23 MDCK cells were kindly provided by Keith Mostov (Univeristy of California, San Francisco) and maintained in DMEM with 10% FBS at 37^{O} in a humidified incubator containing 5% CO_2. All other cells were as described previously.

Anti-Nadrin antibody was primarily B85AP1, made against recombinant, bacterially-produced Nadrin. Anti-RICH-2 was from Fabbgenix. Anti-ZO-1 antibody was from Zymed. Anti-acetylated tubulin antibody was from Sigma.

shRNA sequences (5'-GATATGGGCTGAATACAAA-3' for GL2 Luciferase control; 5'- GAA TGACACAAGTTGCAA -3' for Nadrin of human, mouse, or dog origin and 5'-GAATGGACGCAAGTTGCCA-3' for Nadrin of pig origin) were cloned into pSUPER.retro.puro (Oligoengine) following the manufacturer's instructions. They were packaged in the Pheonix Ampho cell-line, and the supernatant was used to infect target cells, which were then selected in puromycin.

Nadrin siRNA was the following sequnence: 5'-GGUGCUUUAAAAUCCUAUUtt-3'. siRNAs were transfected into Jeg-3 cells using Lipofectamine RNAiMAX (Invitrogen) previously described.

Calcium switch experiments were performed by growing MDCK cells to confluence on coverslips, and then changing the media to SMEM containing 10 % FBS for 18-24 hours, and then switching the media back to DMEM + 10% FBS for indicated times.

All additional procedures were as described in chapters 2 and 3 or appendix A.

RESULTS AND DISCUSSION

The Nadrin gene produces two spliceforms, p120 Nadrin and p100 Nadrin (aka RICH-1). A related gene product called RICH-2 shares homology in the N-terminal region, encoding a membrane-curvature sensing N-BAR domain and a Rho GTPase activating protein domain, but contains almost no discernible homology in the C-terminal region, although both contain polyproline-rich regions which bind a number of SH3 domains. Strikingly, all Nadrins end in the same final 6 amino acids –E-E-S-T-A-L, a predicted PDZ consensus site (Figure B.1.A). Consistently, both Nadrin and RICH-2 can interact with EBP50 from lysates (Figure B.1.B) but this interaction is disrupted by the addition of residues to the C-terminal region (Figure B.1.C). Antibodies against Nadrin and RICH-2 do not cross-react (Figure B.1.D), and so could be used in immunofluorescence where they predominantly illuminate the cytoplasm (Figure B.1.E,F). Some Nadrin can be seen in microvilli when overexpressed (Figure B.1.E).

We first investigated whether Nadrin is requied for microvilli. Jeg-3 cells contain p120 Nadrin but no RICH-2 (Figure B.2.A). When >80% of Nadrin is depleted from Jeg-3 cells, there is no significant decrease in the number of cells with microvilli (Figure B.2.C). A similar lack of

A.

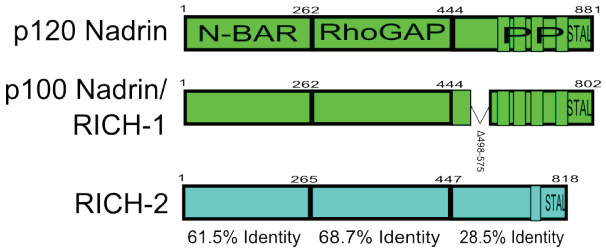
p120 Nadrin
N-BAR
RhoGAP
PP
STAL
1
262
444
881
p100 Nadrin/
RICH-1
802
Δ489-575
RICH-2
265
447
818
61.5% Identity
68.7% Identity
28.5% Identity

B.

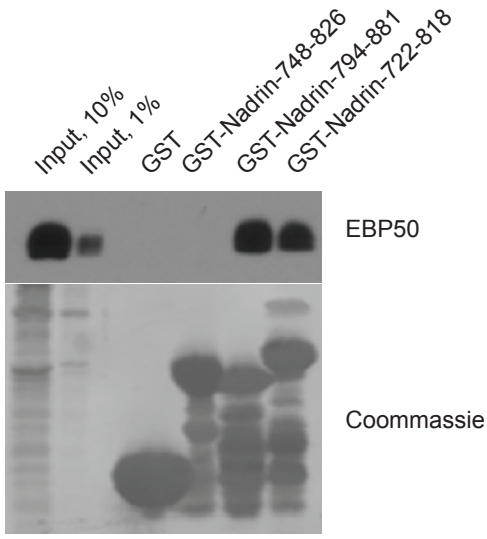
Input, 10%
Input, 1%
GST
GST-Nadrin-748-826
GST-Nadrin-794-881
GST-Nadrin-722-818
EBP50
Coommassie

C.

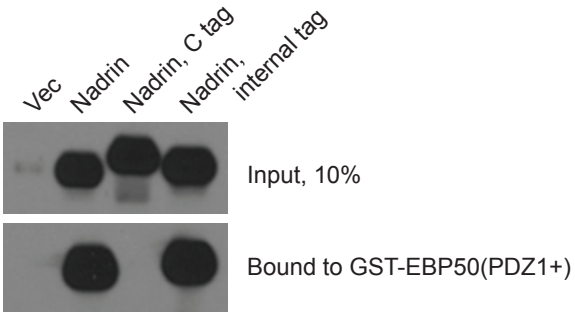
Vec
Nadrin
Nadrin, C tag
Nadrin,
internal tag
Input, 10%
Bound to GST-EBP50(PDZ1+)

D.

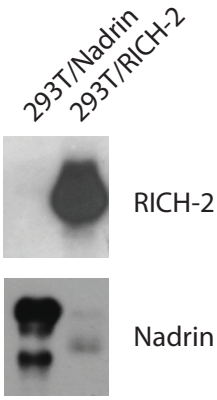
293T/Nadrin
293T/RICH-2
RICH-2
Nadrin

E.

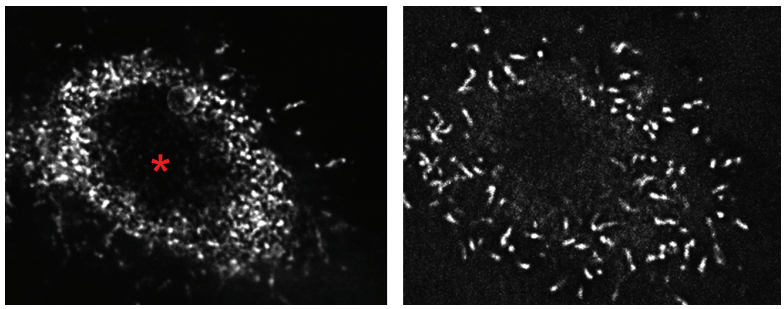
Nadrin
Ezrin

F.

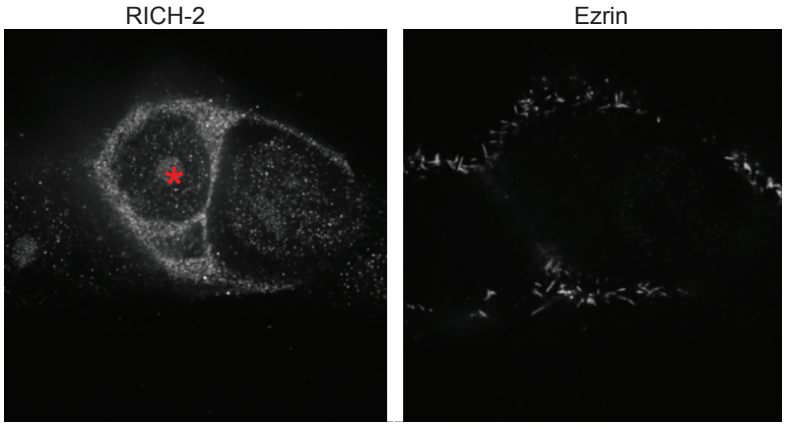
RICH-2
Ezrin

Figure B.1 Nadrin and RICH-2 bind to EBP50 through a C-terminal PDZ motif, and localize primarily to the cytoplasm when expressed in Jeg-3 cells.

(A) Schematic of Nadrin and RICH-2. N-BAR, N-termainl Bin, Amphiphysin, Rvs161/167 domain; RhoGAP, Rho GTPase activating domain; PP, poly proline regions; STAL, C-terminal PDZ binding motifs. (B) Jeg-3 cell extract was subjected to GST-pulldowns using indicated regions of Nadrin or RICH-2 or GST only control, resolved and western blotted for EBP50. EBP50 interacts with the C-termini of both Nadrin and RICH-2. (C) LLC-PK1 cell extract, which has very little endogenous Nadrin, transfected with Nadrin constructs as indicated was subjected to GST-pulldowns using the PDZ1+ region of EBP50 (Reczek and Bretscher, 2001), and western blotted for endogenous and overexpressed Nadrin. Nadrin binds to EBP50 only when the C-terminus is unmodified. (D) 293T cells expressing untagged Nadrin or RICH-2 were western blotted for either Nadrin (B85AP1) or RICH-2 (Fabgennix 1141) validating the antibodies. (E,F) Cells overexpressing untagged Nadrin (E) or RICH-2 (F) were stained with antibodies detecting Nadrin (E) or RICH-2 (F) showing mostly cytoplasmic expression. Nadrin partially localizes in microvilli when overexpressed.

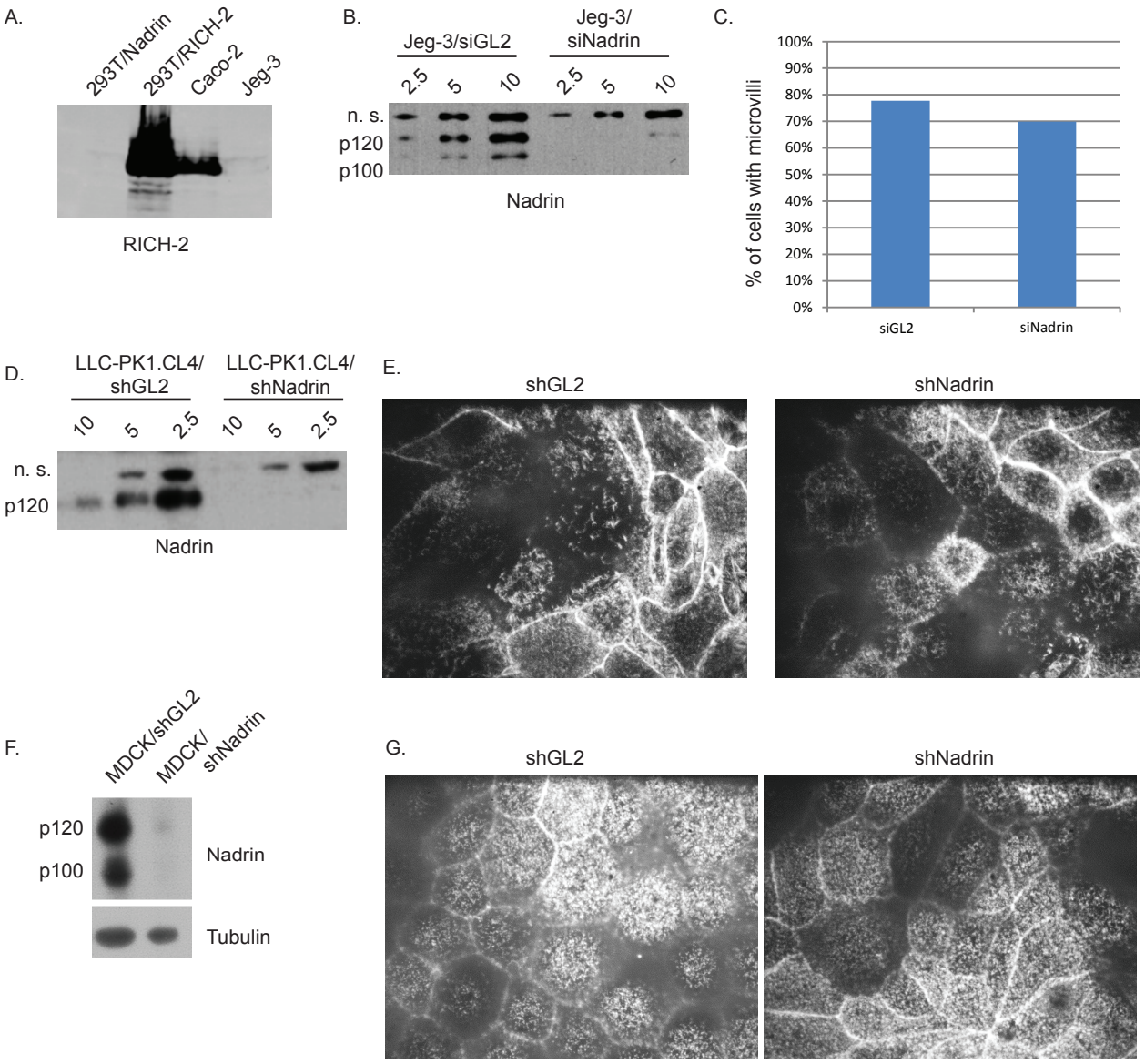

Figure B.2 Nadrin and RICH-2 are not required for microvilli in three epithelial cell-lines.

(A) Cells as indicated were western blotted for RICH-2, revealing that Caco-2 cells express RICH-2 as previously described (Rollason et al., 2009). (B) Nadrin western blot using indicated amounts of Jeg-3 cell lysate transiently transfected with Nadrin siRNAs revealing that ~80% of Nadrin can be depleted from Jeg-3 cells. (C) Cells transfected as in B were fixed and stained with ezrin antibodies and the number of microvilli-baring cells scored revealing no significant differences. (D) Nadrin western blot using indicated amounts of LLC-PK1.CL4 cell lysate transiently transfected with Nadrin siRNAs revealing that ~90% of Nadrin can be depleted stably from LLC-PK1.CL4. (E) Cells as in D were fixed and stained with phalloidin to reveal apical F-actin, revealing no differences. (F) Nadrin western blot using indicated amounts of T23 MDCK cell lysate transiently transfected with Nadrin siRNAs revealing that ~90% of Nadrin can be depleted stably from MDCK. (G) Cells as in F were fixed and stained with phalloidin to reveal apical F-actin, revealing no differences.

effect on microvilli is seen in LLC-PK1.CL4 and MDCK cells stably expressing Nadrin shRNA, which depleted the gene product by greater than 90% in both cases (Figure B.2.D-G). These experiments suggest that Nadrins have no unique role in microvilli biogenesis or maintainance.

We next investigated whether Nadrin-depleted MDCK cells could still recruit ZO-1 into tight junctions, a process which others have claimed is defective in the same cells (Wells et al., 2006). Contrary to the previous report, MDCK cells with a >90% reduction in Nadrin protein levels retained tight junctions at steady-state (Figure B.3.A) and formed them with normal kinetics following calcium switch (Figure B.3.B,C). These experiments suggest that Nadrin has no unique role in tight junction biogenesis or maintainance.

In the course of generating various cells lacking Nadrin, I observed that depleting Nadrin from Caco-2 cells caused a subtle delay in cell spreading (Figure B.4).

In the course of my observations of Nadrin trunctations, I noticed that Nadrin (B.5.A) and especially the Nadrin N-BAR domain (Figure B.5.B), localized in puncta. Some of these were identified as endocytic sites, as they were enriched in PI(3)P. Thus Nadrin localizes to some endosomes, as has been claimed (Wells et al., 2006). We examined degradation of EGF receptor as a model endocytic cargo, and found no significant delay its degradation following activation by EGF treatment (Figure B.5.C). Thus, Nadrin may have a role in endocytosis, but the pertinent cargo is not the EGF receptor.

Because the N-BAR domain of Nadrin localizes to curved membranes *in vitro* and *in vivo* (Peter et al., 2004; Galic et al., 2012) and that the microvillus base (which is partially tapered at the extreme proximal region) potentially represents a curvature hotspot, we examined whether the fine localization of Nadrin relies upon the N-BAR domain. Endogenous Nadrin localizes to

A.

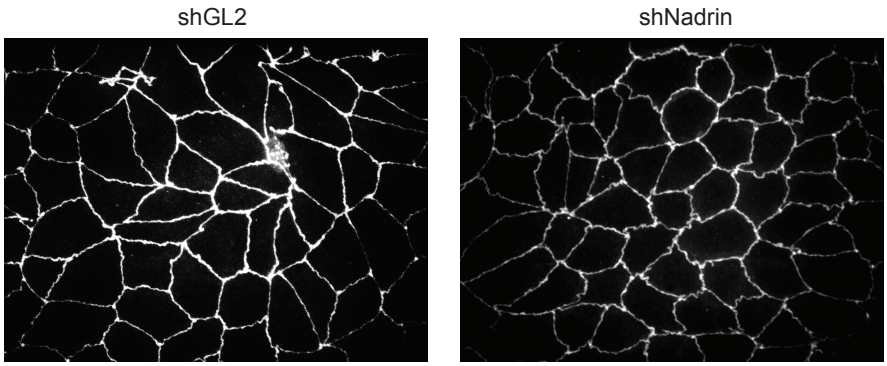
shGL2
shNadrin

B.

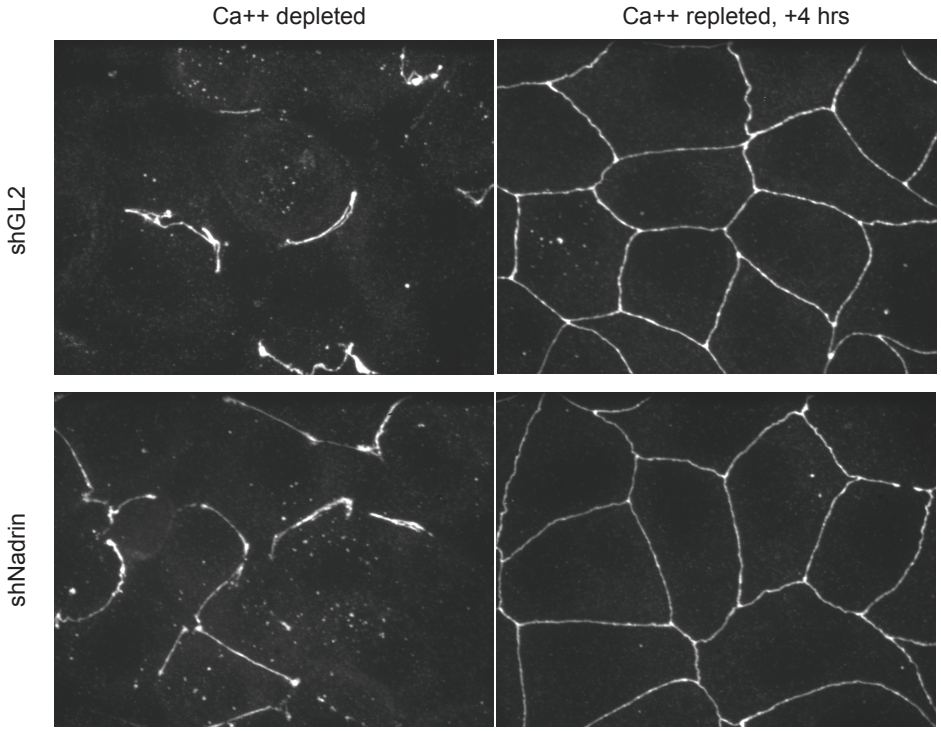
Ca++ depleted
Ca++ repleted, +4 hrs
shGL2
shNadrin

C.

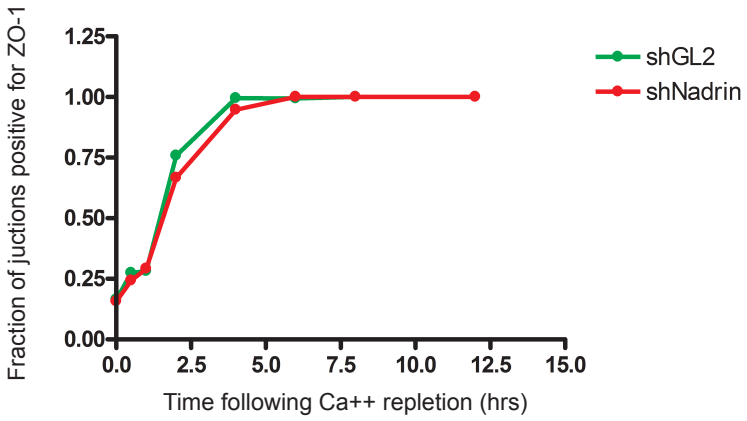
Fraction of junctions positive for ZO-1
1.25
1.00
0.75
0.50
0.25
0.00
0.0
2.5
5.0
7.5
10.0
12.5
15.0
Time following Ca++ repletion (hrs)
shGL2
shNadrin

Figure B.3 Nadrin is not required for ZO-1-labeled tight junctions at steady-state or during reformation.

(A) T23 MDCK stable cell-lines as in B.2.F,G were seeded at confluence for 7 days on 0.4 μ-pore polycarbonate filters, fixed, and stained with ZO-1 antibody (Zymed) revealing no differences. (B) Cells as in B.2.F,G and A were seeded at confluence for 4 days on coverslips and then subjected to calcium depletion and repletion for 4 hours as indicated, then fixed and stained for ZO-1 revealing no differences in contrast with (Wells et al., 2006). (C) Cells as in B were calcium-repleted for indicated times, fixed, and stained for ZO-1 and F-actin (not shown). ~300 cell-cell junctions per treatment were scored for the presence or absence of ZO-1, and the data plotted revealing no significant difference in ZO-1 recruitment to cell-cell junctions following calcium switch in contrast with (Wells et al., 2006).

A.

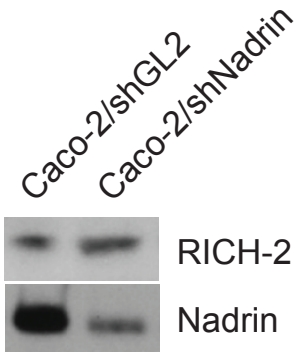

B.

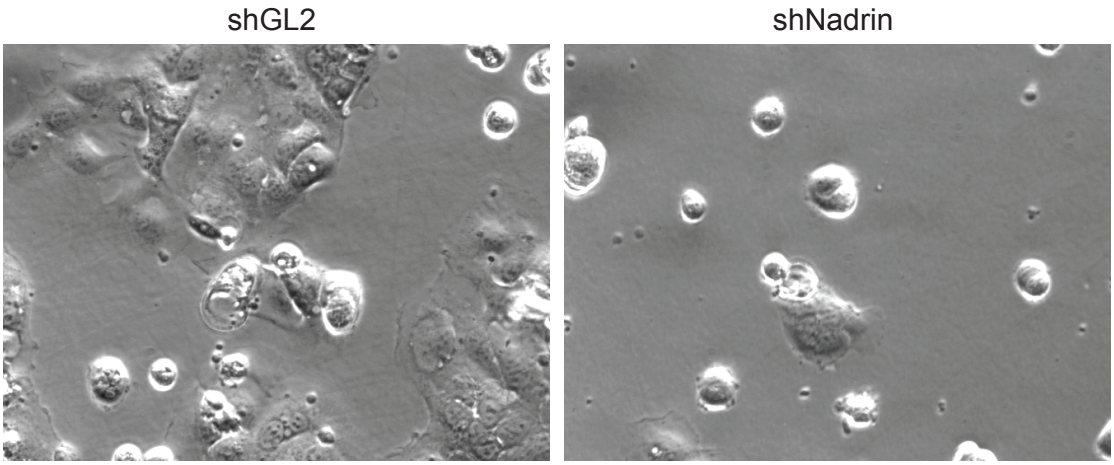

Figure B.4 Nadrin is required for spreading in Caco-2 cells.

(A) Caco-2 cells expressing Nadrin shRNA were western blotted for Nadrin and RICH-2. (B) Cells expressing Nadrin shRNA were analyzed by DIC microscopy after 24 hours of seeding. Nadrin knockdown appears to cause delayed spreading.

A.

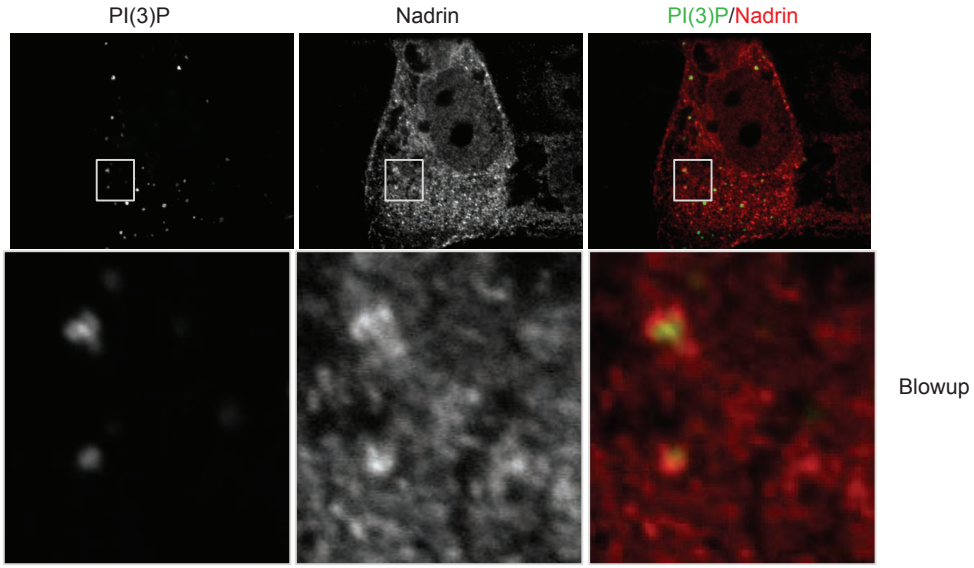
PI(3)P
Nadrin
PI(3)P/Nadrin
Blowup

B.

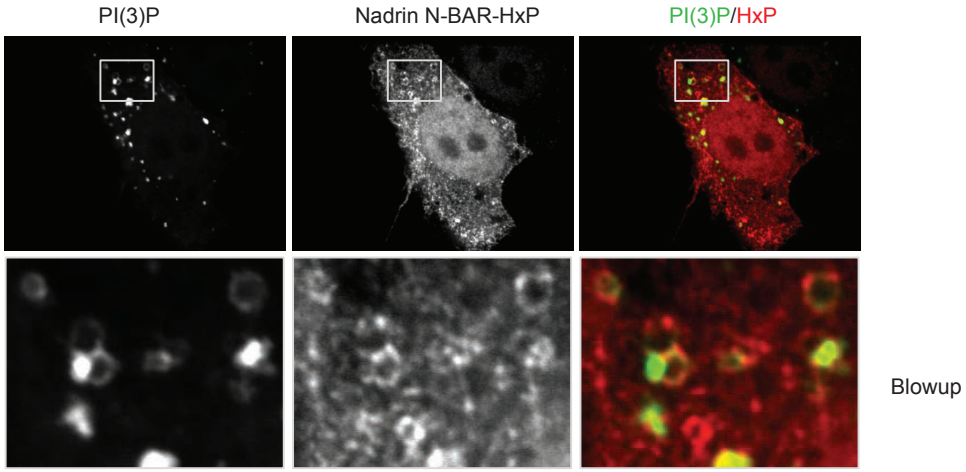
PI(3)P
Nadrin N-BAR-HxP
PI(3)P/HxP
Blowup

C.

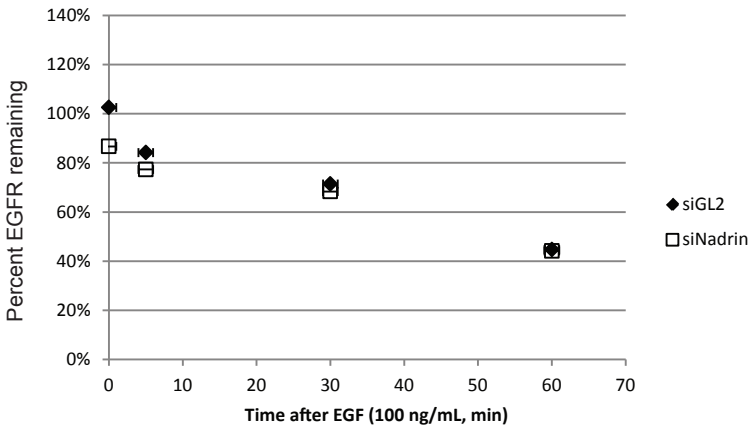
140%
120%
100%
80%
60%
40%
20%
0%
Percent EGFR remaining
0
10
20
30
40
50
60
70
Time after EGF (100 ng/mL, min)
siGL2
siNadrin

Figure B.5 Nadrin is recruited to a subset of endosomes.

(A) Jeg-3 cells overexpressing untagged Nadrin and a PI(3)P-flare, the FYVE domain of EEA-1 tagged with GFP, were stained for Nadrin to reveal partial co-localization. (B) Cells overxpressing the Nadrin N-BAR domain tagged C-terminally with HxP and a PI(3)P-flare were stained for the HxP tag to reveal partial colocalization to a subset of large vacuole-like structures coated with the endosome marker PI(3)P. (C) Jeg-3 cells transfected as in B.2.B,C were treated with 100 ng/mL epidermal growth factor (EGF, Invitrogen) for indicated times, lysed, resolved and western blotted for EGF receptor and loading control E-cadherin. Intensity of EGF receptor divided by E-cadherin (N=1) were graphed. EGF receptor degradation rates are similar to control suggesting that EGF receptor activation and internalization are more or less unaltered following Nadrin depletion.

the cytoplasm but concentrates at the microvillus base (Abraham Hanono, personal communication). This is partially recapitulated by expression of an EBP50-binding-deficient form of Nadrin (tagged on the C-terminus with HxP), suggesting that EBP50 binding is not strictly required for this localization (Figure B.6.A). The ezrin-binding-site (EBS) of EBP50 localizes to the full-length of microvilli (Garbett et al., 2010) by binding directly to ezrin (Reczek et al., 1997; Figure B.6.A). Appending either Nadrin or RICH-2 to the N-terminal end of the EBS forced it to localize specifically to microvilli and accumulate just at the base (Figure B.6.A). A truncation analysis of Nadrin or RICH-2 within the chimera indicated that the N-BAR was necessary and sufficient for the restriction to the base (Figure B.6.B). Western bloting indicates that the chimeras were expressed as expected without degradation (Figure B.6.C). These results are consistent with microvillus base presenting a curved platform to which Nadrin's N-BAR can be recruited. They additionally add to the existing data which suggests that tissue culture cell microvilli can segregate their protein components into discrete domains (Hanono et al., 2006a).

As Nadrin interacts with Par3 (Wells et al., 2006) and EBP50 and its interacting proteins may modulate ciliogenesis (Francis et al., 2011), we investigated whether Nadrin regulates primary ciliogenesis. MDCK cells stably knocked down for Nadrin by >90% were grown at confluence for either 6 or 9 days on 0.4 μ pore-size filters, and then fixed and stained for acetylated tubulin, which accumulates predominantly in primary cilia. Significantly fewer Nadrin knockdown cells had elongated primary cilia at both timepoints (Figure B.7). However, these results could not be recapitulated in either LLC-PK1.CL4 cells or NIH3T3 cells lacking Nadrin, where ciliogenesis proceeded at the normal pace (data not shown). Additionally, neither Nadrin nor EBP50 was found to be a component of primary cilia (data not shown). Therefore, Nadrin

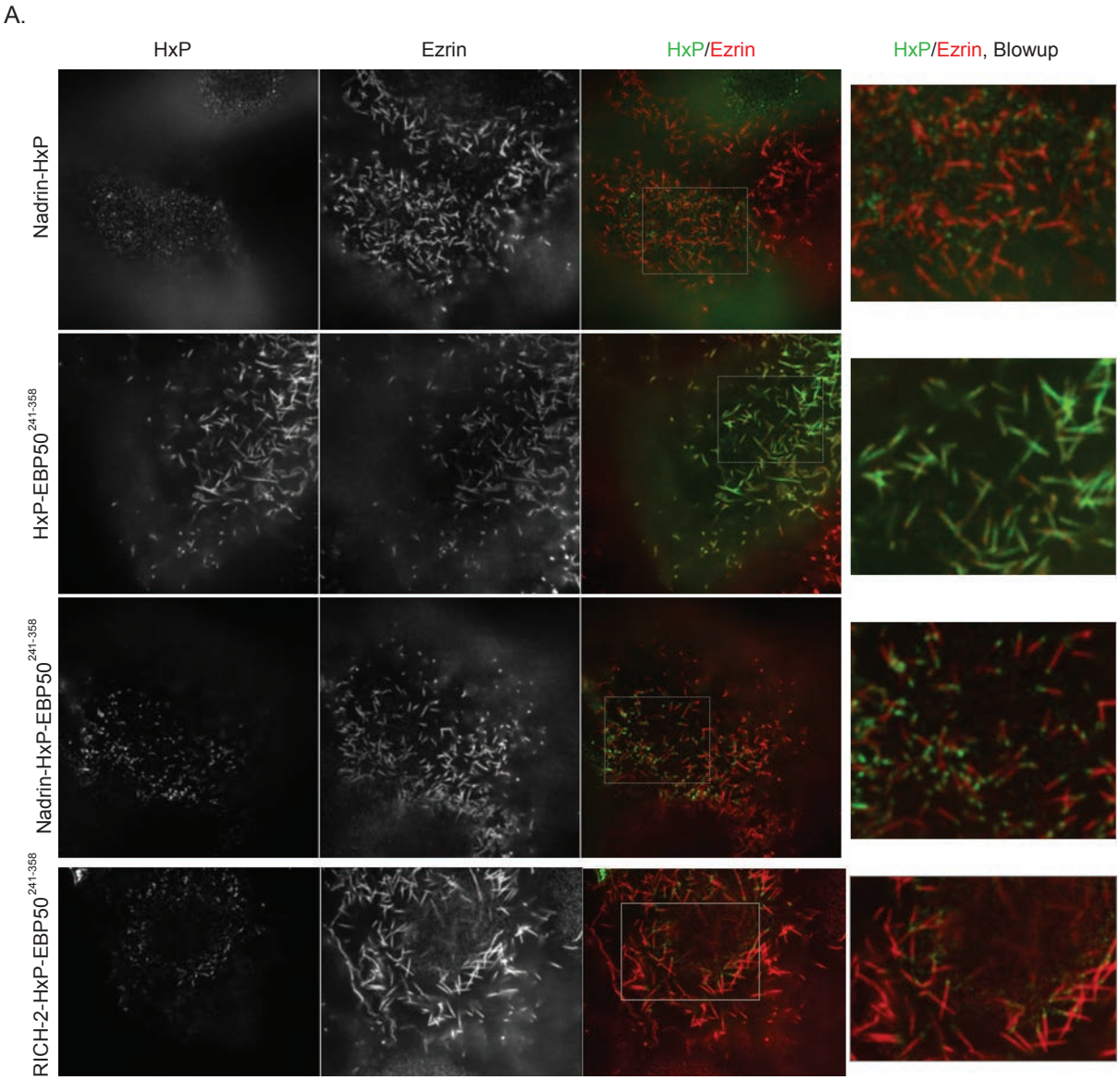
A.
HxP
Ezrin
HxP/Ezrin
HxP/Ezrin, Blowup
Nadrin-HxP
HxP-EBP50241-358
Nadrin-HxP-EBP50241-358
RICH-2-HxP-EBP50241-358
B.
262
444
881
a
N-BAR
RhoGAP
PP
STA
HxP
Diffuse
b
Diffuse
c
EBP50 1-358
MV length
d
MV base
e
EBP50 241-358
MV length
f
MV base
g
MV length
h
MV length
i
50% MV base,
50% MV middle
0% MV length
C.
c e f g
Nadrin1-881-HxP-EBP50241-358
EBP50
HxP-EBP50241-358
EBP50

Figure B.6 Nadrin is recruited to a subset of endosomes.

(A) Jeg-3 cells overexpressing indicated, HxP-tagged proteins and chimeras were fixed and stained for the Xpress tag and ezrin. Whereas, the ezrin-binding site of EBP50 localizes to the full-length of microvilli, Nadrin- or RICH-2 fused to the ezrin-binding site localize specifically to the microvillus base. (B) Summary of localization of indicated truncations and chimeras. The N-BAR domain is necessary and sufficient to localize to the microvillus base in the chimera of Nadrin fused to EBP50's ezrin binding site. (C) Expression of selected, intact fusion proteins was verified by EBP50 western blot.

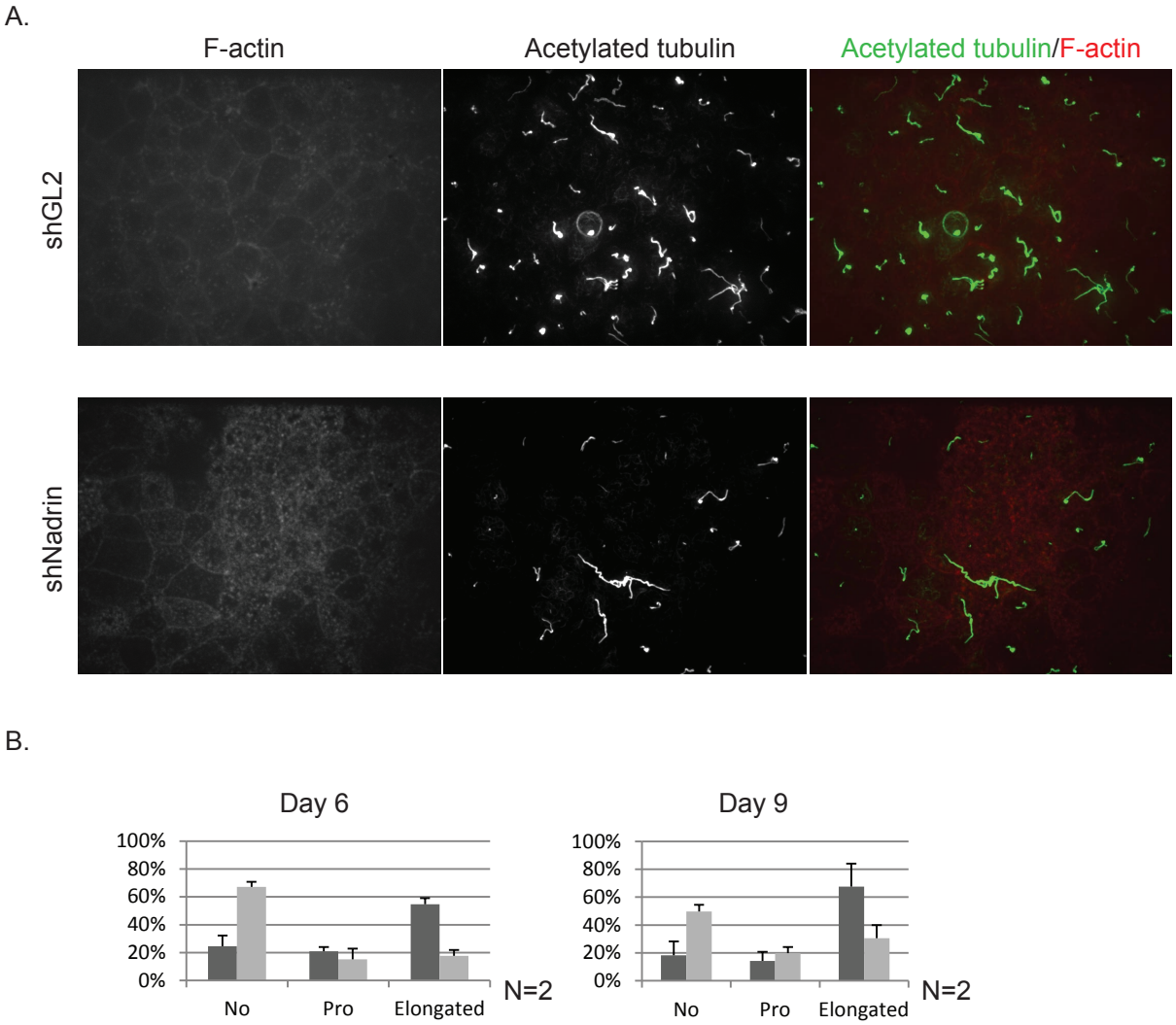

Figure B.7 Nadrin may be required for the proper timing of primary cilium biogenesis

(A) MDCK stable cell-lines expressing control shRNA (shGL2) or Nadrin shRNA (shNadrin) as in Figure B.2.F were grown at confluence on 0.4 μ-pore-size filters for 6 days to induce formation of the primary cilium, and then fixed and stained for acetylated tubulin (marking the primary cilium) and F-actin (phalloidin). (B) shGL2 (dark gray) or shNadrin (light gray) cells as in A were scored for no primary cilium ('No') a punctate pro-cilium ('Pro') or an elongated primary cilium ('Elongated') after indicated number of days at confluence.

knockdown may have an effect on ciliogenesis in MDCK cells, but this may reflect a delay in any of the downstream polarity processes required to be intact prior to ciliogenesis.

Thus, despite interacting tightly with EBP50, Nadrin does not appear to be involved in the same function. Interestingly, Lauffer et al. reached a similar conclusion regarding sorting of the β2 adrenergic receptor (Lauffer et al., 2010). Though the tail of the receptor binds tenaciously to EBP50's first PDZ domain *in vitro* (Cao et al., 1999), it is the PDZ domain from a different protein, SNX27, that regulates its endocytic sorting. Along with many others, such findings imply that evolutionarily recent protein interaction pairs such as the PDZ-PDZ binding motif interaction may have been incompletely selected for specificity.

APPENDIX C

AN ISOFORM-SPECIFIC INTERACTION BETWEEN EBP50 AND IRSP53-T

Work on EBP50 in Jeg-3 cells strongly indicated that an unknown ligand interacting with EBP50's first PDZ domain brings about microvilli (Garbett et al., 2010; Hanono et al., 2006). In the previous appendix, it became clear that Nadrin was not this ligand, because removing it did not affect microvilli in several cell types (Appendix B). Although there is a strong interaction between EBP50 and Nadrin *in vitro*, this interaction could not be recapitulated by immunoprecipitation with or without DSP cross-linking prior to lysis (data not shown). Thus, we sought to determine the EBP50 PDZ1 immunoprecipitation-defined interactome in order to identify the true EBP50 PDZ1 ligand(s).

MATERIALS AND METHODS

EBP50 and PDZ mutant cDNAs were obtained from Damien Garbett (Garbett et al., 2010) and cloned by tailored PCR into pQCXIP-3XFLAG. IRSp53-S and -T were amplified from Jeg-3 cDNA and cloned into pEGFP-C1 or pTagRFP-T-C1.

For immunoprecipitations, 2 x 10^8 cells per construct were grown in SILAC media, scraped directly into lysis buffer (25 mM Tris pH 7.4, 150 mM NaCl, 2.5% glycerol, 1% IGEPAL, 0.1 mM Na3VO4, 50 mM NaF, 10 mM β-GP, 1X Roche Protease inhibitor tablet), homogenized by 5 strokes of a loose-fitting dounce homogenizer, clarified, and immunoprecipitated with 20 μL of Flag-M2 affinity gel (Sigma) for 2 hours and then processed for mass spectrometry as described in Chapter 2. High confidence interactors were those for which at least 2 peptides were identified at a wild-type-to-PDZ1 mutant ratio of at least 4.0.

Liposomes and liposome flotation assays were exactly according to (Santiago-Tirado et al., 2011). GST-EBP50-PDZ1+ was as previously described (Reczek and Bretscher, 2001).

GST-IRSp53 tail was made by PCR amplifying IRSp53 434-520 with or without an additional alanine and inserting it into pGEX6P1, transforming Rosetta2DE3 bacteria with the resulting plasmid, and purification using glutathione agarose resin (GE Healthcare).

The IRSp53 siRNA (5'-CAGAAUCAGCUGGAAGAAAtt-3') was Silencer Select from Ambion.

The pan-IRSp53/58 antibody was from Milipore. All other reagents are as described in chapters 1-3 and appendices A and B.

RESULTS AND DISCUSSION

Jeg-3 cells expressing 3XFLAG-EBP50 and PDZ mutants singly or in combination as well as 3XFLAG-EBP50 incapable of interacting with ezrin (MAWA) (Garbett et al., 2010) were generated. As a control, quantitative flag immunoprecipitates from the stable lines were probed for EPI64, and it was found to associate with all versions of 3XFLAG-EBP50 except those lacking an intact PDZ1 domain (Figure C.1.A). Mutating PDZ2 decreased EPI64 interaction as expected (Garbett et al., 2010). Cells expressing 3XFLAG-EBP50 were grown in light SILAC medium, cells expressing 3XFLAG-EBP50-PDZ1mut in heavy SILAC medium, and immunoprecipitates were prepared and their contents quantitatively compared by mass spectrometrometry. Amongst the small list of high-confidence interactors were two previously identified PDZ1 ligands, EPI64 and PLCβ3, as well as a previously characterized PDZ2 ligand, YAP65 (Mohler et al., 1999), which we determined actually binds to PDZ1 and not PDZ2 in agreement with our results (Damien Garbett, personal communication). Additionally, we

A.

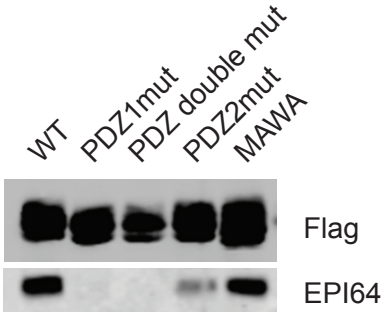

B.

Protein	WT:PDZ1mut	# of peptides	
NEK4	Infinite	2	
IRSp53	18.1	22	
DLGAP4	14.19	3	
EPI64	11.05	8	*
YAP65	8.28	2	*
MAT2A	4.49	24	
PLCβ3	4.15	4	*

C.

MSLSRSEEMH RLTENVYKTI MEQFNPSLRN FIAMGKNYEK ALAGVTYAAK GYFDALVKMG ELASESQGSK
ELGDVLFQMA EVHRQIQNQL EEMLKSFHNE LLTQLEQKVE LDSRYLSAAL KKYQTEQRSK GDALDKCQAE
LKKLRKKSQG SKNPQKYSDK ELQYIDAISN KQGELENYVS DGYKTALTEE RRRFCFLVEK QCAVAKNSAA
YHSKGKELLA QKLPLWQQAC ADPSKIPERA VQLMQQVASN GATLPSALSA SKSNLVISDP IPGAKPLPVP
PELAPFVGRM SAQESTPIMN GVTGPDGEDY SPWADRKAAQ PKSLSPPQSQ SKLSDSYSNT LPVRKSVTPK
NSYATTENKT LPRSSSMAAG LERNGRMRVK AIFSHAAGDN STLLSFKEGD LITLLVPEAR DGWHYGESEK
TKMRGWFPFS YTRVLDSDGS DRLHMSLQQG KSSSTGNLLD KDDLAIPPPD YGAASRAFPA QTASGFKQRP
YSVAVPAFSQ GLDDYGARSM SSADVEVARF

D.

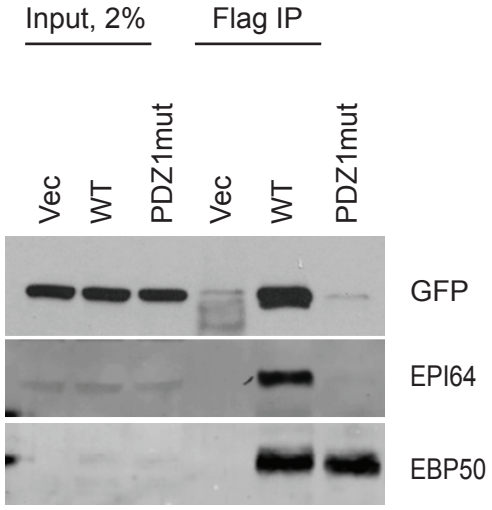

E.

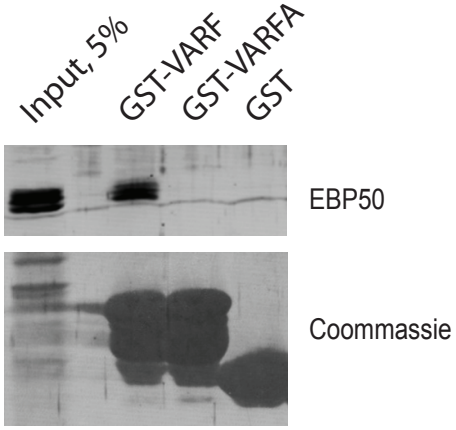

F.

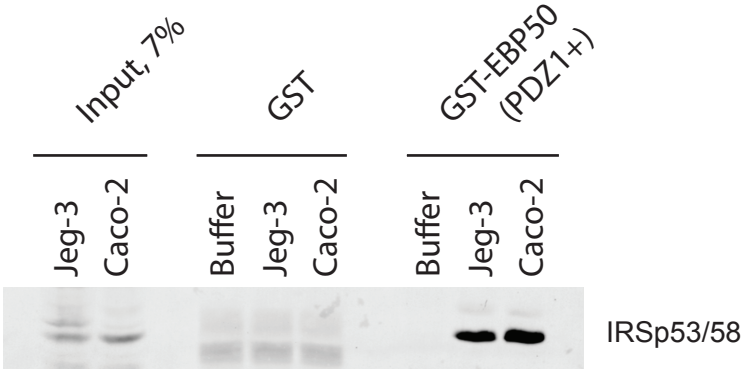

G.

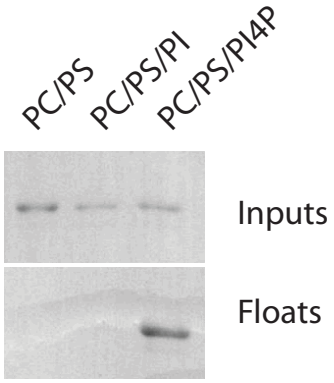

Figure C.1 An isoform of IRSp53 specifically interacts with the PDZ1 domain of EBP50.

(A) Jeg-3 stable cell-lines expressing 3XFlag-EBP50 with indicated mutations (MAWA blocks binding to ezrin, (Garbett and Bretscher, 2012) were subjected to flag immunoprecipitation, and the immunoprecipitates western blotted for known EBP50 PDZ1 ligand, EPI64. (B) Jeg-3 cells expressing either 3XFlag-EBP50 ('WT') or 3XFlag-EBP50_PDZ1mut ('PDZ1mut') were differentially labeled using the SILAC procedure. The flag tag was immunoprecipitated, the immunoprecipitate trypsin-digested, and tryptic fragments subjected to mass spectrometry. Top differential candidates are presented. A red asterisk (*) denotes previously known EBP50 ligands. (C) Sequence of IRSp53-T isoform with sequence coverage mapped in orange. The most C-terminal peptide identified the recovered protein unequivocally as IRSp53-T. (D) Jeg-3 cells transfected with vector control or 3XFlag-EBP50 with indicated mutation and GFP-IRSp53-T were subjected to flag IP. The IP results can be recapitulated manually with western blots. (E) Jeg-3 cell lysate was subjected to GST-pulldown using GST or GST IRSp53-T C-terminus with or without an alanine following the PDZ-binding motif, and the precipitate was western blotted for EBP50. EBP50 interacts with the IRSp53 C-terminus. (F) Jeg-3 or Caco-2 cell lysate as indicated was subjected to GST-pulldown using GST or GST-EBP50-PDZ1+ (Reczek and Bretscher, 2001), and the precipitate western blotted for IRSp53/58. IRSp53 but not IRSp58 interacts with EBP50 PDZ1+ in a GST-pulldown. (G) IRSp53-T was expressed in bacteria and purified using the His-SUMO system and subjected to liposome flotation assay, revealed by amido-black total protein stain. Recombinant IRSp53-T was found to bind only phosphoinositide-phosphate-containing liposomes.

identified a PDZ-interacting MAGUK of unknown function (DLGAP4) and IRSp53, a protein with an N-terminal I-BAR domain and a C-terminal SH3 domain and PDZ-binding motif previously implicated in forming filopodia and microspikes in response to activated Rac1 and Cdc42 (Figure C.1.B; Krugmann et al., 2001; Bockmann et al., 2002; Millard et al., 2005; Disanza et al., 2006).

Sequence analysis of the identified peptides unequivocally identified the bound isoform of IRSp53 as IRSp53-T, which had not previously been characterized, but is predicted to end in –V-A-R-F, a potential PDZ binding motif (Figure C.1.C). Co-expression-immunoprecipitation experiments showed that IRSp53-T interacts directly with wild-type but not PDZ1 mut (Figure C.1.D). Furthermore, the tail of IRSp53 precipitated EBP50 from cell extracts, whereas the addition of a single alanine to the C-terminus blocked the interaction completely (Figure C.1.E). Finally, immobilized EBP50 PDZ1+ precipitated IRSp53 from extracts of placental epithelial Jeg-3 or colon epithelial Caco-2 cells, suggesting that an EBP50-binding isoform of IRSp53 is generally expressed in epithelial cells. In preparation for future studies, I prepared IRSp53 as a SUMO fusion. The C-terminus is intact because it interacts with EBP50 (data not shown) and the N-terminus is intact because it interacts with liposomes in a phospholipid-dependent manner (Figure C.1.F).

Overexpressed IRSp53 localized throughout the full-length of microvilli like EBP50 and Ezrin (Figure C.2.A) as well as minimally to cell-cell junctions and filopodia (data not shown). The best studied isoform of IRSp53 is IRSp53-S, which differs from –T in the last 10 residues (ending in –V-S-T-V rather than –V-A-R-F) and binds to the PDZ domain of cell-cell junction and filopodia-localized protein LIN-7. While the localization of the two isoforms partially overlap, IRSp53-S was more enriched at cell-cell junctions while IRSp53-T was more enriched

in microvilli when expressed in the same cell, reflecting the different localization of their cognate PDZ domains (Figure C.2.B).

We knocked down the expression of IRSp53 by about 70% (Figure C.2.C), and cells were fixed, stained for ezrin, and blindly scored for both microvilli presence and abundance. Unfortunately, loss of IRSp53 resulted in only a small change in which the density of microvilli in the transfected cells was partially reduced according to one scoring strategy (Figure C.2.D) not reduced at all according to another (Damien Garbett, personal communication). These results seem surprising in the face of studies in which overexpression of IRSp53 creates microspikes and filopodia in fibroblastic cells (Krugmann et al., 2001; Bockmann et al., 2002; Millard et al., 2005; Disanza et al., 2006) and one study in which IRSp53 knockdown in MDCK cells caused a dramatic loss of microvilli as well as eliminating stress fibers and delaying cell spreading (Cohen et al., 2011). Thus, we may not have knocked the protein down far enough.

Still, the same conclusions have not been reached by genetic studies of IRSp53. IRSp53 knockout mice have minimal effects (Sawallisch et al., 2009), and the single slime mold ortholog of all I-BAR proteins was found to be dispensible for filopodia (Veltman et al., 2011). This may hint that though it can, IRSp53 does not function in making actin protrusions but in some other process entirely such as endocytosis or cell signaling. Since we have limited assays to probe EBP50 function, we may never know what role this interaction is really serving.

A.

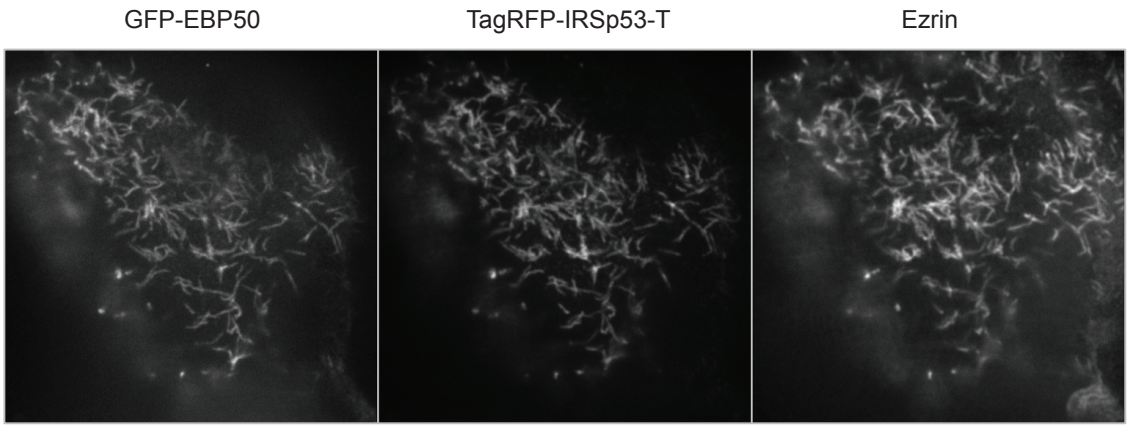
GFP-EBP50
TagRFP-IRSp53-T
Ezrin

B.

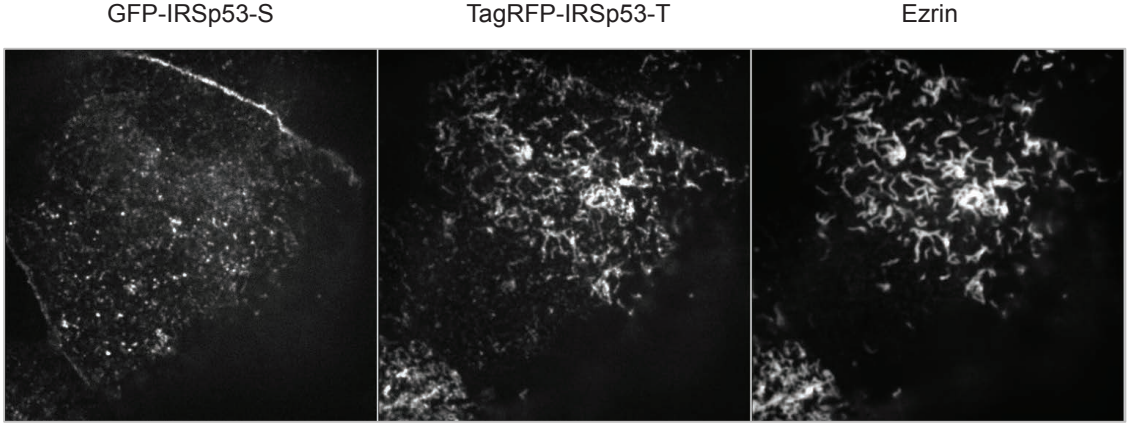
GFP-IRSp53-S
TagRFP-IRSp53-T
Ezrin

C.

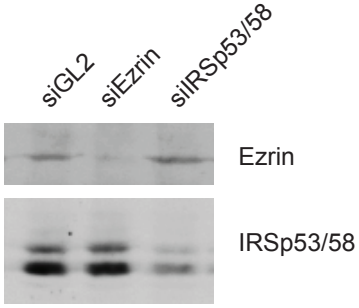
siGL2
siEzrin
siIRSp53/58
Ezrin
IRSp53/58

D.

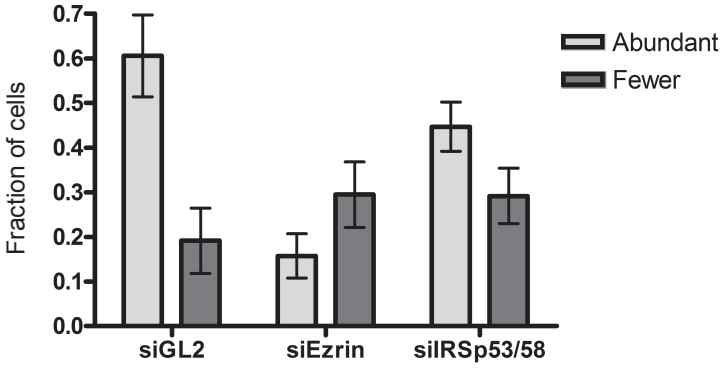
Fraction of cells
0.7
0.6
0.5
0.4
0.3
0.2
0.1
0.0
siGL2
siEzrin
siIRSp53/58
Abundant
Fewer

Figure C.2 IRSp53-T is more highly enriched in microvilli than IRSp53-S, but IRSp53 is dispensible for microvilli.

(A) IRSp53-T was overexpressed in Jeg-3 cells with an N-terminal TagRFP-T tag along with EBP50 with an N-terminal GFP tag, and the cells fixed and stained for ezrin, and the apical projections shown. All three markers colocalize in microvilli. (B) Two isoforms of IRSp53 were differentially tagged and co-expressed in Jeg-3 cells. Whereas IRSp53-S, which has a different C-terminal PDZ binding motif that does not interact with EBP50, localizes more to cell-cell junctions, IRSp53-T localizes more to microvilli. (C) IRSp53/58 or ezrin were knocked down in Jeg-3 cells using siRNAs, and the lysates resolved and western blotted for ezrin and IRSp53/58. (D) Cells as in C were fixed and stained for ezrin, and the presence and density of microvilli were subjectively scored. IRSp53/58 knockdown causes a subtle decrease in microvillus density ($N=4$, $p < 0.03$).

REFERENCES

Algrain, M., O. Turunen, A. Vaheri, D. Louvard, and M. Arpin. 1993. Ezrin contains cytoskeleton and membrane binding domains accounting for its proposed role as a membrane-cytoskeletal linker *J.Cell Biol.* 120:129-139.

Antoine-Bertrand, J., A. Ghogha, V. Luangrath, F.K. Bedford, and N. Lamarche-Vane. 2011. The activation of ezrin-radixin-moesin proteins is regulated by netrin-1 through Src kinase and RhoA/Rho kinase activities and mediates netrin-1-induced axon outgrowth *Mol.Biol.Cell.* 22:3734-3746.

Baas, A.F., J. Kuipers, N.N. van der Wel, E. Batlle, H.K. Koerten, P.J. Peters, and H.C. Clevers. 2004. Complete polarization of single intestinal epithelial cells upon activation of LKB1 by STRAD *Cell.* 116:457-466.

Barret, C., C. Roy, P. Montcourrier, P. Mangeat, and V. Niggli. 2000. Mutagenesis of the phosphatidylinositol 4,5-bisphosphate (PIP(2)) binding site in the NH(2)-terminal domain of ezrin correlates with its altered cellular distribution *J.Cell Biol.* 151:1067-1080.

Basak, S., D. Speicher, S. Eck, W. Wunner, G. Maul, M.S. Simmons, and D. Herlyn. 1998. Colorectal carcinoma invasion inhibition by CO17-1A/GA733 antigen and its murine homologue *J.Natl.Cancer Inst.* 90:691-697.

Batchelor, C.L., J.R. Higginson, Y.J. Chen, C. Vanni, A. Eva, and S.J. Winder. 2007. Recruitment of Dbl by ezrin and dystroglycan drives membrane proximal Cdc42 activation and filopodia formation *Cell.Cycle.* 6:353-363.

Belkina, N.V., Y. Liu, J.J. Hao, H. Karasuyama, and S. Shaw. 2009. LOK is a major ERM kinase in resting lymphocytes and regulates cytoskeletal rearrangement through ERM phosphorylation *Proc.Natl.Acad.Sci.U.S.A.* 106:4707-4712.

Ben-Aissa, K., G. Patino-Lopez, N.V. Belkina, O. Maniti, T. Rosales, J.J. Hao, M.J. Kruhlak, J.R. Knutson, C. Picart, and S. Shaw. 2012. Activation of moesin, a protein that links actin cytoskeleton to the plasma membrane, occurs by phosphatidylinositol 4,5-bisphosphate (PIP2) binding sequentially to two sites and releasing an autoinhibitory linker *J.Biol.Chem.* 287:16311-16323.

Berryman, M., and A. Bretscher. 2000. Identification of a novel member of the chloride intracellular channel gene family (CLIC5) that associates with the actin cytoskeleton of placental microvilli *Mol.Biol.Cell.* 11:1509-1521.

Berryman, M., Z. Franck, and A. Bretscher. 1993. Ezrin is concentrated in the apical microvilli of a wide variety of epithelial cells whereas moesin is found primarily in endothelial cells *J.Cell.Sci.* 105 (Pt 4):1025-1043.

Bockmann, J., M.R. Kreutz, E.D. Gundelfinger, and T.M. Bockers. 2002. ProSAP/Shank postsynaptic density proteins interact with insulin receptor tyrosine kinase substrate IRSp53 *J.Neurochem.* 83:1013-1017.

Bonilha, V.L., S.C. Finnemann, and E. Rodriguez-Boulan. 1999. Ezrin promotes morphogenesis of apical microvilli and basal infoldings in retinal pigment epithelium *J.Cell Biol.* 147:1533-1548.

Bonilha, V.L., M.E. Rayborn, I. Saotome, A.I. McClatchey, and J.G. Hollyfield. 2006. Microvilli defects in retinas of ezrin knockout mice. *Exp.Eye Res.* 82:720-729.

Bretscher, A. 1989. Rapid phosphorylation and reorganization of ezrin and spectrin accompany morphological changes induced in A-431 cells by epidermal growth factor *J.Cell Biol.* 108:921-930.

Bretscher, A. 1983. Purification of an 80,000-dalton protein that is a component of the isolated microvillus cytoskeleton, and its localization in nonmuscle cells *J.Cell Biol.* 97:425-432.

Burakov, A.V., O.V. Kovalenko, E.S. Potekhina, E.S. Nadezhdina, and L.A. Zinovkina. 2005. LOSK (SLK) protein kinase activity is necessary for microtubule organization in the interphase cell centrosome *Dokl.Biol.Sci.* 403:317-319.

Carreno, S., I. Kouranti, E.S. Glusman, M.T. Fuller, A. Echard, and F. Payre. 2008. Moesin and its activating kinase Slik are required for cortical stability and microtubule organization in mitotic cells *J.Cell Biol.* 180:739-746.

Casaletto, J.B., I. Saotome, M. Curto, and A.I. McClatchey. 2011. Ezrin-mediated apical integrity is required for intestinal homeostasis *Proc.Natl.Acad.Sci.U.S.A.* 108:11924-11929.

Chambers, D.N., and A. Bretscher. 2005. Ezrin mutants affecting dimerization and activation *Biochemistry.* 44:3926-3932.

Charras, G.T., C.K. Hu, M. Coughlin, and T.J. Mitchison. 2006. Reassembly of contractile actin cortex in cell blebs *J.Cell Biol.* 175:477-490.

Chen, J., J.A. Cohn, and L.J. Mandel. 1995. Dephosphorylation of ezrin as an early event in renal microvillar breakdown and anoxic injury *Proc.Natl.Acad.Sci.U.S.A.* 92:7495-7499.

Chorna-Ornan, I., V. Tzarfaty, G. Ankri-Eliahoo, T. Joel-Almagor, N.E. Meyer, A. Huber, F. Payre, and B. Minke. 2005. Light-regulated interaction of Dmoesin with TRP and TRPL channels is required for maintenance of photoreceptors *J.Cell Biol.* 171:143-152.

Chuang, J.Z., S.Y. Chou, and C.H. Sung. 2010. Chloride intracellular channel 4 is critical for the epithelial morphogenesis of RPE cells and retinal attachment *Mol.Biol.Cell.* 21:3017-3028.

Cohen, D., D. Fernandez, F. Lazaro-Dieguez, and A. Musch. 2011. The serine/threonine kinase Par1b regulates epithelial lumen polarity via IRSp53-mediated cell-ECM signaling *J.Cell Biol.* 192:525-540.

Coluccio, L.M., and A. Bretscher. 1989. Reassociation of microvillar core proteins: making a microvillar core in vitro *J.Cell Biol.* 108:495-502.

Cordes, N., S. Wagner, C.J. Storbeck, K. Roovers, Z.Y. Chaar, P. Kolodziej, M. McKay, and L.A. Sabourin. 2008. FAK/src-Family Dependent Activation of the Ste20-Like Kinase SLK Is Required for Microtubule-Dependent Focal Adhesion Turnover and Cell Migration *PLoS ONE.* 3:e1868.

Coscoy, S., F. Waharte, A. Gautreau, M. Martin, D. Louvard, P. Mangeat, M. Arpin, and F. Amblard. 2002. Molecular analysis of microscopic ezrin dynamics by two-photon FRAP *Proc.Natl.Acad.Sci.U.S.A.* 99:12813-12818.

Crepaldi, T., A. Gautreau, P.M. Comoglio, D. Louvard, and M. Arpin. 1997. Ezrin is an effector of hepatocyte growth factor-mediated migration and morphogenesis in epithelial cells. *J.Cell Biol.* 138:423-434.

Croce, A., G. Cassata, A. Disanza, M.C. Gagliani, C. Tacchetti, M.G. Malabarba, M.F. Carlier, G. Scita, R. Baumeister, and P.P. Di Fiore. 2004. A novel actin barbed-end-capping activity in EPS-8 regulates apical morphogenesis in intestinal cells of Caenorhabditis elegans *Nat.Cell Biol.* 6:1173-1179.

Dagdas, Y.F., K. Yoshino, G. Dagdas, L.S. Ryder, E. Bielska, G. Steinberg, and N.J. Talbot. 2012. Septin-mediated plant cell invasion by the rice blast fungus, Magnaporthe oryzae *Science.* 336:1590-1595.

D'Angelo, R., S. Aresta, A. Blangy, L. Del Maestro, D. Louvard, and M. Arpin. 2007. Interaction of ezrin with the novel guanine nucleotide exchange factor PLEKHG6 promotes RhoG-dependent apical cytoskeleton rearrangements in epithelial cells *Mol.Biol.Cell.* 18:4780-4793.

Dard, N., S. Louvet, A. Santa-Maria, J. Aghion, M. Martin, P. Mangeat, and B. Maro. 2001. In vivo functional analysis of ezrin during mouse blastocyst formation *Dev.Biol.* 233:161-173.

Dard, N., S. Louvet-Vallee, A. Santa-Maria, and B. Maro. 2004. Phosphorylation of ezrin on threonine T567 plays a crucial role during compaction in the mouse early embryo *Dev.Biol.* 271:87-97.

Delpire, E. 2009. The mammalian family of sterile 20p-like protein kinases *Pflugers Arch.* 458:953-967.

Denker, S.P., and D.L. Barber. 2002. Cell migration requires both ion translocation and cytoskeletal anchoring by the Na-H exchanger NHE1 *J.Cell Biol.* 159:1087-1096.

Denker, S.P., D.C. Huang, J. Orlowski, H. Furthmayr, and D.L. Barber. 2000. Direct binding of the Na--H exchanger NHE1 to ERM proteins regulates the cortical cytoskeleton and cell shape independently of H(+) translocation *Mol.Cell.* 6:1425-1436.

Dent, E.W., S.L. Gupton, and F.B. Gertler. 2011. The growth cone cytoskeleton in axon outgrowth and guidance *Cold Spring Harb Perspect.Biol.* 3:10.1101/cshperspect.a001800.

Disanza, A., S. Mantoani, M. Hertzog, S. Gerboth, E. Frittoli, A. Steffen, K. Berhoerster, H.J. Kreienkamp, F. Milanesi, P.P. Di Fiore, A. Ciliberto, T.E. Stradal, and G. Scita. 2006. Regulation of cell shape by Cdc42 is mediated by the synergic actin-bundling activity of the Eps8-IRSp53 complex *Nat.Cell Biol.* 8:1337-1347.

Doi, Y., M. Itoh, S. Yonemura, S. Ishihara, H. Takano, T. Noda, and S. Tsukita. 1999. Normal development of mice and unimpaired cell adhesion/cell motility/actin-based cytoskeleton without compensatory up-regulation of ezrin or radixin in moesin gene knockout *J.Biol.Chem.* 274:2315-2321.

Estecha, A., L. Sanchez-Martin, A. Puig-Kroger, R.A. Bartolome, J. Teixido, R. Samaniego, and P. Sanchez-Mateos. 2009. Moesin orchestrates cortical polarity of melanoma tumour cells to initiate 3D invasion *J.Cell.Sci.* 122:3492-3501.

Eto, M., J.A. Kirkbride, and D.L. Brautigan. 2005. Assembly of MYPT1 with protein phosphatase-1 in fibroblasts redirects localization and reorganizes the actin cytoskeleton *Cell Motil.Cytoskeleton.* 62:100-109.

Evangelista, M., D. Pruyne, D.C. Amberg, C. Boone, and A. Bretscher. 2002. Formins direct Arp2/3-independent actin filament assembly to polarize cell growth in yeast *Nat.Cell Biol.* 4:260-269.

Fehon, R.G., A.I. McClatchey, and A. Bretscher. 2010. Organizing the cell cortex: the role of ERM proteins *Nat.Rev.Mol.Cell Biol.* 11:276-287.

Fievet, B., D. Louvard, and M. Arpin. 2006. ERM proteins in epithelial cell organization and functions. *Biochim.Biophys.Acta.* 1773:653-60.

Fievet, B.T., A. Gautreau, C. Roy, L. Del Maestro, P. Mangeat, D. Louvard, and M. Arpin. 2004. Phosphoinositide binding and phosphorylation act sequentially in the activation mechanism of ezrin *J.Cell Biol.* 164:653-659.

Finnerty, C.M., D. Chambers, J. Ingraffea, H.R. Faber, P.A. Karplus, and A. Bretscher. 2004. The EBP50-moesin interaction involves a binding site regulated by direct masking on the FERM domain. *J.Cell.Sci.* 117:1547-1552.

Firat-Karalar, E.N., and M.D. Welch. 2011. New mechanisms and functions of actin nucleation *Curr.Opin.Cell Biol.* 23:4-13.

Fornaro, M., R. Dell'Arciprete, M. Stella, C. Bucci, M. Nutini, M.G. Capri, and S. Alberti. 1995. Cloning of the gene encoding Trop-2, a cell-surface glycoprotein expressed by human carcinomas *Int.J.Cancer.* 62:610-618.

Francis, S.S., J. Sfakianos, B. Lo, and I. Mellman. 2011. A hierarchy of signals regulates entry of membrane proteins into the ciliary membrane domain in epithelial cells *J.Cell Biol.* 193:219-233.

Fukata, Y., K. Kimura, N. Oshiro, H. Saya, Y. Matsuura, and K. Kaibuchi. 1998. Association of the myosin-binding subunit of myosin phosphatase and moesin: dual regulation of moesin phosphorylation by Rho-associated kinase and myosin phosphatase *J.Cell Biol.* 141:409-418.

Galic, M., S. Jeong, F.C. Tsai, L.M. Joubert, Y.I. Wu, K.M. Hahn, Y. Cui, and T. Meyer. 2012. External push and internal pull forces recruit curvature-sensing N-BAR domain proteins to the plasma membrane. *Nat.Cell Biol.* 14:874-881.

Galvagni, F., C.T. Baldari, S. Oliviero, and M. Orlandini. 2012. An apical actin-rich domain drives the establishment of cell polarity during cell adhesion *Histochem.Cell Biol.* 138:419-433.

Garbett, D., and A. Bretscher. 2012. PDZ interactions regulate rapid turnover of the scaffolding protein EBP50 in microvilli *J.Cell Biol.* 198:195-203.

Garbett, D., D.P. LaLonde, and A. Bretscher. 2010. The scaffolding protein EBP50 regulates microvillar assembly in a phosphorylation-dependent manner *J.Cell Biol.* 191:397-413.

Gary, R., and A. Bretscher. 1995. Ezrin self-association involves binding of an N-terminal domain to a normally masked C-terminal domain that includes the F-actin binding site *Mol.Biol.Cell.* 6:1061-1075.

Gary, R., and A. Bretscher. 1993. Heterotypic and homotypic associations between ezrin and moesin, two putative membrane-cytoskeletal linking proteins *Proc.Natl.Acad.Sci.U.S.A.* 90:10846-10850.

Gautreau, A., D. Louvard, and M. Arpin. 2000. Morphogenic effects of ezrin require a phosphorylation-induced transition from oligomers to monomers at the plasma membrane. *J.Cell Biol.* 150:193-203.

Gervais, L., S. Claret, J. Januschke, S. Roth, and A. Guichet. 2008. PIP5K-dependent production of PIP2 sustains microtubule organization to establish polarized transport in the Drosophila oocyte *Development.* 135:3829-3838.

Gisler, S.M., S. Pribanic, D. Bacic, P. Forrer, A. Gantenbein, L.A. Sabourin, A. Tsuji, Z.S. Zhao, E. Manser, J. Biber, and H. Murer. 2003. PDZK1: I. a major scaffolder in brush borders of proximal tubular cells *Kidney Int.* 64:1733-1745.

Gloerich, M., J.P. Ten Klooster, M.J. Vliem, T. Koorman, F.J. Zwartkruis, H. Clevers, and J.L. Bos. 2012. Rap2A links intestinal cell polarity to brush border formation *Nat.Cell Biol.* 14:793-801.

Gobel, V., P.L. Barrett, D.H. Hall, and J.T. Fleming. 2004. Lumen morphogenesis in C. elegans requires the membrane-cytoskeleton linker erm-1. *Dev.Cell.* 6:865-873.

Gorelik, J., A.I. Shevchuk, G.I. Frolenkov, I.A. Diakonov, M.J. Lab, C.J. Kros, G.P. Richardson, I. Vodyanoy, C.R. Edwards, D. Klenerman, and Y.E. Korchev. 2003. Dynamic assembly of surface structures in living cells. *Proc.Natl.Acad.Sci.U.S.A.* 100:5819-5822.

Gould, K.L., J.A. Cooper, A. Bretscher, and T. Hunter. 1986. The protein-tyrosine kinase substrate, p81, is homologous to a chicken microvillar core protein *J.Cell Biol.* 102:660-669.

Granes, F., C. Berndt, C. Roy, P. Mangeat, M. Reina, and S. Vilaro. 2003. Identification of a novel Ezrin-binding site in syndecan-2 cytoplasmic domain *FEBS Lett.* 547:212-216.

Granes, F., J.M. Urena, N. Rocamora, and S. Vilaro. 2000. Ezrin links syndecan-2 to the cytoskeleton *J.Cell.Sci.* 113 (Pt 7):1267-1276.

Grimm-Gunter, E.M., C. Revenu, S. Ramos, I. Hurbain, N. Smyth, E. Ferrary, D. Louvard, S. Robine, and F. Rivero. 2009. Plastin 1 binds to keratin and is required for terminal web assembly in the intestinal epithelium *Mol.Biol.Cell.* 20:2549-2562.

Grusche, F.A., C. Hidalgo, G. Fletcher, H.H. Sung, E. Sahai, and B.J. Thompson. 2009. Sds22, a PP1 phosphatase regulatory subunit, regulates epithelial cell polarity and shape *BMC Dev.Biol.* 9:14.

Guerra, E., M. Trerotola, A.L. Aloisi, R. Tripaldi, G. Vacca, R. La Sorda, R. Lattanzio, M. Piantelli, and S. Alberti. 2012. The Trop-2 signalling network in cancer growth *Oncogene.*

Guilluy, C., M. Rolli-Derkinderen, L. Loufrani, A. Bourge, D. Henrion, L. Sabourin, G. Loirand, and P. Pacaud. 2008. Ste20-related kinase SLK phosphorylates Ser188 of RhoA to induce vasodilation in response to angiotensin II Type 2 receptor activation *Circ.Res.* 102:1265-1274.

Hamada, K., T. Shimizu, T. Matsui, S. Tsukita, and T. Hakoshima. 2000. Structural basis of the membrane-targeting and unmasking mechanisms of the radixin FERM domain *EMBO J.* 19:4449-4462.

Hamada, K., T. Shimizu, S. Yonemura, S. Tsukita, S. Tsukita, and T. Hakoshima. 2003. Structural basis of adhesion-molecule recognition by ERM proteins revealed by the crystal structure of the radixin-ICAM-2 complex *EMBO J.* 22:502-514.

Hanono, A., D. Garbett, D. Reczek, D.N. Chambers, and A. Bretscher. 2006. EPI64 regulates microvillar subdomains and structure *J.Cell Biol.* 175:803-813.

Hao, J.J., Y. Liu, M. Kruhlak, K.E. Debell, B.L. Rellahan, and S. Shaw. 2009. Phospholipase C-mediated hydrolysis of PIP2 releases ERM proteins from lymphocyte membrane *J.Cell Biol.* 184:451-462.

Harris, E.S., T.J. Gauvin, E.G. Heimsath, and H.N. Higgs. 2010. Assembly of filopodia by the formin FRL2 (FMNL3) *Cytoskeleton (Hoboken).* 67:755-772.

Harris, M.J., M. Kuwano, M. Webb, and P.G. Board. 2001. Identification of the apical membrane-targeting signal of the multidrug resistance-associated protein 2 (MRP2/MOAT) *J.Biol.Chem.* 276:20876-20881.

Hayashi, K., S. Yonemura, T. Matsui, and S. Tsukita. 1999. Immunofluorescence detection of ezrin/radixin/moesin (ERM) proteins with their carboxyl-terminal threonine phosphorylated in cultured cells and tissues *J.Cell.Sci.* 112 (Pt 8):1149-1158.

Heiska, L., and O. Carpen. 2005. Src phosphorylates ezrin at tyrosine 477 and induces a phosphospecific association between ezrin and a kelch-repeat protein family member *J.Biol.Chem.* 280:10244-10252.

Hipfner, D.R., and S.M. Cohen. 2003. The Drosophila sterile-20 kinase slik controls cell proliferation and apoptosis during imaginal disc development *PLoS Biol.* 1:E35.

Hipfner, D.R., N. Keller, and S.M. Cohen. 2004. Slik Sterile-20 kinase regulates Moesin activity to promote epithelial integrity during tissue growth *Genes Dev.* 18:2243-2248.

Hirao, M., N. Sato, T. Kondo, S. Yonemura, M. Monden, T. Sasaki, Y. Takai, S. Tsukita, and S. Tsukita. 1996. Regulation mechanism of ERM (ezrin/radixin/moesin) protein/plasma membrane association: possible involvement of phosphatidylinositol turnover and Rho-dependent signaling pathway. *J.Cell Biol.* 135:37-51.

Hornbeck, P.V., J.M. Kornhauser, S. Tkachev, B. Zhang, E. Skrzypek, B. Murray, V. Latham, and M. Sullivan. 2012. PhosphoSitePlus: a comprehensive resource for investigating the structure and function of experimentally determined post-translational modifications in man and mouse *Nucleic Acids Res.* 40:D261-70.

Hughes, S.C., and R.G. Fehon. 2006. Phosphorylation and activity of the tumor suppressor Merlin and the ERM protein Moesin are coordinately regulated by the Slik kinase. *J.Cell Biol.* 175:305-313.

Hughes, S.C., E. Formstecher, and R.G. Fehon. 2010. Sip1, the Drosophila orthologue of EBP50/NHERF1, functions with the sterile 20 family kinase Slik to regulate Moesin activity *J.Cell.Sci.* 123:1099-1107.

Ingraffea, J., D. Reczek, and A. Bretscher. 2002. Distinct cell type-specific expression of scaffolding proteins EBP50 and E3KARP: EBP50 is generally expressed with ezrin in specific epithelia, whereas E3KARP is not. *Eur.J.Cell Biol.* 81:61-68.

Jackson, D.I., and C. Dickson. 1999. Protein techniques. Immunoprecipitation, in vitro kinase assays, and western blotting *Methods Mol.Biol.* 97:699-708.

Jankovics, F., R. Sinka, T. Lukacsovich, and M. Erdelyi. 2002. MOESIN crosslinks actin and cell membrane in Drosophila oocytes and is required for OSKAR anchoring *Curr.Biol.* 12:2060-2065.

Karagiosis, S.A., and D.F. Ready. 2004. Moesin contributes an essential structural role in Drosophila photoreceptor morphogenesis. *Development.* 131:725-732.

Kikuchi, S., M. Hata, K. Fukumoto, Y. Yamane, T. Matsui, A. Tamura, S. Yonemura, H. Yamagishi, D. Keppler, S. Tsukita, and S. Tsukita. 2002. Radixin deficiency causes conjugated hyperbilirubinemia with loss of Mrp2 from bile canalicular membranes. *Nat.Genet.* 31:320-325.

Kinoshita, E., E. Kinoshita-Kikuta, K. Takiyama, and T. Koike. 2006. Phosphate-binding tag, a new tool to visualize phosphorylated proteins *Mol.Cell.Proteomics.* 5:749-757.

Kitajiri, S., K. Fukumoto, M. Hata, H. Sasaki, T. Katsuno, T. Nakagawa, J. Ito, S. Tsukita, and S. Tsukita. 2004. Radixin deficiency causes deafness associated with progressive degeneration of cochlear stereocilia. *J.Cell Biol.* 166:559-570.

Krugmann, S., I. Jordens, K. Gevaert, M. Driessens, J. Vandekerckhove, and A. Hall. 2001. Cdc42 induces filopodia by promoting the formation of an IRSp53:Mena complex *Curr.Biol.* 11:1645-1655.

Kunda, P., A.E. Pelling, T. Liu, and B. Baum. 2008. Moesin controls cortical rigidity, cell rounding, and spindle morphogenesis during mitosis *Curr.Biol.* 18:91-101.

Kunda, P., N.T. Rodrigues, E. Moeendarbary, T. Liu, A. Ivetic, G. Charras, and B. Baum. 2012a. PP1-mediated moesin dephosphorylation couples polar relaxation to mitotic exit *Curr.Biol.* 22:231-236.

LaLonde, D.P., D. Garbett, and A. Bretscher. 2010. A regulated complex of the scaffolding proteins PDZK1 and EBP50 with ezrin contribute to microvillar organization *Mol.Biol.Cell.* 21:1519-1529.

Lange, K. 2011. Fundamental role of microvilli in the main functions of differentiated cells: Outline of an universal regulating and signaling system at the cell periphery *J.Cell.Physiol.* 226:896-927.

Lauffer, B.E., C. Melero, P. Temkin, C. Lei, W. Hong, T. Kortemme, and M. von Zastrow. 2010. SNX27 mediates PDZ-directed sorting from endosomes to the plasma membrane. J.Cell Biol. 190:565-574.

Lee, A., and J.E. Treisman. 2004. Excessive Myosin activity in mbs mutants causes photoreceptor movement out of the Drosophila eye disc epithelium *Mol.Biol.Cell.* 15:3285-3295.

Legg, J.W., and C.M. Isacke. 1998. Identification and functional analysis of the ezrin-binding site in the hyaluronan receptor, CD44 *Curr.Biol.* 8:705-708.

Legg, J.W., C.A. Lewis, M. Parsons, T. Ng, and C.M. Isacke. 2002. A novel PKC-regulated mechanism controls CD44 ezrin association and directional cell motility *Nat.Cell Biol.* 4:399-407.

Leung, T., X.Q. Chen, I. Tan, E. Manser, and L. Lim. 1998. Myotonic dystrophy kinase-related Cdc42-binding kinase acts as a Cdc42 effector in promoting cytoskeletal reorganization *Mol.Cell.Biol.* 18:130-140.

Li, M., W. Wang, C.J. Soroka, A. Mennone, K. Harry, E.J. Weinman, and J.L. Boyer. 2010. NHERF-1 binds to Mrp2 and regulates hepatic Mrp2 expression and function *J.Biol.Chem.* 285:19299-19307.

Li, Q., M.R. Nance, R. Kulikauskas, K. Nyberg, R. Fehon, P.A. Karplus, A. Bretscher, and J.J. Tesmer. 2007. Self-masking in an intact ERM-merlin protein: an active role for the central alpha-helical domain *J.Mol.Biol.* 365:1446-1459.

Liu, Y., N.V. Belkina, C. Park, R. Nambiar, S.M. Loughhead, G. Patino-Lopez, K. Ben-Aissa, J.J. Hao, M.J. Kruhlak, H. Qi, U.H. von Andrian, J.H. Kehrl, M.J. Tyska, and S. Shaw. 2012. Constitutively active ezrin increases membrane tension, slows migration, and impedes endothelial transmigration of lymphocytes in vivo in mice *Blood.* 119:445-453.

Louvet, S., J. Aghion, A. Santa-Maria, P. Mangeat, and B. Maro. 1996. Ezrin becomes restricted to outer cells following asymmetrical division in the preimplantation mouse embryo *Dev.Biol.* 177:568-579.

Maniti, O., N. Khalifat, K. Goggia, F. Dalonneau, C. Guerin, L. Blanchoin, L. Ramos, and C. Picart. 2012. Binding of Moesin and Ezrin to membranes containing phophatidylinositol (4,5) bisphosphate: A comparative study of the affinity constants and conformational changes *Biochim.Biophys.Acta.*

Martin-Belmonte, F., A. Gassama, A. Datta, W. Yu, U. Rescher, V. Gerke, and K. Mostov. 2007. PTEN-mediated apical segregation of phosphoinositides controls epithelial morphogenesis through Cdc42 *Cell.* 128:383-397.

Matsui, T., M. Maeda, Y. Doi, S. Yonemura, M. Amano, K. Kaibuchi, S. Tsukita, and S. Tsukita. 1998. Rho-kinase phosphorylates COOH-terminal threonines of ezrin/radixin/moesin (ERM) proteins and regulates their head-to-tail association. *J.Cell Biol.* 140:647-657.

Matsui, T., M. Maeda, Y. Doi, S. Yonemura, M. Amano, K. Kaibuchi, S. Tsukita, and S. Tsukita. 1998b. Rho-kinase phosphorylates COOH-terminal threonines of ezrin/radixin/moesin (ERM) proteins and regulates their head-to-tail association *J.Cell Biol.* 140:647-657.

Matsui, T., S. Yonemura, S. Tsukita, and S. Tsukita. 1999. Activation of ERM proteins in vivo by Rho involves phosphatidyl-inositol 4-phosphate 5-kinase and not ROCK kinases. *Curr.Biol.* 9:1259-1262.

McClatchey, A.I., and R.G. Fehon. 2009. Merlin and the ERM proteins--regulators of receptor distribution and signaling at the cell cortex *Trends Cell Biol.* 19:198-206.

McConnell, R.E., J.N. Higginbotham, D.A. Shifrin Jr, D.L. Tabb, R.J. Coffey, and M.J. Tyska. 2009. The enterocyte microvillus is a vesicle-generating organelle *J.Cell Biol.* 185:1285-1298.

Meder, D., A. Shevchenko, K. Simons, and J. Fullekrug. 2005. Gp135/podocalyxin and NHERF-2 participate in the formation of a preapical domain during polarization of MDCK cells *J.Cell Biol.* 168:303-313.

Medina, E., J. Williams, E. Klipfell, D. Zarnescu, G. Thomas, and A. Le Bivic. 2002. Crumbs interacts with moesin and beta(Heavy)-spectrin in the apical membrane skeleton of Drosophila. *J.Cell Biol.* 158:941-951.

Millard, T.H., G. Bompard, M.Y. Heung, T.R. Dafforn, D.J. Scott, L.M. Machesky, and K. Futterer. 2005. Structural basis of filopodia formation induced by the IRSp53/MIM homology domain of human IRSp53 *EMBO J.* 24:240-250.

Mohler, P.J., S.M. Kreda, R.C. Boucher, M. Sudol, M.J. Stutts, and S.L. Milgram. 1999. Yes-associated protein 65 localizes p62(c-Yes) to the apical compartment of airway epithelia by association with EBP50 *J.Cell Biol.* 147:879-890.

Mooseker, M.S., and L.G. Tilney. 1975. Organization of an actin filament-membrane complex. Filament polarity and membrane attachment in the microvilli of intestinal epithelial cells *J.Cell Biol.* 67:725-743.

Morales, F.C., Y. Takahashi, E.L. Kreimann, and M.M. Georgescu. 2004. Ezrin-radixin-moesin (ERM)-binding phosphoprotein 50 organizes ERM proteins at the apical membrane of polarized epithelia *Proc.Natl.Acad.Sci.U.S.A.* 101:17705-17710.

Mori, T., K. Kitano, S. Terawaki, R. Maesaki, Y. Fukami, and T. Hakoshima. 2008. Structural basis for CD44 recognition by ERM proteins *J.Biol.Chem.* 283:29602-29612.

Mosevitsky, M.I., J.P. Capony, G.Y. Skladchikova, V.A. Novitskaya, A.Y. Plekhanov, and V.V. Zakharov. 1997. The BASP1 family of myristoylated proteins abundant in axonal termini. Primary structure analysis and physico-chemical properties *Biochimie.* 79:373-384.

Naba, A., C. Reverdy, D. Louvard, and M. Arpin. 2008. Spatial recruitment and activation of the Fes kinase by ezrin promotes HGF-induced cell scattering *EMBO J.* 27:38-50.

Nakamura, F., M.R. Amieva, and H. Furthmayr. 1995. Phosphorylation of threonine 558 in the carboxyl-terminal actin-binding domain of moesin by thrombin activation of human platelets. *J.Biol.Chem.* 270:31377-31385.

Nakamura, F., M.R. Amieva, C. Hirota, Y. Mizuno, and H. Furthmayr. 1996. Phosphorylation of 558T of moesin detected by site-specific antibodies in RAW264.7 macrophages *Biochem.Biophys.Res.Commun.* 226:650-656.

Nakamura, N., N. Oshiro, Y. Fukata, M. Amano, M. Fukata, S. Kuroda, Y. Matsuura, T. Leung, L. Lim, and K. Kaibuchi. 2000. Phosphorylation of ERM proteins at filopodia induced by Cdc42 *Genes Cells.* 5:571-581.

Nambiar, R., R.E. McConnell, and M.J. Tyska. 2010. Myosin motor function: the ins and outs of actin-based membrane protrusions *Cell Mol.Life Sci.* 67:1239-1254.

Neubueser, D., and D.R. Hipfner. 2010. Overlapping roles of Drosophila Drak and Rok kinases in epithelial tissue morphogenesis *Mol.Biol.Cell.* 21:2869-2879.

Ng, T., M. Parsons, W.E. Hughes, J. Monypenny, D. Zicha, A. Gautreau, M. Arpin, S. Gschmeissner, P.J. Verveer, P.I. Bastiaens, and P.J. Parker. 2001. Ezrin is a downstream effector of trafficking PKC-integrin complexes involved in the control of cell motility *EMBO J.* 20:2723-2741.

Niggli, V., C. Andreoli, C. Roy, and P. Mangeat. 1995. Identification of a phosphatidylinositol-4,5-bisphosphate-binding domain in the N-terminal region of ezrin *FEBS Lett.* 376:172-176.

Ong, S.E., B. Blagoev, I. Kratchmarova, D.B. Kristensen, H. Steen, A. Pandey, and M. Mann. 2002. Stable isotope labeling by amino acids in cell culture, SILAC, as a simple and accurate approach to expression proteomics *Mol.Cell.Proteomics.* 1:376-386.

Oshiro, N., Y. Fukata, and K. Kaibuchi. 1998. Phosphorylation of moesin by rho-associated kinase (Rho-kinase) plays a crucial role in the formation of microvilli-like structures *J.Biol.Chem.* 273:34663-34666.

Pakkanen, R., K. Hedman, O. Turunen, T. Wahlstrom, and A. Vaheri. 1987. Microvillus-specific Mr 75,000 plasma membrane protein of human choriocarcinoma cells *J.Histochem.Cytochem.* 35:809-816.

Pao, W., and J. Chmielecki. 2010. Rational, biologically based treatment of EGFR-mutant non-small-cell lung cancer *Nat.Rev.Cancer.* 10:760-774.

Pao, W., V.A. Miller, K.A. Politi, G.J. Riely, R. Somwar, M.F. Zakowski, M.G. Kris, and H. Varmus. 2005. Acquired resistance of lung adenocarcinomas to gefitinib or erlotinib is associated with a second mutation in the EGFR kinase domain *PLoS Med.* 2:e73.

Pearson, M.A., D. Reczek, A. Bretscher, and P.A. Karplus. 2000. Structure of the ERM protein moesin reveals the FERM domain fold masked by an extended actin binding tail domain *Cell.* 101:259-270.

Peter, B.J., H.M. Kent, I.G. Mills, Y. Vallis, P.J. Butler, P.R. Evans, and H.T. McMahon. 2004. BAR domains as sensors of membrane curvature: the amphiphysin BAR structure. *Science.* 303:495-499.

Pietromonaco, S.F., P.C. Simons, A. Altman, and L. Elias. 1998. Protein kinase C-theta phosphorylation of moesin in the actin-binding sequence *J.Biol.Chem.* 273:7594-7603.

Pilot, F., J.M. Philippe, C. Lemmers, and T. Lecuit. 2006. Spatial control of actin organization at adherens junctions by a synaptotagmin-like protein Btsz *Nature.* 442:580-584.

Polesello, C., I. Delon, P. Valenti, P. Ferrer, and F. Payre. 2002. Dmoesin controls actin-based cell shape and polarity during Drosophila melanogaster oogenesis. *Nat.Cell Biol.* 4:782-789.

Prag, S., M. Parsons, M.D. Keppler, S.M. Ameer-Beg, P. Barber, J. Hunt, A.J. Beavil, R. Calvert, M. Arpin, B. Vojnovic, and T. Ng. 2007. Activated ezrin promotes cell migration through recruitment of the GEF Dbl to lipid rafts and preferential downstream activation of Cdc42 *Mol.Biol.Cell.* 18:2935-2948.

Pruyne, D., A. Legesse-Miller, L. Gao, Y. Dong, and A. Bretscher. 2004. Mechanisms of polarized growth and organelle segregation in yeast *Annu.Rev.Cell Dev.Biol.* 20:559-591.

Pujuguet, P., L. Del Maestro, A. Gautreau, D. Louvard, and M. Arpin. 2003. Ezrin regulates E-cadherin-dependent adherens junction assembly through Rac1 activation. *Mol.Biol.Cell.* 14:2181-2191.

Reczek, D., M. Berryman, and A. Bretscher. 1997. Identification of EBP50: A PDZ-containing phosphoprotein that associates with members of the ezrin-radixin-moesin family. *J.Cell Biol.* 139:169-179.

Reczek, D., and A. Bretscher. 2001. Identification of EPI64, a TBC/rabGAP domain-containing microvillar protein that binds to the first PDZ domain of EBP50 and E3KARP. *J.Cell Biol.* 153:191-206.

Reczek, D., and A. Bretscher. 1998. The carboxyl-terminal region of EBP50 binds to a site in the amino-terminal domain of ezrin that is masked in the dormant molecule *J.Biol.Chem.* 273:18452-18458.

Revenu, C., F. Ubelmann, I. Hurbain, F. El-Marjou, F. Dingli, D. Loew, D. Delacour, J. Gilet, E. Brot-Laroche, F. Rivero, D. Louvard, and S. Robine. 2012. A new role for the architecture of microvillar actin bundles in apical retention of membrane proteins *Mol.Biol.Cell.* 23:324-336.

Ripani, E., A. Sacchetti, D. Corda, and S. Alberti. 1998. Human Trop-2 is a tumor-associated calcium signal transducer *Int.J.Cancer.* 76:671-676.

Roch, F., C. Polesello, C. Roubinet, M. Martin, C. Roy, P. Valenti, S. Carreno, P. Mangeat, and F. Payre. 2010. Differential roles of PtdIns(4,5)P2 and phosphorylation in moesin activation during Drosophila development *J.Cell.Sci.* 123:2058-2067.

Roubinet, C., B. Decelle, G. Chicanne, J.F. Dorn, B. Payrastre, F. Payre, and S. Carreno. 2011. Molecular networks linked by Moesin drive remodeling of the cell cortex during mitosis *J.Cell Biol.* 195:99-112.

Sabourin, L.A., and M.A. Rudnicki. 1999. Induction of apoptosis by SLK, a Ste20-related kinase *Oncogene.* 18:7566-7575.

Sabourin, L.A., K. Tamai, P. Seale, J. Wagner, and M.A. Rudnicki. 2000. Caspase 3 cleavage of the Ste20-related kinase SLK releases and activates an apoptosis-inducing kinase domain and an actin-disassembling region *Mol.Cell.Biol.* 20:684-696.

Santiago-Tirado, F.H., A. Legesse-Miller, D. Schott, and A. Bretscher. 2011. PI4P and Rab inputs collaborate in myosin-V-dependent transport of secretory compartments in yeast *Dev.Cell.* 20:47-59.

Saotome, I., M. Curto, and A.I. McClatchey. 2004. Ezrin is essential for epithelial organization and villus morphogenesis in the developing intestine. *Dev.Cell.* 6:855-864.

Sawallisch, C., K. Berhorster, A. Disanza, S. Mantoani, M. Kintscher, L. Stoenica, A. Dityatev, S. Sieber, S. Kindler, F. Morellini, M. Schweizer, T.M. Boeckers, M. Korte, G. Scita, and H.J. Kreienkamp. 2009. The insulin receptor substrate of 53 kDa (IRSp53) limits hippocampal synaptic plasticity *J.Biol.Chem.* 284:9225-9236.

Schon, M.P., and C.E. Orfanos. 1995. Transformation of human keratinocytes is characterized by quantitative and qualitative alterations of the T-16 antigen (Trop-2, MOv-16) *Int.J.Cancer.* 60:88-92.

Segbert, C., K. Johnson, C. Theres, D. van Furden, and O. Bossinger. 2004. Molecular and functional analysis of apical junction formation in the gut epithelium of Caenorhabditis elegans. *Dev.Biol.* 266:17-26.

Serrador, J.M., A. Urzainqui, J.L. Alonso-Lebrero, J.R. Cabrero, M.C. Montoya, M. Vicente-Manzanares, M. Yanez-Mo, and F. Sanchez-Madrid. 2002. A juxta-membrane amino acid sequence of P-selectin glycoprotein ligand-1 is involved in moesin binding and ezrin/radixin/moesin-directed targeting at the trailing edge of migrating lymphocytes *Eur.J.Immunol.* 32:1560-1566.

Sfakianos, J., A. Togawa, S. Maday, M. Hull, M. Pypaert, L. Cantley, D. Toomre, and I. Mellman. 2007. Par3 functions in the biogenesis of the primary cilium in polarized epithelial cells *J.Cell Biol.* 179:1133-1140.

Shcherbina, A. 1999. Moesin, the major ERM protein of lymphocytes and platelets, differs from ezrin in its insensitivity to calpain *FEBS Lett.* 443:31-36.

Shifrin, D.A.,Jr, R.E. McConnell, R. Nambiar, J.N. Higginbotham, R.J. Coffey, and M.J. Tyska. 2012. Enterocyte microvillus-derived vesicles detoxify bacterial products and regulate epithelial-microbial interactions *Curr.Biol.* 22:627-631.

Simons, P.C., S.F. Pietromonaco, D. Reczek, A. Bretscher, and L. Elias. 1998. C-terminal threonine phosphorylation activates ERM proteins to link the cell's cortical lipid bilayer to the cytoskeleton *Biochem.Biophys.Res.Commun.* 253:561-565.

Smolka, M.B., C.P. Albuquerque, S.H. Chen, and H. Zhou. 2007. Proteome-wide identification of in vivo targets of DNA damage checkpoint kinases *Proc.Natl.Acad.Sci.U.S.A.* 104:10364-10369.

Song, Z., M. Postma, S.A. Billings, D. Coca, R.C. Hardie, and M. Juusola. 2012. Stochastic, Adaptive Sampling of Information by Microvilli in Fly Photoreceptors *Curr.Biol.* 22:1371-80.

Speck, O., S.C. Hughes, N.K. Noren, R.M. Kulikauskas, and R.G. Fehon. 2003. Moesin functions antagonistically to the Rho pathway to maintain epithelial integrity. *Nature.* 421:83-87.

Spence, H.J., Y.J. Chen, C.L. Batchelor, J.R. Higginson, H. Suila, O. Carpen, and S.J. Winder. 2004. Ezrin-dependent regulation of the actin cytoskeleton by beta-dystroglycan *Hum.Mol.Genet.* 13:1657-1668.

Storbeck, C.J., S. Wagner, P. O'Reilly, M. McKay, R.J. Parks, H. Westphal, and L.A. Sabourin. 2009. The Ldb1 and Ldb2 transcriptional cofactors interact with the Ste20-like kinase SLK and regulate cell migration *Mol.Biol.Cell.* 20:4174-4182.

Sullivan, A., C.R. Uff, C.M. Isacke, and R.F. Thorne. 2003. PACE-1, a novel protein that interacts with the C-terminal domain of ezrin *Exp.Cell Res.* 284:224-238.

Surace, E.I., C.A. Haipek, and D.H. Gutmann. 2004. Effect of merlin phosphorylation on neurofibromatosis 2 (NF2) gene function *Oncogene.* 23:580-587.

Takai, Y., K. Kitano, S. Terawaki, R. Maesaki, and T. Hakoshima. 2007. Structural basis of PSGL-1 binding to ERM proteins *Genes Cells.* 12:1329-1338.

Takaichi, R., S. Odagaki, H. Kumanogoh, S. Nakamura, M. Morita, and S. Maekawa. 2012. Inhibitory effect of NAP-22 on the phosphatase activity of synaptojanin-1 *J.Neurosci.Res.* 90:21-27.

Takeuchi, K., N. Sato, H. Kasahara, N. Funayama, A. Nagafuchi, S. Yonemura, S. Tsukita, and S. Tsukita. 1994. Perturbation of cell adhesion and microvilli formation by antisense oligonucleotides to ERM family members. *J.Cell Biol.* 125:1371-1384.

ten Klooster, J.P., M. Jansen, J. Yuan, V. Oorschot, H. Begthel, V. Di Giacomo, F. Colland, J. de Koning, M.M. Maurice, P. Hornbeck, and H. Clevers. 2009. Mst4 and Ezrin induce brush borders downstream of the Lkb1/Strad/Mo25 polarization complex *Dev.Cell.* 16:551-562.

Tocchetti, A., C.B. Soppo, F. Zani, F. Bianchi, M.C. Gagliani, B. Pozzi, J. Rozman, R. Elvert, N. Ehrhardt, B. Rathkolb, C. Moerth, M. Horsch, H. Fuchs, V. Gailus-Durner, J. Beckers, M. Klingenspor, E. Wolf, M. Hrabe de Angelis, E. Scanziani, C. Tacchetti, G. Scita, P.P. Di Fiore, and N. Offenhauser. 2010. Loss of the actin remodeler Eps8 causes intestinal defects and improved metabolic status in mice *PLoS One.* 5:e9468.

Toska, E., H.A. Campbell, J. Shandilya, S.J. Goodfellow, P. Shore, K.F. Medler, and S.G. Roberts. 2012. Repression of Transcription by WT1-BASP1 Requires the Myristoylation of BASP1 and the PIP2-Dependent Recruitment of Histone Deacetylase *Cell.Rep.* 2:462-9.

Trebak, M., G.E. Begg, J.M. Chong, E.V. Kanazireva, D. Herlyn, and D.W. Speicher. 2001. Oligomeric state of the colon carcinoma-associated glycoprotein GA733-2 (Ep-CAM/EGP40) and its role in GA733-mediated homotypic cell-cell adhesion *J.Biol.Chem.* 276:2299-2309.

Trerotola, M., P. Cantanelli, E. Guerra, R. Tripaldi, A.L. Aloisi, V. Bonasera, R. Lattanzio, R.D. Lange, U.H. Weidle, M. Piantelli, and S. Alberti. 2012. Upregulation of Trop-2 quantitatively stimulates human cancer growth *Oncogene.* Epub ahead of print.

Tsukita, S., K. Oishi, N. Sato, J. Sagara, A. Kawai, and S. Tsukita. 1994. ERM family members as molecular linkers between the cell surface glycoprotein CD44 and actin-based cytoskeletons *J.Cell Biol.* 126:391-401.

Turunen, O., T. Wahlstrom, and A. Vaheri. 1994. Ezrin has a COOH-terminal actin-binding site that is conserved in the ezrin protein family *J.Cell Biol.* 126:1445-1453.

Tyska, M.J., A.T. Mackey, J.D. Huang, N.G. Copeland, N.A. Jenkins, and M.S. Mooseker. 2005. Myosin-1a is critical for normal brush border structure and composition *Mol.Biol.Cell.* 16:2443-2457.

Van Furden, D., K. Johnson, C. Segbert, and O. Bossinger. 2004. The C. elegans ezrin-radixin-moesin protein ERM-1 is necessary for apical junction remodelling and tubulogenesis in the intestine. *Dev.Biol.* 272:262-276.

Veltman, D.M., G. Auciello, H.J. Spence, L.M. Machesky, J.Z. Rappoport, and R.H. Insall. 2011. Functional analysis of Dictyostelium IBARa reveals a conserved role of the I-BAR domain in endocytosis *Biochem.J.* 436:45-52.

Verdier, V., J.E. Johndrow, M. Betson, G.C. Chen, D.A. Hughes, S.M. Parkhurst, and J. Settleman. 2006. Drosophila Rho-kinase (DRok) is required for tissue morphogenesis in diverse compartments of the egg chamber during oogenesis *Dev.Biol.* 297:417-432.

Verner, K., and A. Bretscher. 1983. Induced morphological changes in isolated microvilli: regulation of membrane topology in vitro by submembranous microfilaments *Eur.J.Cell Biol.* 29:187-192.

Viswanatha, R., Ohouo P.Y., Smolka, M.B., and A. Bretscher. 2012. Local phosphocycling mediated by LOK/SLK restricts ezrin function to the apical aspect of epithelial cells. *J. Cell Biol.* In press.

Wagner, S., T.A. Flood, P. O'Reilly, K. Hume, and L.A. Sabourin. 2002. Association of the Ste20-like kinase (SLK) with the microtubule. Role in Rac1-mediated regulation of actin dynamics during cell adhesion and spreading *J.Biol.Chem.* 277:37685-37692.

Wald, F.A., A.S. Oriolo, A. Mashukova, N.L. Fregien, A.H. Langshaw, and P.J. Salas. 2008. Atypical protein kinase C (iota) activates ezrin in the apical domain of intestinal epithelial cells *J.Cell.Sci.* 121:644-654.

Wang, J., R. Day, Y. Dong, S.J. Weintraub, and L. Michel. 2008. Identification of Trop-2 as an oncogene and an attractive therapeutic target in colon cancers *Mol.Cancer.Ther.* 7:280-285.

Wang, J., K. Zhang, D. Grabowska, A. Li, Y. Dong, R. Day, P. Humphrey, J. Lewis, R.D. Kladney, J.M. Arbeit, J.D. Weber, C.H. Chung, and L.S. Michel. 2011. Loss of Trop2 promotes carcinogenesis and features of epithelial to mesenchymal transition in squamous cell carcinoma *Mol.Cancer.Res.* 9:1686-1695.

Wells, C.D., J.P. Fawcett, A. Traweger, Y. Yamanaka, M. Goudreault, K. Elder, S. Kulkarni, G. Gish, C. Virag, C. Lim, K. Colwill, A. Starostine, P. Metalnikov, and T. Pawson. 2006. A Rich1/Amot complex regulates the Cdc42 GTPase and apical-polarity proteins in epithelial cells. *Cell.* 125:535-548.

Xing, B., A. Jedsadayanmata, and S.C. Lam. 2001. Localization of an integrin binding site to the C terminus of talin *J.Biol.Chem.* 276:44373-44378.

Xu, X., T. Omelchenko, and A. Hall. 2010. LKB1 tumor suppressor protein regulates actin filament assembly through Rho and its exchange factor Dbl independently of kinase activity *BMC Cell Biol.* 11:77. 11:77.

Yamamoto, M., D.H. Hilgemann, S. Feng, H. Bito, H. Ishihara, Y. Shibasaki, and H.L. Yin. 2001. Phosphatidylinositol 4,5-bisphosphate induces actin stress-fiber formation and inhibits membrane ruffling in CV1 cells *J.Cell Biol.* 152:867-876.

Yamamoto, N., M. Honma, and H. Suzuki. 2011. Off-target serine/threonine kinase 10 inhibition by erlotinib enhances lymphocytic activity leading to severe skin disorders *Mol.Pharmacol.* 80:466-475.

Yang, H.S., and P.W. Hinds. 2006. Phosphorylation of ezrin by cyclin-dependent kinase 5 induces the release of Rho GDP dissociation inhibitor to inhibit Rac1 activity in senescent cells *Cancer Res.* 66:2708-2715.

Yang, H.S., and P.W. Hinds. 2003. Increased ezrin expression and activation by CDK5 coincident with acquisition of the senescent phenotype *Mol.Cell.* 11:1163-1176.

Yang, Y., D.A. Primrose, A.C. Leung, R.B. Fitzsimmons, M.C. McDermand, A. Missellbrook, J. Haskins, A.S. Smylie, and S.C. Hughes. 2012. The PP1 phosphatase flapwing regulates the activity of Merlin and Moesin in Drosophila *Dev.Biol.* 361:412-426.

Yokoyama, T., H. Goto, I. Izawa, H. Mizutani, and M. Inagaki. 2005. Aurora-B and Rho-kinase/ROCK, the two cleavage furrow kinases, independently regulate the progression of cytokinesis: possible existence of a novel cleavage furrow kinase phosphorylates ezrin/radixin/moesin (ERM) *Genes Cells.* 10:127-137.

Yonemura, S., M. Hirao, Y. Doi, N. Takahashi, T. Kondo, S. Tsukita, and S. Tsukita. 1998. Ezrin/radixin/moesin (ERM) proteins bind to a positively charged amino acid cluster in the juxta-membrane cytoplasmic domain of CD44, CD43, and ICAM-2 *J.Cell Biol.* 140:885-895.

Yonemura, S., T. Matsui, S. Tsukita, and S. Tsukita. 2002. Rho-dependent and -independent activation mechanisms of ezrin/radixin/moesin proteins: an essential role for polyphosphoinositides in vivo. *J.Cell.Sci.* 115:2569-2580.

Yonemura, S., S. Tsukita, and S. Tsukita. 1999. Direct involvement of ezrin/radixin/moesin (ERM)-binding membrane proteins in the organization of microvilli in collaboration with activated ERM proteins *J.Cell Biol.* 145:1497-1509.

Zaarour, R.F., D. Chirivino, L. Del Maestro, L. Daviet, A. Atfi, D. Louvard, and M. Arpin. 2012. Ezrin ubiquitylation by the E3 ubiquitin ligase, WWP1, and consequent regulation of hepatocyte growth factor receptor activity *PLoS One.* 7:e37490.

Zakharov, V.V., and M.I. Mosevitsky. 2010. Oligomeric structure of brain abundant proteins GAP-43 and BASP1 *J.Struct.Biol.* 170:470-483.

Zhou, R., X. Cao, C. Watson, Y. Miao, Z. Guo, J.G. Forte, and X. Yao. 2003. Characterization of protein kinase A-mediated phosphorylation of ezrin in gastric parietal cell activation *J.Biol.Chem.* 278:35651-35659.

Zwaenepoel, I., A. Naba, M.M. Da Cunha, L. Del Maestro, E. Formstecher, D. Louvard, and M. Arpin. 2012. Ezrin regulates microvillus morphogenesis by promoting distinct activities of Eps8 proteins *Mol.Biol.Cell.* 23:1080-1094.